NONLINEAR AND ANISOTROPIC BEHAVIOR OF HIGH PERFORMANCE FIBERS

by

MAUREEN THERESA FAHEY
S.B. Mat. Sci. and Eng., MIT
(1990)

submitted to
The Department of Materials Science and Engineering
in partial fulfillment of the requirement for the degree of

DOCTOR OF SCIENCE

at the
Massachusetts Institute of Technology
September, 1993

Signature of Author _____
Department of Materials Science and Engineering
August 6, 1993

Certified by _____
Frederick J. McGarry
Professor of Polymer Engineering
Thesis Supervisor

Accepted by _____
Carl V. Thompson III
Professor of Electronic Materials
Chair, Departmental Committee on Graduate Students

NONLINEAR AND ANISOTROPIC BEHAVIOR OF HIGH PERFORMANCE FIBERS

by

MAUREEN THERESA FAHEY

Submitted to the Department of Materials Science and Engineering
on August 6, 1993 in partial fulfillment of the requirement for the
degree of Doctor of Science in Materials Science and Engineering

ABSTRACT:

Two novel test methods for the direct measurement of single fiber tensile and compressive properties have been developed and are used to describe the strain dependent behavior of polyacrylonitrile- and pitch-based carbon fibers and aramid polymeric fibers. Fiber microstructure is responsible for nonlinear behavior and causes distinctly different tensile and compressive properties.

The tensile modulus of five DuPont aramid fibers (Kevlar 119, Kevlar 29, Kevlar 129, Kevlar 49 and Kevlar 149), four Hercules PAN- based carbon fibers (AS-4, IM-7, IM-8 and HMS-4) and three Amoco pitch- based fibers (P25, P55, and P75) are measured with the Fiber Incremental Tensile Tester, a device built to measure fiber extension as a function of dead- weight loading. Increasing tensile strain enhances microstructural orientation, leading to a non-linear stress- strain curve. During the first 0.2% strain, the tensile modulii of Kevlar 119, 29, 129 and 49 and PAN-based AS4, IM7 and IM8 increase by less than 5% while the tensile modulii of the more oriented Kevlar 149 and HMS4 increase almost 10%. The tensile modulii of P25, P55 and P75 increase an average of 12%, 21% and 16%, respectively, during the first 0.2% strain.

Compressive strain reduces microstructural orientation leading to softening and lower strengths than in tension. The Micro- Flex bending test was developed to measure the bending stiffness and yield stress from which the compressive modulus and strength are calculated. During the first 0.2% strain, the compressive modulus of Kevlar 149 drops almost 35% from the zero strain value while the compressive modulii of the other Kevlar fibers decrease 20- 30%. Compressive modulii of Kevlar 149 and the other Kevlar fibers at compressive failure are approximately 33% and 50%, respectively, of the tensile modulus. Compressive strengths range from 0.2 GPa to 0.3 GPa. The compressive modulus of HMS4 decreases 20%, compared to a decrease of 10-15% for the other PAN- based fibers. At 0.3- 0.4% bending strain, a range typically encountered in aerospace composites, the compressive modulii of PAN- based fibers are approximately 60% of the tensile modulii. The compressive modulus of P25 decreases approximately 20% in the first 0.2% strain, while the higher modulus P55 and P75 fibers lose 30% of the zero strain compressive modulus. The compressive modulus of P25 at 0.6% strain is approximately 55% of the tensile modulus while the compressive modulii of P55 and P75 are approximately 40% of the tensile modulii at 0.2% strain.

A sensitivity analysis based on the precision of the test variables indicates a standard error of ± 1.6% in the measured tensile modulus and ± 3.5% in the measured bending modulus. Error in the calculated compressive modulus depends on the degree of anisotropy, but generally is less than ± 7% for the compressive modulus and stress at failure. The Fiber Incremental Tensile Test and Micro- Flex Test are simple methods for assessing tensile, flexural and compressive behaviors of high performance fibers with a minimum amount of fiber required.

Thesis Supervisor: Professor Frederick J. McGarry

Title: Professor of Polymer Engineering

Table of Contents

List of Figures

Chapter 1

Chapter 2

List of Tables

Chapter 1

Chapter 2

Chapter 3

Acknowledgements

My family has always supported my endeavors, and to them I give my greatest thanks. The love in the Fahey family is apparent to all who know me, and the escapades of Mom and Dad, Katie, Mike, Tim and Pat are a constant source of amazement, amusement, and general good cheer. Katie deserves special thanks for trading her brand new computer for my slow old one while we were both working on graduate theses.

I would like to thank Professor McGarry, for his guidance and support over the years. He has helped me learn my personal and professional strengths and weaknesses, and has advised me how to make the best of them. From an eager UROP with limited skills, to the engineer I am today, Professor McGarry has provided me with many opportunities for which I will always be grateful.

In the hustle and bustle of MIT, there have been many who have helped me keep the world in perspective. Though too numerous to mention them all, I would particularly like to recognize the following contributors to my sanity: Daniel Aalberts, Morgan Conn, Kirk Kolenbrander, John Moalli, Susan Noe, Steph Ragucci, Gus Rancatore, Maria Raposo, Ramnath Subramaniam, Mike Vale, Debbie Vezie and from miles away, Jeff Drake.

I would like to thank those who have helped advance my project in addition to teaching me invaluable practical skills: Mike Frongillo and Tony Garratt-Reed for giving me access to my "dungeon," where I was able to test the fibers in a vibration free area; Stephen and Arthur Rudolph, whose outstanding workmanship is reflected in the testing devices and fixtures they built; Hong Li and Alex Pfajfer for helping me with the micro-electrodischarge machining; Peter Flüeller for reviewing the tests and suggesting the air shield; Rob Lescanec, who patiently explained error analysis and even got me the book; and most of all, CJ Doane, my UROP, who has developed the touch for fiber testing and without whose help I could not have finished as planned. There are others, not mentioned, whose contributions are nonetheless appreciated.

Materials for this study were provided by the duPont Textile Fibers Department, Hercules, Inc., and Amoco Performance Products, Inc., while partial funding was provided by Dow Chemical.

Introduction

Composite materials reinforced with high performance polymeric and carbon fibers are replacing traditional structural materials in many applications. Kevlar rigid- rod polymer fibers and PAN- and pitch- based carbon fibers have tensile strengths and modulii many times greater than many typical materials and so with densities in the range of 1-2.5 g/cc, composites based on them have attractive properties when weight considerations are important. Much effort has gone into the improvement of their properties by adjusting the starting materials and processing conditions to optimize microstructural factors. With Kevlar, for example, orienting the primary bonds along the fiber axis improves tensile properties, but it can also have the opposite effect on compressive behavior. In carbon fibers, transverse properties can be similarly reduced.

To monitor such changes, often special tests are necessary. Axial compression of single fibers is difficult because of their long slender geometry. Typical diameters of glass fibers are 14-18 μm, of Kevlar and pitch- based carbon fibers are 9-12 μm, and of PAN-based fibers are 4- 7 μm. (The diameter of human hair is 70-100 μm.) In axial compression, buckling occurs if the fiber is too long compared to its diameter, but end-effects from grips may require a lower bound on the test length. Such opposing factors have led to the development of many indirect test methods with which to measure fiber compressive properties. The oriented microstructure may cause nonlinear stress-strain behavior, both in tension and in compression. If these are used in structural composites, simple, reliable tests are needed to measure the complete stress- strain curves. Developing such tests was one purpose of this research. Two, single fiber, test methods are described; when performed sequentially, a complete set of fiber properties can be obtained. The tests are well suited to experimental fibers because of the minimal sample requirements.

In Chapter 1, the current state of high performance fiber testing is reviewed. Chapter 2 presents a new tensile test procedure, the Fiber Incremental Tensile Test (FITT) in which dead- weight loading simple displacement measurements are used. The tensile

stress- strain curves for each of twelve synthetic fiber types and for glass fibers are presented.

The Micro- Flex bending test, which measures single fiber bending stiffness and yield load, is described in Chapter 3. If the tensile and bending modulii of a fiber are measured, the compressive modulus of it can be calculated. Knowing the compressive modulus and the strain at failure permits the calculation of the compressive strength. Thus this approach is especially important to study anisotropic fibers and its accuracy can be monitored by testing such isotropic fibers as glass. Rayon- based carbon and other fibers with nonuniform cross sections were not studied because the bending analysis requires calculation of the fiber centroidal moment of inertia, which is related to the fiber shape. Bending load- deflection curves for each fiber type are given. Bending stress- strain curves are compared to tensile stress-strain curves. Bending and compressive modulii and their strain-dependence are reported. Compressive failure stress is calculated from the compressive modulus and compressive failure strain when the latter is small enough to avoid excessive bending deflections. (This requirement excluded the carbon fibers.) Error propagation analysis indicates a maximum uncertainty of ± 7% of the compressive properties;typically the range is ± 5.5%.

Chapter 4 summarizes the work, presents conclusions and suggests recommendations for further applications of the test.

1. Fiber Structure and Properties

1.1. Kevlar Fibers

The fibers tested in this study are commercially available: Kevlar 119, 29, 129, 49 and 149 fibers were provided by duPont Fibers and Textiles division. Kevlar fibers are PPTA, poly(paraphenylene terephthalamide), which has been processed by dry jet- wet spinning to orient the rigid polymer chains with the fiber axis. The PPTA repeat unit is shown in Figure 1.1. The extended chain conformation of the molecules is responsible for the high tensile modulus and strength. The two phenyl rings give strength and stiffness to the chain, increasing the number of covalent bonds parallel to the fiber axis. The extended conformation is maintained because stearic hindrance discourages rotation of the rings around the amide linkage. Dobb, Johnson and Saville[1] report radially arranged pleated sheets in the structure of Kevlar 29 and 49 (Figure 1.2A). The sidestep in the repeat unit introduced by the amide linkage and the pleated structure both affect mechanical properties, particularly the modulus. The pleats in Kevlar 29 and 49 will open or close with applied tensile or compressive stress. At full extension or in the absence of pleats, the modulus will be higher than when the pleat is acting as a hinge.

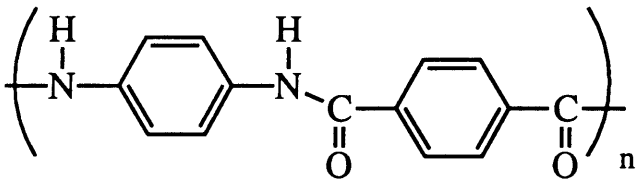

Figure 1.1. Repeat unit of poly(paraphenylene terephthalamide), which is processed and sold by duPont as Kevlar fiber.

Rigid- rod fibers exhibit a fibrillar microstructure (Figure 1.2B), similar to that proposed by Sawyer and Jaffe.[2] Applied axial tensile forces can further orient the fibrils, increasing stiffness, while axial compressive forces lead to fibril buckling and kinking. Figure 1.3A is a micrograph of a Kevlar 149 fiber showing a characteristic splitting along the fiber length due to the extreme processing conditions. Microfibrils are visible across

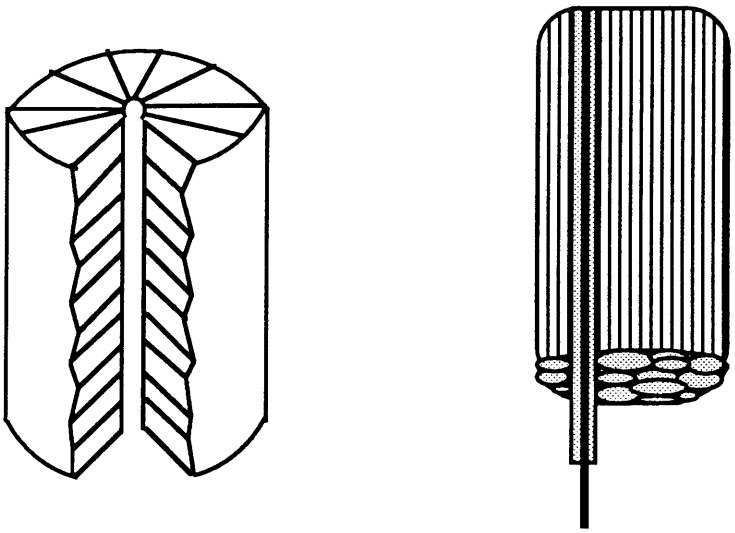

1.2A 1.2B

Figure 1.2. Structure of Kevlar fibers. A) Radially oriented pleated sheet structure described by Dobb, Johnson and Saville. B) Fiber is made of fibrils of various size, after Sawyer and Jaffe.

the split. Figure 1.3B is a micrograph of a Kevlar 49 fiber with the skin peeled back to reveal the fibrillar structure. Kink bands have different appearances depending on how they are formed. Failures in fibers subjected to pure compression and to bending are shown schematically in Figure 1.4A and 1.4B. Frequently, the visible failure region from pure compression consists of more than one kink band. Bending failure is characterized by two opposite kinks or groups of kinks initiated at the fiber edge under greatest compressive strain. An SEM micrograph of a Kevlar 129 fiber kinked during flexure is shown in Figure 1.5.

After spinning and drying, Kevlar 49 and 149 fibers experience a heat treatment: exposure to elevated temperature while under tension, to improve the orientation of the structure. (Kevlar 119, 29 and 129 receive no separate heat treatment.) The heat treatment on the Kevlar 149 fibers is severe enough to eliminate the pleated sheet structure, but all of the fibers show the fibrillar microstructure, irrespective of heat treatment.

Figure 1.3A. SEM micrograph of typical Kevlar 149 fiber showing axial splitting. Microfibrils connect the fiber across the split.

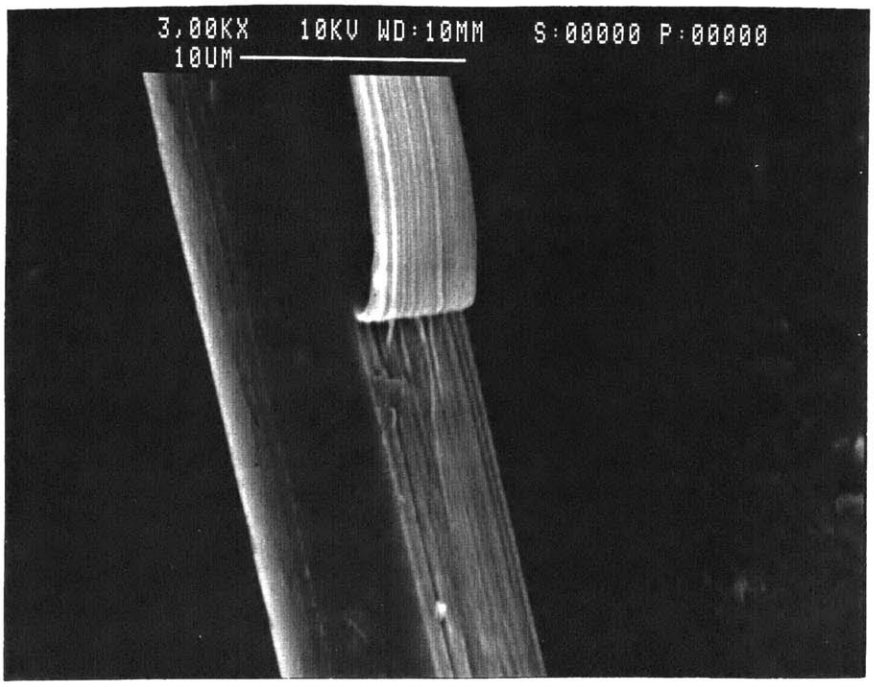

Figure 1.3B. SEM micrograph of Kevlar 49 fiber. Skin is peeled back to show fibrillar microstructure.

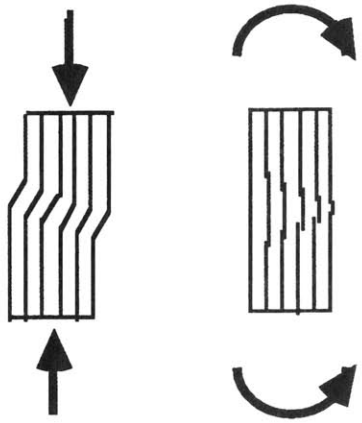

1.4A 1.4B

Figure 1.4. Schematic of kink formation in rigid- rod fibers. Arrows represent applied forces. Figures are not to scale. A) Compression B) Bending.

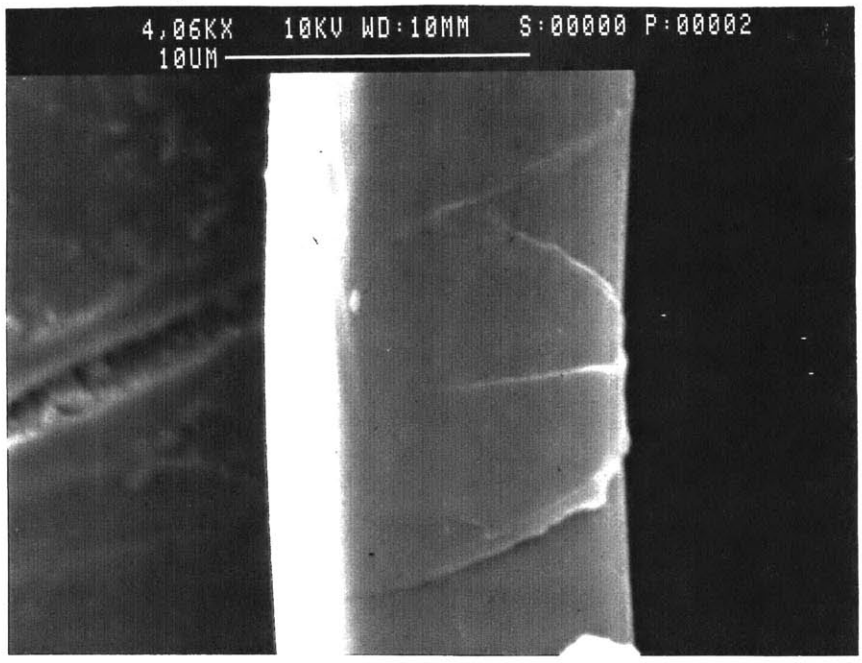

Figure 1.5. SEM Micrograph of kink band region in Kevlar 129.

1.2. Carbon Fibers

A flow chart describing carbon fiber processing is shown in Figure 1.6[3]. The first several steps are precursor- dependent. A two- dimensional structure develops during the

stabilization phase, then non- carbon atoms are removed during carbonization. Graphitization, in which crystallite size is increased and orientation is improved, is necessary to develop high modulus.

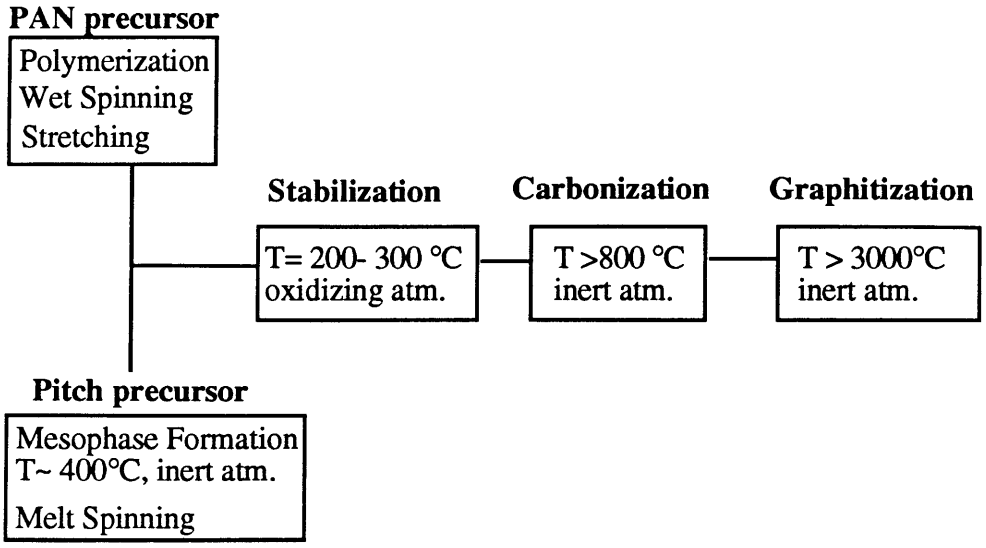

Figure 1.6. Carbon fiber processing. Figure after S. Lin.

1.2.1 PAN- based

Hercules provided PAN- based AS4, IM7, IM8 and HMS4 carbon fibers. These have circular cross-sections which permits the analysis of test results. Other PAN- based fibers and rayon based fibers have kidney-shaped or crenulated cross-sections, which make tit impossible to analyze the results of the bending stiffness test.

The precursor of PAN- based carbon fiber is poly(acrylonitrile), usually randomly copolymerized with small amounts of methyl acrylate and vinyl acetate, shown in Figure 1.7. The fiber is made in a process similar to that outlined in Figure 1.6. As the polymer chain is heated, cyclization occurs. The ladder formation is not confined to a single plane, since the polymer twists and coils, nor is the ladder formation within a single chain, since side groups from other chains may be more accessible. The result is an interwoven net of turbostratic graphite crystallites, shown schematically in Figure 1.8A. Some non- carbon atoms are retained, disrupting lateral order, but the interweaving helps maintain lateral integrity under compression.

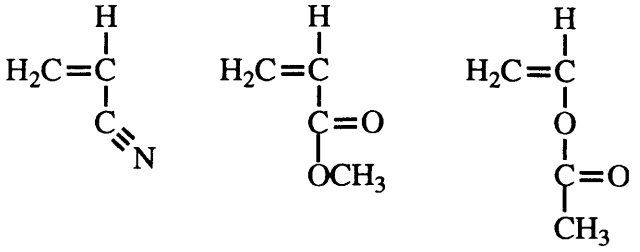

acrylonitrile methyl acrylate vinyl acetate

Figure 1.7. Monomers used in precursor copolymer for poly(acrylonitrile)- based carbon fibers.

PAN- based fibers fractured in tension or in flexure have a transverse morphology which resembles concrete, or particles in a matrix.[4] A schematic of the fiber cross section is shown in Figure 1.8B. Based on TEM, Johnson and Dyson[5] suggest the matrix phase in PAN- based fibers is disordered. Similar to Kevlar fibrils, the crystallite-ribbon orientation with respect to the fiber axis increases with applied tension and decreases with applied compression, leading to a strain dependent modulus.

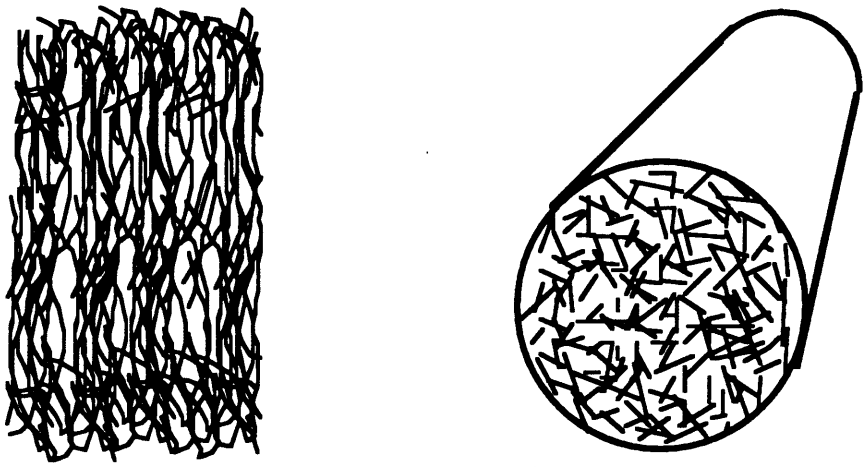

1.8A 1.8B

Figure 1.8A and B. Schematic of microstructure of PAN-based carbon fibers. A) ribbon- network along fiber axis B) transverse isotropic cross section.

1.2.2 Pitch- based

The pitch- based Thornel P25 HT, P55s and P75 carbon fibers were provided by Amoco. The P25 HT tow has a permanent twist so single fibers extracted from the tow are

wavy. Short straight sections were selected for the bending test. P55s has a sizing which makes single fiber separation from the tow easier compared to the other fibers.

Vezie and Adams[4] describe the folded sheet- like structure of the pitch- based fibers (Figure 1.9). The precursor of this fiber type is the asphaltene fraction of coal- tar pitch, which contains high-molecular-weight molecules, generally in the form of plates of rings containing carbon, nitrogen and sulfur. The fraction forms a liquid crystalline phase in the melt and is processed as described in Figure 1.6. The plate- like molecules join and form turbostratic graphite sheets aligned with the fiber axis. WAXS studies have been used to confirm three dimensional order in P75 and P100,[6] which have the most developed sheet structure. The lower modulus P25 and P55 do not have such order, but the sheets are well developed. The fracture surfaces of pitch- based fibers show a skin of radially oriented sheets around a randomly oriented core but Figure 1.10, which is an SEM micrograph of a P25 fiber fracture along the axis, shows only the sheet like structure and does not discriminate between the core and skin. The intersheet- spacing and relative size of the core depend on the processing parameters and directly influence the mechanical properties. Vezie[7] has shown that the higher modulus fibers have more distinct and faceted sheets with a smaller core region. The sheet structure provides an easy direction for crack propagation across the fiber, so the pitch- based fibers tend to have lower tensile and compressive strengths than the PAN- based fibers, but higher tensile modulii. The nonlinear tensile stress strain behavior of the pitch based fibers is much greater than the PAN- based ones: the sheets orient and the fibers become stiffer.

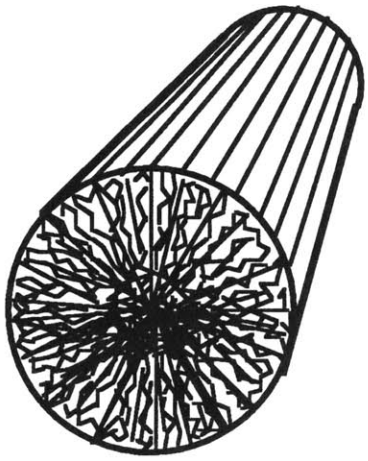

Figure 1.9. Schematic of microstructure of pitch- based carbon fibers in cross section: graphitic sheets arrange radially and fold in a core region. Sheets fold back at fiber surface giving characteristic ridged appearance.

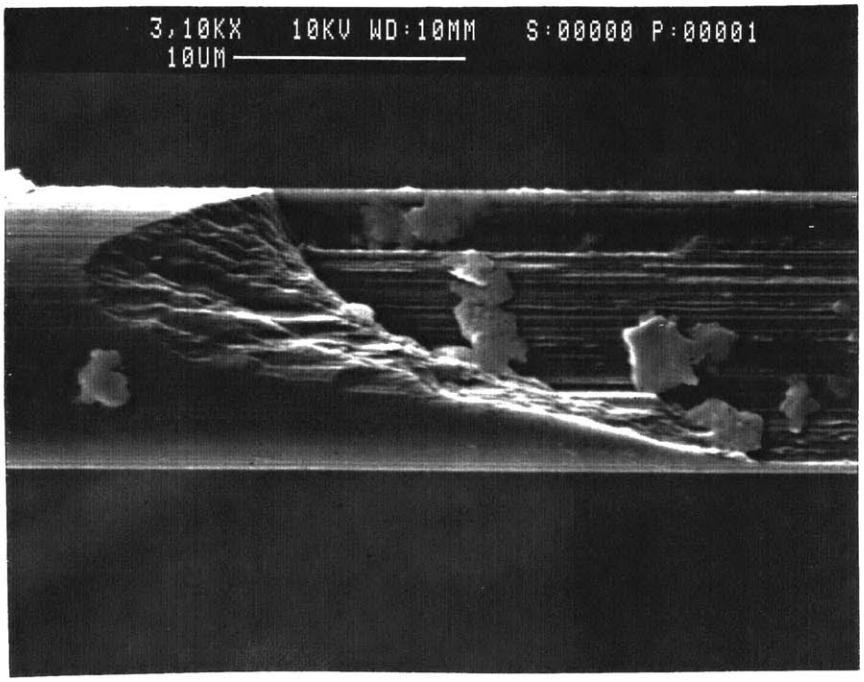

Figure 1.10. SEM of P25 fiber, showing sheet structure in fracture surface.

1.3. Elasticity of Composites

A difference between tensile and compressive properties in uniaxial composites has been observed in both Kevlar- and carbon- reinforced plastics (KRP and CRP), but not in glass- reinforced plastics (GRP). Harper and Heumann[8] proposed a difference in carbon fiber compressive and tensile modulus after comparing GRP, CRP and hybrid G/CRP mechanical behavior. The CRP modulus increases with tensile strain, decreases with compressive strain, and is continuous through the origin. The modulus of GRP is independent of strain and the hybrid follows a rule of mixtures. Crasto and Kim[9] showed that the compression- softening and tension- stiffening are reversible in carbon fiber composites and can be seen at low strains, suggesting that they are the result of fiber properties, not fiber placement. Kumar, Adams and Helminiak[10] report the compressive modulus of CRP as 84-100% of the tensile modulus. In Lubin's Handbook of Composites[11], PAN- based HMS/ epoxy composites exhibit an compressive modulus which is only 52% of the tensile modulus. The ratio of compressive to tensile modulii is 0.95 for AS/ epoxy and 1.0 for GY-70/ epoxy, indicating that not all carbon fibers exhibit this kind of anisotropy.

Greenwood and Rose[12] noted that KRPs yield at compressive stresses lower than those required for matrix yield and concluded that fiber failure was responsible. Fisher and Marom[13] tested Kevlar 49 composites in flexure and found a slightly lower compressive than tensile modulus. Kumar and Helminiak[14] cite duPont literature which gives compressive modulii of Kevlar 29, 49 and 149 fibers as approximately 80, 90 and 60% of the corresponding tensile modulii, based on composite testing. Piggott and Harris[15] found the tensile and compressive modulii of GRP to be equal, but for CRP the compressive modulus was 76-84% of the rule-of-mixtures value calculated using the tensile modulus and for KRP it was 55% of the rule-of-mixtures value. Compressive strengths lower than the tensile ones were measured for Kevlar- and carbon- fiber composites. In compression,

failure occurs while the matrix is still elastic, suggesting that the fibers are the limiting element.

The ICAN code[16] for predicting composite properties, like many such codes, recognizes that there may be a difference in tensile and compressive strengths, but it ignores any modulus difference and any strain dependent modulus changes. Despite the code, the lower compressive modulus and strength of Kevlar and other rigid- rod fibers is recognized, and it is a limiting factor in the use of these fibers in composites. On the other hand, carbon fibers are attributed different tensile and compressive strengths, but only one modulus. Mrse and Piggott[17] postulated a single fiber modulus and tried to show that the nonlinear stress- strain relationship and the lower observed compressive modulus for AS-4 fibers in CRP was a result of fiber waviness. Swift's analysis[18] applied to a similar system showed that while waviness did contribute, it could not account completely for the observed behavior. Theoretical modeling of pitch-based fibers by Klunziger *et al.*[19] showed that nonlinear stress- strain behavior arises principally from crystallite orientation effects but that bond stretching may also contribute.

1.4. Elasticity of Fibers

1.4.1 Carbon Fibers

As early as 1968, Curtis, Milne and Reynolds reported a strain dependence in the tensile modulus of PAN- based carbon fibers measured by ultrasonic methods,[20] while Gill,[21] in a general text published in 1972, described carbon fibers as perfectly linear and elastic. However, the strain- dependence has become more frequently recognized. For example, Hughes[22] criticized the carbon fiber manufacturers for not including strain-dependent tensile modulus data in their publications. SACMA,[23] the Suppliers of Advanced Composite Materials Association, addressed the issue in its 1990 recommendation for standardized test methods. It recommends the impregnated tow test and reporting the secant modulus, where the secant defining endpoints vary and depend

upon the modulus and the strain to failure of the fiber. The increase in modulus with strain is described by Equation 1.1, where E_0 is the modulus at zero strain, ε_1 and ε_2 are the strain measurement endpoints and F is the measured nonlinearity factor. The SACMA standard gives E_0 and F as 228 GPa and 1.97 GPa for standard fibers such as AS-4, 290 GPa and 2.34 GPa for intermediate modulus fibers such as IM-7 and IM-8 and 345 GPa and 3.10 GPa for high modulus fibers such as HMS-4.

$$E = E_0 + F(\varepsilon_1 + \varepsilon_2) \tag{1.1}$$

To describe fiber behavior, Hughes uses Equation 1.2, where f is the nonlinearity factor: the change in modulus per percent increase in strain. The nonlinearity factor varies from 16- 17% both for high strength and high strain fibers, to 25-30% for high modulus fibers. SACMA's nonlinearity constants correspond to nonlinearity factors, f, of approximately 16- 18%.

$$E = E_0(1 + f\varepsilon) \tag{1.2}$$

The non- Hookean behavior is more pronounced in the pitch-based fibers than the PAN based fibers, and this has been attributed to the differences in microstructure. Crasto and Kim[9] measured tensile stress strain curves for P25, P55 and P75 as well as glass and AS4 fibers. The tangent modulus equation, from the slope of the stress-strain curve, is in the form of Equation 1.2. The nonlinearity factor, f, for glass is 0% and for AS4 is 18.5%. For P25, P55 and P75 they are 52%, 91% and 88% respectively.

WAXS shows that the tensile modulus of carbon fibers measured by sonic means is a function of orientation, ease of basal plane shear and basal dislocations.[24] Curtis *et al.*[20] proposed that the very sharp early increase in sonic tensile modulus is a result of dislocation motion to the crystallite boundaries, while the more gradual increase is due to orientation of the ribbon network which is reminiscent of the PAN precursor structure. In pitch- based fibers, the weaker interactions between graphite basal planes allow sheet sliding to increase alignment with the applied stress. Nonlinearity is more severe in the

lower modulus pitch fibers, which have less initial orientation. Kumar and Helminiak attribute the higher compressive strengths of PAN- based fibers relative to pitch based fibers to residual nitrogen, which disrupts the development of three dimensional order.[14]

1.4.2 Kevlar Fibers

Changes in the modulus of Kevlar aramid fibers with applied strain have also been measured. Kawabata reports two regions of approximately constant tensile modulus for Kevlar 49 and 29, and three tensile modulus regions for Kevlar 149.[25] The increase with applied tensile strain is attributed to the opening of the pleated sheet structure in Figure 1.2A. Allen and Roche[26] report two regions of approximately constant modulus in Kevlar 49 and 29 and a more continuous change in the modulus of Kevlar 149. The pleated sheet structure is absent in Kevlar 149, so the increase in orientation is on a smaller structural scale. In both papers, the first constant-modulus range for Kevlar 29 and 49 extends to approximately 1% strain.

1.5. Tensile Property Measurement Techniques

Both the ASTM race track method[27] for single fibers and the impregnated tow method recommended by SACMA are widely used to measure static tensile properties. Because strain is inferred from crosshead displacement in the ASTM method, machine compliance must be measured to correct the collected data. The impregnated tow method has the advantage of being able to support an extensometer or strain gage, while single fibers cannot, but the mechanical contribution of the matrix is ignored. Dynamic tensile modulus[28] is measured with ultrasonic pulses. The resonant frequency of longitudinal vibrations in a fiber is directly related to the modulus of the fiber.

The challenge in tensile testing is not the execution of the test, but the data analysis. If the stress- strain behavior is linear, Hooke's law operates. The modulus is single valued and equal to the slope of the stress- strain curve. However, the modulus of high

performance fibers frequently is a function of applied strain. The modulus can be calculated from the linear regression fit of the early part of the curve, from the secant between two strains, or from the tangent at a specific point along the curve. Manufacturers' data typically cite one or two modulus values and how they were obtained, but this is not detailed enough for a complete prediction of behavior.

1.6. Fiber Anisotropy

In general, single fiber tests show low compressive strengths. Schoppee and Skelton[29] compared loop efficiencies, defined as the ratio of the failure tensile strain in a fiber wrapped around a mandrel to the failure tensile strain of the fiber in pure tension, of many filaments. The efficiency should decrease from one to zero as the bending strain in the fiber increases. The efficiencies of glass and high-modulus carbon fibers decrease as expected, but the efficiencies of standard carbon fibers are high for no apparent reason, while the efficiencies of polyester, stainless steel and Kevlar 49 are high due to yielding. Jones and Johnson[30] suggested the nonlinear knot test results for carbon fibers were due to a high modulus core and a low modulus skin, however, since the skin is more oriented from processing, this is unlikely.

Macturk *et al.*[31] directly compressed single P75 carbon fibers and found the compressive modulus to be 90% of the tensile modulus. Measured compressive strengths from this test compare well with values from tensile recoil testing for P55, P75 and P100, but recoil results for carbon fibers are lower than the compressive strengths measured from composites, probably because of bending in the recoil test.[32] Fawaz *et al.*,[33] used the opto- mechanical Tecam Micro- tensile Machine (MTM), their own design, in which fiber displacement is measured by realigning the support-anvil image after an applied moment causes anvil translation. By this method, the measured compressive modulii of Kevlar 29 and 49 fibers are 79% and 90% of the tensile modulii.

Carbon fibers are perfectly elastic in compression and tension, but show a nonlinear stress- strain curve. Kevlar fibers have a linear stress strain curve at low strains but deviation occurs in tension at higher strain and in compression when kink bands form. Large scale kink band formation, which defines compressive failure and the ultimate compressive strength, occurs at much lower stresses than the ultimate tensile strength. The kinked region acts as a plastic hinge, lowering the effective modulus measured in compression or in flexure.

1.7. Compressive Property Measurement Techniques

1.7.1 Composite stress- strain tests:

Composite testing in compression and flexure requires many fibers but does provide a stress- strain curve. Problems with composite testing include fracturing composites within the gage length and not at the grips,[34] off- axis loading, and the effect of different fixtures.[35] For uniaxial tests, fiber and matrix contributions can be separated according to the rule of mixtures, assuming perfect interfacial adhesion and fiber alignment, and the absence of matrix- specific interactions. Single fiber composites[36] and embedded bundles[37] have been used to eliminate the need for large amounts of fiber but suffer from many of the same problems.

1.7.2 Single fiber compressive strain tests:

The elastica loop or knot test was developed by Sinclair[38] to measure the tensile strength of isotropic glass fibers with very short gage lengths, but is now used to measure the compressive failure strain of oriented fibers. The failure strain is calculated from the loop radius of curvature and the fiber diameter. The ratio of the major to minor axes of the loop should remain constant as the loop size decreases until failure occurs.

Support- beam tests use a fiber affixed to the surface of a beam of GRP or an isotropic plastic. The beam is subjected to a moment in three or four point bending[39] or as

a cantilever. The beam depth is much larger than the fiber diameter, so the strain at the beam surface is the strain in the fiber. Shifts in a Raman spectrum peak along fibers on the face of a cantilever beam have been used to measure the failure strain of Kevlar fibers and estimate the compressive modulus.[40] Strain softening is observed, but there is significant scatter in the data.

The piezoresistive method[41] requires a conductive fiber attached to the side of a block of isotropic plastic. The fiber resistivity is recorded as the block is compressed. When the fiber fails, the resistivity becomes infinite, so the method does not require visual identification of failure. DeTeresa has shown that PAN- based AS-4 and IM-7 fail at larger compressive strains than those achievable in composite testing. He concluded that these fibers do not limit the performance of such composites in compression.

1.7.3 Single fiber compressive strength tests:

Carbon fibers show a distribution of tensile strengths and Miwa *et al.*[42] assumed that the shape of the strength distribution is the same in compression as in tension. After determining the tensile strength distribution, isotropic beams with single fiber embedded near the surface were subjected to four point bending. The single fiber, near either the tensile or the compressive face of the beam exhibits multiple breaks. The fragments from bending failure show a distribution of lengths. Comparison of the fragment lengths from compression to those from tension permits an estimate of the ratio of compressive and tensile strengths. The length comparison gives the shift applied to the same distribution curve.

Tensile recoil[43] is an iterative method for establishing the stress range in which compressive failure occurs. A fiber is held at a fixed tensile load, and then carefully cut in half. The released tensile stress wave is reflected from the grip and returns along the fiber as a compressive wave. If the magnitude of the wave exceeds the compressive strength of the fiber, failure occurs. The test is repeated until the range between failure and no failure is sufficiently narrow to report compressive strength. Eccentricity in the load induces

bending failure, leading to lower values of the compressive strength as measured in composite tests. The method has been modified from the original form to include strand recoil[44] and recoil of greased fibers,[45] as well as improved methods of cutting.[46]

1.7.4 Single fiber stress- strain tests:

Macturk's direct compression method for very short fibers has a low success rate. Fiber alignment is difficult and test length restrictions compete: the fiber must be short enough to avoid buckling yet long enough to avoid gripping effects at the ends, which persist over longer lengths than in isotropic materials.[47] Fiber length is also an issue with the MTM used by Fawaz *et al.*; both compressive and tensile modulii varied with gage length when measured with this device.

Freeston and Schoppee[48] developed a test for measuring the bending moment as a function of imposed curvature for a cantilevered fiber. The compressive modulus is calculated from the known tensile modulus and the measured bending modulus. The test is sound, but the analysis may faulty: the neutral axis shift factor is 20-30% lower than the actual value, which depends upon the ratio of the compressive to the tensile modulii.

1.7.5 Single Fiber bend tests:

Dmitruk *et al.*[49] used a simple single- fiber four- point- bend test to measure the tensile strength of sapphire fibers, which are difficult to grip for conventional tensile tests. Flexural tests are a simple way to measure tensile modulus and strength because sapphire fibers, similar to glass, have a single modulus and strength. Moalli and McGarry[50] used single- fiber three- point bending to measure the compressive modulus of oriented polymeric fibers from the bending stiffness and tensile modulus. Strengths are not measured because failure is obscured by the loading point. This last method was the basis for the Micro- Flex single fiber bending test.

1.8. Conclusion

With the exception of Macturk and Fawaz, the tests mentioned above measure either compressive strain or stress at failure, but not both. Frequently, the compressive modulus is assumed to be the same as the tensile modulus so the ultimate compressive strength can be calculated from the failure strain by Hooke's law. Different test methods give very different results. Table 1.1 contains the compressive strength of Kevlar 49 measured in five ways, as reported by Allen and Farris[51] in the US and Kozey and Berlin[44] in the former Soviet Union. One significant cause of the difference between the measured strengths is the use of the tensile modulus to calculate stress from strain in most analyses, and the neglect of the resulting neutral axis shift in bending tests.

Table 1.1 Compressive failure strength of Kevlar 49 fibers. (GPa)

Author \ method	loop	cantilever	recoil	strand recoil	composite
Allen and Farris	740	620	365		400
Kozey and Berlin	510- 850		384	420	405

The microstructure of high-performance fibers is responsible for the observed nonlinear and anisotropic mechanical behavior. Since fiber properties change with magnitude and direction of the applied stress, precise quantification of the tensile, bending and compressive properties and their dependence on strain are necessary. The FITT and Micro-Flex tests described in Chapters 2 and 3 offer an efficient, reliable means of measuring the mechanical properties of single fibers.

2. Tensile Modulus Measurements with the Fiber Incremental Tensile Tester

2.1. Test

The Fiber Incremental Tensile Test (FITT) was developed to measure the tensile modulus of a single fiber without the need for system compliance corrections required by ASTM D3379. A fiber loop is placed around rigid posts in the FITT fixtures. One fixture is attached to a stationary block and the other to a highly polished rod which slides in a nitrogen gas bushing. The core of a linear variable differential transducer (LVDT) is attached to the free face of the sliding fixture and measures displacement. Weights are added incrementally to a basket connected over a pulley to the sliding rod and the loop extension is measured. Measurement of the initial length and the fiber diameter allow the calculation of stress, strain and the tangent modulus.

2.1.1. Equipment

Platform

The basic platform, described earlier by Moalli and McGarry,[50] is an aluminum table, measuring 24" x 6" x 5" with solid side legs. (Figure 2.1) The 4" x 2" section in the front center of the table top is cut out for the work area. At one end, a foot is attached to the side leg. An inch- long thumbscrew fits in a threaded hole in the foot. By turning the screw, the height of one end of the platform can be raised or lowered to balance the fixture on the sliding rod in a neutral starting position. The height difference between the two ends is typically 0.25- 0.375 inches.

Attached to the top of the platform are two blocks holding Dover Air Lube bushings, models LB-2 and LB-5. The bushing nearer the work area is one inch long and has a 0.25" inside diameter for the sliding rod. The other, at the platform end, a bushing with 0.50" inside diameter, is oriented such that the spindle which fits inside is

perpendicular to the sliding rod and functions as a pulley. Nitrogen gas at 20 psi activates the bushing, reducing friction between the rod or spindle and the sleeve to a negligible level: after initial finger twirling, the pulley will rotate for 60 minutes.

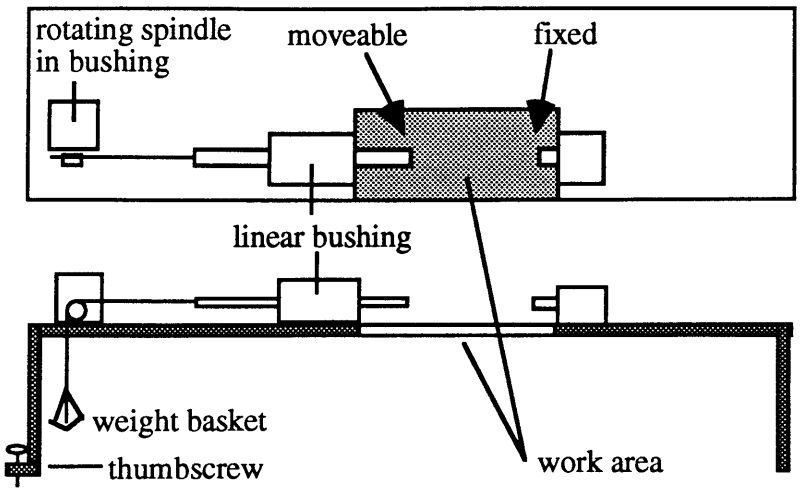

Figure 2.1. Top and side views of basic platform. Fixed rod is on right, moveable on left. Fixtures are attached to rod ends. Resting position of sliding rod is determined by thumbscrew height adjustment..

Both the rod and the spindle are made of stainless steel which has been polished in a lathe with metallography paper up to 1200 grit. The spindle diameter is 0.5" and is capped on the back so it does not slide through the bushing. A circumfrential groove 0.125" from the front end guides the cable. The sliding rod is made of 0.25" diameter stainless steel. Test- specific fixtures are attached to the end in the work area. A wire hook is adhered to the other end of the rod. A cable of PBO fibers is tied to the hook, fed over the rotating spindle and down through a hole in the platform. The other end is tied to a small hook which holds the weight basket.

The weight basket is a rectangular piece of heavy cardboard, approximately 1.25" long and 0.75" wide, supported at the corners by wires which join at a center knot where the hook is attached. By adjusting the platform end-height with the thumbscrew, the weight of the basket is balanced against the weight of the fixtures. Both should be as

light as possible, or the platform adjustment will be too large to ignore the effect of the vertical force component due to gravity.

FITT fixtures

The FITT fixtures, shown in Figure 2.2A and 2.2B, consist of blocks and the screws. The aluminum blocks are attached to the fixed and moveable rods with set screws on the top and bottom. The blocks are 0.25" square and approximately 0.75" long. Each block has a centered slot, 0.25" high and 0.50" deep, where the fiber loop fits. The moveable block has been further machined to remove excess weight, so the corners are rounded, and the piece is shorter than the fixed block. Steel hex screws with smooth necks and a 0.188" diameter are used to transfer the load to the fiber loop. The screws fit vertically in the blocks and are supported above and below the centerline. Only the smooth neck is visible in the centered slot. The screw for the moveable block has been cut short to reduce weight and the bottom hole in the block is threaded so no nut is needed. The screw for the fixed block is the original 1.25" length and is secured with a nut. The top hole in the fixed block is slightly elongated to ease screw removal after testing, when that screw has a spot of adhesive where the loop is attached.

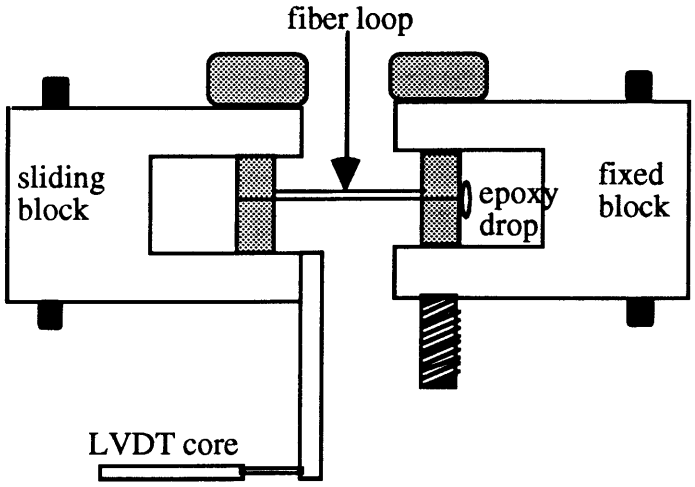

Figure 2.2A. FITT fixtures, side view. Fiber loops around smooth neck of screws. Fixtures attach to fixed and moveable rods via set screws indicated in black. LVDT core hangs from free face of block on sliding rod. Figure is not to scale.

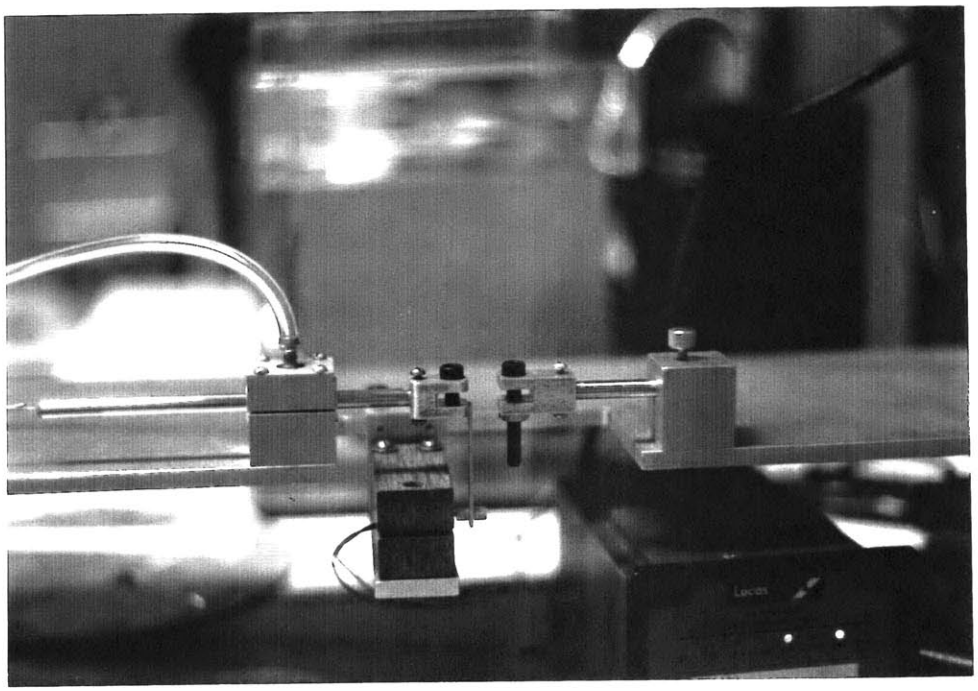

Figure 2.2B. Photograph of FITT fixtures before a test. Left block slides, right block is fixed. The LVDT cylinder is in the holder below the work area.

Measuring System

A strip of aluminum, 0.125" wide and 1.50" long is attached by a screw to the inside, bottom face of the moveable block. The core for the Lucas Schaevitz MHR-100 LVDT is aligned with the rod and is attached by a 1-72 stainless steel screw to the aluminum strip. The LVDT cylinder is held in a support block and is suspended below the test area so the core slides in the cylinder without touching the sides (Figure 2.2B).

The full scale displacement of the LVDT is ±0.100 inches. Its output is calibrated with the MP-1000 controller readout by inserting a brass shim, measured in the SEM to be 0.0450 inch thick, between the blocks and entering the distance traveled into the MP-1000 memory. The system is operated at 10 kHz, with 3 Vrms excitation voltage and 1.2 Vrms full scale sensitivity (low gain).

Sample Preparation Tubes

The tubes used for making fiber loops are cardboard, approximately 1.75" in diameter, which have been cut into one inch lengths and wrapped with 2 strips of colored labeling tape. Purple tape is used for glass and Kevlar fiber preparation; yellow for carbon fibers. The colors are chosen to contrast with the fiber color. The tubes are cut along the axis, wrapped to a smaller diameter and held with a paper clip until the ends remain overlapped when the clip is removed. The outside flap is capped with wax paper during sample preparation to protect the fiber and to ease removal of the epoxy drop. (Figure 2.3)

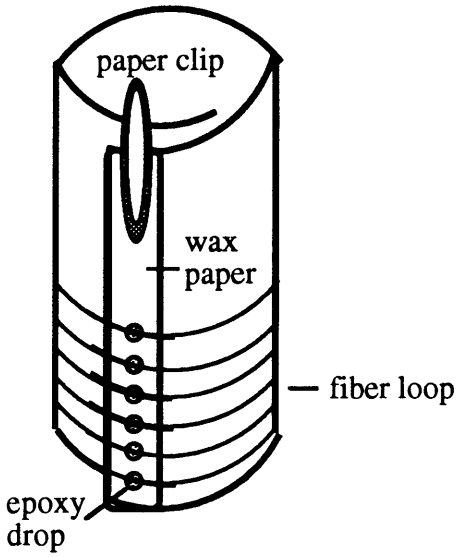

Figure 2.3. Cardboard sample preparation tube for single fiber loops. Four to six loops can be made on each tube.

2.1.2. Sample Preparation

Several single fibers 5-7 inches long are removed from the tow and placed on smooth colored paper. Kevlar fibers are handled with No. 5 tweezers and visually checked for fraying, excessive waviness or kinked regions. Carbon fibers are handled by fingertip, since tweezers fracture them.

The tube is end-capped with the wax paper sleeve and held with a paper clip. Epoxi-Patch clear adhesive (Dexter Adhesives and Structural Materials Division, Seabrook, NH) is mixed and a drop approximately 0.05" in diameter is placed on the wax paper. The end section of a fiber is held against the tube with a finger while the rest of the fiber is wrapped around the tube so the fiber passes through the drop twice. The loop is not necessarily tight against the tube because the epoxy should not be drawn onto the fiber outside the drop location. Also, tension increases the probability of fiber damage during preparation. A toothpick with more epoxy on the end is used to press the fibers through the drop to the tube surface. The process is repeated until the lower section of the tube is wrapped with fibers, spaced approximately 0.15" apart. The tube is left for at least 24 hours at room temperature while the epoxy cures.

The outer surface of a 10 μm fiber undergoes approximately 0.1% strain when held against the FITT screws. Combined with the epoxy drop size relative to the screw curvature, the strain is enough to break the pitch- based fibers against the screw posts. Thus, the above process is slightly modified for the pitch-based carbon fibers. A second paper clip is put on the tube before end-capping with the wax- paper sleeve so the arm of the clip causes a ridge under the paper. In this configuration, the epoxy drops tend to be smaller and the fibers enter the epoxy at a sharper angle, reducing the frequency of premature breaks.

When the epoxy is dry, the loop is removed from the tube. The tube sides are held while the paper clip is removed, then the tube is tightened to reduce the diameter. The clip is replaced to maintain the smaller size while the wax-paper sleeve is removed from the tube end. The loops are free of the tube and move with the wax paper. The strip, with attached loops, is placed on smooth paper for individual loop removal. For more fragile fibers such as the pitch- based carbon, the wax paper cap is kept on the shrunken tube for loop removal.

The tip of Aesculap BD 330 tweezers is worked under the epoxy drop to pop the drop free of the wax paper. The 330's are not as fine as No. 5 tweezers and do not pierce the paper as easily. Usually the wax provides a weak interface and easy separation, but, if the epoxy bonds to the paper, the drop is difficult to remove, and the fiber usually breaks at the edge of the drop during removal. The success rate for removal of carbon fiber loops is approximately 50%.

Once a single loop is free, it is held by the epoxy drop and moved to the testing area. The end away from the drop is inserted in the moveable fixture and the screw tightened. Keeping plenty of slack in the loop, the drop end is inserted in the fixed block, the screw inserted and the nut tightened. The fixtures are moved into the starting position, so the LVDT core is within its range and there is little slack in the loop. Then the platform is balanced: the sliding rod moves away from the fixed end, bringing the loop against the screws when the gas bushings are activated.

The height of the ends and the alignment of the arms of the loop are checked visually and corrected if necessary. Then 910 cyanoacrylate adhesive (Permabond International, Englewood, NJ) is dropped over the epoxy on the fixed end screw. A weight of 0.5-2.0 grams is placed in the weight basket while the 910 dries, keeping the epoxy drop against the screw, and centering the other loop end so both sections of the fiber experience equal loads.

2.1.3. Test Procedure

The fixed block rod is moved to locate the LVDT core to a position where the controller readout is in the range of -0.08000 to -0.09900 inches. This initial position leaves most of the full 0.2 inch range available for the test. With the nitrogen flowing to the linear bushing but not to the pulley, the end of the pulley spindle is manually rotated to extend the loop. When the resisting force of the loop is greater than the frictional force

between the cable and the spindle, the fiber will not extend further. This becomes the zero position for testing.

After zeroing, the gas is turned on in both bushings. Usually the zeroed readout is usually -0.00010 to -0.00080 inches, depending on the fibers ability to maintain an undeformed loop shape. One to two gram weights are added to the basket and the resulting extension recorded to the nearest 0.01 mil. The fiber is loaded, unloaded, and reloaded at least once. The test ends when the fiber breaks or when the strain has exceeded 1.0%.

The tested fiber is removed from the FITT fixtures with tweezers and placed in a sample box on smooth paper for storage until Micro-Flex testing. Then the distance between the screw heads when the LVDT is at the zero position for the test is measured with a Mitutoyo digital micrometer; this avoids loop breakage if the micrometer slips.

2.1.4. Analysis

In a test the fiber extension is measured as a function of the load on two parallel lengths of the fiber. The fixtures insure the load has no off-axis component. The analysis assumes the fiber strains uniformly. The diameters of the FITT samples (which have been subsequently Micro-Flex tested) are measured in the SEM at 10 keV acceleration voltage and a 10 mm working distance. Magnification ranges from 2000x-5000x, depending on the fiber size. The fiber is viewed along the length and the diameter measured at 5-15 equally spaced locations, or approximately every 100-200μm. The average diameter is used to calculate the tensile stress: force divided by original cross-sectional area.

The contribution of screw bending to the measured extension is on the order of 10^{-9} inches, which is not measurable with this system. Strain in the fiber in contact with the screw at either end is assumed to be negligible. Calculation of the actual rate of decay of strain around the screw depends on the assumption of a coefficient of friction, and is

not performed. The loop arm length, or center-to-center distance between screws is used to calculate the strain: change in length normalized by original length.

The stress-strain data are plotted using Cricket Graph software for the Macintosh. Linear regression accurately describes the load- extension behavior of the glass fiber and Kevlar 119 and 49 fibers. Second-order polynomial regressions are needed to fit the data from the other fibers. The first derivative of the data expression, m_t, is converted to modulus, E_t, according to Equation 2.1, where L_O is the gage or loop arm length, r is the average fiber radius, and X is a units conversion factor. The factor of two in the denominator arises because the load is shared between the two arms.

$$E_t = \frac{\sigma}{\varepsilon} = X\frac{m_t L_0}{2\pi r^2} \tag{2.1}$$

2.2. Results

The measured tensile modulii for all fibers are listed in tables in each fiber section. The tables list sample, fiber diameter, FITT slope and gage length. The tensile modulus is calculated using Equation. 2.1 and is reported in both GPa and Msi. The modulus is strain-dependent to some degree in all of the fibers except glass, Kevlar 119 and Kevlar 49. The tables have columns headed B and C for the coefficients in the force-displacement equation used to represent the data, Equation 2.2, where (2P) is the applied load and ΔL is the loop arm extension. The slope used to calculate the tangent modulus at a specific strain is the first derivative of this, given in Equation 2.3. The extension and corresponding strain at which the modulus is calculated are listed where appropriate. The average and standard deviation of the measured modulii are at the bottom of each table.

$$(2P) = A + B(\Delta L) + C(\Delta L)^2 \tag{2.2}$$

$$m_t = B + 2C(\Delta L) \tag{2.3}$$

Appendix B contains graphs of the FITT data. Fiber type, gage length and average diameter are listed in the upper corner of each graph. The letters "L" and "U" in the legends represent loading and unloading, respectively.

2.2.1. Glass Fibers

The average tensile modulus of glass fiber measured by the Fiber Increment Tensile Tester is 76.5 GPa (11.1 Msi) with a standard deviation of 5.1%. The results are listed in Table 2.1. Figure 2.4 is a representative graph of the tensile stress-strain behavior of glass fibers, showing a linear elastic response to loading.

Table 2.1. Glass Fiber FITT results.

sample	diameter (μm)	m_t (g/ mil)	Lo (in)	**Et** (GPa)	**Et** (Msi)
6/2.1T	15.50	1.6775	1.6670	72.7	10.5
	15.60	1.6775	1.6670	71.7	10.4
	15.40	1.6775	1.6670	73.6	10.7
	15.40	1.6775	1.6670	73.6	10.7
	15.70	1.6775	1.6670	70.8	10.3
6/2.2T	18.10	2.3095	1.6275	71.6	10.4
6/7.2T	15.60	1.9799	1.5195	77.2	11.2
	15.60	1.9799	1.5195	77.2	11.2
	15.60	1.9799	1.5195	77.2	11.2
	15.60	1.9799	1.5195	77.2	11.2
6/7.3T	16.10	2.1900	1.5355	81.0	11.7
	16.10	2.1900	1.5355	81.0	11.7
6/15.1T	15.20	2.0044	1.5055	81.5	11.8
	15.30	2.0044	1.5055	80.5	11.7
	15.30	2.0044	1.5055	80.5	11.7
			average:	**76.5**	**11.1**
			std. dev:	3.9	0.6

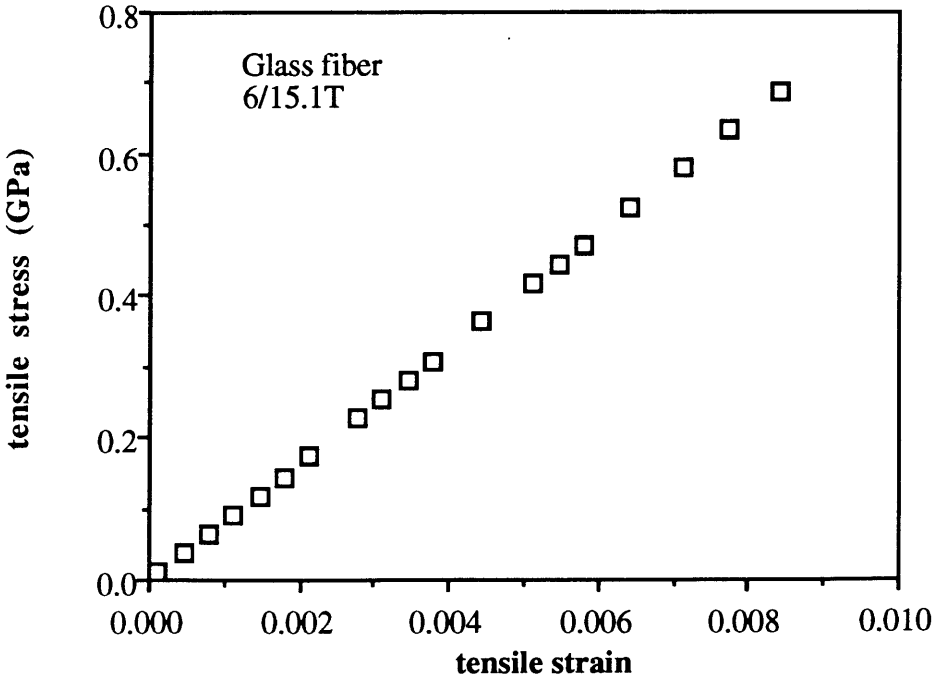

Figure 2.4. Tensile stress- strain behavior of a typical glass fiber, sample 6/15.1T.

2.2.2. Kevlar Fibers

The extension of all Kevlar fibers except Kevlar 149 increases with time, so the extension was recorded 20 seconds after each loading, which took about 10 seconds; thus the extension was measured every 30 seconds. This timing was selected to match the deformation rate in the Micro- Flex bending test. Upward curvature in Kevlar 29, 129 and 149 fibers is evident in the second and subsequent load-unload cycles but during the first cycle either the curvature is absent or slightly downward. The data are fit with Equation 2.2 and then Equation 2.3 is used to calculate the tangent modulus at a specified strain. (The stress- strain behaviors of Kevlar 119 and Kevlar 49 fibers are better described by linear regression: C = 0 in Equation 2.2.)

Kevlar 119 has the lowest tensile modulus of the Kevlar series: the reported value is 62 -69 GPa (9-10 Msi).[52] The average of six samples measured in the FITT mode was 71.9 GPa (10.4 Msi) with a standard deviation of 3.6%. Results are listed in Table 2.2 and Figure 2.5 shows a typical tensile stress-strain curve.

The tensile modulus of Kevlar 29 fiber is reported by Kawabata as 80.0 GPa (11.6 Msi)[25] and in the Kevlar technical guide as 83 GPa (12.0 Msi)[53]. The average of twelve samples measured in the FITT mode was 78.3 GPa (11.4 Msi) with a standard deviation of 5.0% at 0.15% strain and 80.0 GPa (11.6 Msi) with a standard deviation of 5.3% at 0.3% strain. The results at 0.3% strain are given in Table 2.3. The strain-dependent behavior of a typical Kevlar 29 fiber in tension is shown in Figure 2.6.

The tensile modulus of Kevlar 129 is reported as approximately 96.5 GPa (14 Msi)[52]. The average of six samples measured in the FITT mode was 96.4 GPa (14.0 Msi) with a standard deviation of 6.8% at 0.15% strain. It increases to 98.7 GPa (14.3 Msi) with a standard deviation of 6.5% at 0.3% strain. The test results at 0.3% strain are given in Table 2.4. The stress-strain behavior of a typical Kevlar 129 fiber is shown in Figure 2.7.

Kevlar 49 is the most widely studied Kevlar fiber. Kawabata reports a tensile modulus of 113 GPa (16.4 Msi)[25] while the Kevlar technical guide suggests 24 GPa (18 Msi).[53] The stress- strain behavior is linear. The average of 11 samples measured in the FITT mode was 128.5 GPa (18.6 Msi) with standard deviation of 5.6%. The results are given in Table 2.5, and a typical stress-strain curve is shown in Figure 2.8.

Kevlar 149 has the highest tensile modulus of the Kevlar series, reported by both Kawabata[25] and duPont[53] as 179 GPa (26 Msi). Kawabata reports an increase in modulus to 209 GPa (30.3 Msi) above approximately 0.8% strain. The average of eight samples measured in the FITT mode was 162.4 GPa (23.6 Msi) with a standard deviation of 2.1% at 0.15% strain. At 0.3% strain, the average was 171.4 GPa (24.9 Msi) with a standard deviation of 1.8%. These results are presented in Table 2.6. The modulus continues to increase with strain. At 0.9% strain, the average tensile modulus was 207.5 GPa (30.1 Msi) with a standard deviation of 1.4%. Figure 2.9 shows the strain-dependent tensile behavior of a typical Kevlar 149 fiber.

Table 2.2. Kevlar 119 FITT results: response is linear.

sample	diameter (μm)	mt (g/mil)	Lo (in)	**Et (GPa)**	**Et (Msi)**
6/12.5T	10.7	0.8240	1.6870	75.8	11.0
2L	11.2	0.8240	1.6870	69.2	10.0
	11.1	0.8240	1.6870	70.4	10.2
	10.9	0.8240	1.6870	73.0	10.6
6/12.6T	10.8	0.7987	1.7205	73.6	10.7
1.5L	11.1	0.7987	1.7205	69.6	10.1
			average	**71.9**	**10.4**
			std. dev	2.6	0.4

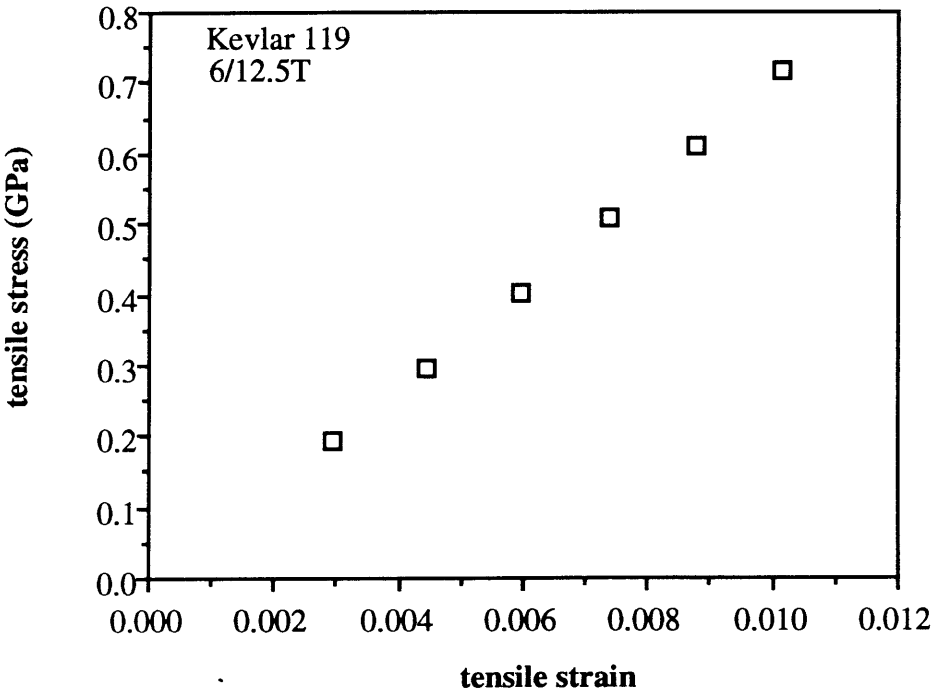

Figure 2.5 Typical stress- strain behavior of Kevlar 119 fiber tested in tension.

Table 2.3. Kevlar 29 FITT results at 0.3% strain.

sample	diameter (μm)	mt (g/mil)	B	C	Lo (in)	ΔL (mil)	strain	**Et (GPa)**	**Et (Msi)**
6/7.5T	12.2	0.9838	0.9599	2.13e-3	1.8720	5.60	0.30%	77.2	11.2
3L	12.1	0.9838	0.9599	2.13e-3	1.8720	5.60	0.30%	78.5	11.4
	11.4	0.9838	0.9599	2.13e-3	1.8720	5.60	0.30%	88.5	12.8
	12.1	0.9838	0.9599	2.13e-3	1.8720	5.60	0.30%	78.5	11.4
6/11.1T	12.3	1.1350	1.0456	8.94e-3	1.6570	5.00	0.30%	77.6	11.3
2L	11.8	1.1350	1.0456	8.94e-3	1.6570	5.00	0.30%	84.3	12.2
	11.7	1.1350	1.0456	8.94e-3	1.6570	5.00	0.30%	85.8	12.4
6/11.3T	11.7	1.0004	0.9705	2.99e-3	1.6560	5.00	0.30%	75.6	11.0
2L	11.5	1.0004	0.9705	2.99e-3	1.6560	5.00	0.30%	78.2	11.3
	11.8	1.0004	0.9705	2.99e-3	1.6560	5.00	0.30%	74.3	10.8
6/12.1T	11.9	1.0971	1.0484	4.87e-3	1.6580	5.00	0.30%	80.2	11.6
2L	11.8	1.0971	1.0484	4.87e-3	1.6580	5.00	0.30%	81.6	11.8
							average	**80.0**	**11.6**
							std dev	4.3	0.6

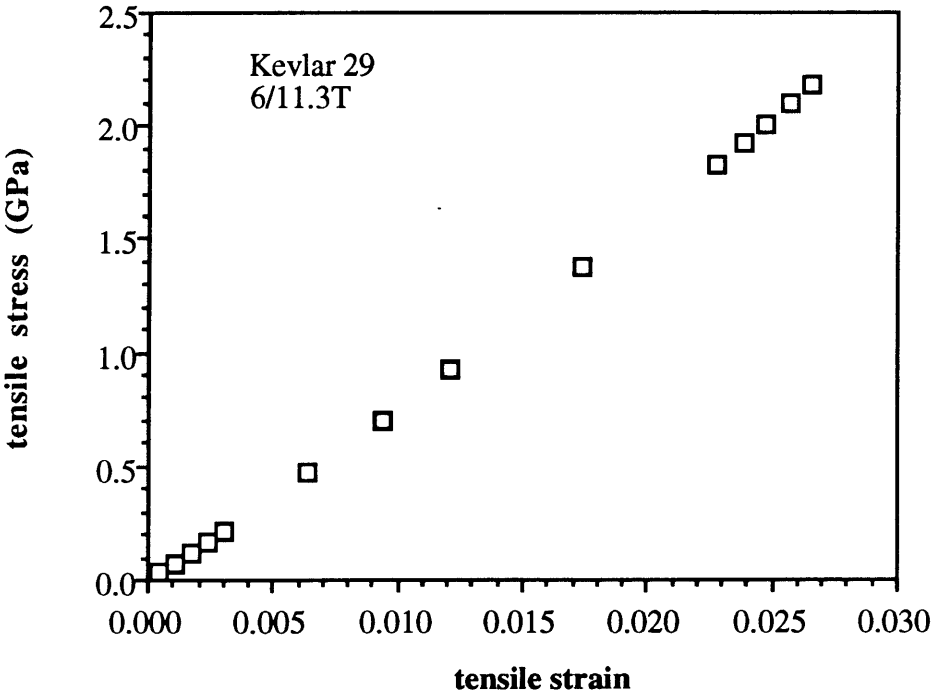

Figure 2.6. Typical stress- strain curve for Kevlar 29 fiber in tension. Upward curvature indicates the modulus is increasing with strain.

Table 2.4. FITT results at 0.3% strain for Kevlar 129 fibers.

sample	diameter (μm)	mt (g/mil)	B	C	Lo (in)	ΔL (mil)	strain	**Et (GPa)**	**Et (Msi)**
6/12.3T	11.5	1.1298	1.072	5.28e-3	1.8420	5.50	0.30%	98.2	14.2
2L	12.0	1.1298	1.072	5.28e-3	1.8420	5.50	0.30%	90.2	13.1
	11.7	1.1298	1.072	5.28e-3	1.8420	5.50	0.30%	94.9	13.8
	11.6	1.1298	1.072	5.28e-3	1.8420	5.50	0.30%	96.6	14.0
6/12.4T	11.8	1.4092	1.354	5.52e-3	1.6945	5.00	0.30%	107.1	15.5
2L	11.9	1.4092	1.354	5.52e-3	1.6945	5.00	0.30%	105.3	15.3
							average	**98.7**	**14.3**
							std dev	6.4	0.9

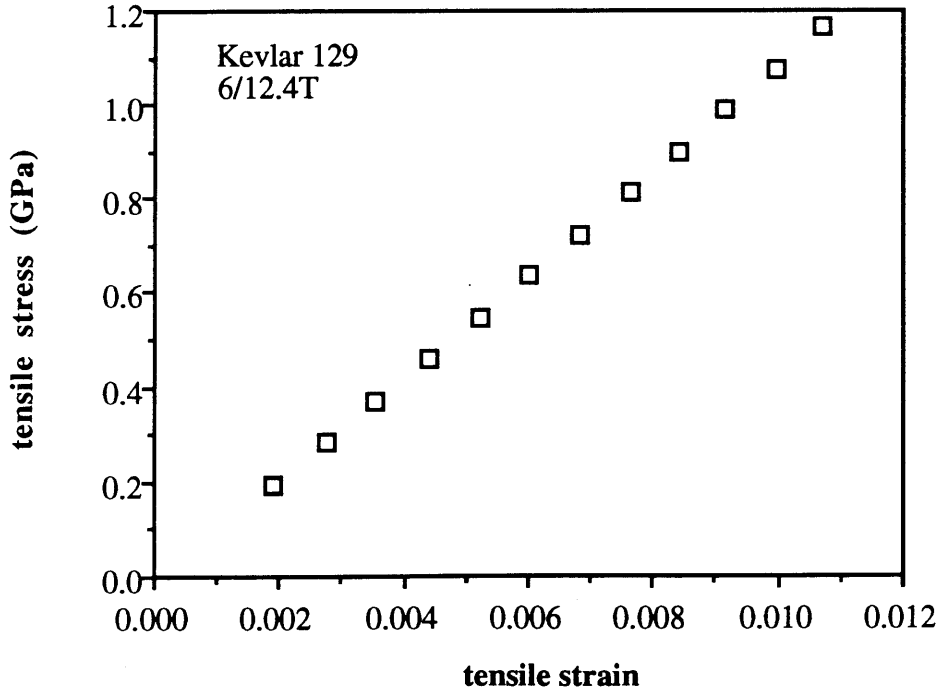

Figure 2.7. Stress- strain curve of a typical Kevlar 129 fiber in tension.

Table 2.5. FITT results for Kevlar 49 fibers. Loop 6/17.1T was two fibers which appeared as one during sample preparation.

sample	diameter (μm)	mt (g/mil)	Lo (in)	**Et (GPa)**	**Et (Msi)**
6/15.4	11.3	1.7267	1.4700	124.1	18.00
6/17.1T	11.5	3.6524	1.4455	124.6	18.07
2L	11.8	3.6524	1.4455	118.4	17.17
	11.9	3.6524	1.4455	116.4	16.88
	11.4	3.6524	1.4455	126.8	18.39
6/20.1T	11.1	1.7853	1.4855	134.4	19.49
1L	10.8	1.7853	1.4855	141.9	20.59
	11.2	1.7853	1.4855	132.0	19.14
6/20.2T	11.9	1.9599	1.5170	131.1	19.01
2L	11.8	1.9599	1.5170	133.3	19.33
	11.9	1.9599	1.5170	131.1	19.01
			average	**128.5**	**18.6**
			std. dev.	7.4	1.1

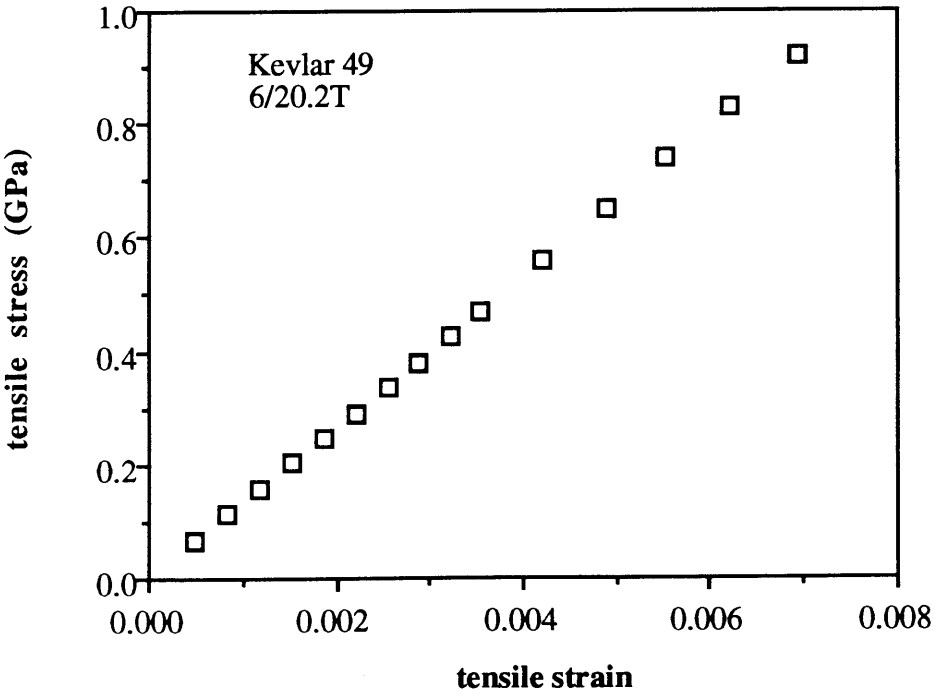

Figure 2.8. Linear stress- strain response of Kevlar 49 in tension.

Table 2.6. FITT results for Kevlar 149 fibers at 0.3% strain.

sample	diameter (μm)	mt (g/mil)	B	C	Lo (in)	ΔL (mil)	strain	**Et (GPa)**	**Et (Msi)**
6/15.2T	10.6	1.7584	1.587	1.60e-2	1.7945	5.38	0.300%	175.3	25.43
1L	10.7	1.7584	1.587	1.60e-2	1.7945	5.38	0.300%	172.1	24.96
	10.6	1.7584	1.587	1.60e-2	1.7945	5.38	0.300%	175.3	25.43
6/15.3T	11.5	1.9783	1.771	1.92e-2	1.8030	5.40	0.300%	168.4	24.42
2L	11.4	1.9783	1.771	1.92e-2	1.8030	5.40	0.300%	171.3	24.85
6/17.2T	10.9	1.7921	1.588	1.89e-2	1.8005	5.40	0.300%	169.5	24.59
1L	10.8	1.7921	1.588	1.89e-2	1.8005	5.40	0.300%	172.7	25.05
	11.0	1.7921	1.588	1.89e-2	1.8005	5.40	0.300%	166.5	24.15
							average	**171.4**	**24.9**
							std dev	3.2	0.5

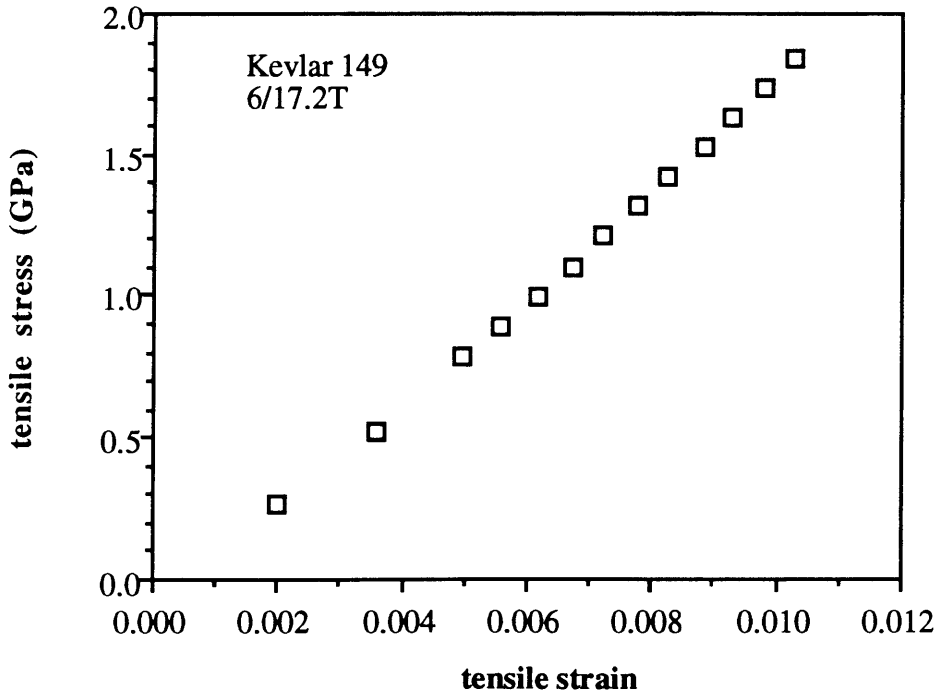

Figure 2.9. Nonlinear stress-strain response of typical Kevlar 149 fiber.

2.2.3. Carbon Fibers

Similar to the glass fibers, both the pitch- based and the PAN- based carbon fibers do not exhibit time dependence in the extension under load so the "10 seconds to load/ 20 seconds before recording" schedule was not necessary. However, the carbon fibers do exhibit distinctly nonlinear elasticity, the modulus increasing with strain. Hercules, the manufacturer of the PAN-based fibers used in this study, reports the tensile modulus at 0.4% strain and at half of the tensile breaking load.[54] These differ by as much as 7.6% for AS4 fibers. In the case of high modulus HMS4, half of the breaking load actually corresponds to approximately 0.4% strain, so the difference is only 0.7%. Amoco, the manufacturer of the pitch- based fibers used in this study, reports "typical fiber properties," without any indication of method of measurement or any reference to nonlinearity in the stress-strain response[55].

PAN- based

The standard PAN fiber is AS4, with a 0.4% strain modulus of 226 GPa (32.8 Msi) and a half of breaking load modulus of 243 GPa (35.3 Msi). Ten samples were used in the FITT mode to measure the tensile modulus. At 0.15% strain, the average was 248.6 GPa (36.1 Msi) with a standard deviation of 2.8%. At 0.4% strain, the average was 260.6 GPa (37.8 Msi) with a standard deviation of 2.6%. These results are listed in Table 2.7. Figure 2.10 shows the tensile stress-strain behavior of a typical AS4 fiber.

The intermediate modulus IM7 fibers have a modulus of 269 GPa (39.0 Msi) at 0.4% strain and 289 GPa (41.9 Msi) at half the breaking load. The average of six samples measured by FITT was 283.1 GPa (41.1 Msi) with a standard deviation of 7.6% at 0.15% strain and 299.9 GPa (43.5 Msi) with a standard deviation of 6.9% at 0.4% strain. The results at 0.4% strain are given in Table 2.8, and a typical stress- strain curve is shown in Figure 2.11.

The reported tensile modulus of IM8 fibers is 309 GPa (44.8 Msi) at 0.4% strain and 328 GPa (47.6 Msi) at half the breaking load. The average of five samples measured with FITT was 326.8 GPa (47.4 Msi) with a standard deviation of 4.6% at 0.15% strain. This increased to 346.8 GPa (50.3 Msi) with a standard deviation of 4.2% at 0.4% strain, as seen in Table 2.9. An IM8 tensile stress-strain curve is shown in Figure 2.12.

The highest modulus PAN-based fiber is HMS4. The reported modulii at 0.4% strain and at half of the breaking load are 368 GPa (53.4 Msi) and 366 GPa (53.0 Msi) respectively. The average of seven samples measured with FITT was 337.6 GPa (49.0 Msi) with a standard deviation of 2.5% at 0.15% strain, and 375.2 GPa (54.4 Msi) with a standard deviation of 3.1% at 0.4% strain. The results at 0.4% strain are given in Table 2.10, and a typical stress-strain curve is shown in Figure 2.13.

Table 2.7. FITT results for AS4 fibers at 0.4% strain

sample	diameter (μm)	mt (g/mil)	B	C	Lo (in)	ΔL (mil)	strain	**Et (GPa)**	**Et (Msi)**
6/21.1T	6.20	0.9304	0.872	4.23e-3	1.7240	6.90	0.40%	260.5	37.8
	6.20	0.9304	0.872	4.23e-3	1.7240	6.90	0.40%	260.5	37.8
	6.24	0.9304	0.872	4.23e-3	1.7240	6.90	0.40%	257.2	37.3
	6.04	0.9304	0.872	4.23e-3	1.7240	6.90	0.40%	274.5	39.8
6/21.2T	6.31	0.9439	0.852	6.68e-3	1.7075	6.90	0.40%	252.7	36.7
	6.19	0.9439	0.852	6.68e-3	1.7075	6.90	0.40%	262.6	38.1
	6.12	0.9439	0.852	6.68e-3	1.7075	6.90	0.40%	268.6	39.0
6/21.3T	6.53	1.0431	0.980	4.63e-3	1.6990	6.80	0.40%	259.5	37.6
	6.63	1.0431	0.980	4.63e-3	1.6990	6.80	0.40%	251.7	36.5
	6.54	1.0431	0.980	4.63e-3	1.6990	6.80	0.40%	258.7	37.5
							average	**260.6**	**37.8**
							std dev	6.8	1.0

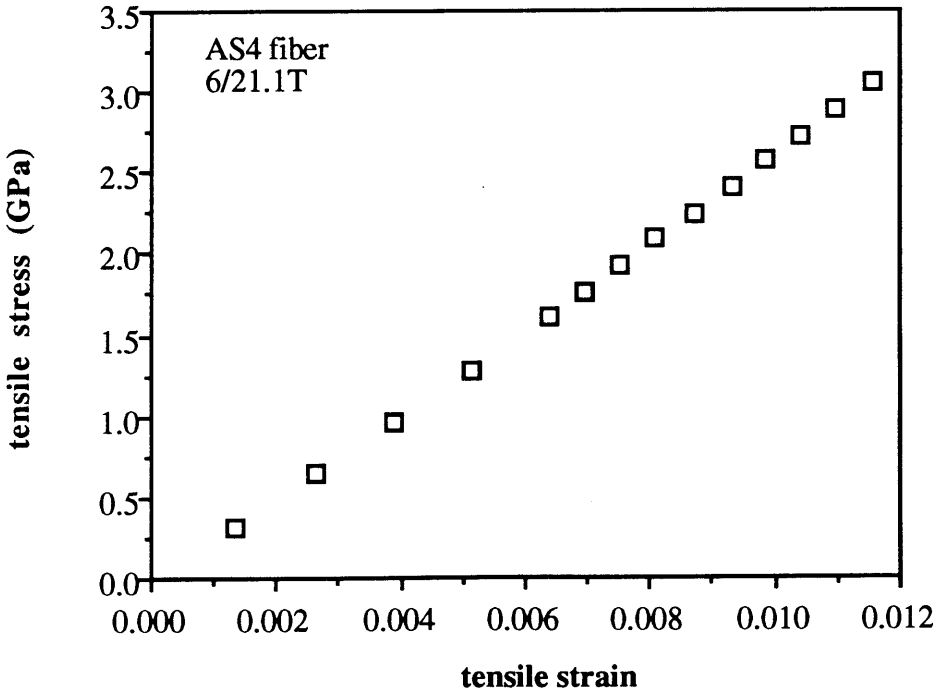

Figure 2.10. Tensile stress-strain behavior for a typical AS4 fiber.

Table 2.8. FITT results for IM7 fibers at 0.4% strain.

sample	diameter (μm)	mt (g/mil)	B	C	Lo (in)	ΔL (mil)	strain	**Et (GPa)**	**Et (Msi)**
6/26.3T	4.65	0.6610	0.5949	5.60e-3	1.4650	5.90	0.40%	279.6	40.6
	4.63	0.6610	0.5949	5.60e-3	1.4650	5.90	0.40%	282.0	40.9
	4.63	0.6610	0.5949	5.60e-3	1.4650	5.90	0.40%	282.0	40.9
6/27.1T	5.13	0.7708	0.7098	4.42e-3	1.7155	6.90	0.40%	313.7	45.5
	5.06	0.7708	0.7098	4.42e-3	1.7155	6.90	0.40%	322.4	46.8
	5.08	0.7708	0.7098	4.42e-3	1.7155	6.90	0.40%	319.9	46.4
							average	**299.9**	**43.5**
							std dev	20.7	3.0

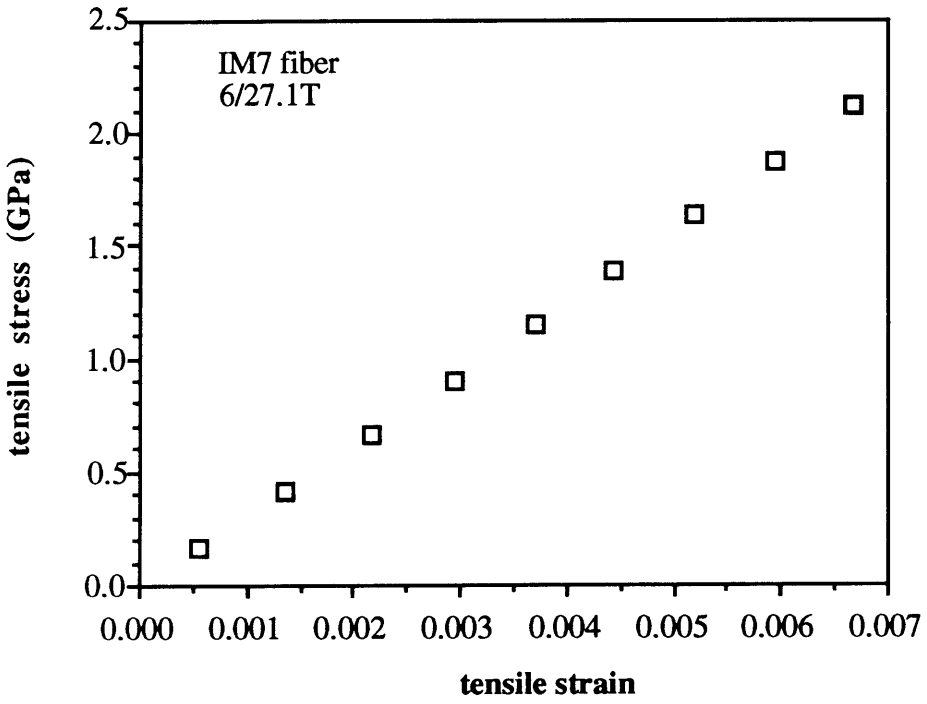

Figure 2.11. Tensile stress-strain behavior of a typical IM7 fiber.

Table 2.9. FITT results at 0.4% strain for IM8 fibers. Loop 6/26.2T was two fibers which appeared to be one during sample preparation.

sample	diameter (μm)	mt (g/mil)	B	C	Lo (in)	ΔL (mil)	strain	**Et (GPa)**	**Et (Msi)**
6/27.2T	4.80	1.2480	1.1237	7.97e-3	1.9320	7.80	0.40%	326.7	47.4
	4.71	1.2480	1.1237	7.97e-3	1.9320	7.80	0.40%	339.3	49.2
6/27.3T	4.90	0.7078	0.6462	3.95e-3	1.9260	7.80	0.40%	354.4	51.4
	4.83	0.7078	0.6462	3.95e-3	1.9260	7.80	0.40%	364.8	52.9
	4.94	0.7078	0.6462	3.95e-3	1.9260	7.80	0.40%	348.7	50.6
							average	**346.8**	**50.3**
							std dev	14.6	2.1

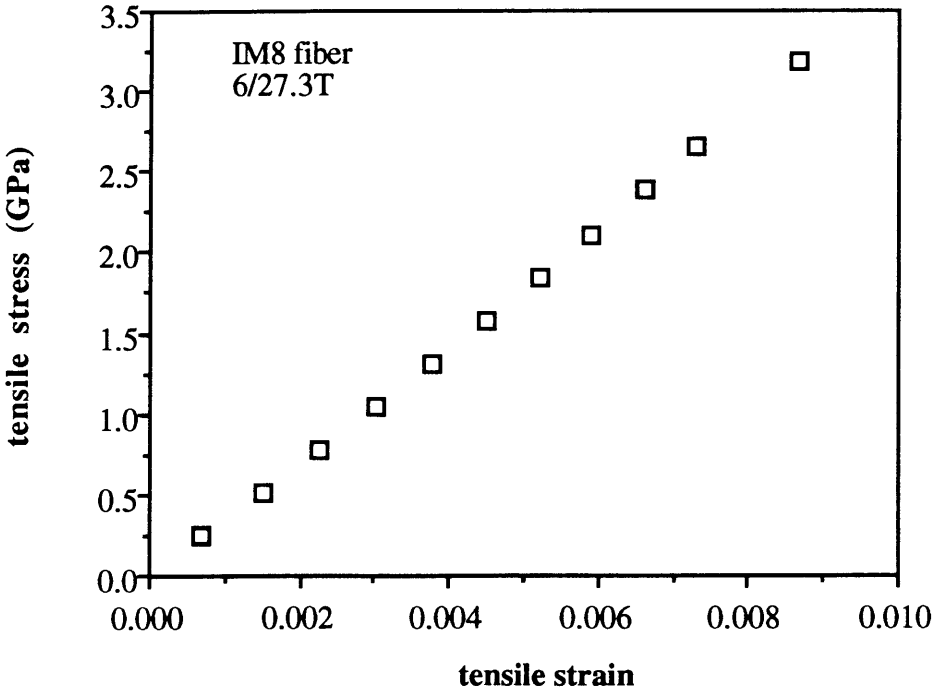

Figure 2.12. Measured tensile stress-strain behavior for an IM8 fiber.

Table 2.10. FITT results for HMS4 fibers at 0.4% strain.

sample	diameter (μm)	mt (g/mil)	B	C	Lo (in)	ΔL (mil)	strain	**Et (GPa)**	**Et (Msi)**
6/20.3T	6.97	2.1045	1.7505	3.16e-2	1.40	5.60	0.40%	378.6	54.9
	6.95	2.1045	1.7505	3.16e-2	1.40	5.60	0.40%	380.8	55.2
	6.87	2.1045	1.7505	3.16e-2	1.40	5.60	0.40%	389.7	56.5
	6.90	2.1045	1.7505	3.16e-2	1.40	5.60	0.40%	386.3	56.0
6/20.4T	7.14	2.1234	1.8061	2.83e-2	1.4130	5.60	0.40%	367.4	53.3
	7.16	2.1234	1.8061	2.83e-2	1.4130	5.60	0.40%	365.4	53.0
	7.23	2.1234	1.8061	2.83e-2	1.4130	5.60	0.40%	358.3	52.0
							average	**375.2**	**54.4**
							std dev	11.7	1.7

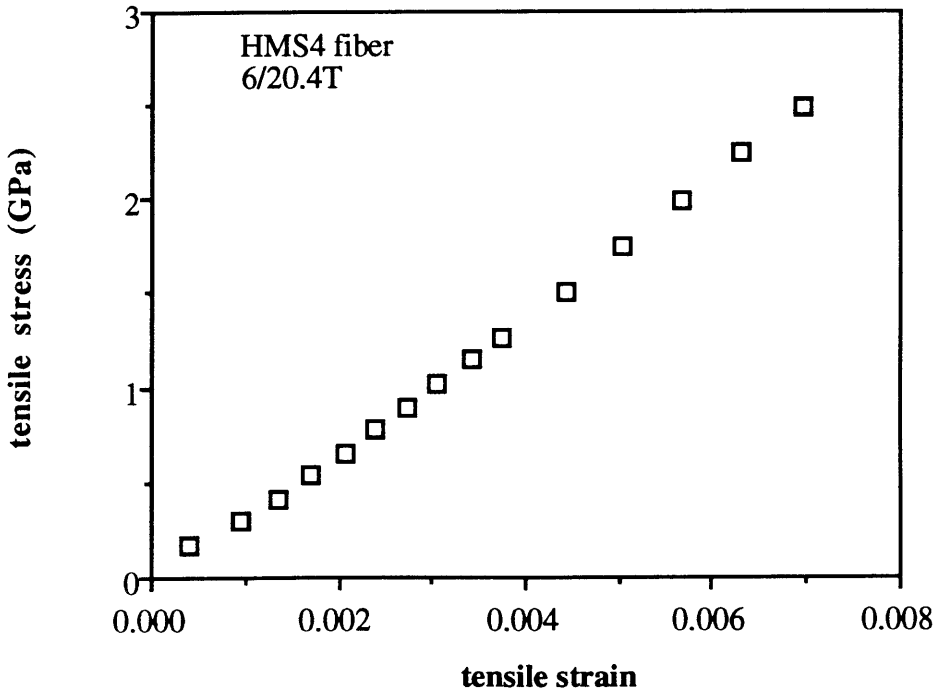

Figure 2.13. Tensile stress-strain curve for a typical HMS4 fiber.

Pitch- based

The pitch-based fibers have a more developed microstructure and were expected to show the most nonlinear behavior of all the fibers. Also, they are the most brittle and fail at the lowest strains: only the P25 fiber reached 1% strain before failure. P55 failed between 0.1% and 0.2% strain and P75 failed between 0.2% and 0.4% strain.

The reported tensile modulus of P25 is 160 GPa (23 Msi).[55] The average FITT results with nine samples was 117.3 GPa (17.0 Msi) with a standard deviation of 8.3% at 0.1% strain and 153.1 GPa (22.2 Msi) with a standard deviation of 10.7% at 1.0% strain. Curvature was most pronounced a strains less that 0.6%. Above 0.6%, the slopes from a linear fit gave an average modulus of 145.3 GPa (21.1 Msi) with a standard deviation of 8.4%. In fact, the difference between 145 and 153 GPa may not be significant, recognizing the standard deviations present. The results at 0.1 % strain are given in Table 2.11. Typical P25 fiber stress-strain behavior is shown in Figure 2.14.

The reported tensile modulus of P55 fiber is 380 GPa (55 Msi).[55] The average of seven samples in the FITT test was 442.6 GPa (64.2 Msi) with a standard deviation of 7.6% at 0.05% strain and 468.3 GPa (67.9 Msi) with a standard deviation of 8.7% at 0.1% strain. Results at 0.1% strain are given in Table 2.12 and typical stress-strain behavior is shown in Figure 2.15.

The reported tensile modulus of P75 fiber is 520 GPa (75 Msi).[55] The average of ten samples in the FITT mode was 498.2 GPa (72.3 Msi) with a standard deviation of 3.2% at 0.1% strain and 545.7 GPa (79.1 Msi) with a standard deviation of 4.5% at 0.2% strain. Results at 0.1 % strain are given in Table 2.13 and typical stress-strain behavior is shown in Figure 2.16.

Table 2.11. FITT results from P25 fiber at 0.1% strain.

sample	diameter (μm)	mt (g/mil)	B	C	Lo (in)	**Et (GPa)**	**Et (Msi)**
6/21.4	10.40	1.1692	1.1046	1.8356e-2	1.7645	119.1	17.3
	11.10	1.1692	1.1046	1.8356e-2	1.7645	104.5	15.2
	10.70	1.1692	1.1046	1.8356e-2	1.7645	112.5	16.3
7/15.1T	10.58	1.1575	1.1314	7.8959e-3	1.6575	107.0	15.5
	10.60	1.1575	1.1314	7.8959e-3	1.6575	106.6	15.5
	9.77	1.1575	1.1314	7.8959e-3	1.6575	125.5	18.2
7/15.2T	10.20	1.3065	1.2739	9.9305e-3	1.6380	128.4	18.6
	10.40	1.3065	1.2739	9.9305e-3	1.6380	123.5	17.9
	10.20	1.3065	1.2739	9.9305e-3	1.6380	128.4	18.6
					average:	**117.3**	**17.0**
					std. dev:	9.8	1.4

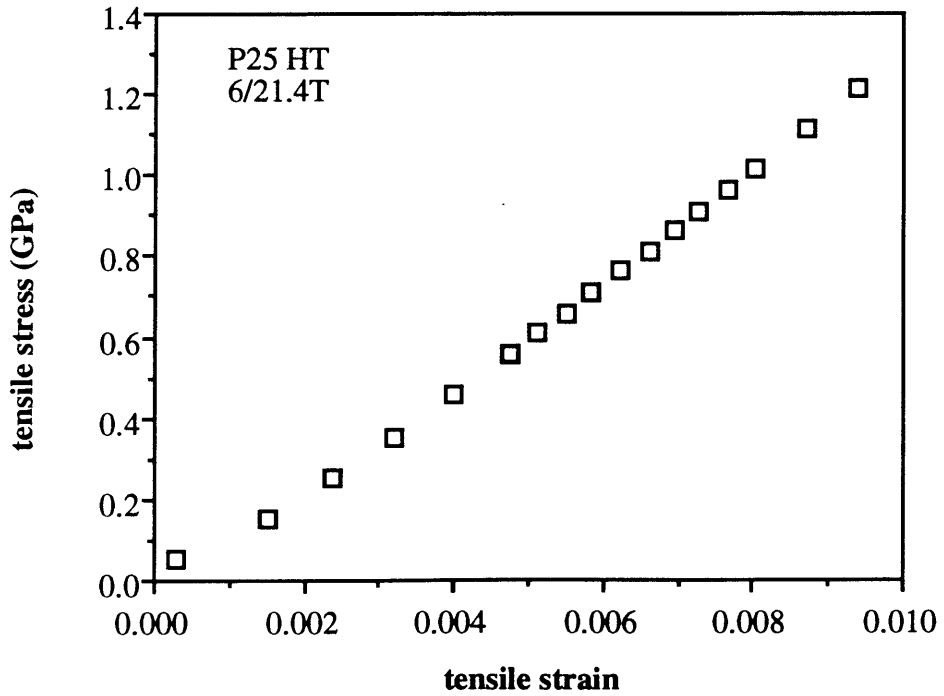

Figure 2.14. Slope of tensile stress- strain curve for P25 fiber increases noticeably in the first 0.6% strain. Stress-strain behavior is more linear at higher strains.

Table 2.12. FITT results fro P55 fiber at 0.1% strain

sample	diameter (μm)	mT (g/mil)	B	C	Lo (in)	**Et (GPa)**	**Et (Msi)**
7/20.1T	9.79	4.7840	4.2439	1.7424e-1	1.5470	482.1	69.9
	9.68	4.7840	4.2439	1.7424e-1	1.5470	493.1	71.5
7/21.1T	9.24	4.3776	3.7779	1.8860e-1	1.5915	509.5	73.9
	9.19	4.3776	3.7779	1.8860e-1	1.5915	515.0	74.7
7/21.2T	9.00	3.4135	3.1164	9.2831e-2	1.5995	420.8	61.0
	8.87	3.4135	3.1164	9.2831e-2	1.5995	433.2	62.8
	8.96	3.4135	3.1164	9.2831e-2	1.5995	424.6	61.6
					average:	**468.3**	**67.9**
					std. dev:	41.0	5.9

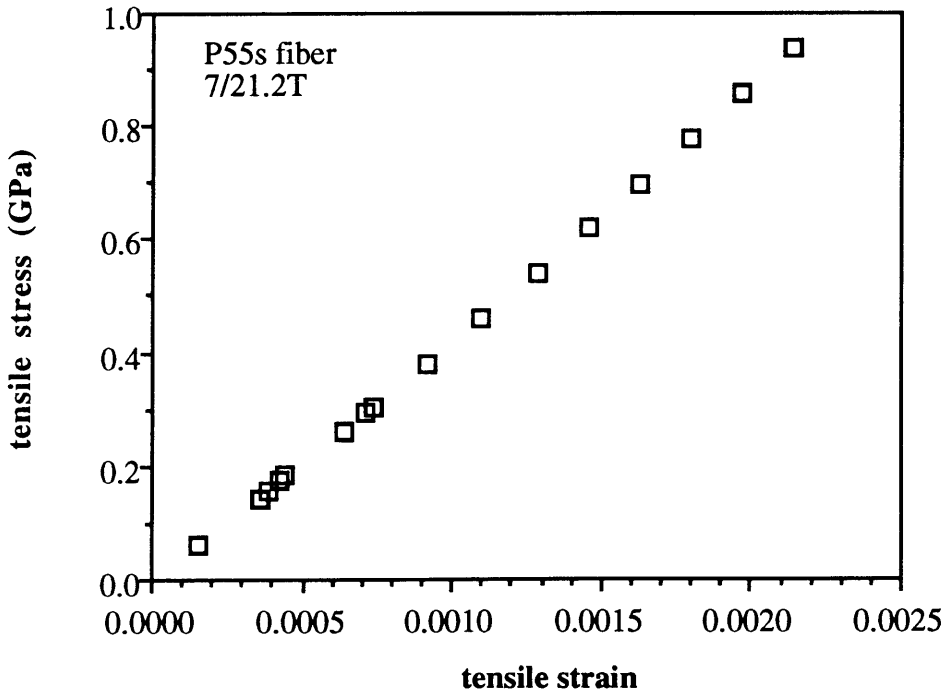

Figure 2.15. Typical stress- strain curve of P55 fiber under tension. Fiber failure occurred at approxmately 50% of typical tensile strength.

Table 2.13. FITT results for P75 fibers at 0.1% strain.

sample	diameter (μm)	mt (g/mil)	B	C	Lo (in)	**Et (GPa)**	**Et (Msi)**
7/14.5T	10.60	5.0648	4.4306	1.8987e-1	1.6710	470.2	68.2
	10.40	5.0648	4.4306	1.8987e-1	1.6710	488.5	70.9
	10.40	5.0648	4.4306	1.8987e-1	1.6710	488.5	70.9
	10.40	5.0648	4.4306	1.8987e-1	1.6710	488.5	70.9
	10.10	5.0648	4.4306	1.8987e-1	1.6710	518.0	75.1
	10.00	5.0648	4.4306	1.8987e-1	1.6710	528.4	76.6
7/17.1	9.06	4.1028	3.7919	9.7769e-2	1.5900	496.2	72.0
	9.11	4.1028	3.7919	9.7769e-2	1.5900	490.7	71.2
	8.96	4.1028	3.7919	9.7769e-2	1.5900	507.3	73.6
7/22.1T	10.20	4.8389	4.6743	4.8121e-2	1.7110	496.8	72.1
	10.10	4.8389	4.6743	4.8121e-2	1.7110	506.7	73.5
					average:	**498.2**	**72.3**
					std. dev:	16.1	2.3

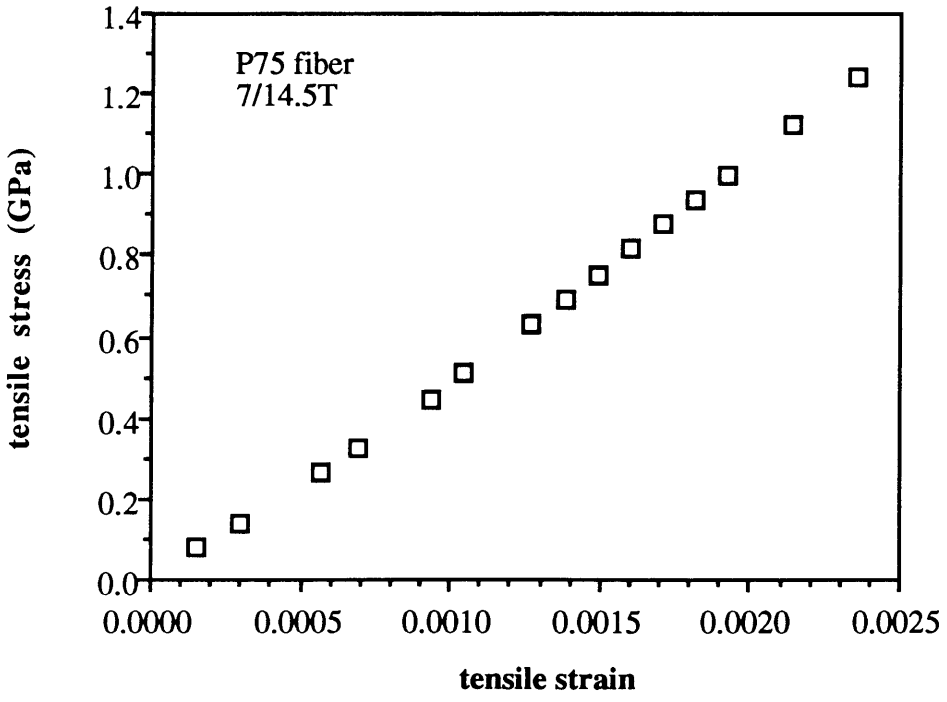

Figure 2.16. P75 fiber stress-strain response in nonlinear, especially at lower strains. Fiber failed at approximately 65% of typical tensile strength.

2.3. Discussion

The Fiber Incremental Tensile Test is useful for measuring the modulus of a wide variety of fibers. The stress- strain curves are consistent with earlier studies and predictions based on the microstructures of the fibers.[9, 19-20, 24-26] Table 2.14 lists all of the fibers tested and the average nonlinearity factor for each type. The nonlinearity factor, f, describes the change in modulus with strain as given in Equation 2.4, where E is the modulus, E_0 is the modulus at zero strain and ε is the strain.

$$E = E_0(1 + f\varepsilon) \tag{2.4}$$

Table 2.14. Zero- strain modulus and nonlinearity factor for all tested fiber types. Equation 2.4 is valid over at least 1% strain for all fibers except those marked with asterisks, which failed at lower strains.

fiber type	E_0 GPa	E_0 Msi	f %/ %strain
glass	76.5	11.1	0%
Kevlar 119	71.9	10.4	0%
Kevlar 29	74.2	10.8	16%
Kevlar 129	98.0	14.2	16%
Kevlar 49	128.5	18.6	0%
Kevlar 149	153.1	22.2	39%
AS4	238.7	34.6	20%
IM7*	263.9	38.3	25%
IM8*	308.9	44.8	25%
HMS4*	313.7	45.5	47%
P25	117.5	17.0	36%
P55*	324.3	47.0	127%
P75*	393.9	57.1	113%

The fiber strength was not measured in this test series because the fixtures are not designed to eliminate stress concentrations which would cause early failure. In fact, the failures which did occur were located in the loop arm and at the epoxy drop edge with equal frequency. Kevlar was not tested to failure because such could damage the fiber, rendering it unusable in the subsequent Micro-Flex testing. Flexure samples for the carbon fibers were taken at locations removed from the fracture region and which appeared to have suffered no damage.

2.3.1. Error Propagation

Propagation of the error associated with each variable in Equation 2.1 indicates the error in the measured modulus is on the order of ± 1.5%, and is primarily due to the measurement of the fiber diameter. The standard error in the regression of the load-extension data typically is less than 0.1%, while the standard deviation of the six slopes calculated by linear regression from a glass fiber loaded and unloaded three times (Figure 2.17) is 0.56%.

The gage length, typically one to two inches, was measured to the nearest 0.0005 inch with a digital micrometer, so the error from this source is negligible. The fiber diameter was measured in a Cambridge Stereoscan 240 scanning electron microscope with cursor overlay. The measuring system resolution is 1.0%, so the fiber radius is correct to within 0.5%. Actual variations in the fiber diameter was a more practical limit. Glass and PAN- based fibers do not vary in diameter along a single fiber but pitch-based carbon and Kevlar fibers are not as constant over lengths of 5 mm or more. The diameters of samples selected for the Micro-Flex testing generally vary by 1.5% along the 5-7 mm test length. (The error analysis is presented in more detail in Appendix A.)

The widely accepted value for the modulus of E-glass fibers is 77.4 GPa (10.5 Msi).[56] The FITT values averaged 76.5 GPa (11.1 Msi) which confirms the validity of the procedure, since it is also well known that the actual modulus of E- glass can vary

with its heat history.[56] (It should be noted that if glass fibers are used for system compliance calibration in ASTM Procedure D3379, some error may result from this variability.)

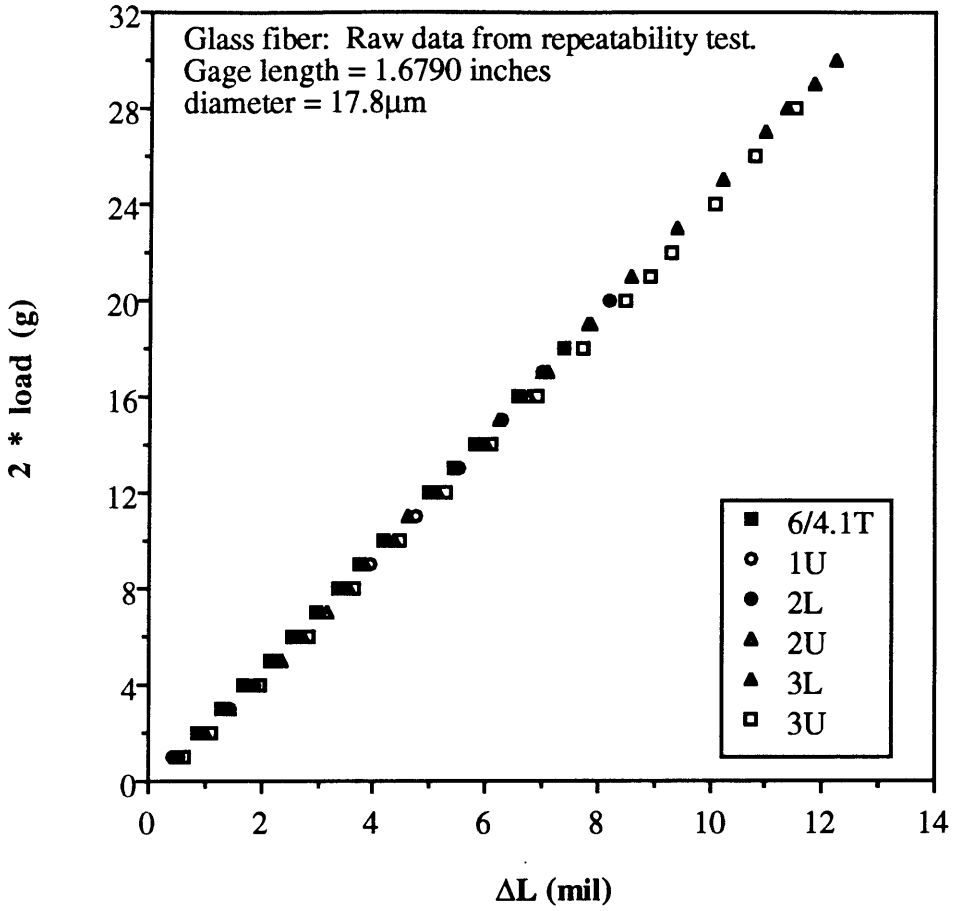

Figure 2.17. Collected data for glass fiber loaded and unloaded three times, showing the expected linear and elastic behavior. Standard deviation of the six slopes is 0.56%.

2.3.2 Kevlar Fibers

The five Kevlar fibers in Figure 2.18 show different modulii. These derive from different processing histories and, with the exception of Kevlar 49, as the modulus increases so does the nonlinearity in behavior. Allen and Roche[26] have shown a correlation between opening of the pleated sheet structure and nonlinear mechanical behavior. The processing conditions for Kevlar 149 are severe enough such that the pleated sheet structure is fully open. This leads to the most nonlinear behavior because

the primary valence bonds increasingly are distorted, in contrast to the easier rotation of the sheets. In fact, the increase is 40%, as found in both studies. The Kevlar 49 modulus shows little change over 1% strain, while the tensile modulus of Kevlar 29 increases approximately 5% according to Allen and 15% by the FITT approach. It is believed the FITT method provides greater accuracy.

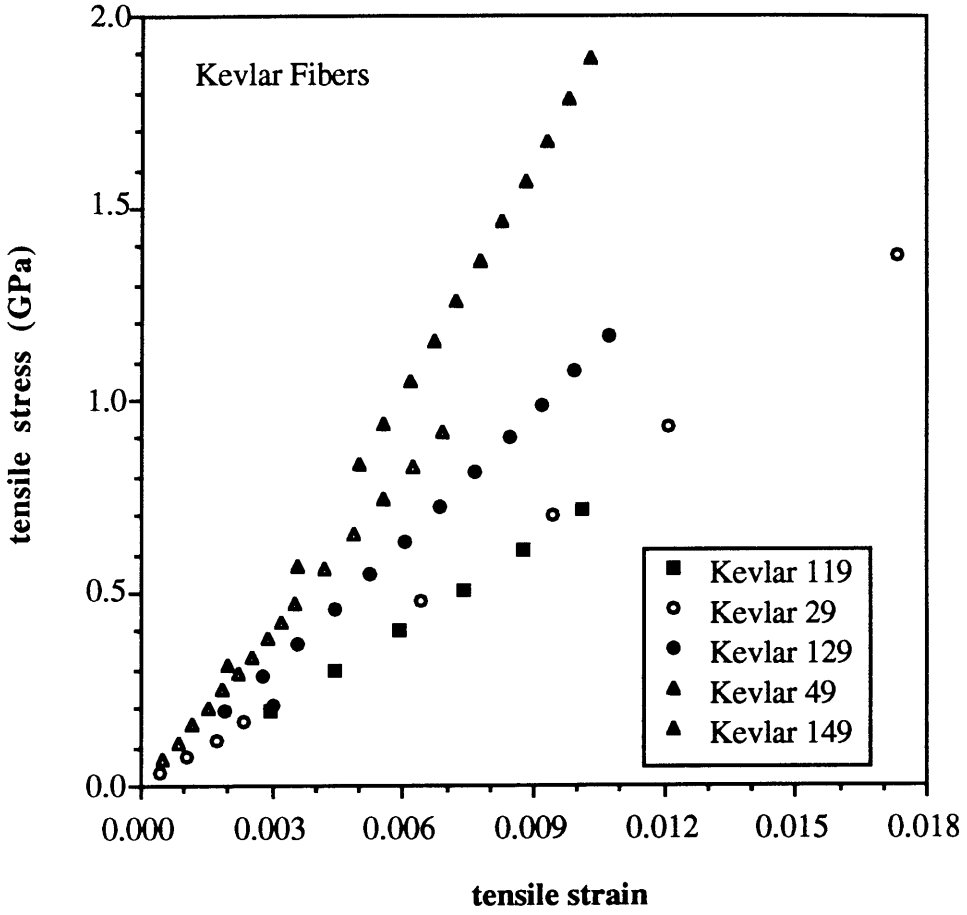

Figure 2.18. Tensile stress- strain curves for Kevlar fibers. Non-linearity is most pronounced in the highest modulus Kevlar 149.

Allen and Roche also showed that deformations from tensile loading do not change the fiber orientation: the modulus was unchanged after repeated loading and unloading. In the FITT mode, the second loading sequence was used to minimize the transient creep behavior encountered in the first sequence; such was more convenient.

2.3.3. Carbon Fibers

The carbon fibers from both precursors exhibit nonlinear elasticity; the degree increases with the modulus, and is higher in the pitch- based fibers than in the PAN based fibers. The latter is consistent with the granular structure of PAN- based fibers which cannot orient as easily as the axially aligned sheet structure in the pitch- based fibers.

PAN- based

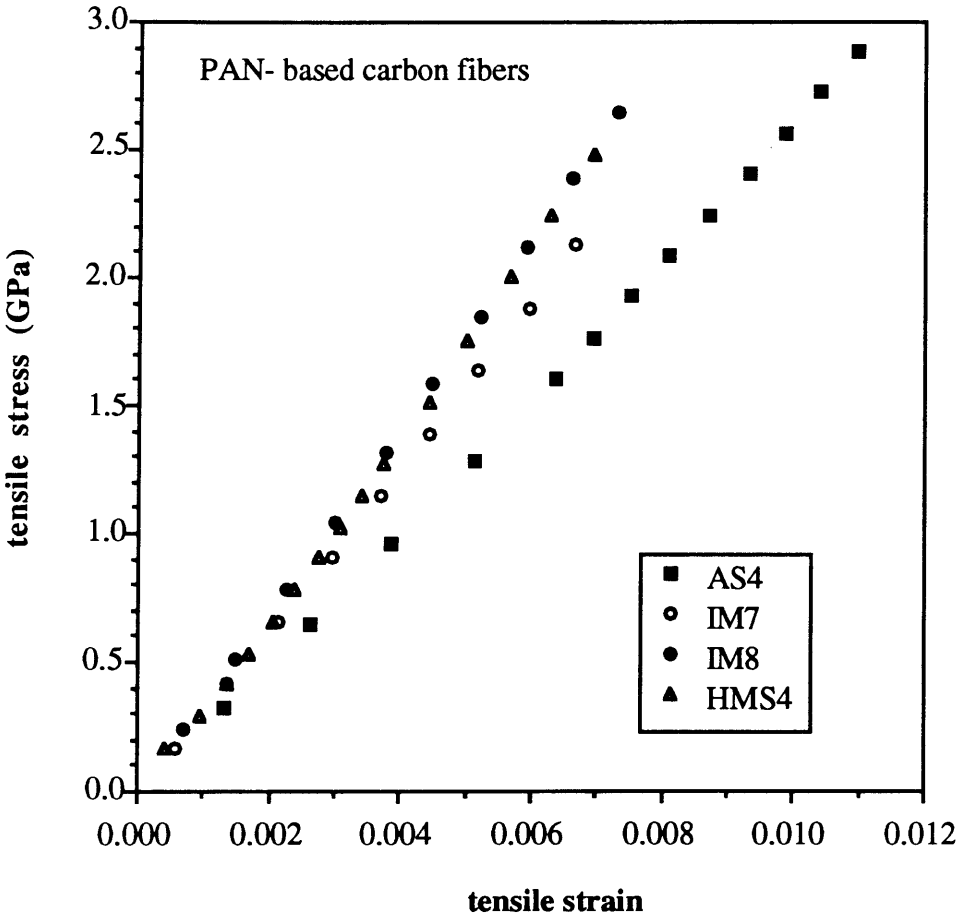

Figure 2.19. Stress-strain curves for PAN- based carbon fibers. Nonlinearity increases with increasing modulus.

The measured tensile modulii for AS4, IM7 and IM8 fibers are higher than those reported by Hercules, while the HMS4 results are about the same. In all of them, the modulus increases with increasing strain, as seen in Figure 2.19. Hughes[22] and SACMA[23] give typical nonlinearity factors for standard and intermediate PAN- based

fibers of 16-18%, consistent with the FITT measured values of 20% for AS4 and 25% for IM7 and IM8. Hughes presents nonlinearity factors almost twice as much (25- 30%) for high modulus fibers. The FITT measured change in HMS4 fibers is 47%, almost twice as much as measured for the other three.

Pitch- based

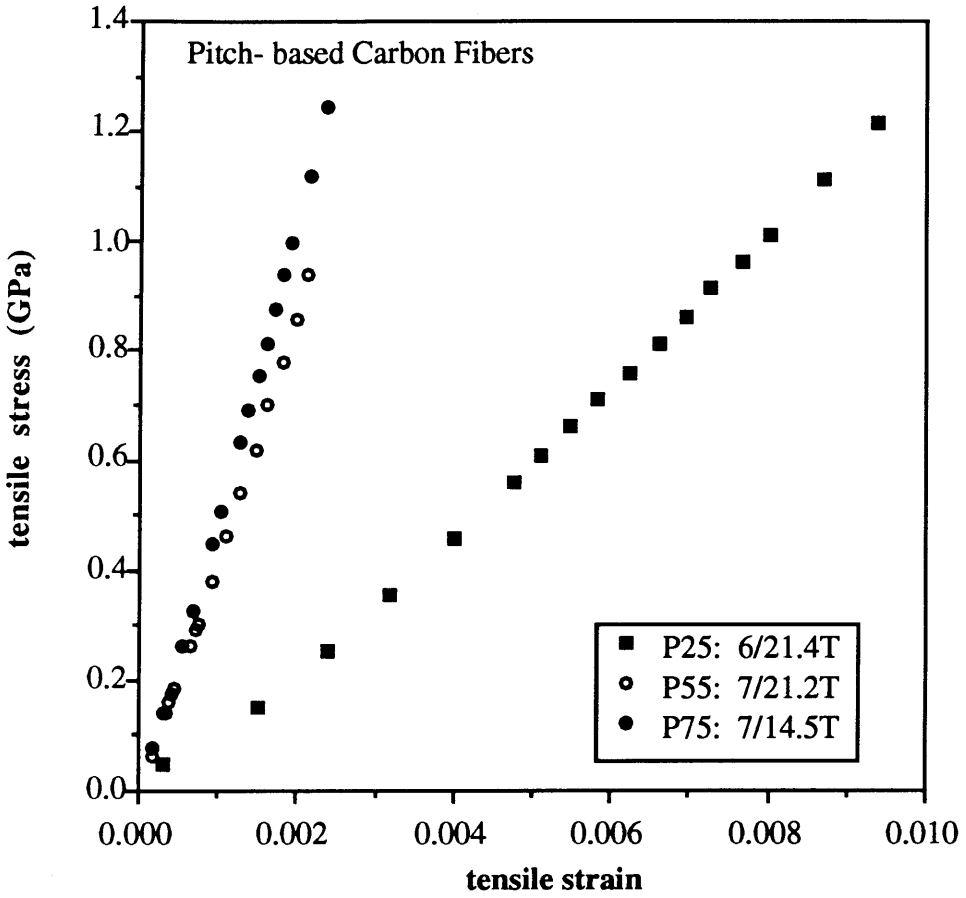

Figure 2.20. Pitch based carbon fiber stress- strain curves. The foot of the P25 curve extends over the largest strain range. P55 and P75 fail at low strains and are also distinctly nonlinear.

The P25 tow provided by Amoco had a permanent twist, which made the individual fibers wavy until the first load increment was applied. The modulus increased slowly and reached the manufacturer's reported value (23 Msi) at approximately 1% strain. The large "foot" region near the origin for P25, which is less evident in P55 and P75 (See Figure 2.20), is consistent with the observations of Arsenovic *et al.* [24] who used

laser- generated ultrasound to measure Young's modulus as a function of orientation under stress. Since the sheet microstructure of the P25 is less ordered compared to the other two fibers; its overall orientation increases more rapidly with strain so the modulus also increases.[4]

The pitch fibers are more brittle and fragile than glass or PAN- based fibers: sample preparation is difficult and successfully prepared samples are prone to fail at the epoxy drop. The stress-strain curves of these fibers are the most nonlinear, as expected. Crasto and Kim[9] measured nonlinearity factors of 52%, 91% and 88% for P25, P55 and P75 fibers respectively, consistent with the FITT measured values of 36%, 127% and 113%. The better developed graphite sheets in the P55 and P75 fibers increase the modulus but reduce the strain to failure. The sheet structure is directly reflected in the large nonlinearity factors: the modulii of P55 and P75 do not level off at higher strains, as does P25, because the degree of structural perfection is higher, which allows continued sheet sliding until failure occurs.

3. Micro-Flex Test for the Flexural and Compressive Properties of Single Fibers

3.1. Test

In contrast to composite testing and to other single fiber tests, the Micro-Flex bend test involves only one test on a small amount of fiber to determine the compressive modulus, the compressive failure stress and the failure strain. The bending stiffness is measured from the load-deflection behavior of a single fiber which had been previously tested in the Fiber Incremental Tensile Tester.

A beam in pure bending experiences tension on one side of the neutral axis and compression on the other. The bending stiffness is a function both of material properties and beam geometry. If the fiber is isotropic, the bending modulus, the stiffness divided by the moment of inertia around the centroidal axis, will be equal to the tensile and compressive modulii; all values are the same. If the fiber is anisotropic, the compressive modulus can be calculated from the measured Micro-Flex bending stiffness and FITT tensile modulus. Once the compressive modulus and the resulting neutral axis shift are determined, the compressive stress and strain can be calculated.

The Micro-Flex Test was developed from the three point bend test used by Moalli to measure the compressive modulus of high performance fibers such as commercially available Kevlar and experimental PBO.[46] The new, four- point loading (Figure 3.1) eliminates shear in the center test region and makes it easier to see the fiber and the kink-band formation process.

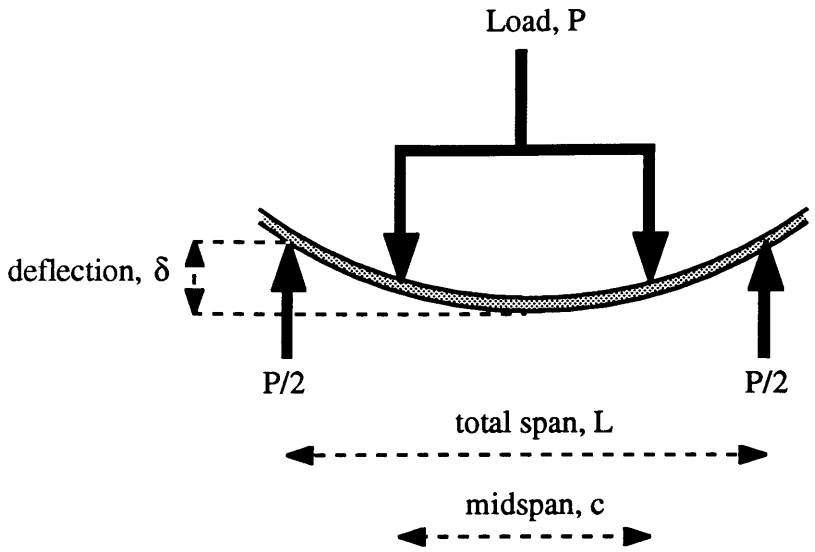

Figure 3.1. Diagram of four point loading. Dark arrows represent forces. Beam deflection is measured as a function of loading.

1. Equipment

Platform

Figure 3.2A is a schematic of the test apparatus. The basic platform is a duplicate of the FITT platform, except two thumbscrews adjust platform end height, instead of one. Dover Air Lube LB-2 and LB-5 Bushings are situated as before: the 0.25" i.d. LB-2 is a linear bearing next to the work area for the highly polished sliding rod; the 0.5" i.d. LB-5 supports the rotating spindle at the end of the test platform. The weight basket is paper, 0.75" x 1.00", held by wire at the four corners. A single PBO fiber connects the weight basket over the rotating spindle to a mini binder clip clamped to the sliding rod.

Gas flow from the linear bearing can disturb the fiber sample, making precise measurement of deflection difficult. Because the Micro-Flex fixtures are lighter than the FITT fixtures, the system is adequately activated with nitrogen gas at 5 instead of 20 psi. Flow in the test area is further reduced by a simple air shield. The shield is an inverted T of aluminum sheet, 4" wide, with a 0.4" diameter hole through which the sliding rod passes.

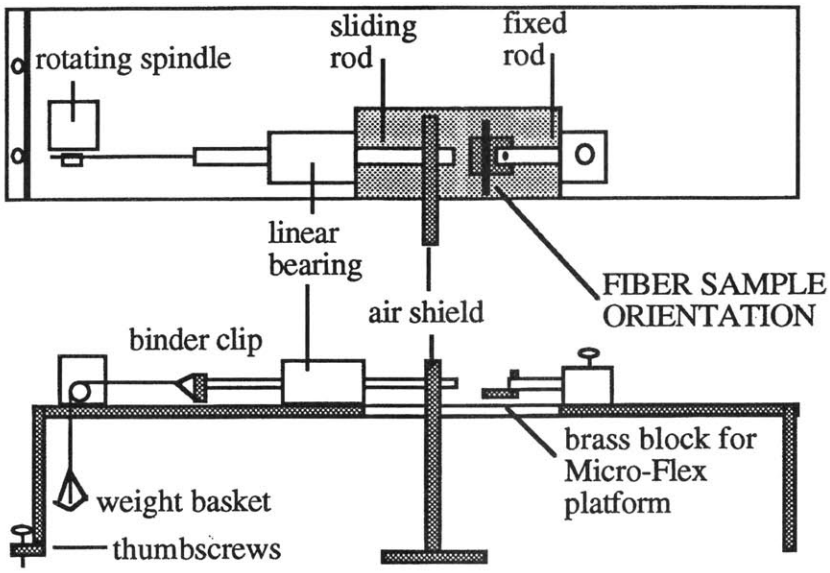

Figure 3.2A. Top and side views of Micro-Flex platform without fixtures. Fixed rod is on right, moveable on left. Fixtures are attached to rod ends. Resting position of sliding rod is determined by thumbscrew height adjustment. Air shield reduces flow from linear bearing in test area.

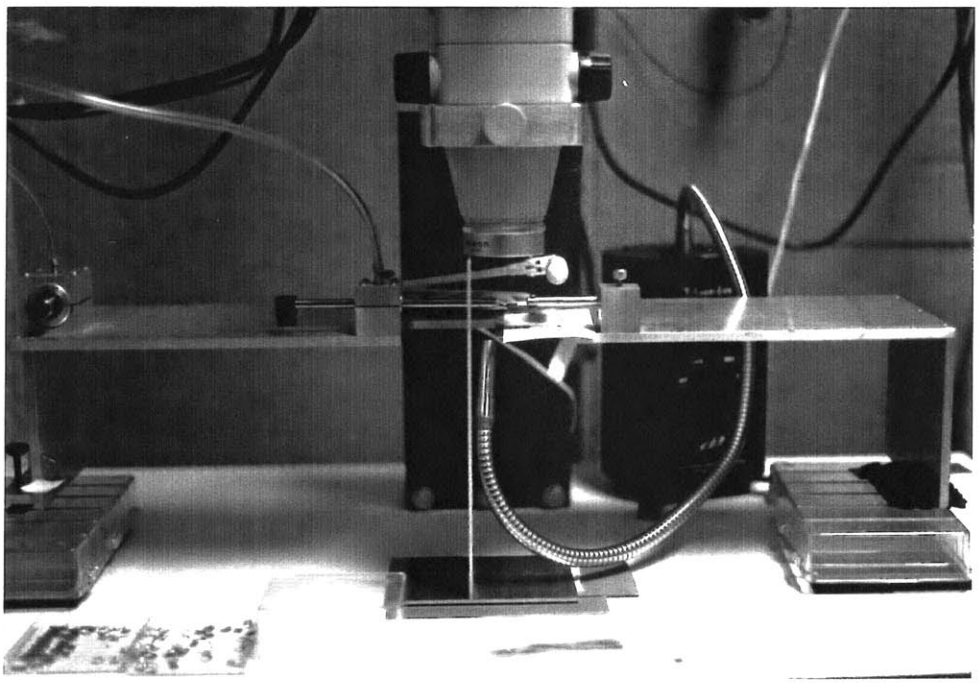

Figure 3.2B. Photograph of Micro-Flex work area.

Both the fixed and sliding rods are 0.25" diameter stainless steel. The fixed rod is clamped in an aluminum block with a set screw. A screw through the end of the rod holds a brass block, 0.75" x 0.50" x 0.125", to which the support platform is attached. The probe fits in a slot in the work-area end of the sliding rod. The mini binder clip is attached to hang below the rod, keeping the slot perpendicular to the table so the Micro-Flex probe is properly positioned. Figure 3.2B is a photograph of the test apparatus.

The test is sensitive to vibration in the work area because of the very small distances measured in the balanced, frictionless system. The test platform sits on a steel table top, 2' x 3' x 1", on top of a standard lab table in an area of low traffic selected for its relatively vibration- free environment. The test is not suitable for use on the manufacturing floor.

Micro- Flex fixtures

The probe and support platform, shown schematically in Figure 3.3, attach to the fixed and sliding rods of the test platform. The load probe is wedged in the slot at the end of the sliding rod and held by friction. The support platform is secured to the brass block on the fixed rod with Permabond 910 cyanoacrylate adhesive. The trough of the two parts, where the fiber sits for testing, is perpendicular to the rods and parallel to the ground. The fixtures are designed to place a single fiber in four point bending such that the fiber deflection can be measured when the sliding rod and load probe travel under an applied load.

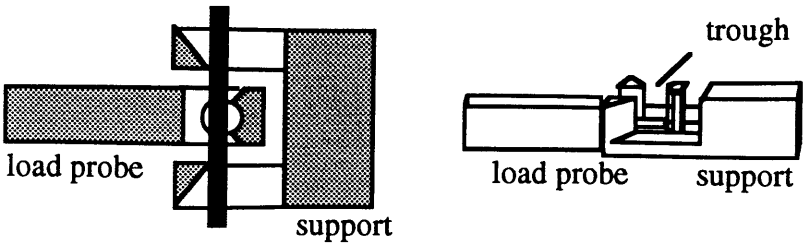

Figure 3.3. Schematic of Micro-Flex fixtures. Test fiber fits in trough between columns of support platform and columns of load probe. During test, load probe travels to the left while the support platform remains fixed.

Micro Electrodischarge Machining (μEDM)

Both the support platform and the load probe are machined from brass which is 0.125" thick. The original test fixtures were made with a Panasonic micro-electrodischarge machining (μEDM) system using 300 μm- diameter tungsten electrodes. The machining rate is 20- 30 μm/ min. when the electrode is operated at 110 volts and 3300 picoFarads. A finer surface finish is achieved with smaller capacitors, but the maximum machining rate is 10 μm/ min. Narrow columns are formed by overlapping holes where the electrode has vaporized the metal (Figure 3.4A). Perfectly straight and aligned columns with widths of 2-5 μm are possible (Figure 3.4B).

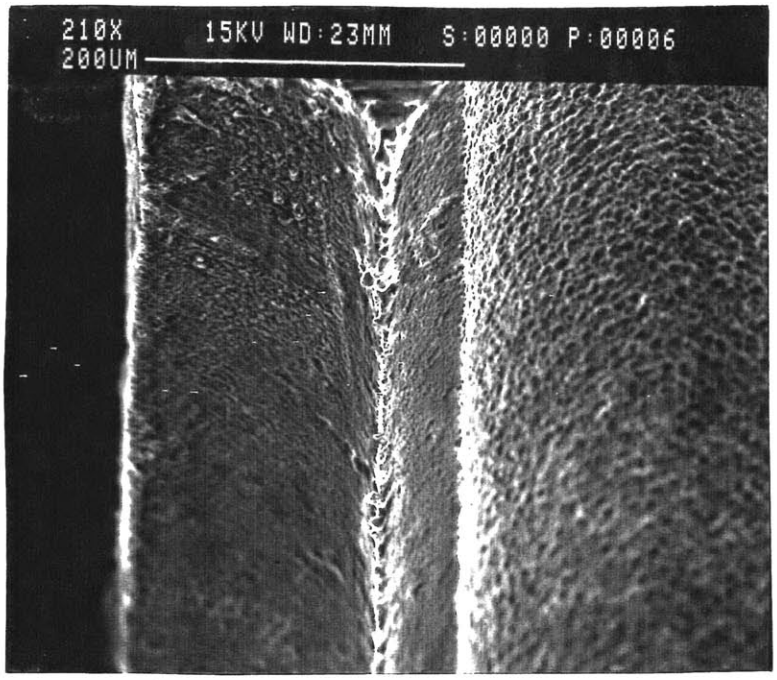

Figure 3.4A. SEM micrograph of micro-machined column for four point loading viewed at 45° tilt. Columns width is approximately 2 μm.

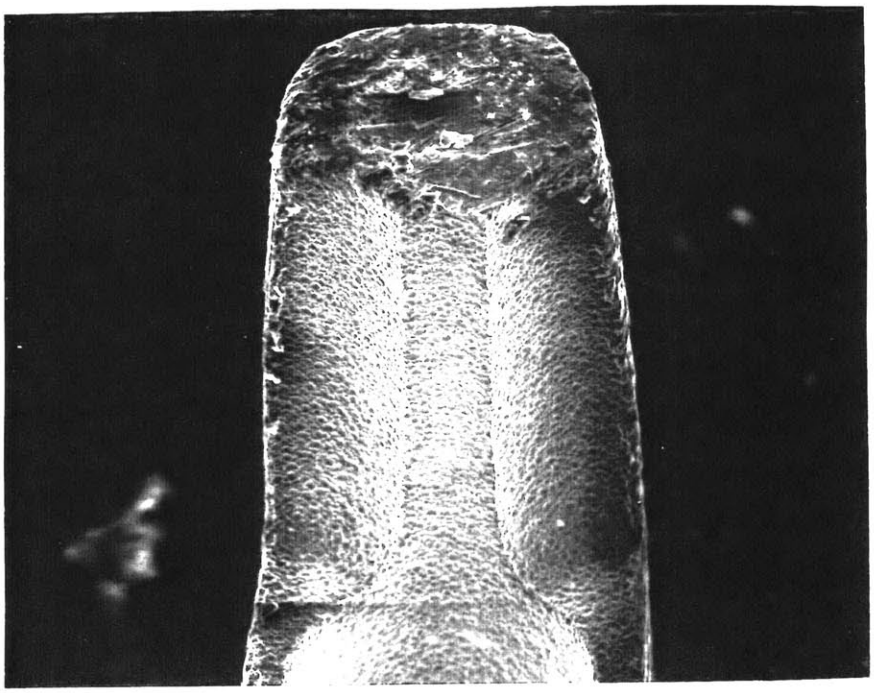

Figure 3.4B. Micrograph (124x magnification) of micro-machined load probe. Columns are straight and aligned, separation is 90 μm. (View angle is 45°)

The load probe starting piece is rectangular in section, 0.5" x 0.02", with a trough cut half through the thickness at one end. The loading columns are micro-machined from the wall on one side of the trough (Figure 3.5). The first cut is a circular, centered hole completely through the thickness. This is needed for backlighting if the fiber edges and kinks are to be seen clearly for deflection measurements during the test. The second and third cuts are holes displaced from the first position by the electrode radius plus and minus half of the midspan distance along the trough wall. These holes are cut only to the trough depth. The load probe used for this study is shown in Figure 3.6. The distance between the columns is 90 μm.

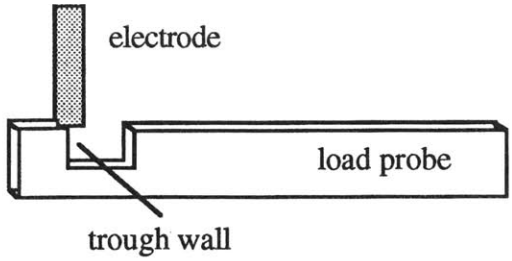

Figure 3.5. Electrode positioned over trough wall for cutting load probe.

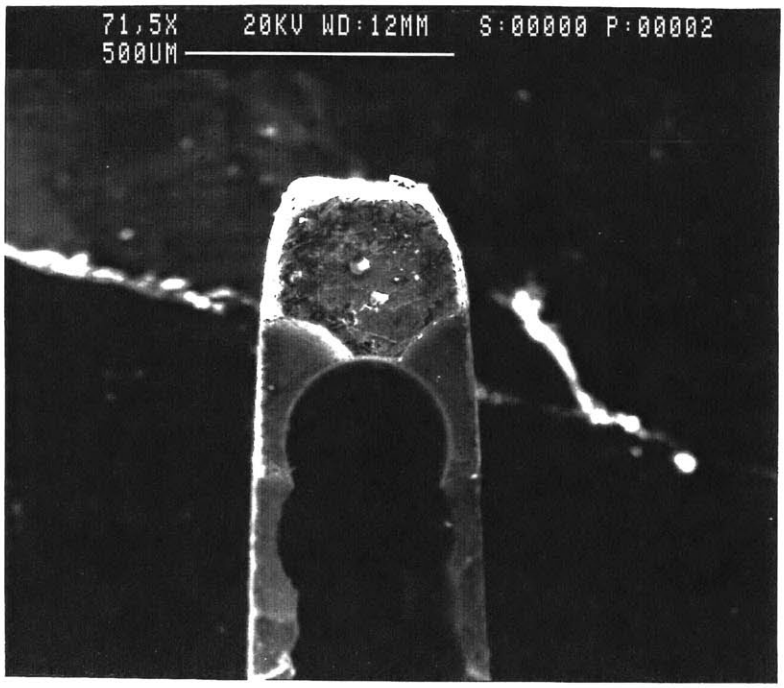

Figure 3.6. Top view of micromachined load probe used for all tests in this study.

The support platform starting piece has a rectangular section, 0.5" x 0.375", with two arms, 0.2" x 0.1", separated by a distance less than or equal to the desired test span and it has a trough approximately 0.05" deep running across both arms. The first of two different support platforms used for these tests was micromachined (Figure 3.7) to have a span of 542 μm between the columns. As with the load probe, the columns were formed by cutting the trough wall (Figure 3.8). The electrode was positioned over the inside corner of the trough for the first cut: a hole as deep as the trough. The second cut is a slot; the electrode travels between the outside of the arm and a position slightly less than the electrode diameter away from the first position along the trough wall until the trough bottom meets the slotted area. The two cuts are repeated on the opposite arm. The removal of material away from the columns is useful for aligning the test fixtures, since the platform must be twisted to make the four columns collinear and properly spaced.

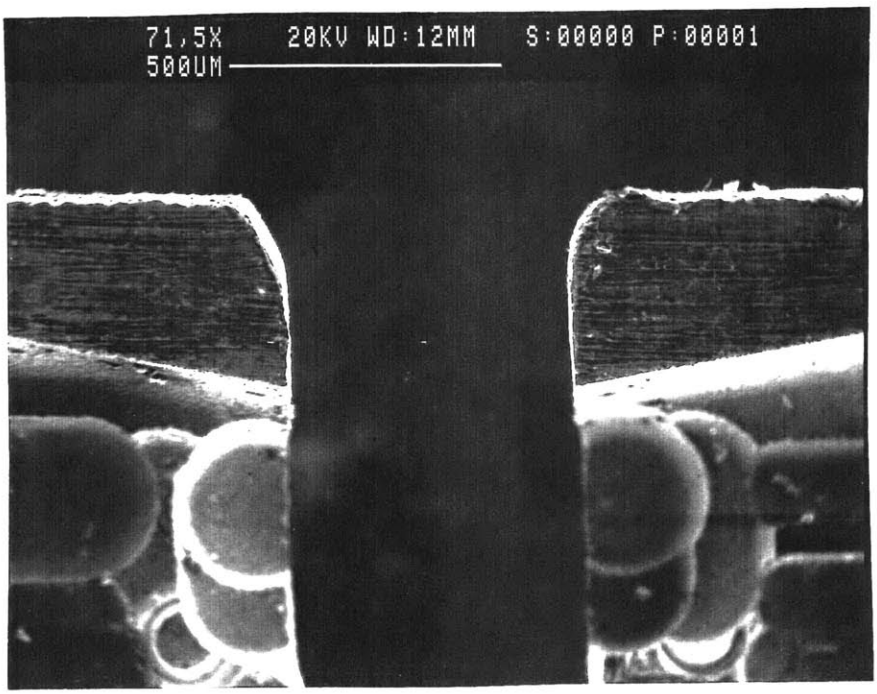

Figure 3.7. SEM Micrograph of small support platform made by μEDM. Span between columns is 542 μm. Columns were formed by angled slots.

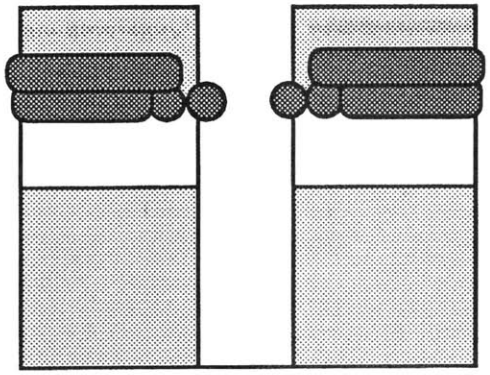

Figure 3.8. Schematic of μEDM cuts for support platform. Pre-slotted arms are viewed from the top. Holes to form columns are cut first, then horizontal or angled slots remove excess material, freeing fiber ends.

Conventional Machining

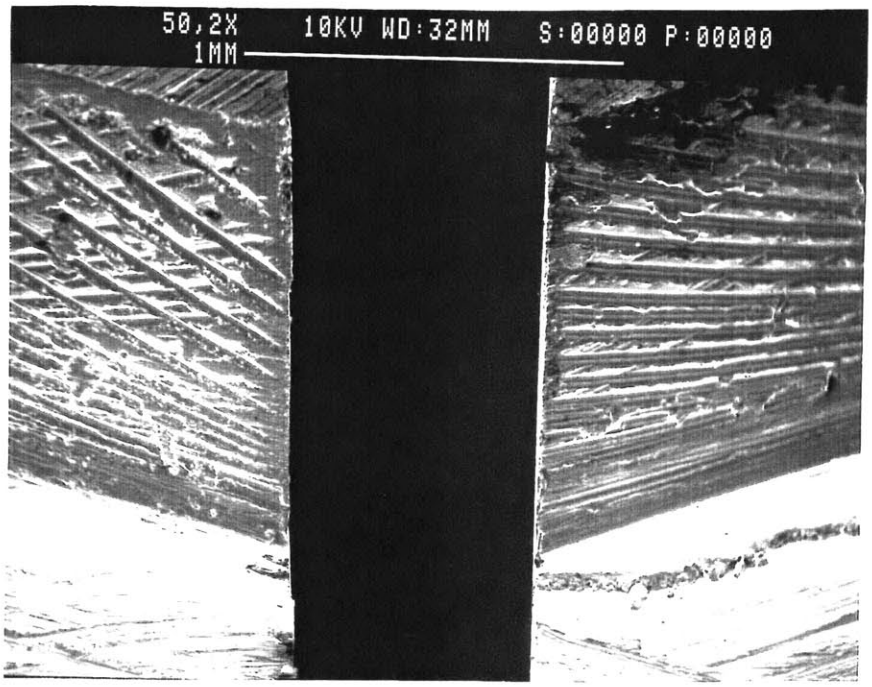

Figure 3.9. SEM micrograph of large support platform (666 μm span) made by conventional machining. Platform is tilted 45° so view is from inside the trough.

Conventional machining is faster and easier than μEDM. The second support platform, which has a span of 666 μm, was made by conventional methods (Figure 3.9). The center slot was carefully cut with a fine blade saw to the desired span, then the piece

was turned for milling at angles to form the columns at the inner faces (Figure 3.10). The support platform made by conventional machining has a rougher surface, but this does not affect results since the fiber contacts only the smooth inner columns.

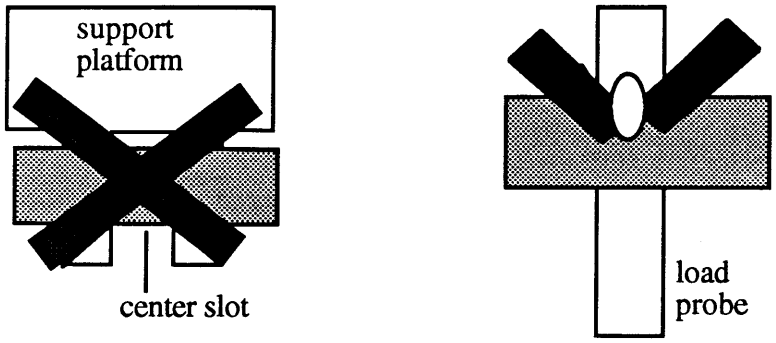

Figure 3.10. Conventional machining cuts for Micro-Flex fixtures. Light shaded area is trough cut. Dark shaded areas are milled. Center hole in load probe should be drilled first. Drawing is not to scale.

Measuring system

The work area for the Micro-Flex test is viewed with a Nikon light microscope with standard magnification of 55x. The microscope is held in a collar which is mounted on steel plate 0.25" thick and bolted to the steel tabletop thereby eliminating separate vibrations in the measurement system. A Hitachi camera sits at the top of the microscope column and sends the image through a Boeckler VIA-100 videomicrometer to the black and white Hitachi monitor. Videomicrometer cursor position, thickness and intensity are controlled with a joystick. The video system is calibrated with a standard diamond-etched slide with grid lines 10 μm apart for the first 100 μm and 100 μm apart for the rest of the 1 mm distance. At 350 x magnification, the cursor resolution is 0.5 μm.

Two sources of illumination are used for fiber viewing during setup and testing. A portable book lamp sits on the platform behind the work area for illumination at low magnification. A Cole-Parmer Fiber-Lite Fiber Optic Illuminator with polarizing film over the source is positioned under the work area to backlight the fiber and to more clearly define the edges at high magnification.

The loading is accomplished by the sequential addition of small weights made of aluminum foil. The foil pieces are cut with a scalpel and weighed with a Mettler 2000 balance to the nearest 0.05 mg. The measured weight is written on the foil with pen, then groups of 2-8 foil weights are weighed to reduce the accumulated error.

3.1.1. Test Setup and Alignment

The load probe position is fixed by the slot in the sliding rod. The support platform is fixed to the brass block so the fiber touches all four columns, two load and two support, without deformation. Then a glass fiber is used to check alignment. The support is glued in position and the load probe brought to the starting position. A glass fiber is placed in the trough and the bearings are activated. The platform end height is adjusted so the load probe moves slightly to the left, bringing the fiber against the support columns. The test area is viewed at low magnification so the tops of all four columns are visible. The distances between the support and load columns on each side are compared and the brass block is twisted until the load probe is centered. If the four columns are not collinear when the spacing is correct, the fiber is removed and the support platform is popped off the brass block. The support platform is glued on again in a slightly different position, based on the observed misalignment. The fiber is reinserted and spacing and alignment are checked. The process is repeated until the setup is satisfactory.

To further check alignment as well as friction in the system, the Micro-Flex test is run on a clean glass fiber from an FITT loop. Fiber curvature under load should be symmetric around the center of the loading midspan. The measured bending modulus should match the tensile modulus from the FITT test. The setup procedure, including platform realignment is continued until the Micro-Flex and FITT results match within experimental error.

3.1.2. Test Procedure

A 3 to 5 mm long section of a single fiber free of noticeable waviness, peels and defects is cut from an FITT loop. The fiber is handled with fine-tip tweezers, and stored

on smooth paper in plastic sample boxes. The test piece is placed in the trough of the Micro-Flex fixtures and further checked for defects or extraneous debris before testing. If the sample is a Kevlar fiber, the test section of is checked for kink bands, which appear as dark spots, lines or wedges in an otherwise translucent fiber. Pre- kinked fibers are discarded.

The fiber is brought against the support columns by the load probe when the gas bearings are activated. The mounted fiber is viewed at 350 x magnification. The light tube is adjusted for best definition of the fiber edges. A small but finite load from the balanced fixtures is necessary to hold the fiber against the columns, so the data are slightly shifted from the true origin. Video- micrometer cursors overlay one edge of the fiber at the zero- deflection point. Weights are added, and the fiber deflection measured, until the fiber fails or the deflection exceeds the limits of simple beam theory. Sometimes the fiber then is unloaded, but this is more difficult: if the weight basket is bumped or the fiber rolls in the columns, the focus changes and the cursor measurements are no longer valid.

Typical weight increments are 0.5 - 10 mg, depending on fiber type. The time to add a weight and record the fiber deflection is approximately 30 seconds because of the care taken to avoid dropping the weight or hitting the weight basket. In addition, at very low deflections, fibers have a tendency to vibrate slightly before settling to a fixed deflection under a given load. These vibrations occur more frequently in fibers with diameters larger than 15 μm (glass) or smaller than 6 μm (carbon); Kevlar fibers damp more.

3.1.3. Sample Recovery and Assessment

After the test is complete, the gas flow to the bearings is turned off. If the fiber was not unloaded, the weights are carefully removed, then the gas is turned on briefly to move the load probe away from the fiber. If the fiber was unloaded, the gas to the linear bearing is turned on while the spindle in the other bearing is rotated manually to move the

probe away from the fiber. The fiber is removed from the test area with tweezers and placed on an SEM stub. The ends are tacked down with colloidal silver paint. When the stub is full of test pieces, it is gold coated. Typically the gold is 200 Å thick and improves the quality of the fiber image in the SEM.

Fibers are viewed in a Cambridge Stereoscan 240 Scanning Electron Microscope at 10 keV acceleration voltage and 10 mm working distance. The viewing system is fitted with a calibrated cursor overlay. Fibers are viewed along the length and the diameters measured at 5-15 equally spaced intervals. The presence of kinks and other defects as well as any diameter variation greater than 2% are noted and correlated with the test results.

3.2. Bending Analysis

3.2.1. Beam Theory

The relationship between load and deflection is derived from the change in moment along the arc length of the beam as described by Equation 3.1. $d\theta/ds$ is the change in angle between the undeflected and deflected beam along the arc of the beam, M is the bending moment and EI is the bending stiffness. The arc length can be approximated as the horizontal distance from the support if the total deflection is small enough for $\sin\theta$ and θ to be equal. The maximum deflection for this approximation to hold occurs is $\sin\theta = \theta = 0.5$. For a particular combination of span, L, and midspan, c, the deflection limit is given by Equation 3.2, which is derived from the expression for the beam angle at the support column. Thus for a midspan of 90 μm and a total span of 666 μm, the maximum deflection is 55 μm; for a total span of 542 μm it is 45 μm.

$$\frac{d\theta}{ds} = \frac{M}{EI} \tag{3.1}$$

$$\text{maximum } \delta = \frac{3L^2 - (L - c)^2}{24(L + c)} \tag{3.2}$$

To remain within the small deflection region and still achieve high compressive stresses at the outer edges of the fiber, a small span and midspan must be used. In some cases it is impossible to achieve the desired stress and stay within the limits of the theory. This is a limiting factor to the full characterization of many carbon fibers. Although numerical integration can be used to solve for the relationship between load and deflection at larger deflections, the reaction force at the support begins to have a significant component parallel to the fiber length. To assess the consequences of this, the resulting friction force would need to be known; this involves many uncertainties and thus was avoided by keeping the deflections within the cited limit.

3.2.2. Bending Stiffness

When the small deflection assumption restriction obtains, integration of Equation 3.1 yields Equation 3.3 in which the fiber deflection, δ, is related to applied load, P, by the bending stiffness, EI. The geometric factor, G, given in Equation 3.4, is a function of the support span, L, and the mid- or loading- span, c. Since load and deflection are measured, the slope of the linear region of the load- deflection curve is used to calculate the bending stiffness. For non-Hookean behavior, the curve fit is quadratic, and the derivative represents the tangent bending stiffness.

$$\delta = \frac{P}{EI} G \tag{3.3}$$

$$G = \frac{L^2(L - c)}{32} - \frac{(L - c)^3}{96} \tag{3.4}$$

3.2.3 Bending Modulus, Stress and Strain

If the fiber were isotropic such as E- glass, its behavior in tension and compression would be the same. Then the bending stiffness would simply be the product of the Young's modulus, E, and the centroidal moment of inertia, I. The modulus is a material property while the centroidal moment of inertia is a geometric property, defined by Equation. 3.5, where y' is the distance of each area element from the centroidal axis and A is the section area.

$$I_0 = \int y'^2 \, dA \tag{3.5}$$

The bending modulus is the modulus calculated from the bending stiffness assuming no shift in the neutral axis, and is given by Equation 3.6 for a fiber of circular cross section. $(EI)_f$ is the measured bending stiffness, m_b is the slope of the load deflection curve, G is the geometric factor and r is the fiber radius. The bending stress and strain are calculated with Equation 3.7 and 3.8. M is the bending moment, P is the applied load and L and c are the test span and midspan. The strain is greatest at the outer

edge of the fiber, where y = r. The bending modulus and bending stress-strain behavior are the same as the modulus and stress- strain behavior measured in tensile tests for an isotropic fiber.

$$E_b = \frac{(EI)_f}{I} = \frac{4m_b G}{\pi r^4} \tag{3.6}$$

$$\sigma = \frac{My}{I_f} = \frac{P(L-c)r}{\pi r^4} \tag{3.7}$$

$$\varepsilon = \frac{My}{(EI)_f} = \frac{P(L-c)r}{4m_b G} \tag{3.8}$$

3.2.3. Compressive Modulus

In high performance fibers the tensile and compressive modulii often are different, so the fiber neutral axis shifts away from the fiber centroidal one. The following discussion assumes the tensile modulus is larger than the compressive modulus, so the neutral axis shifts to reduce the area in tension. The bending stiffness is the sum of the stiffness of the regions in tension and in compression, so the compressive modulus can be calculated with Equation 3.9, where the subscripts f, c and t refer to fiber, compression and tension. The parallel axis theorem (Equation 3.10) must be employed to determine both the whole fiber and tensile section moments of inertia around the neutral axis because the neutral and centroidal axes no longer coincide; they are separated by the shift distance, y, shown in Figure 3.11.

$$E_c = \frac{(EI)_f - E_t I_t}{I_f - I_t} \tag{3.9}$$

$$I = I_0 + Ay^2 \tag{3.10}$$

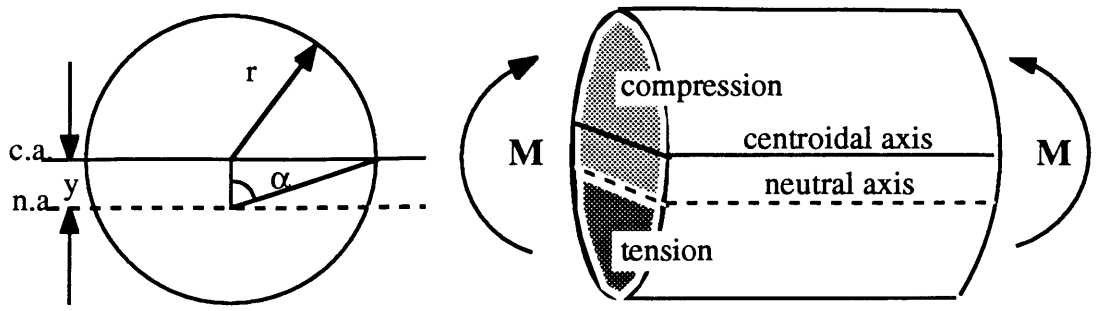

Figure 3.11. Anisotropic fiber in bending. The lower modulus in compression causes the neutral axis to shift away from the centroidal axis, increasing the amount of fiber in compression. The shift distance, y, is related to the ratio of tensile to compressive moduli.

The shift factor, k, given in Equation 3.11, is the distance the neutral axis moves relative to the fiber radius, and is a function of the ratio of the tensile to compressive modulii. The shift factor is also the cosine of the angle α which describes the size of the sectors in tension and compression. The centroidal moments of inertia about the neutral axis are given by Equations 3.12 and 3.13 for a fiber of circular cross section. If the tensile modulus and fiber radius are known, the compressive modulus can be determined.

$$k = \frac{y}{r} = \cos\alpha = \frac{\sqrt{\frac{E_t}{E_c}} - 1}{\sqrt{\frac{E_t}{E_c}} + 1} \tag{3.11}$$

$$I_f = \pi r^4 (0.25 + k^2) \tag{3.12}$$

$$I_t = r^4 \left[\frac{a}{2} (0.25 + k^2) - \frac{5}{6} k (1-k^2)^{1.5} \right] \tag{3.13}$$

$$a = \alpha - k (1-k^2)^{0.5}$$

The fibers selected for this study have circular cross sections to simplify the analysis. Spectra polyethylene fiber, rayon-based carbon fiber, and many PAN- based carbon fibers such as Amoco T-300, BASF G40-700 and G45- 700 are excluded because of their irregular cross sections.

3.2.4. Compressive Stress and Strain

The failure stress and strain also can be determined by this method. The bending moment, M, increases linearly along the beam from the support to the load column. The failure load, P, defined as the onset of kinking or fracture, corresponds to a failure moment which can be calculated using Equation 3.14. The failure moment is used to determine the compressive failure strain, ε_C, and the compressive failure stress, UCS.

$$M = \frac{P\,(L - c)}{4} \tag{3.14}$$

Fiber strain increases linearly from zero at the neutral axis to a maximum at the fiber surface. The radius, plus or minus the shift distance, defines the distance from the neutral axis: y*. In Kevlar fibers, microfibril buckling in compression occurs before tensile failure. The compressive failure stress is defined as the point of large scale kink band formation or significant deviation from linearity of the load- deflection data. PAN- and pitch- based carbon fiber failures do not occur within the limits of the test.

The compressive strain and stress at failure, ε_C and UCS, are calculated using y* from Equation 3.15 in Equations 3.16 and Equation 3.17. The ratio of tensile to compressive modulus determines the shift factor, which is needed to calculate y*, so E_C must be calculated before ε_C and UCS. When both the tensile modulus and bending stiffness vary with strain, the compressive modulus must be found iteratively, so that the tensile strain in the fiber during bending is the same for which the tensile modulus initially used to start the analysis was assumed. Usually, three or four cycles of iteration are required to fulfill this condition.

$$y^* = r(1 + k) \tag{3.15}$$

$$\varepsilon = \frac{M\,y^*}{(EI)_f} \tag{3.16}$$

$$UCS = \frac{My^*}{I_C} = E_C\varepsilon_C \tag{3.17}$$

3.3. Error Analysis-Bending

The first derivative of an expression, y, is the first order measure of the change in the calculated value with a small change in an input variable, x_i. The standard error of the expression, S(y), is defined by Equation 3.18, where $\partial y/\partial x_i$ is the first derivative with respect to x_i and $S(x_i)$ is the error in x_i.

$$S(y) = \sqrt{\sum \left(\frac{\partial y}{\partial x_i}\right)^2 (S(x_i))^2} \tag{3.18}$$

For this analysis, the relevant expressions are Equations 2.1, 3.6, 3.9, 3.16 and 3.17 for E_t, E_b, E_c, ε_c and compressive stress, σ. The first derivatives with respect to the measured parameters and the error equations are in Appendix B. (Second derivatives have been calculated and are negligible compared to the first order contributions.) The appropriate formulae have been compiled in a spreadsheet which allows the calculation of error for specific tests. Table 3.1 lists the variables which affect the five expressions. The percent error in the tensile and bending modulii are simple combinations of the percent error in the input variables, but because of shift factor, the error in the compressive modulus, strain and stress depends on the ratio of tensile to compressive modulus as well as the magnitude of the other input variables.

Table 3.1. Test variables are listed under the calculated fiber properties which they affect. Some test variables are functions of more basic input variables.

tensile modulus, E_t	bending modulus, E_b	compressive modulus, E_c	compressive strain, ε_c	compressive stress, σ
$m_t = f(2P, \Delta L)$	$m_b = f(P, \delta)$	$EI = f(m_b, G)$	$M = f(P, L, c)$	E_c (column 3)
L_0	$G = f(L, c)$	$E_t = f(m_t, Lo, r)$	$y^* = f(r, k)$	ε_c (column 4)
radius	radius	$I_t = f(r, k)$	$EI = f(m_b, G)$	
		$I_f = f(r, k)$		

3.3.1. Sources of Error: measurements

The analysis employs standard error propagation techniques, as described by Barford.[57] The standard error of each variable, $S(x_i)$, is determined by material and equipment limits. The variables and the precision with which they can be measured are listed in Table 3.2A. The error in the calculated values from the error in the relevant measured parameters is presented in Table 3.2B. These influence the various calculated values to the degrees shown.

Table 3.2A. Precision of measured parameters for Micro-Flex test.

Measured Parameter	Precision
Load, P	± 0.05 mg per increment of load
Deflection, δ	± 0.5 μm
Span, L	± 2.5 μm
Midspan, c	± 1 μm
Fiber Radius, r	± 0.75%

Table 3.2B. Error in calculated values from Micro-Flex test.

Calculated Value	Error
Tensile Modulus, Et	± 1.6% (from Chapter 2)
slope, mB	± 1.0%
Geometric Factor, G (666 μm span)	± 1.1%
Bending Modulus, Eb (666 μm span)	± 3.4%
Geometric Factor, G (542 μm span)	± 1.4%
Bending Modulus, Eb (542 μm span)	± 3.5%

The modulus dependence on radius is very strong, especially at higher values of bending stiffness. The fiber diameters are measured with the SEM at 2000 to 4000 times magnification. The glass and the carbon fibers in this study are very uniform in size.

Their cross section is circular and the diameter does not vary by more than 0.2 μm over the test length. In contrast, polymer fiber diameters often vary by as much as 1 μm over the test length. If the diameter varies by more than 0.2 μm from the average over the test length the bending test results are viewed as invalid.

All variables in Table 3.2A are necessary to calculate the bending modulus. The slope of the bending load-deflection plot is calculated by linear or polynomial regression. The error from the fit is negligible, but repeated tests on the same glass or AS4 fibers show a variation of approximately 1%. Span and midspan measurements with the SEM are accurate to within a few microns so the test dimensions are not a major source of error, unless the test pieces are not positioned correctly in the SEM for the measurement.

The tensile modulus is used to determine the compressive modulus from the bending stiffness, according to Equation 3.9. The most significant errors in the calculation of the compressive modulus comes from the radius, because of its fourth power dependence in the equations for the centroidal moment of inertia, and from the tensile modulus, because of its multiple and variable appearances via the shift factor.

3.3.2. Sources of Error: Testing System

Friction and Alignment

Glass fibers are isotropic, well characterized, and have a very uniform cross-section so 36 tests were run on them to calibrate the Micro- Flex Test. The average modulus was 72.4 GPa (10.5 Msi), with a standard deviation of 0.1, or 0.84%. This result, which matches the literature value,[56] shows that the assumption of frictionless bearings is valid and that errors from misalignment and videomicrometer precision are minimal. The primary source of error is the nonuniformity of the fiber cross section as described by the measured radius.

In a later series, glass fibers which had been FITT tested were bend tested. The results of 15 Micro-Flex tests match the FITT results, sample by sample, within the

propagated error (See Figure 3.12) It should be noted that the modulus determinations were independent, literally: neither was used to calculate the other.

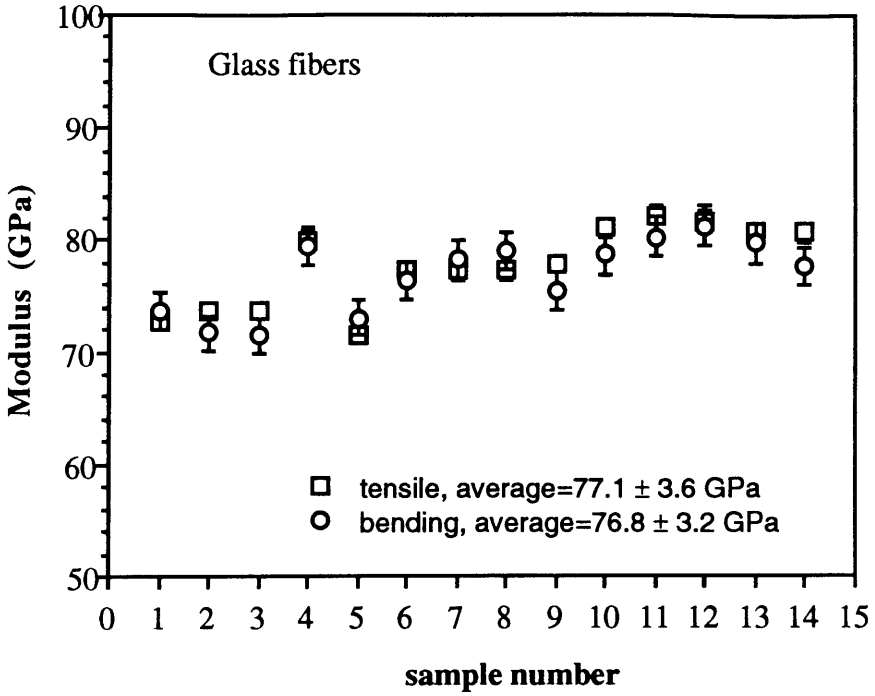

Figure 3.12. Glass Fibers sequentially FITT and Micro-Flex tested. Measurements confirm isotropic mechanical behavior

Physical setup

If the fiber is not horizontal when placed in the apparatus, the span and midspan distances increase by a factor equal to the secant of the angle with the horizontal. Before each test this angle is checked visually against a permissible maximum of 8° which had been set with a protractor. At angles less than 8°, the dimension increases are within the error of the dimension measurements themselves.

Load probe centering is a time- consuming but necessary step. An eccentricity of 2-3% is easily observable and is corrected before testing. An eccentricity of 2% raises the error in the bending modulus from ±3.4% to ±4.4%. The eccentricity of 2% also increases the error both in the compressive modulus and in the compressive stress from approximately ±6% to approximately ±8%.

3.3.3. Propagation of Error:

Representative test results and the corresponding errors for each fiber type are presented in Table 3.3A, B and C for pitch- and PAN- based carbon and Kevlar fibers, respectively. The total error for each property is given as a percentage below that property and these are averaged for each fiber family. Generally, the error in the tensile modulus is ±1.6%, the error in the bending modulus is ±3.5%, and the error in the compressive modulus is ±6%. The errors in the bending, compressive and tensile strains are less than ±2%, and the error in the compressive stress is essentially the same as the error in the compressive modulus, since the error in the strain is so small.

Compressive strain and stress values for the Kevlar samples correspond to kink band formation or failure by softening. The bending stress at which the analysis is performed for the PAN- and pitch- based fibers is listed in the last column. AS4 and HMS4 are analyzed at 0.4% bending strain to compare with the manufacturer's data. The IM7 and IM8 fibers did not reach 0.4% bending strain during the tests, so the analysis is performed at 0.3% strain. P25 is analyzed at 0.6% bending strain, the point at which the tensile modulus is approximately constant. The P55 and P75 fibers are analyzed at 0.2% bending strain because tensile modulus data are not available at higher strains.

Table 3.3A. Error Calculation results for representative tests on pitch- based carbon fiber. Percent error is listed below each measured value.

Fiber Type	**Et** (GPa)	**Eb** (GPa)	**Ec** (GPa)	**Ec/Et** (%)	**c-strain** (MPa)	**c-stress**	**bending strain**
P25	126.7	83.0	57.6	0.45	0.72	412.5	0.6%
6/21.10B	±1.6%	±3.4%	±5.3%	±2.5%	±1.6%	±5.5%	
P55	454.7	283.6	190.3	0.42	0.24	461.3	0.2%
7/21.20B	±1.6%	±3.4%	±5.2%	±2.3%	±1.6%	±5.4%	
P75	549.0	305.4	189.6	0.35	0.25	477.0	0.2%
7/21.11B	±1.6%	±3.4%	±5.0%	±1.8%	±1.6%	±5.2%	
avg. of total error	**±1.6%**	**±3.4%**	**±5.2%**	**±2.2%**	**±1.6%**	**±5.4%**	

Table 3.3B. Error Calculation results for representative tests on PAN- based carbon fibers. Percent error is listed below each measured value.

Fiber Type	**Et** (GPa)	**Eb** (GPa)	**Ec** (GPa)	**Ec/Et** (%)	**c-strain** (MPa)	**c-stress**	**bending strain**
AS4	255.3	199.0	158.7	0.62	0.45	710.1	0.4%
6/25.4B	±1.6%	±3.5%	±6.0%	±3.8%	±1.7%	±6.2%	
IM7	313.1	226.8	170.4	0.54	0.35	588.0	0.3%
6/27.5B	±1.6%	±3.5%	±5.7%	±3.2%	±1.6%	±6.0%	
IM8	353.6	270.0	211.6	0.60	0.34	716.6	0.3%
6/27.11B	±1.6%	±3.5%	±5.9%	±3.7%	±1.6%	±6.1%	
HMS4	360.5	294.1	244.8	0.68	0.44	1073.9	0.4%
6/21.5B	±1.6%	±3.4%	±5.9%	±4.3%	±1.6%	±6.1%	
avg. of total error	**±1.6%**	**±3.5%**	**±5.9%**	**±3.8%**	**±1.6%**	**±6.1%**	

Table 3.3C. Error Calculation results for representative tests on Kevlar fibers. Percent error is listed below each measured value.

Fiber Type	**Et** (GPa)	**Eb** (GPa)	**Ec** (GPa)	**Ec/Et** (%)	**c-strain** (MPa)	**c-stress**	**bending strain**
Kevlar 119	73.0	51.8	38.3	0.52	0.50	192.7	fail
6/19.3B	±1.6%	±3.4%	±5.5%	±3.0%	±1.6%	±5.7%	
Kevlar 29	75.4	60.5	49.5	0.66	0.48	237.5	fail
6/13.11B	±1.6%	±3.4%	±5.9%	±4.0%	±1.6%	±6.1%	
Kevlar 129	105.7	73.4	53.4	0.51	0.46	243.9	fail
6/14.2B	±1.6%	±3.4%	±5.5%	±2.9%	±1.6%	±5.7%	
Kevlar 49	133.3	78.8	51.0	0.38	0.81	414.8	fail
6/20.10B	±1.6%	±3.4%	±5.5%	±3.0%	±1.6%	±5.7%	
Kevlar 149	170.3	90.4	54.5	0.32	0.55	300.5	fail
6/19.10B	±1.6%	±3.4%	±4.8%	±1.6%	±1.6%	±5.1%	
avg. of total error	**±1.6%**	**±3.4%**	**±5.4%**	**±2.9%**	**±1.6%**	**±5.7%**	

3.4. Results

3.4.1. Glass Fiber

Micro- Flex tests were performed on E- glass fibers for system calibration. The results are linear- elastic and repeatable. A typical load- deflection curve is shown in Figure 3.13 for two sections of the FITT tested fiber reported in Section 2.4. The slight offset from the origin of the load-deflection curves has been corrected by subtracting the y-intercept of the equation for the load-deflection data before converting to stress using Equations 3.7 and 3.8. Figure 3.14 is the bending stress-strain curve. The bending and tensile stress-strain curves from the fiber are shown in Figure 3.15: the stress-strain behaviors are identical, confirming that glass is an isotropic material.

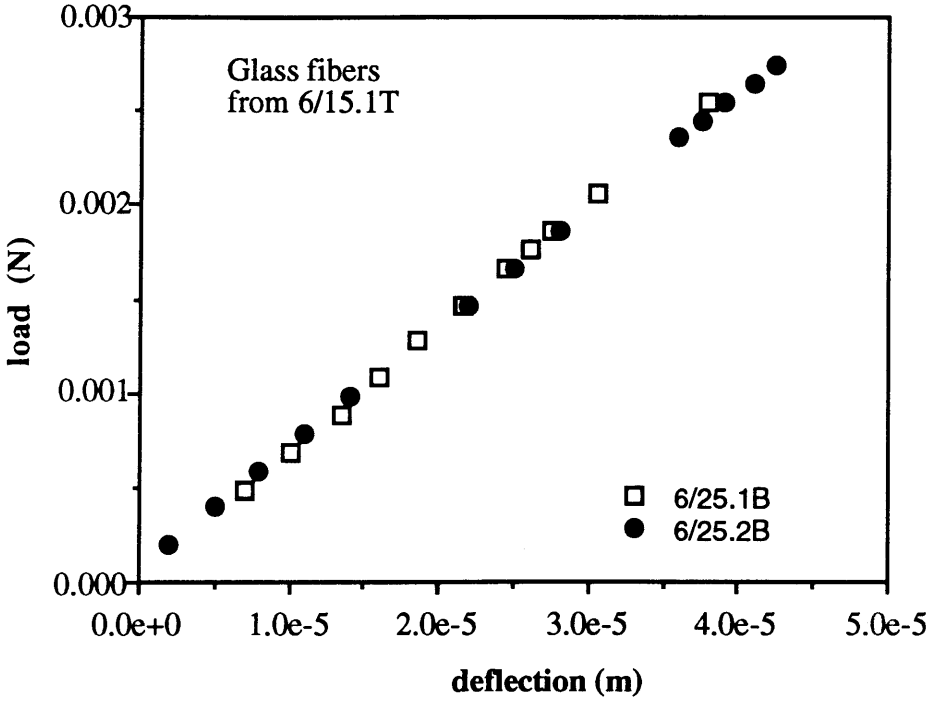

Figure 3.13. Load- deflection curve for two sections of glass fiber from the same FITT loop specimen.

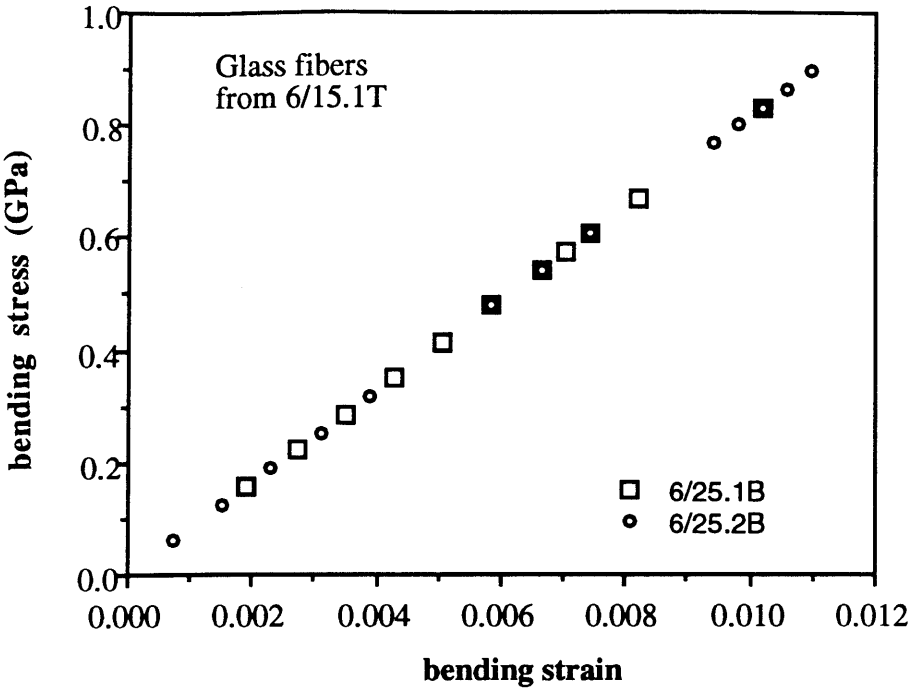

Figure 3.14. Bending stress-strain behavior of glass fibers is linear.

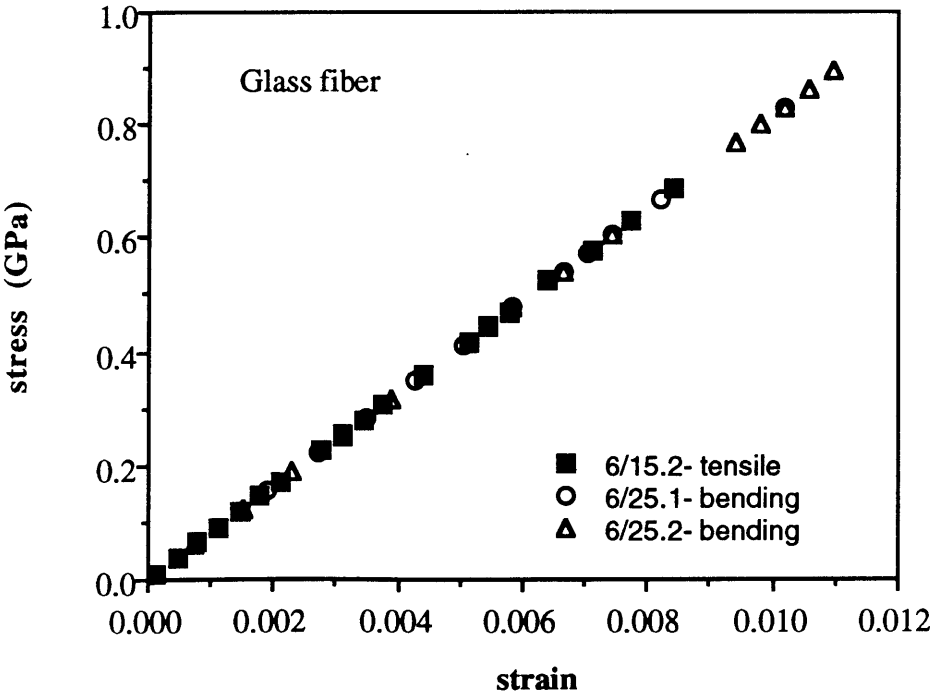

Figure 3.15. Glass fibers exhibit the same linear stress-strain behavior in tension and in bending.

3.4.2. Kevlar Fibers

Figures 3.16 and 3.17 are typical load-deflection and bending stress-strain curves for Kevlar 119. Overlaying the tensile stress-strain curve (Figure 3.18) emphasizes the anisotropy which increases after kink formation. The average tensile, bending and compressive modulii at three strains are presented in Table 3.4. At zero strain, the fiber bending and tensile are essentially the same. This means the compressive modulus also has that value, and therefore it is not calculated from the bending and tensile data at zero strain. At 0.15% strain, the bending modulus has decreased to 74% of the tensile modulus, but the most noticeable change in bending modulus is after large scale kink formation. At approximately 0.39% bending strain, kinks are visible and the compressive modulus has dropped to 56% of the tensile modulus. On average, compressive failure in the six samples occurs at 0.45% strain and 178.1 MPa (25.8 ksi) ± 11.6%. Figures 3.19 and 3.20 show the measured tensile, bending, and compressive modulii at 0.15% bending strain and at the compressive failure strain. Figure 3.21 shows the measured compressive failure stress compared to the compressive failure strain.

Table 3.4. Tensile, Bending and Compressive modulii of Kevlar 119 fiber at three strains. Results are the average of tests on six samples, standard deviations are given.

Modulus	zero strain	0.15% bending strain	compressive failure strain
Tensile (GPa)	71.9±2.6	71.9 ±2.6	71.9 ±2.6
(Msi)	10.4±0.4	10.4±0.4	10.4±0.4
Bending (GPa)	67.4±4.3	61.3±3.6	52.6±2.3
(Msi)	9.8±0.6	8.9±0.5	7.6±0.3
Compressive (GPa)	(isotropic)	52.9±6.1	39.9±3.7
(Msi)		7.7 ±0.9	5.8±0.5

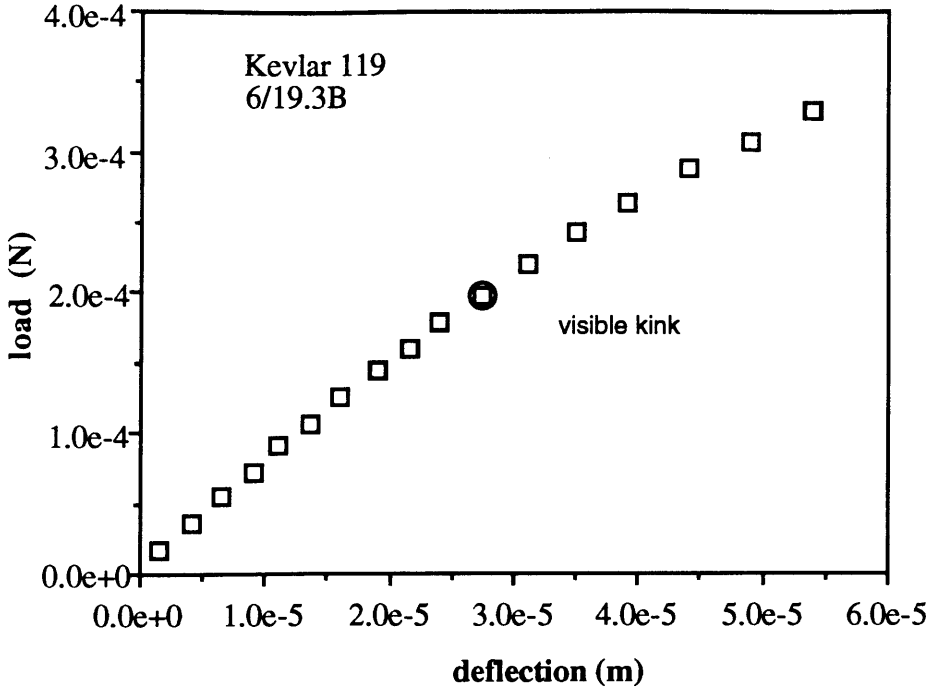

Figure 3.16. Load-deflection curve for Kevlar 119 fiber with diameter of 10.9 μm. Test span is 666 mm, midspan is 90 μm. Significant nonlinearity and visible kink formation coincide.

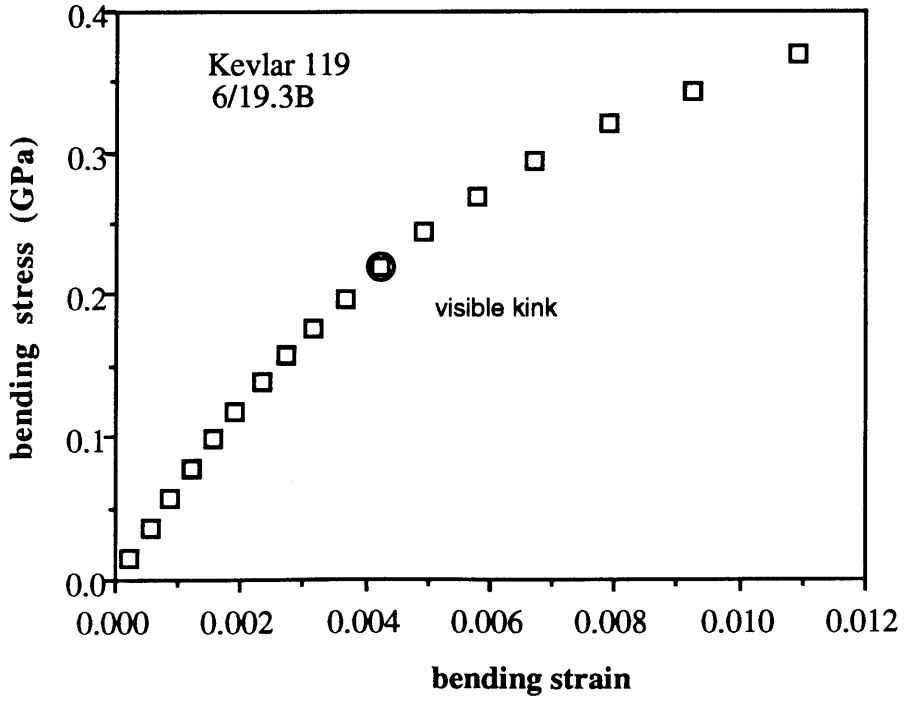

Figure 3.17. Bending stress-strain curve for Kevlar 119 fiber.

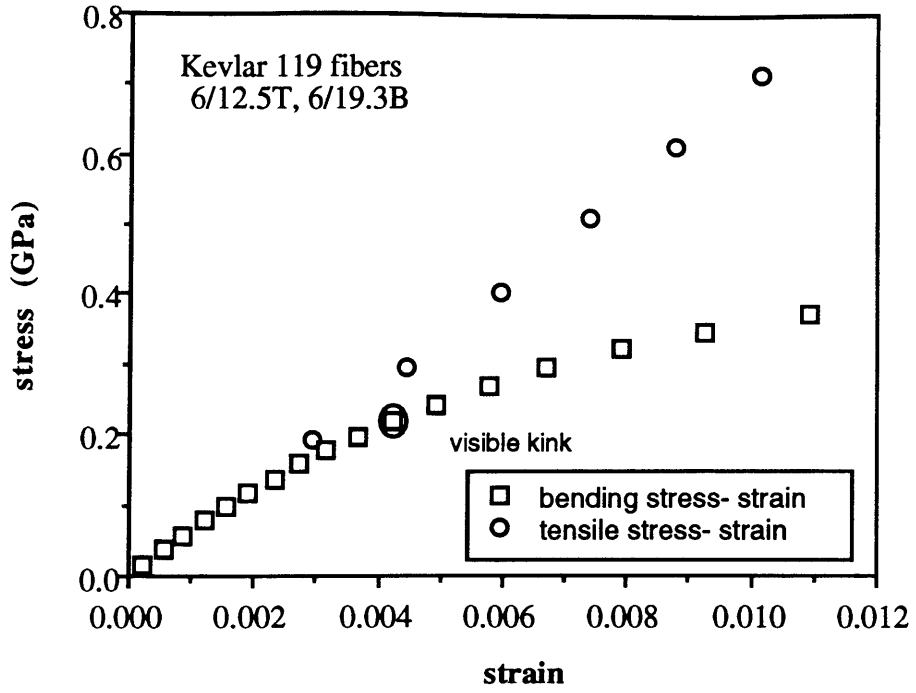

Figure 3.18. FITT and Micro-Flex stress-strain curves for Kevlar 119. Obvious anisotropy appears just before visible kink band formation.

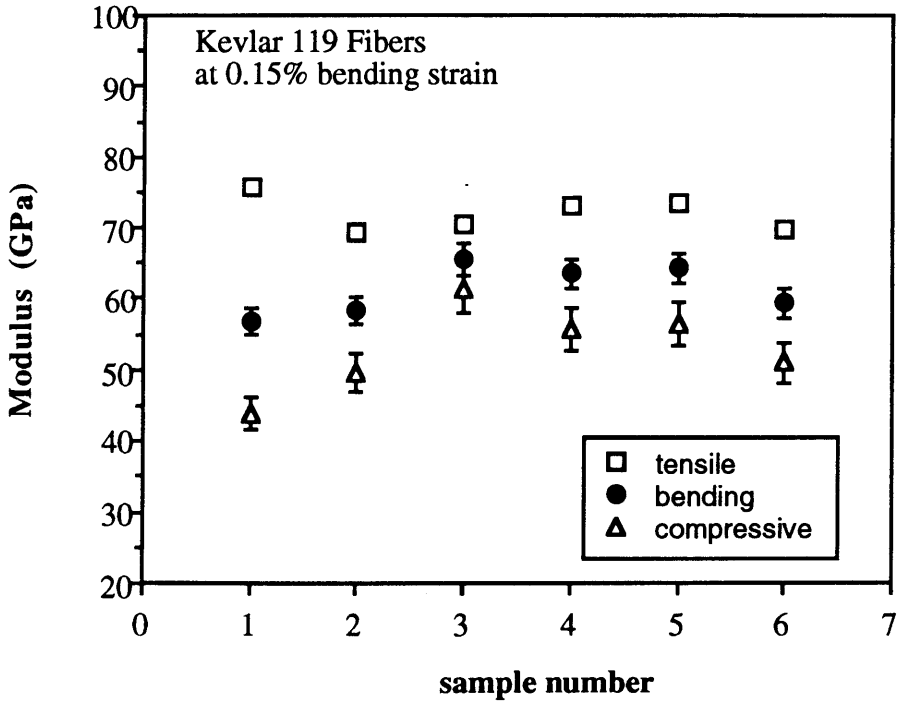

Figure 3.19. Measured tensile, bending and compressive modulii of Kevlar 119 fibers at 0.15% bending strain.

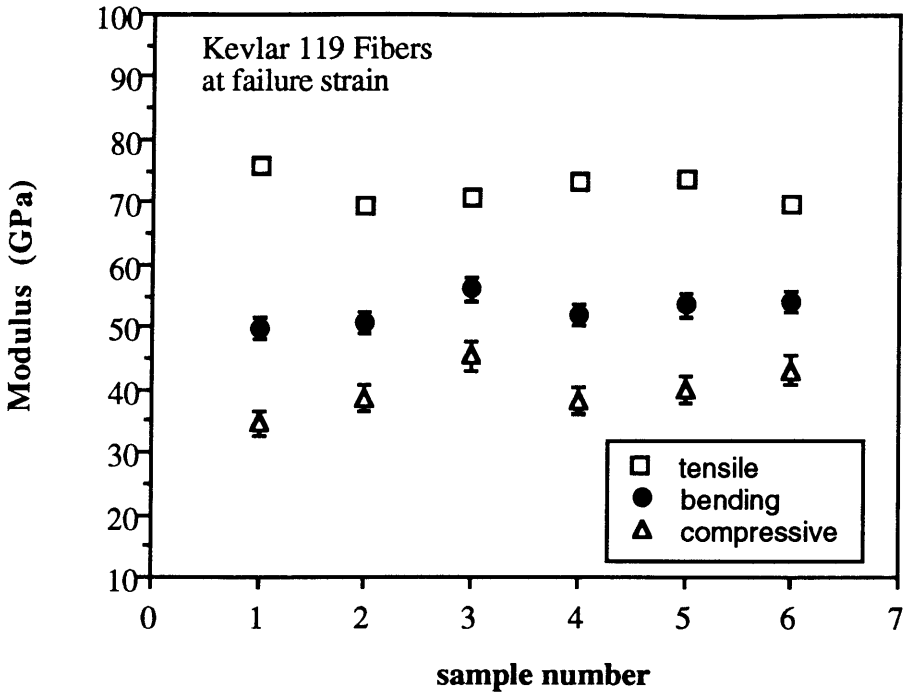

Figure 3.20. Measured tensile, bending and compressive modulii of Kevlar 119 fibers at the failure strain.

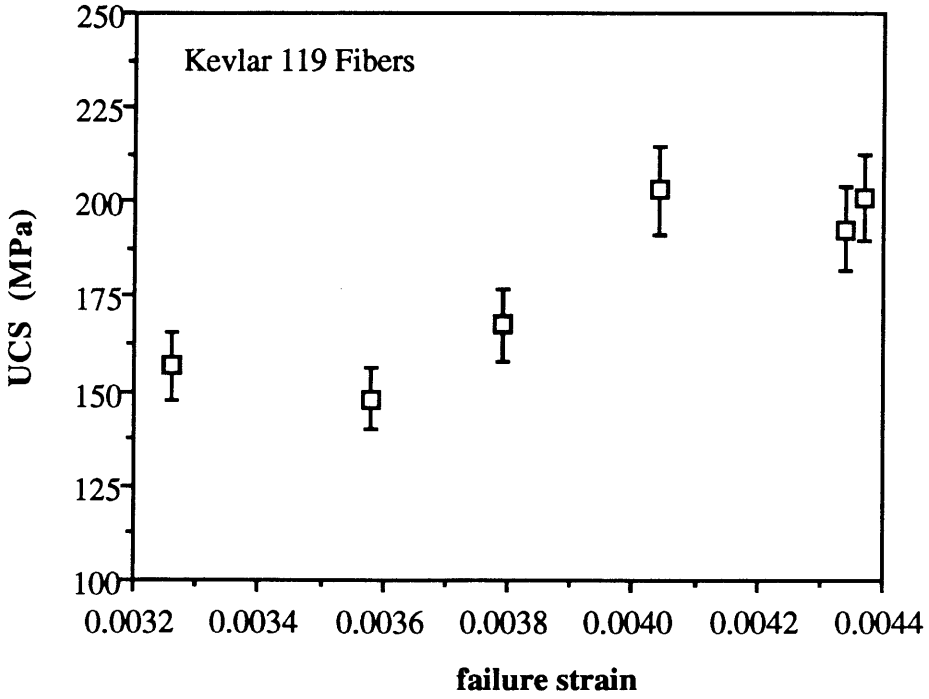

Figure 3.21. Kevlar 119 measured compressive strength versus compressive strain for six different fibers. (Error bars denote propagated error.)

The load-deflection and bending stress-strain curves for a typical Kevlar 29 fiber are shown in Figures 3.22 and 3.23. Comparing the bending and tensile stress-strain curves, Figure 3.24, indicates the fiber is isotropic at low strains, but the bending stiffness greatly decreases after kink band formation. Average measured modulii at zero-, 0.15%- and the failure strain are presented in Table 3.5. At approximately 0.42% bending strain, kinks are visible and the compressive modulus has dropped to 59% of the tensile modulus. Compressive failure in the twelve samples corresponds to 0.48% strain and 229.3 MPa (33.3 ksi) ± 18.1%. Figures 3.25 and 3.26 show the measured tensile, bending, and compressive modulii at 0.15% bending stress and at the compressive failure strain. Single kinks which develop before full compressive failure comprise the low stress data in Figure 3.27; the higher stress data represents sudden multiple kinks.

Table 3.5. Modulus of Kevlar 29 fibers before and after kink band formation. Results are the average of tests on twelve samples, standard deviations are given.

Modulus	zero strain	0.15% bending strain	compressive failure strain
Tensile (GPa)	76.7±3.7	78.4 ±3.8	81.1 ±4.5
(Msi)	11.1±0.5	11.4±0.6	11.8±0.7
Bending (GPa)	85.4±9.1	75.8±7.0	61.3±3.6
(Msi)	12.4±1.3	11.0±1.0	8.9±0.5
Compressive (GPa)	(isotropic)	73.8±12.2	47.8±4.4
(Msi)		10.7 ±1.8	6.9±0.6

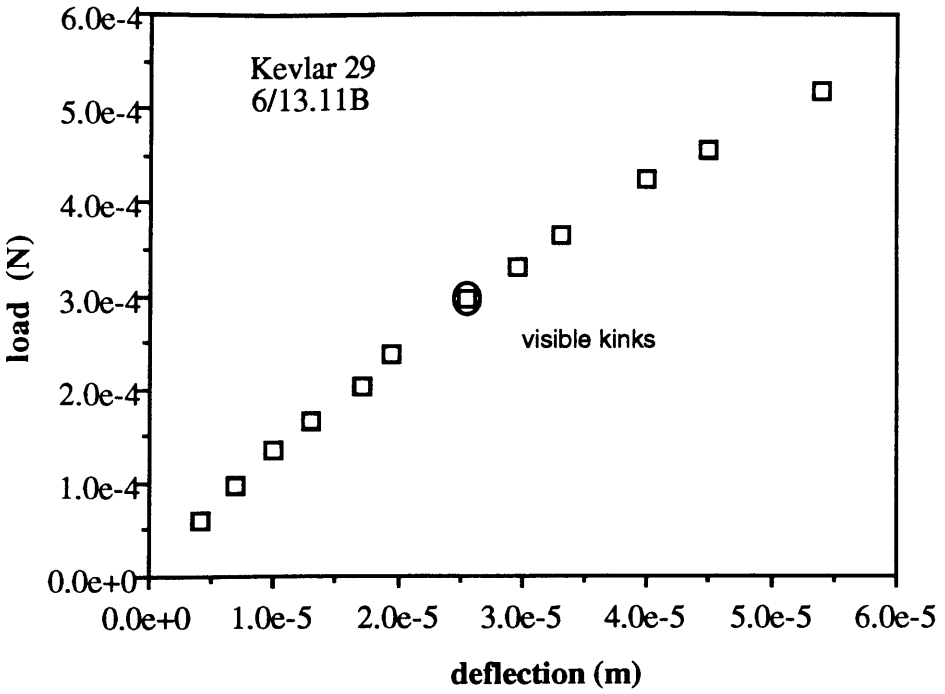

Figure 3.22. Load- deflection curve of 11.8 μm diameter Kevlar 29 fiber. Micro- Flex span = 666 μm, midspan = 90 μm.

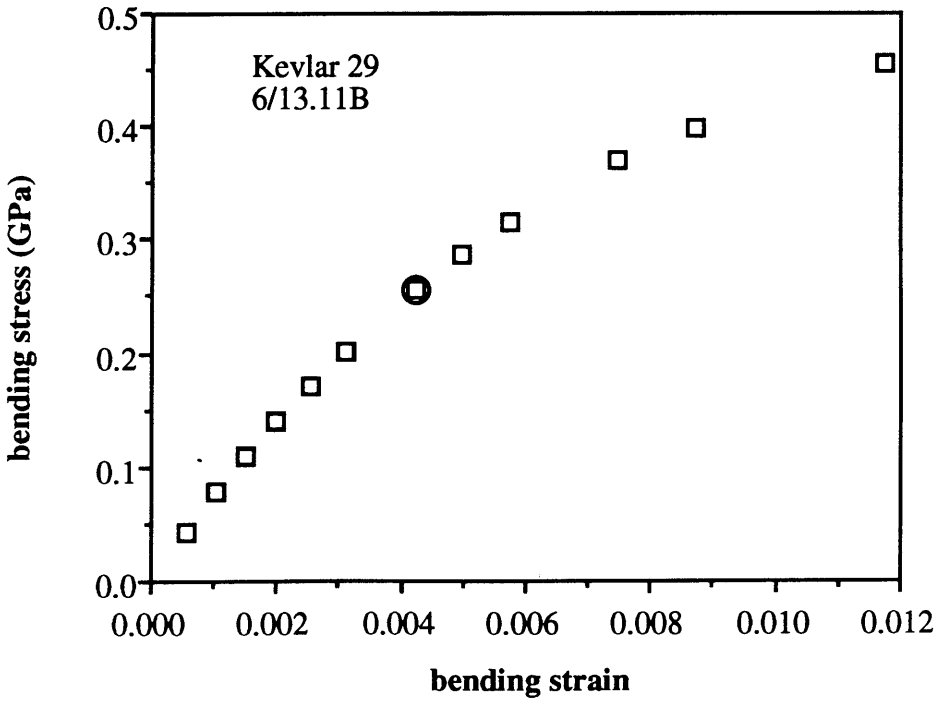

Figure 3.23. Bending stress-strain curve calculated from collected data in Figure 3.22. Circled mark indicates visible kink bands.

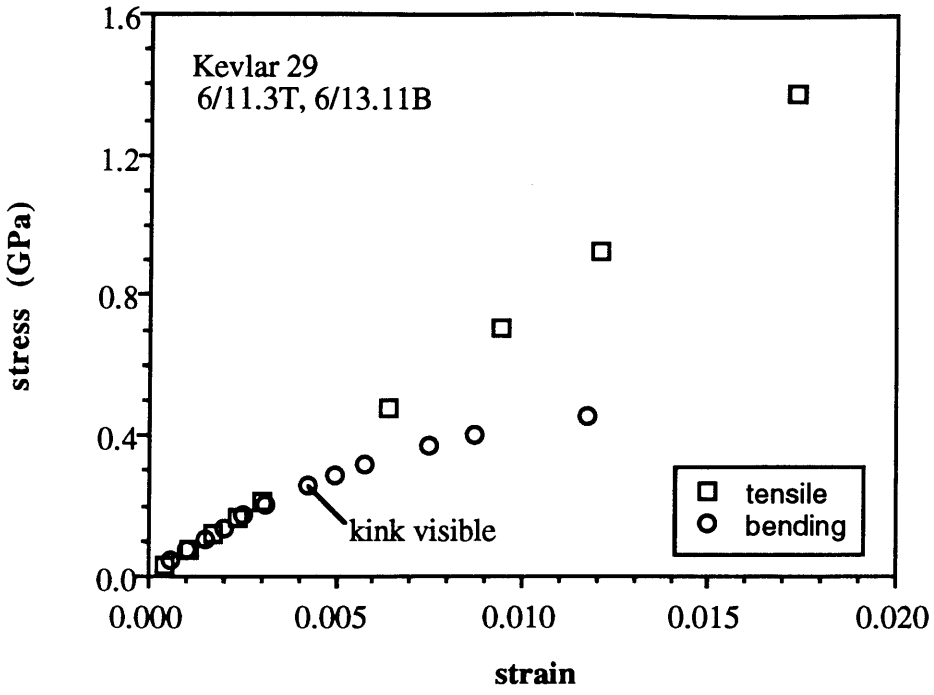

Figure 3.24. Stress- strain curves for Kevlar 29 fiber tested sequentially in tension and bending. Fiber is isotropic until kink band formation at approximately 0.4% strain.

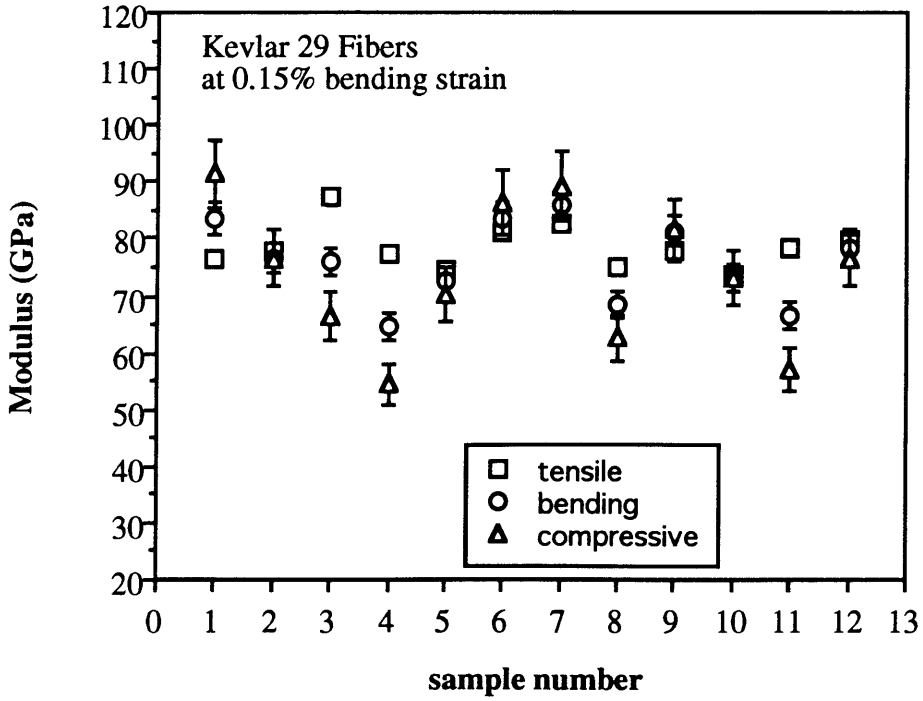

Figure 3.25. Measured tensile and bending modulii and calculated compressive modulii for twelve Kevlar 29 samples. Fiber is essentailly isotropic at low strain.

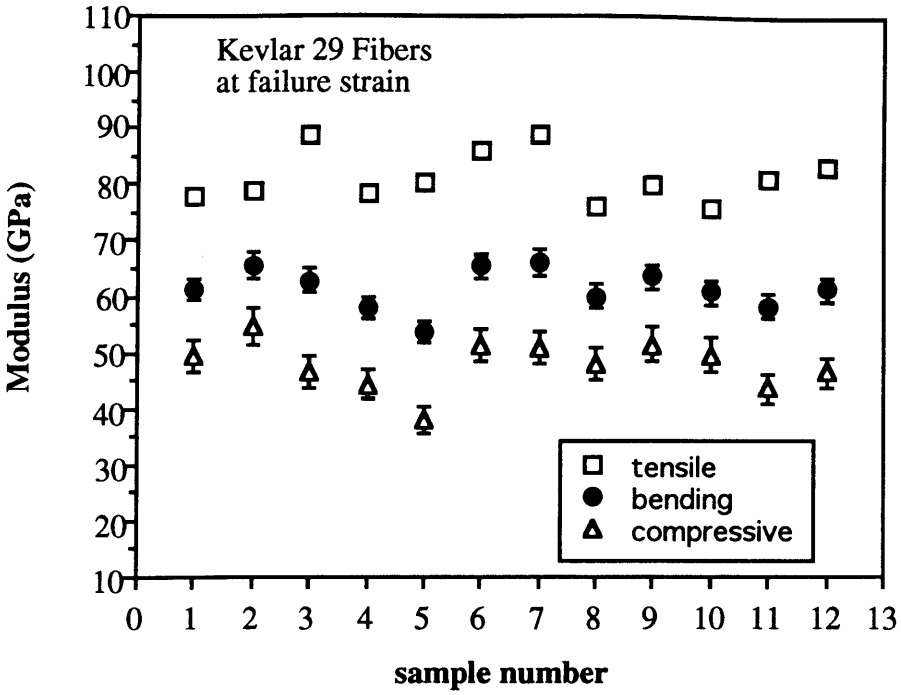

Figure 3.26. Measured bending modulus of Kevlar 29 fibers at compressive failure strain is approximately 75% of the measured tensile modulus. Calculated compressive modulus is approximately 60% of the tensile modulus.

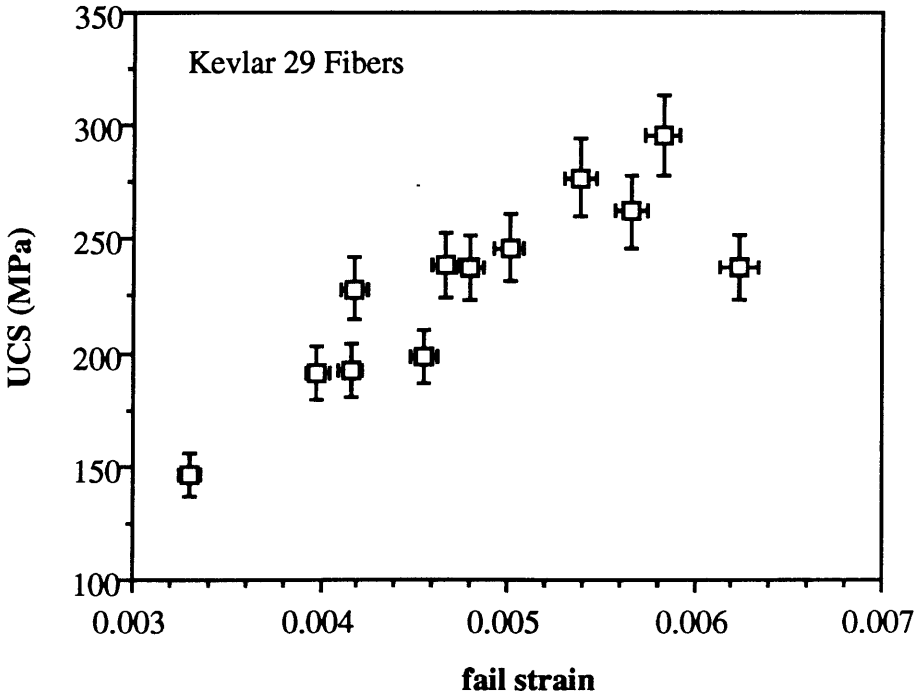

Figure 3.27. Compressive stress and strain at kink band formation for twelve Kevlar 29 fibers tested in bending.

The load-deflection and bending stress-strain curves for a typical Kevlar 129 fiber are shown in Figures 3.28 and 3.29. The fiber behavior deviates from isotropy before noticeable kink band formation (Figure 3.30). The average measured modulii at zero-, 0.15%- and the failure strain are presented in Table 3.6. At approximately 0.38% bending strain, kinks are visible; this corresponds to a compressive strain of 0.44% and a compressive stress of 228.4 MPa (33.1 ksi) ± 13.3%. Figures 3.31 and 3.32 show the measured tensile, bending, and compressive modulii at 0.15% bending strain and at the compressive failure strain. Figure 3.33 shows the measured compressive failure stress compared to the compressive failure strain.

Table 3.6. Modulus of Kevlar 129 fibers before and after kink band formation. Results are the average of tests on six samples, standard deviations are given.

Modulus	zero strain	0.15% bending strain	compressive failure strain
Tensile (GPa)	94.1 ±6.7	96.2 ±6.5	99.0 ±6.6
(Msi)	13.6 ±1.0	14.0 ±0.9	14.4 ±1.0
Bending (GPa)	89.1 ±8.2	81.0 ±6.7	70.0 ±4.4
(Msi)	12.9 ±1.2	11.7 ±1.0	10.2 ±0.6
Compressive (GPa)		69.5 ±10.0	51.9 ±6.0
(Msi)		10.1 ±1.5	7.5 ±0.9

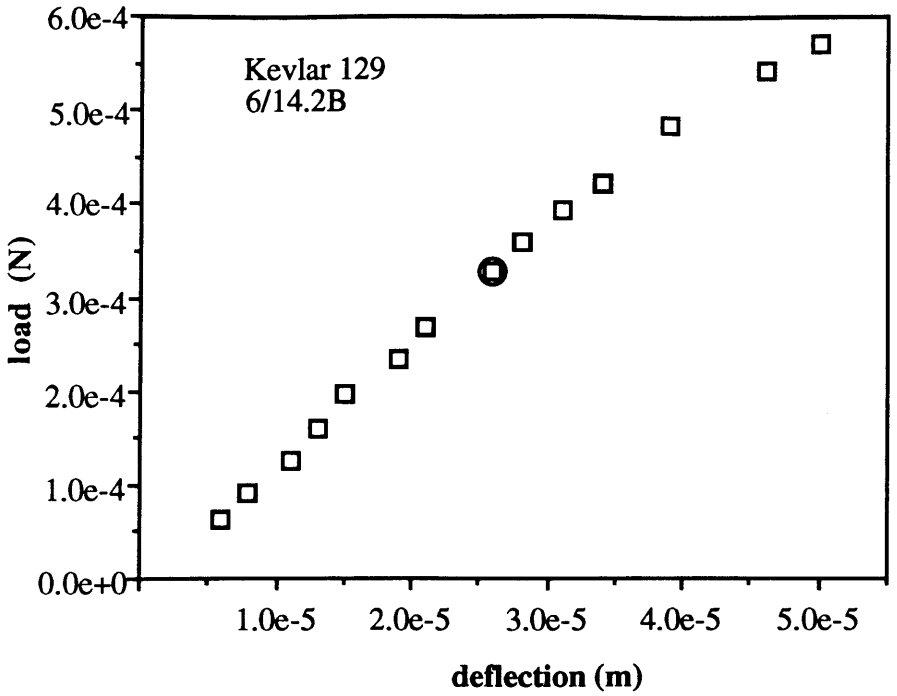

Figure 3.28. Load -deflection curve of a Kevlar 129 fiber with diameter 11.9 μm. Test span = 666 μm, midspan = 90 μm. Kinks observed at circled mark.

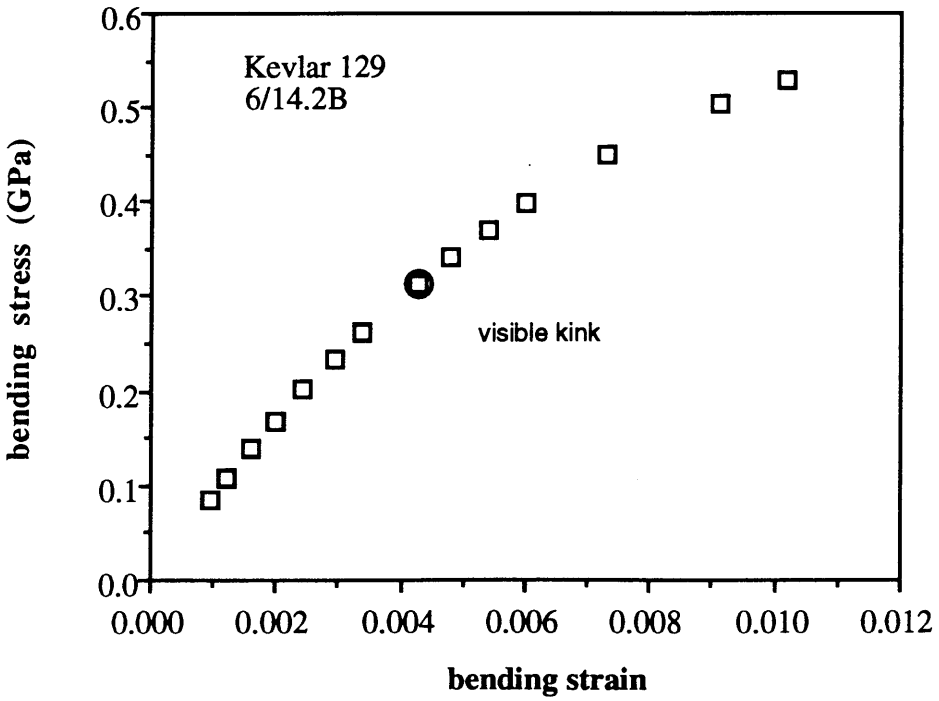

Figure 3.29. Bending stress-strain curve from data shown in Figure 3.28. Significant nonlinearity occurs after kink band formation.

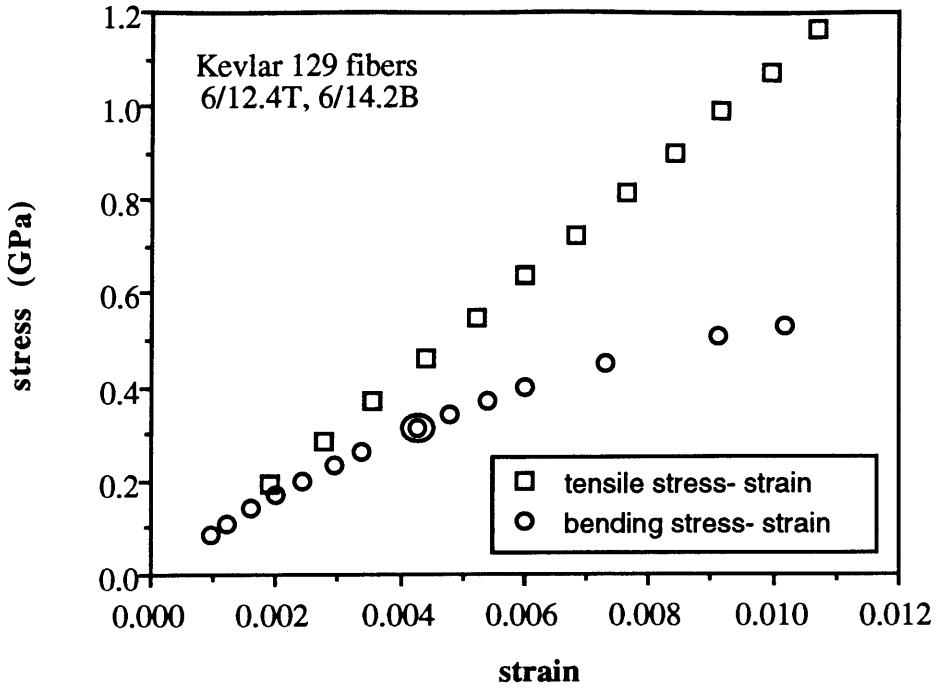

Figure 3.30. Tensile and bending stress- strain curves for a typical Kevlar 129 fiber. Anisotropic behavior begins before kink band are seen, circled mark.

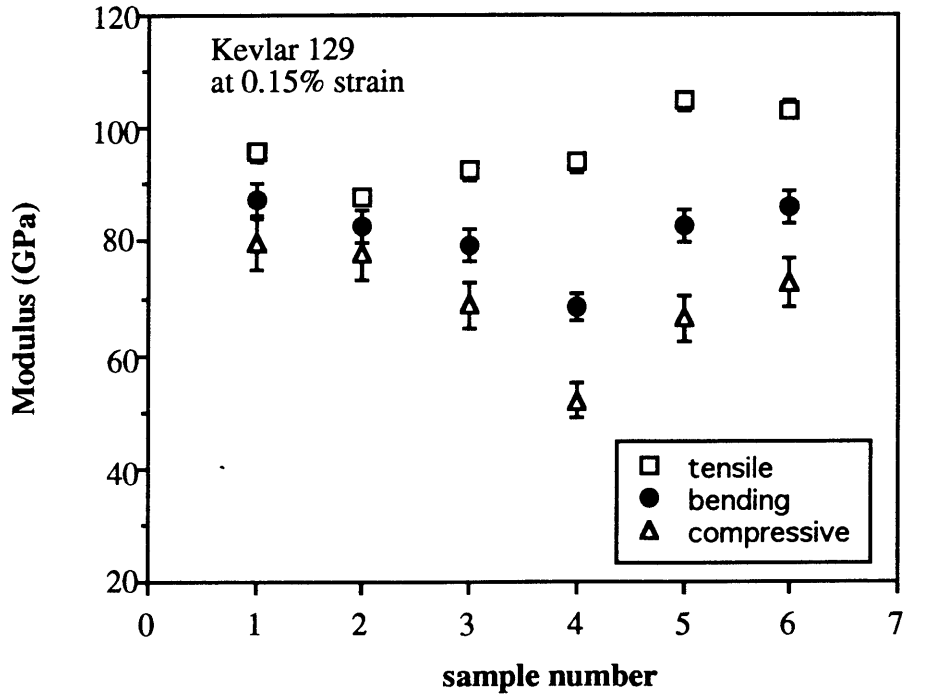

Figure 3.31. Tensile, bending and compressive modulii of Kevlar 129 fibers at 0.15% bending strain. The average bending and compressive modulii are 84% and 73% of the average tensile modulus.

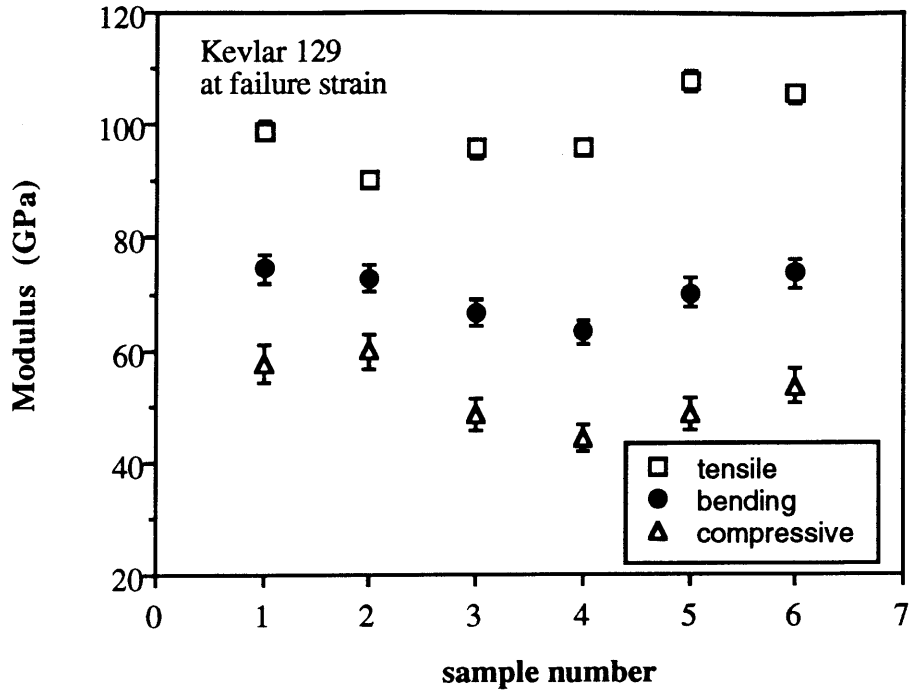

Figure 3.32. Tensile, bending and compressive modulii of Kevlar 129 fibers at the compressive failure strain, approximately 0.45%. The average bending and compressive modulii are 71% and 53% of the average tensile modulus.

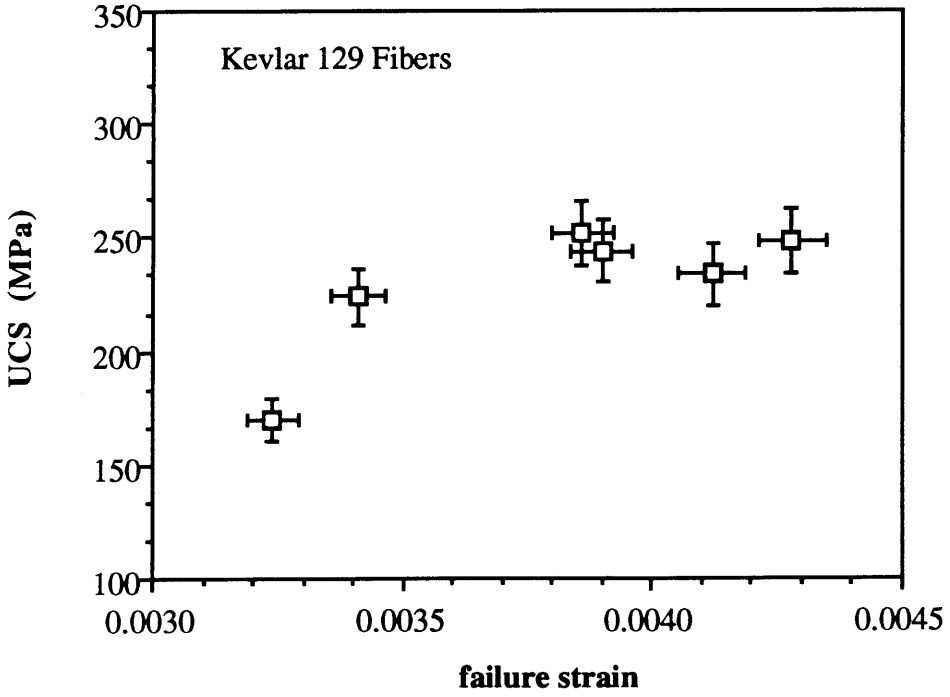

Figure 3.33. Compressive failure stress and strain, defined by large scale kink formation and significant deviation from linearity in the bending stress- strain curve.

Figures 3.34 and 3.35 are typical load-deflection and bending stress-strain curves for Kevlar 49. Overlaying the tensile stress-strain curve (Figure 3.36) shows that pronounced anisotropy exists both before and after kink formation. In Table 3.7, the average tensile, bending and compressive modulii of nine Kevlar 49 samples are listed along with the standard deviation of the data. Though the fiber appears to be isotropic at low strains, the bending modulus has decreased to 82% of the tensile modulus at 0.15% strain and then to 65% of the tensile modulus at the failure strain. The compressive modulus decreases to 69% of the tensile modulus at 0.15% bending strain and 46% of the tensile modulus at the failure strain, which is approximately 0.51% bending strain or 0.62% compressive strain. The average stress for visible kink band formation is 335.3 MPa (48.6 ksi) ± 32.9%. Figures 3.37 and 3.38 show the measured tensile, bending, and compressive modulii at 0.15% bending strain and at the compressive failure strain. Figure 3.39 shows the measured compressive failure stress and the compressive failure strain for nine different samples.

Table 3.7. Tensile, Bending and Compressive modulii of Kevlar 49 fiber at three strains. Results are the average of tests on nine samples, standard deviations are given.

Modulus	zero strain	0.15% bending strain	compressive failure strain
Tensile (GPa)	128.5 ±7.1	128.5 ±7.1	128.5 ±7.1
(Msi)	18.6 ±1.1	18.6 ±1.1	18.6 ±1.1
Bending (GPa)	117.9 ±15.5	106.1 ±12.7	84.0 ±12.5
(Msi)	17.1 ±2.3	15.4 ±1.8	12.3 ±1.8
Compressive (GPa)	(isotropic)	89.3 ±16.0	59.0 ±14.1
(Msi)		13.0 ±2.3	8.6 ±2.0

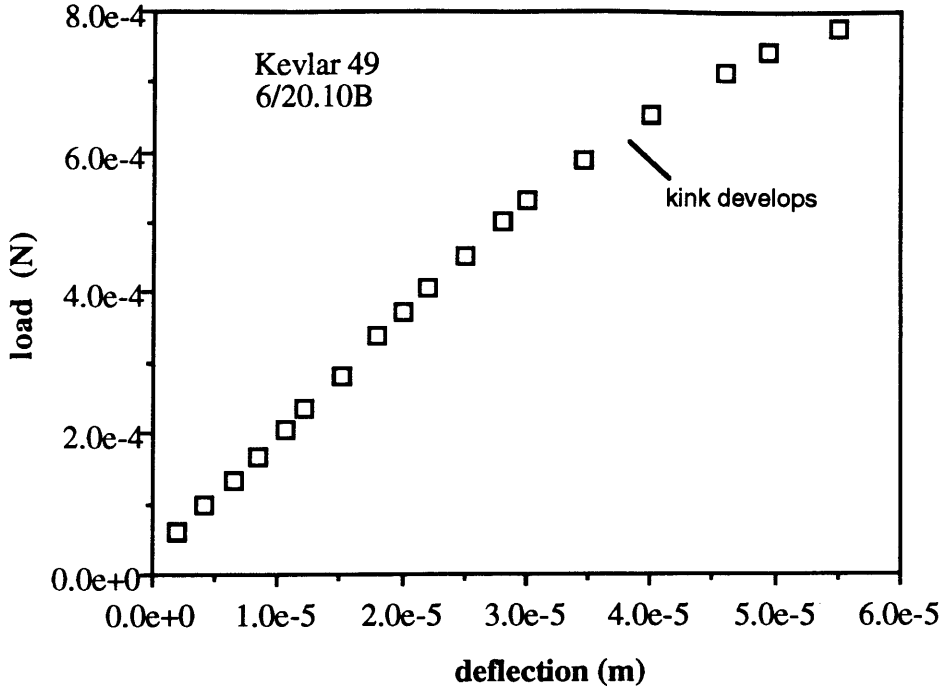

Figure 3.34. Load deflection curve of an 11.8 μm diameter Kevlar 49 fiber. Micro-Flex test span = 666 μm, midspan = 90 μm.

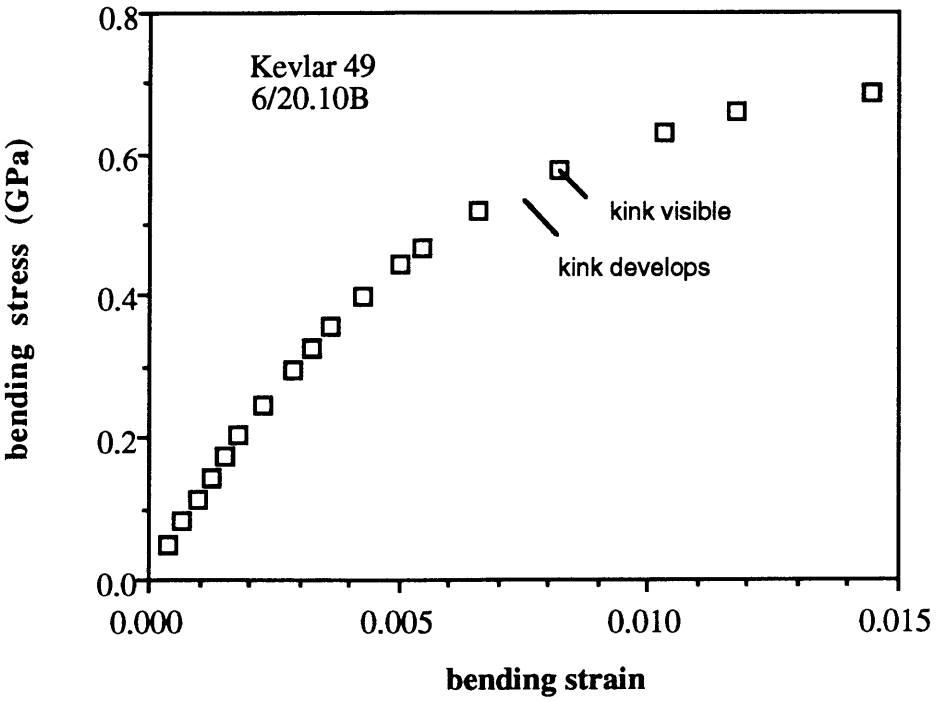

Figure 3.35. Bending stress-strain curve for Kevlar 49 fiber in figure 3.34. Fiber softens gradually until fully developed kink is observed, then load- carrying ability levels off.

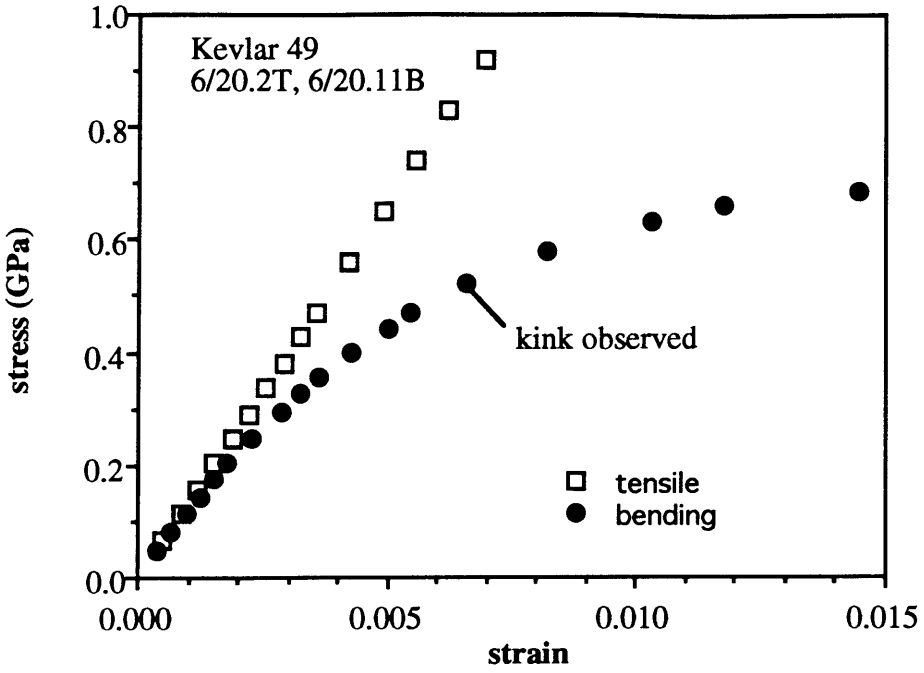

Figure 3.36. Tensile and Bending stress- strain curves for a typical Kevlar 49 fiber. The fiber deviates from linear, isotropic behavior before kinks are large enough to observe.

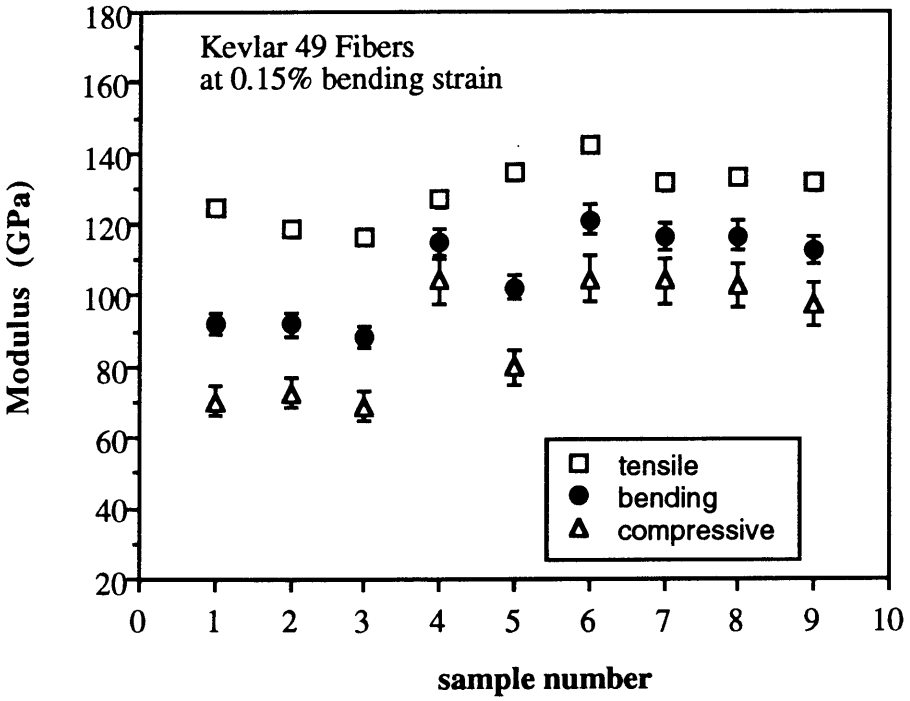

Figure 3.37. Kevlar 49 tensile, bending and compressive modulii at 0.15% bending strain. Bending modulus is 75-90% of the tensile modulus, while the compressive modulus is 55- 80% of the tensile modulus.

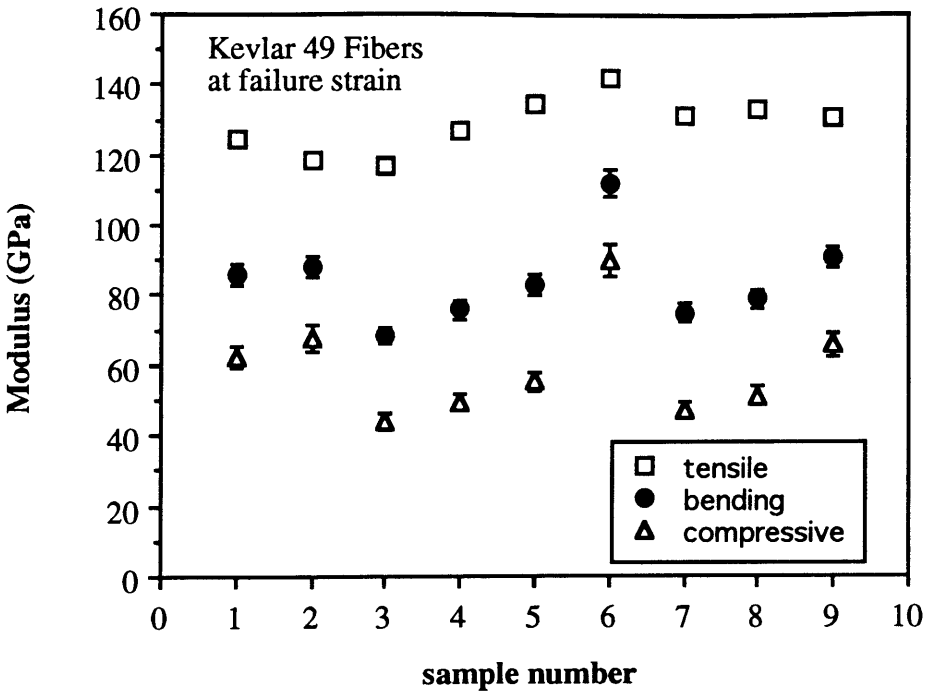

Figure 3.38. Modulii of Kevlar 49 fibers in tension, bending and compression. Measured bending modulus is 60-75% of the measured tensile modulus, which gives a compressive modulus 40-60% of the tensile modulus.

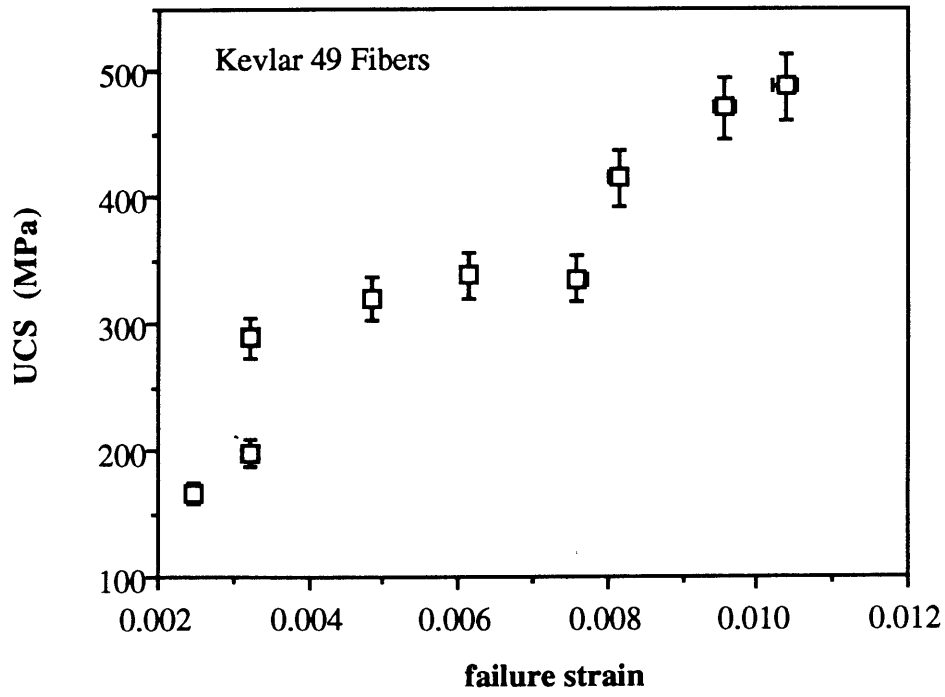

Figure 3.39. The strength of Kevlar 49 fibers increases as the strain before failure increases. Since failure is defined as the onset of large scale kink band formation, single kinks in various stages of development are responsible for this trend.

The load- deflection behavior of a typical section of Kevlar 149 fiber is given in Figure 3.40. The curvature of the bending stress- strain curve, Figure 3.41, is very strong, and when compared to the tensile stress strain curve, Figure 3.42, it indicates a highly oriented and anisotropic structure. No kinks are observed during bending, though the fiber load- carrying ability does reach a limit. The average modulii in tension, bending and compression are given in Table 3.8, based on eight samples of Kevlar 149. The modulii of each of the samples at 0.15% bending strain is presented graphically in Figure 3.43. Since kink bands were not observed during the test, failure is defined as the onset of significant nonlinearity in the bending stress- strain curve. The modulii of the eight samples are shown in Figure 3.44, while the compressive stress and corresponding strains are shown in Figure 3.45. The average stress at nonlinearity is 306.2 MPa (44.4 ksi) ± 10.3%. This corresponds to an average bending strain of 0.44% and an average compressive strain of 0.56%.

Table 3.8. Tensile, Bending and Compressive modulii of Kevlar 149 fiber at three strains. Results are the average of tests on eight samples, standard deviations are given.

Modulus	zero strain	0.15% bending strain	compressive failure strain
Tensile (GPa)	153.3 ±3.8	161.3 ±3.4	172.3 ±2.3
(Msi)	22.2 ±0.6	23.4 ±0.5	25.0 ±0.3
Bending (GPa)	152.7 ±3.6	127.3 ±2.8	84.0 ±12.5
(Msi)	22.1 ±0.5	18.5 ±0.4	12.3 ±1.8
Compressive (GPa)	(isotropic)	102.5 ±4.3	56.4 ±8.7
(Msi)		14.9 ±0.6	8.2 ±1.3

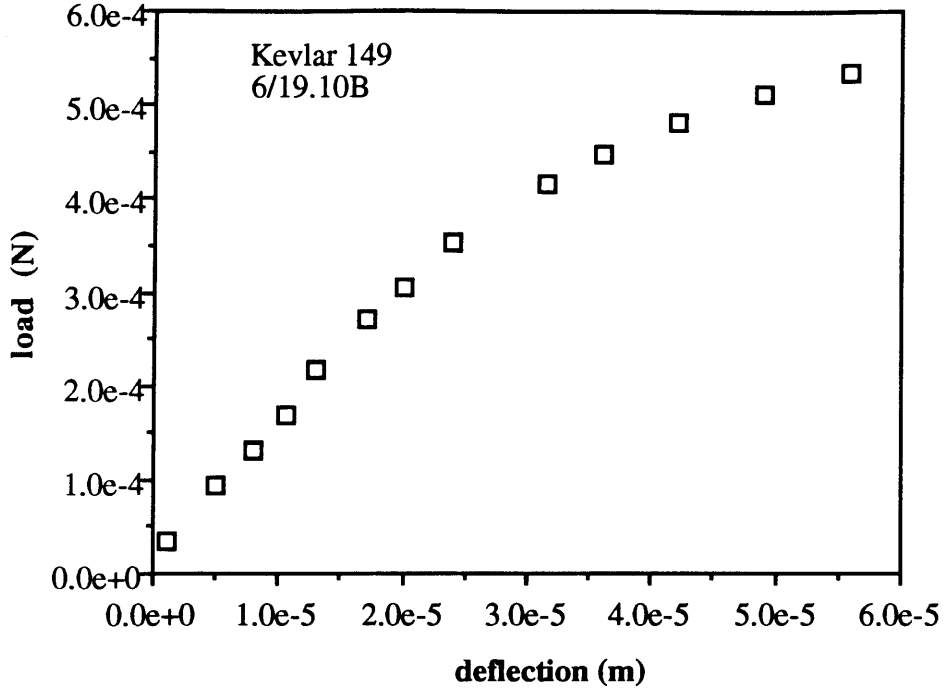

Figure 3.40. Load -deflection curve for a typical section of Kevlar 149 fiber. Fiber diameter is 10.9 μm. Test span is 666 μm, midspan is 90 μm.

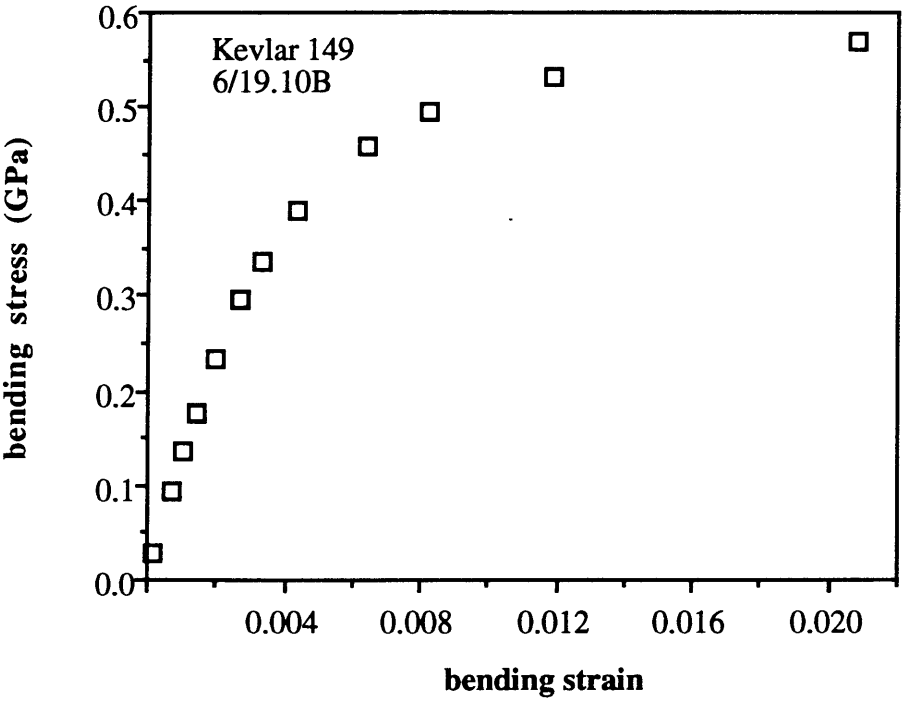

Figure 3.41. Bending stress- strain curve from load- deflection data in Figure 3.40. Curvature is significant, especially above 0.4% strain.

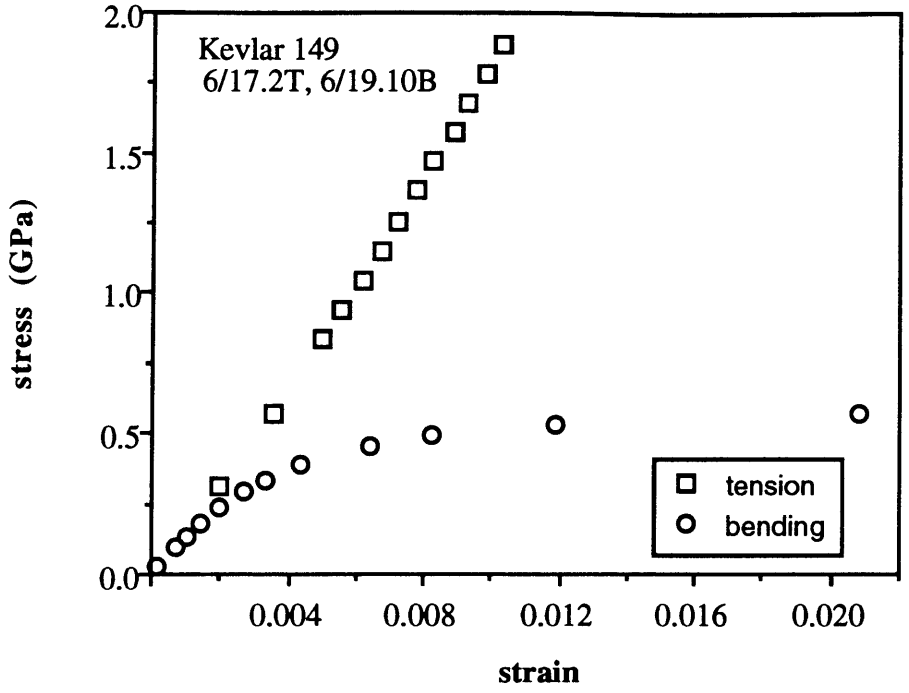

Figure 3.42. Both the tensile and bending stress strain curves show significant curvature, but the two coincide at strains less than 0.2%.

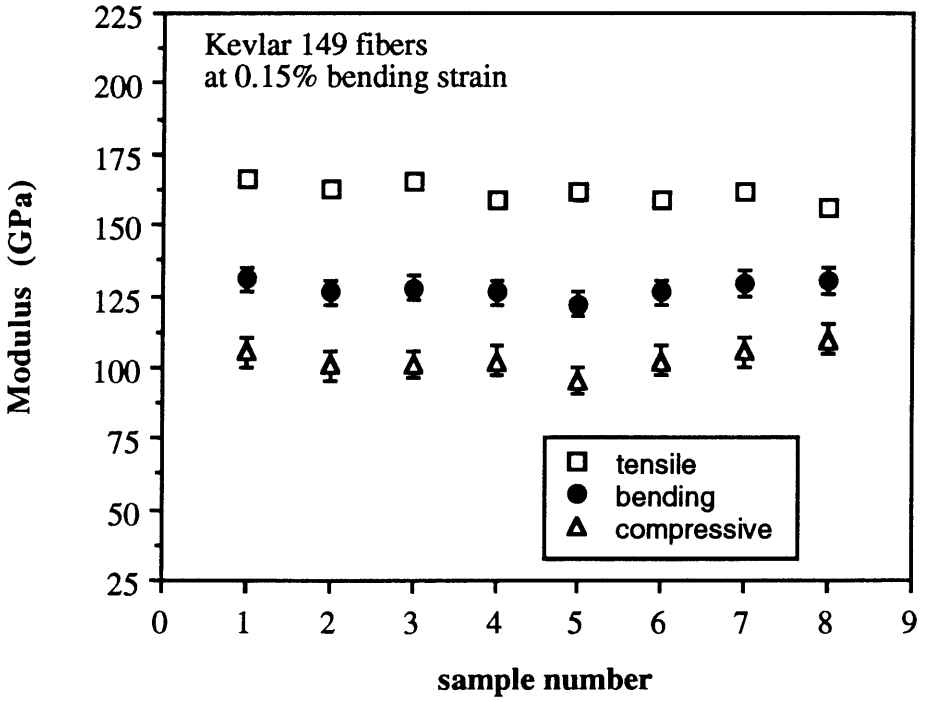

Figure 3.43. The bending and compressive modulii of Kevlar 149 fibers are approximately 80% and 65% of the tensile moduli at 0.15% bending strain.

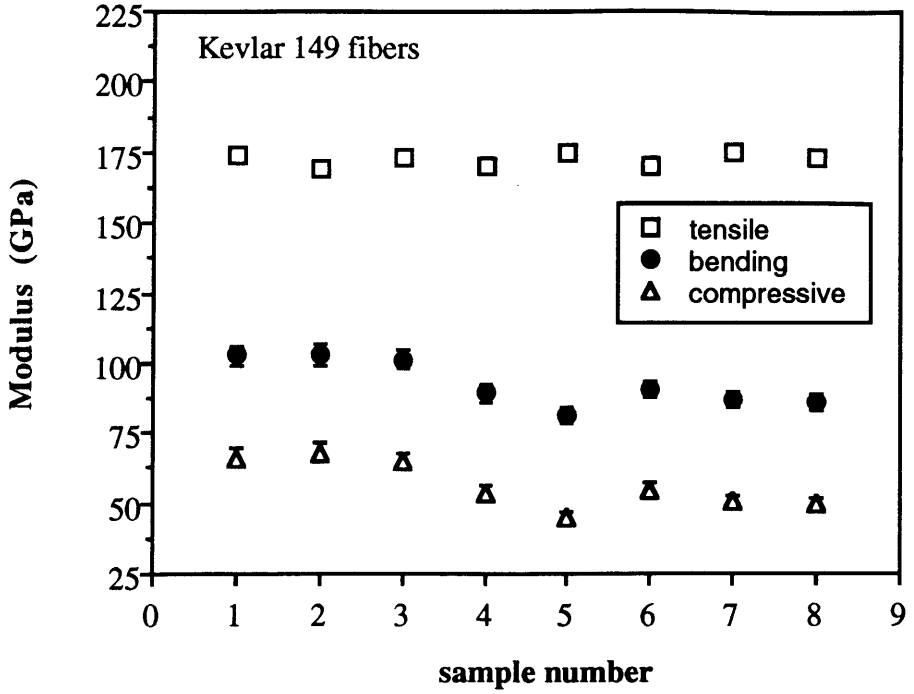

Figure 3.44. The bending and compressive modulii of Kevlar 149 fibers have dropped to approximately 55% and 33% of the tensile modulii when significant nonlinearity in the bending stress- strain curve is apparent.

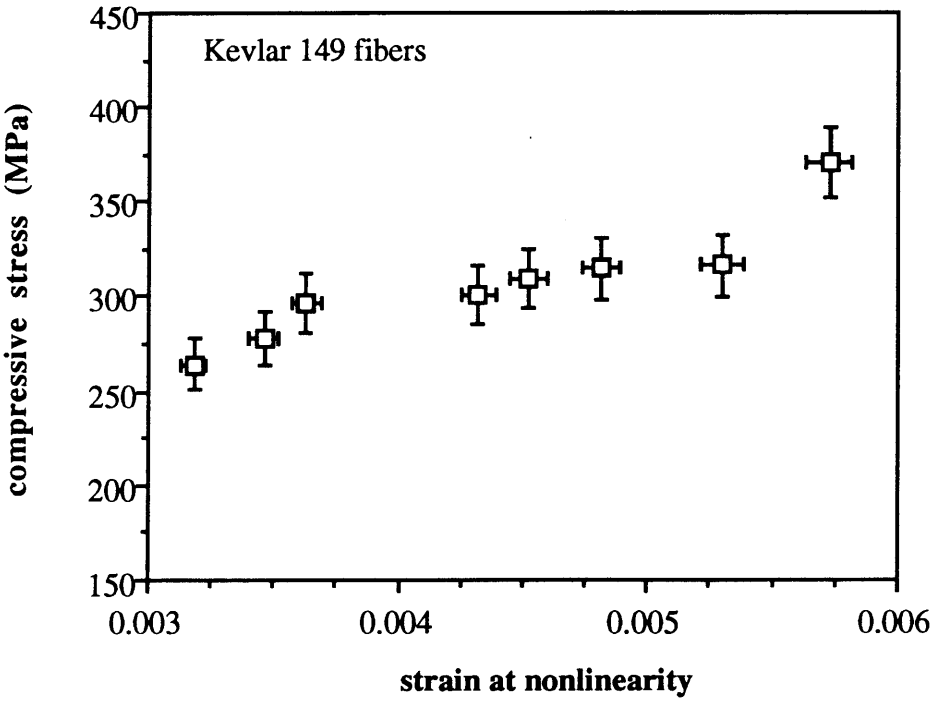

Figure 3.45. Compressive stress at which significant nonlinearity in the bending stress-strain curve occurs is approximately constant, even as the compressive strain at nonlinearity varies.

3.4.3. Carbon Fibers

PAN-based

The load-deflection curves of PAN- based fibers have slight downward curvature, in contrast to the slight upward curvature of the tensile stress strain curves. The standard AS4 fiber exhibits only slight softening with strain in bending (Figures 3.46 and 3.47). At low strains the fiber behavior is isotropic, as seen in Figure 3.48 but at strains higher than approximately 0.3%, the tensile and bending stress-strain curves diverge, indicating a decreasing compressive modulus. Ten samples of AS4 were tested in tension and bending. The measured tensile and bending modulii and the calculated compressive modulii are presented graphically in Figures 3.49 and 3.50 for the fibers at 0.1% and 0.4% bending strain. These should be compared to Figure 3.12 to emphasize the anisotropy observed at higher strains. The average modulus values at the two strains are given in Table 3.9. At 0.1% bending strain the bending and compressive modulii are 90-95% and 80-95% of the tensile modulii, respectively. At 0.4% bending strain, the bending modulii are 70-85% of the tensile modulii, which corresponds to compressive modulii 55-70% of the tensile modulii.

Table 3.9. Average tensile, bending and compressive modulii of AS4 fibers at 0.1% and 0.4% bending strain.

Modulus	0.1% bending strain	0.4% bending strain
Tensile (GPa)	246.3 ±7.0	258.4 ±6.5
(Msi)	35.7 ±1.0	37.5 ±0.9
Bending (GPa)	227.4 ±11.5	201.8 ±8.1
(Msi)	33.0 ±1.7	29.3 ±1.2
Compressive (GPa)	213.6 ±18.1	158.1 ±12.7
(Msi)	31.0 ±2.6	22.9 ±1.8

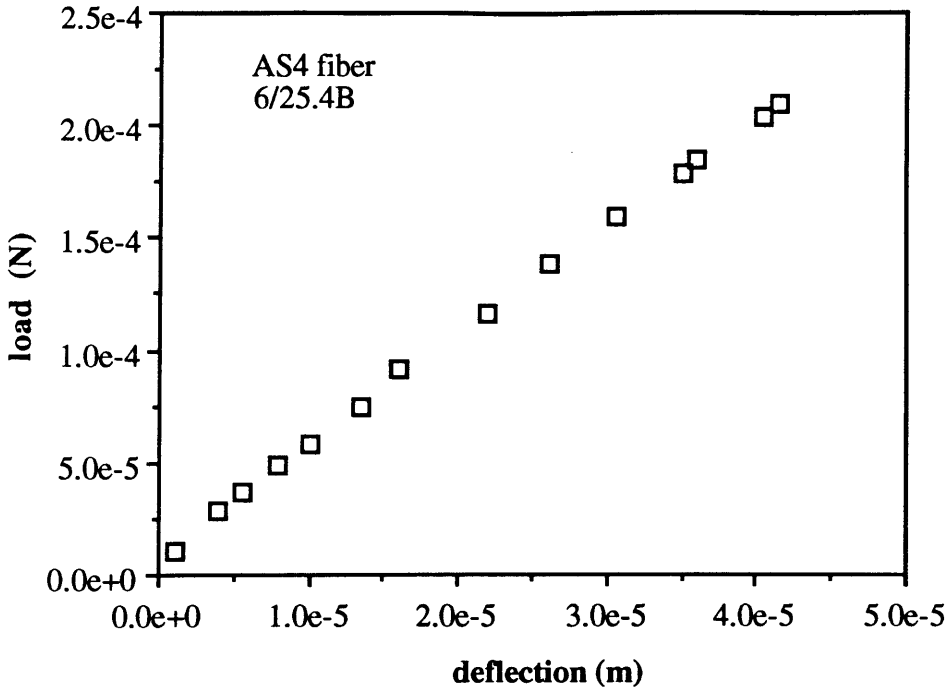

Figure 3.46. Load- deflection curve for typical AS4 fiber. Fiber diameter is 6.24 μm. Test span is 542 μm, midspan is 90 μm,

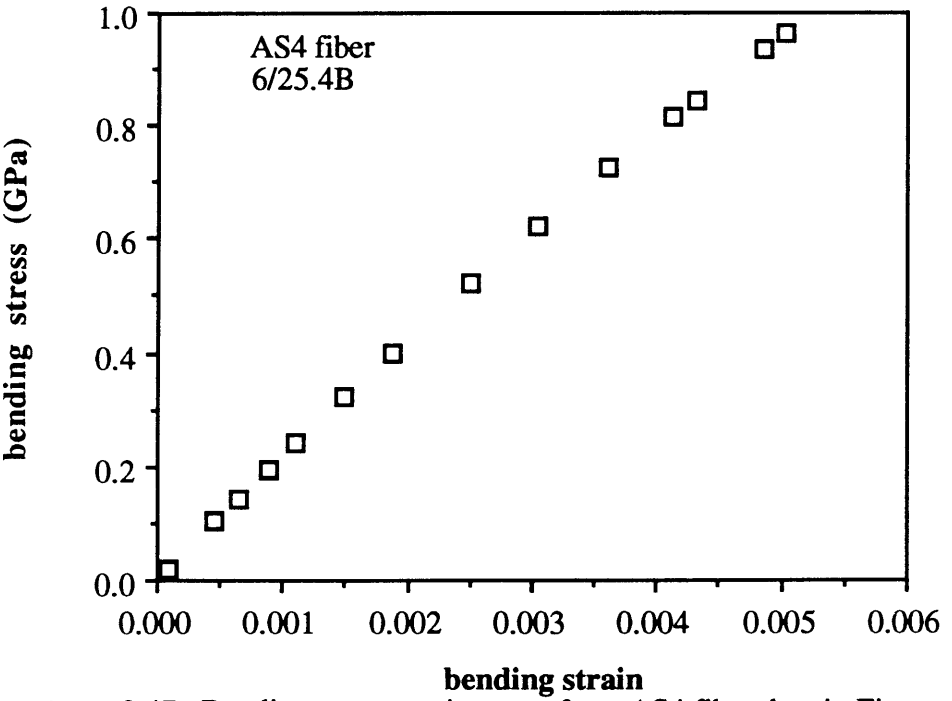

Figure 3.47. Bending stress-strain curve from AS4 fiber data in Figure 3.46. Fiber exceeds deflection limits before failure occurs.

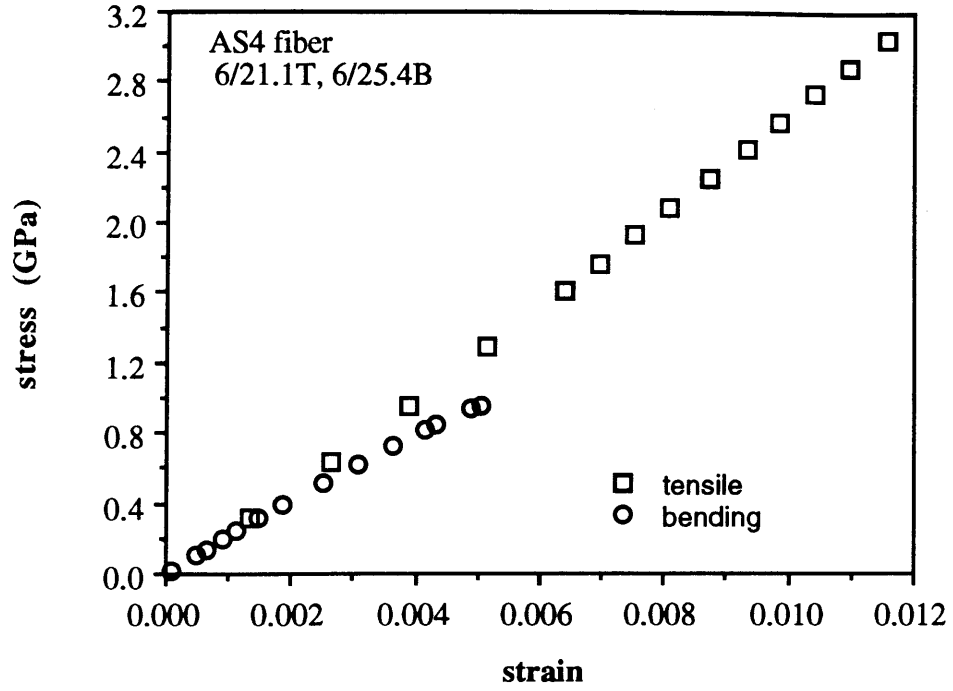

Figure 3.48. Tensile and bending stress- strain curves for a typical AS4 fiber. Fiber behavior is isotropic at low strains. No sign of damage or change is visible when anisotropy develops.

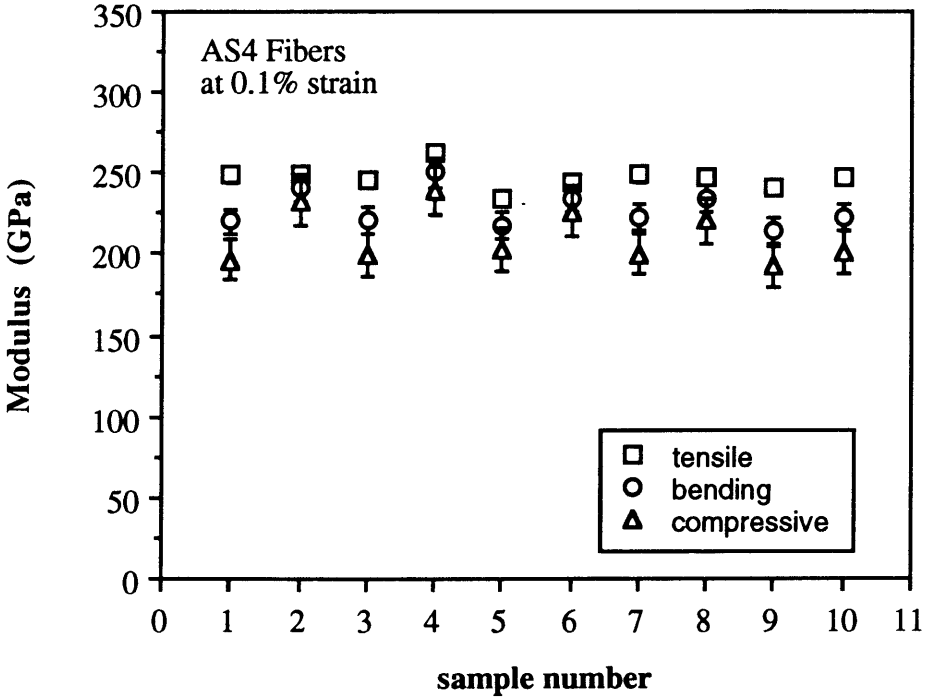

Figure 3.49. Fiber modulus in tension is only slightly greater than in bending and compression at 0.1% bending strain.

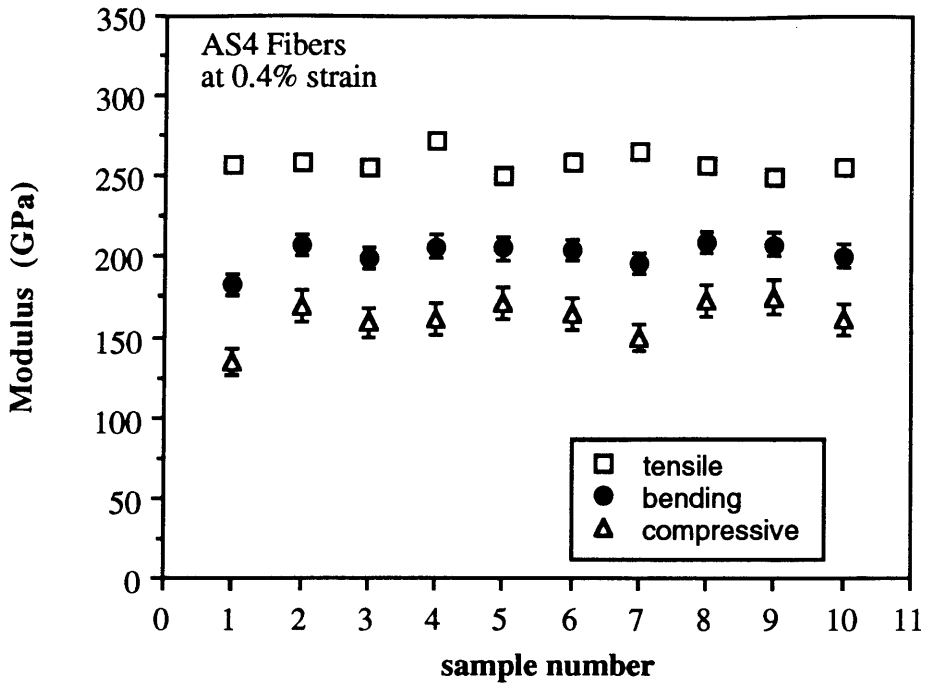

Figure 3.50. The bending modulus and tensile modulus no longer coincide at 0.4% bending strain. The compressive modulus is approximately 60% of the tensile modulus for all the samples.

Intermediate modulus IM7 and IM8 fibers have very small diameters (4-6 μm) and reach the deflection limit under low loads, as seen in Figure 3.51. The bending stress-strain behavior is shown in Figure 3.52 and it deviates from the tensile behavior above approximately 0.1% strain. See Figure 3.53. The average modulii in tension, bending and compression at 0.1% and 0.3% bending strains are presented in Table 3.10, while the values for the six samples are shown in Figures 3.54 and 3.55.

Table 3.10. Average tensile, bending and compressive modulii of six IM7 fibers at 0.1% and 0.3% bending strain.

Modulus	0.1% bending strain	0.3% bending strain
Tensile (GPa)	279.4 ±21.7	290.8 ±20.4
(Msi)	40.5 ±3.1	42.2 ±3.0
Bending (GPa)	236.1 ±8.9	225.7 ±9.3
(Msi)	31.7 ±2.2	32.7 ±1.3
Compressive (GPa)	203.3 ±21.3	180.8 ±21.9
(Msi)	29.5 ±3.1	26.2 ±3.2

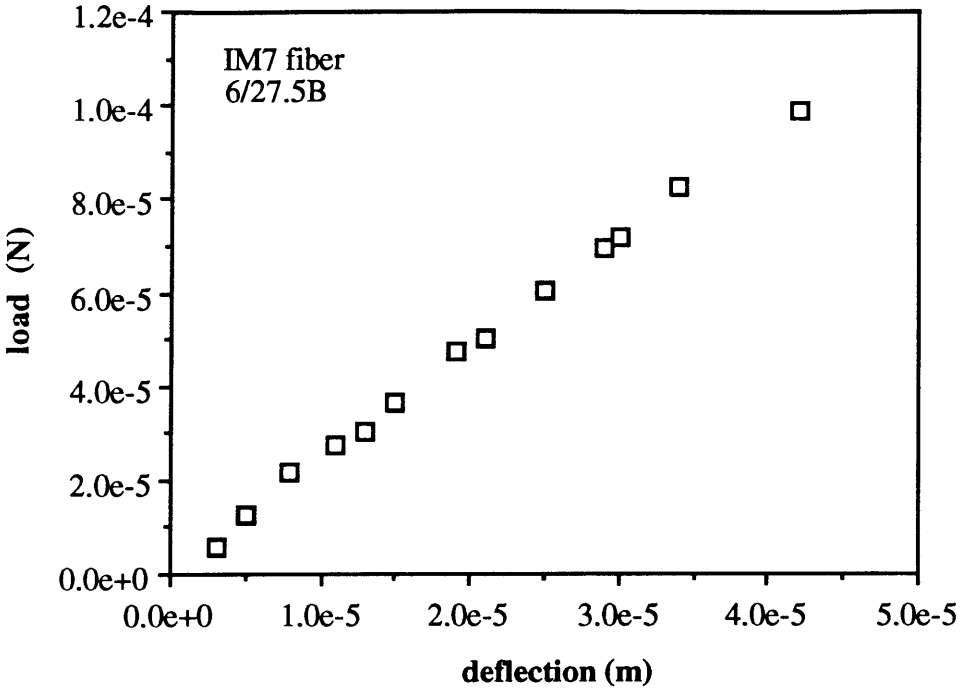

Figure 3.51. Load-deflection curve of a 5.06 μm diameter IM7 fiber. Test span is 542 μm, midspan is 90 μm.

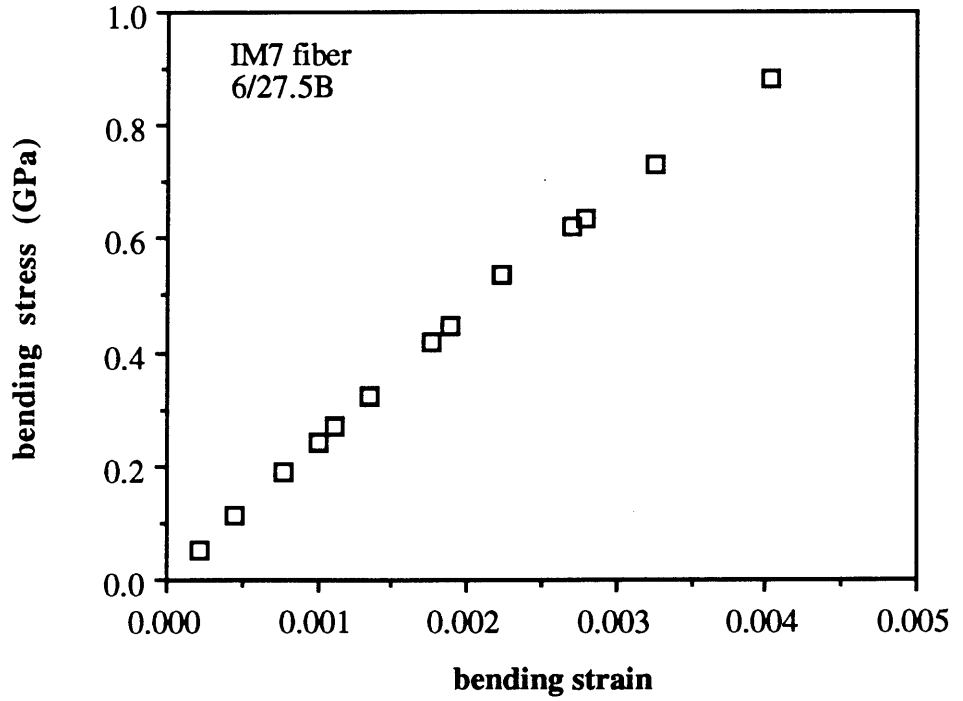

Figure 3.52. Bending stress-strain curve of IM7 fiber from Figure 3.51. Fiber exceeds test deflection limits at approximately 0.4% strain.

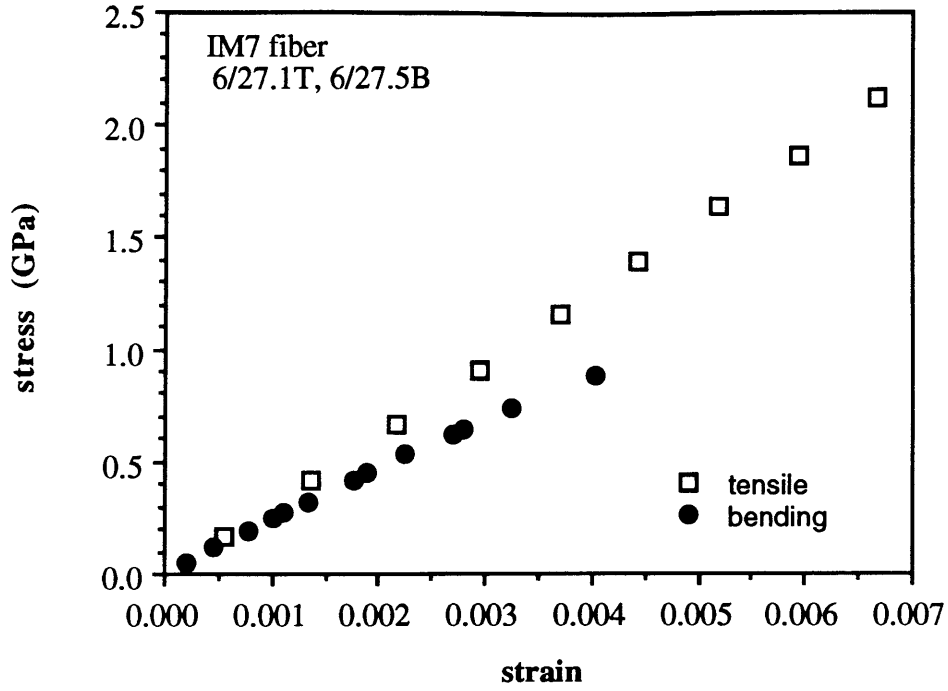

Figure 3.53. Tensile and bending stress- strain curves for IM7 fiber coincide at low strains. Above approximately 0.1% strain, the tensile modulus increases while the bending and compressive modulii decrease.

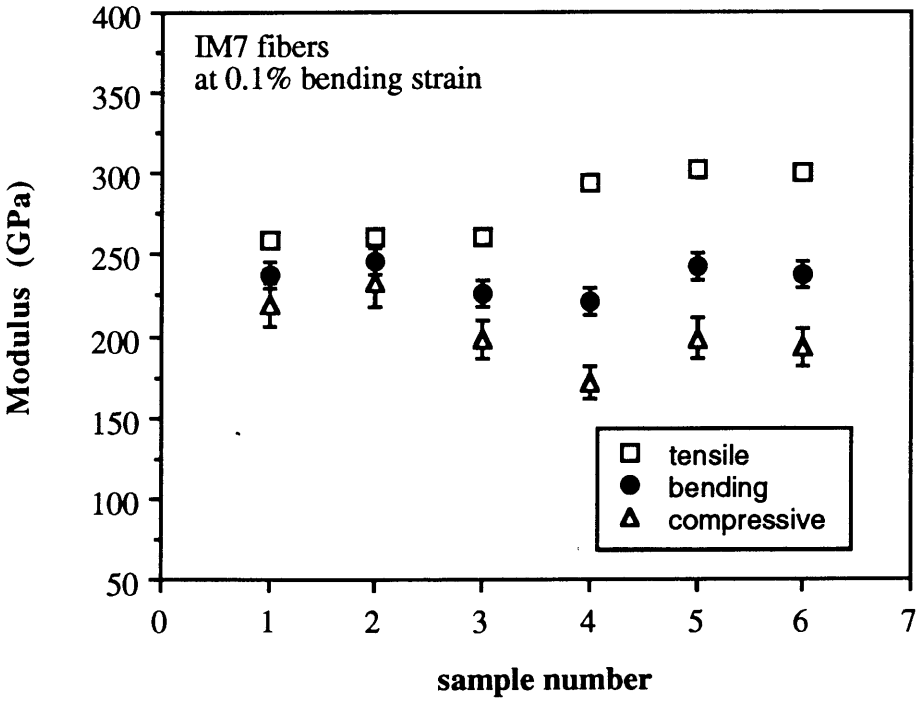

Figure 3.54. Tensile, bending and compressive modulii of six IM7 fiber samples at 0.1% bending strain. The gap between tensile and compressive modulus is just beginning to appear.

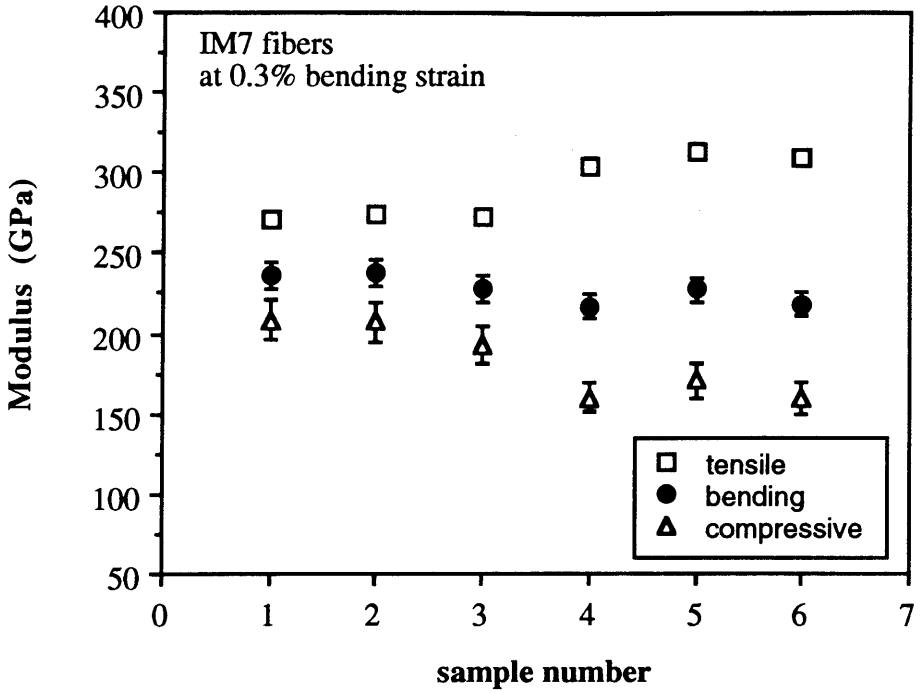

Figure 3.55. Bending and compressive modulii are approximately 80% and 65% of the tensile modulus at 0.4% bending strain.

Figures 3.56 is the load-deflection curve of a typical IM8 fiber. The data have been converted to bending stress- and strain, Figure 3.57, which are compared to the tensile stress strain curve in Figure 3.58. The two diverge above approximately 0.1% strain. The fiber deflection exceeds the test limit at approximately 0.4% strain. IM8 tensile bending and compressive modulus at 0.1% and 0.3% bending strain are given in Table 3.11, based on five samples (Figures 3.59 and 3.60). The average bending modulus drops from 82% of the tensile modulus at 0.1% bending strain to 74% of the tensile modulus at 0.3% bending strain. The corresponding change in the compressive modulus is from 68% to 57% of the tensile modulus.

Table 3.11. Average tensile, bending and compressive modulii of five IM8 fibers at 0.1% and 0.3% bending strain.

Modulus	0.1% bending strain	0.3% bending strain
Tensile (GPa)	322.1 ±15.1	335.2 ±15.2
(Msi)	46.7 ±2.2	48.6 ±2.2
Bending (GPa)	264.3 ±14.3	248.2±22.2
(Msi)	38.3 ±2.1	36.0 ±3.2
Compressive (GPa)	220.3 ±16.1	190.1 ±24.3
(Msi)	32.0 ±2.3	27.6 ±3.5

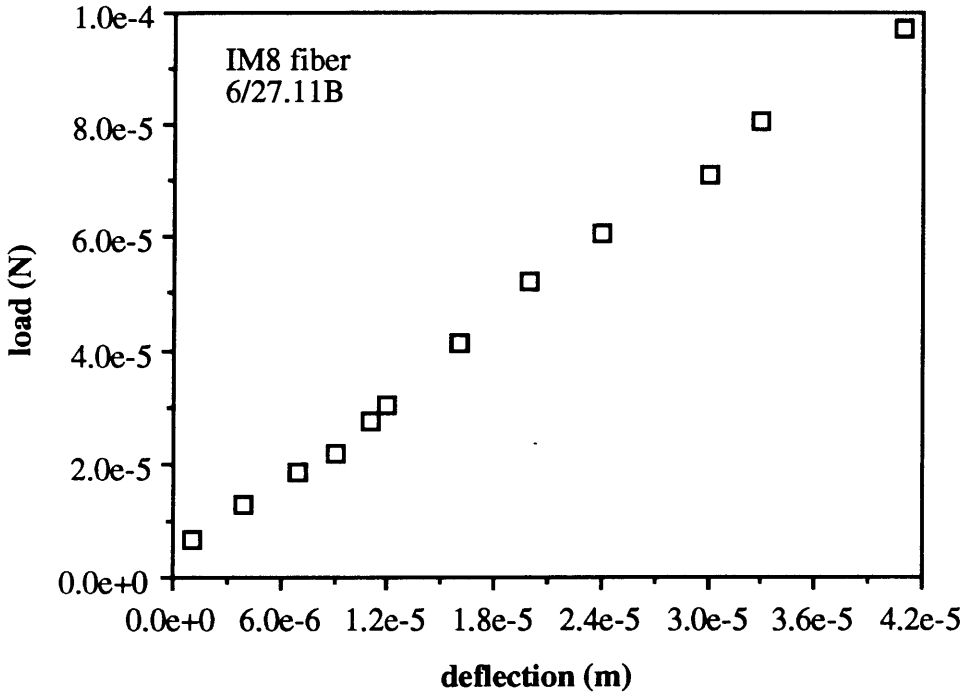

Figure 3.56. Load- deflection behavior of IM8 fiber is more erratic than other fibers because the small fiber size makes it more susceptable to vibrations. Fiber diameter is 4.83 μm. Test span is 542 μm, midspan is 90 μm.

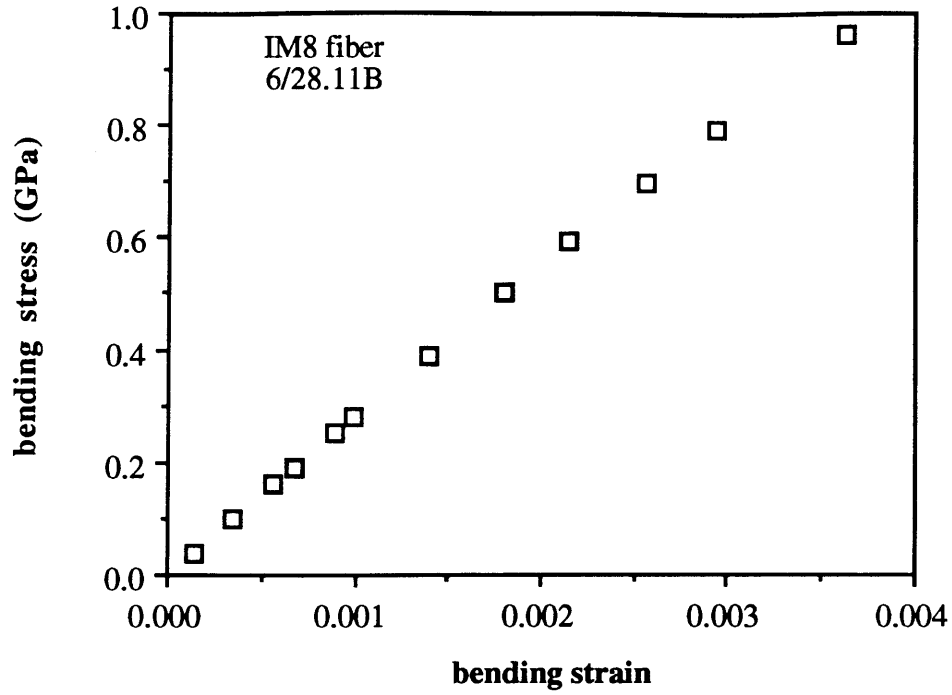

Figure 3.57. Bending stress- strain curve for IM8 fiber in Figure 3.56.

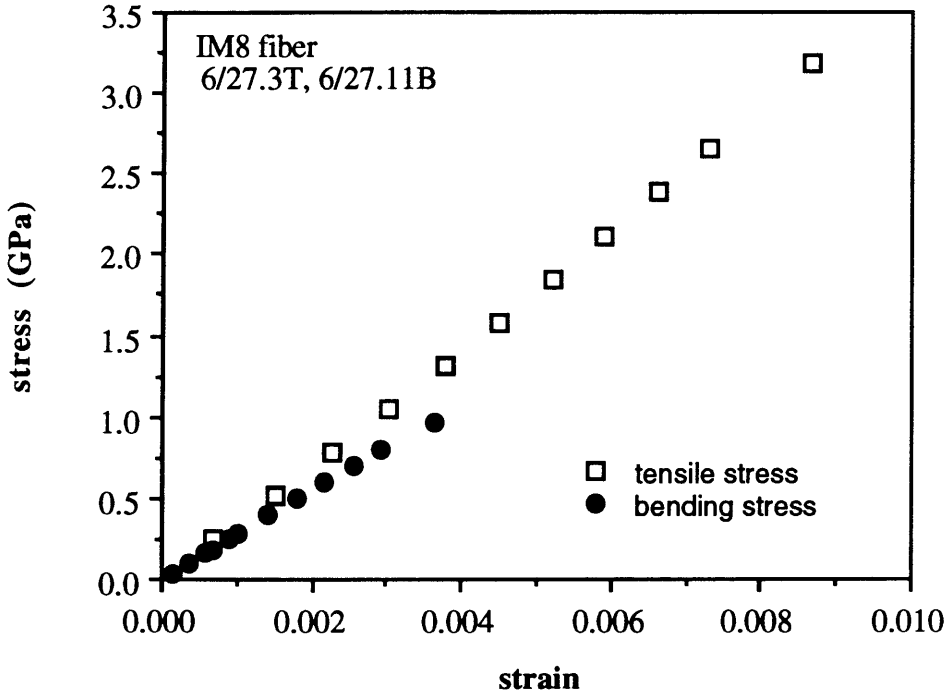

Figure 3.58. Stress- strain behavior of an IM8 fiber in tension and bending overlaps at strains less than approximately 0.1%.

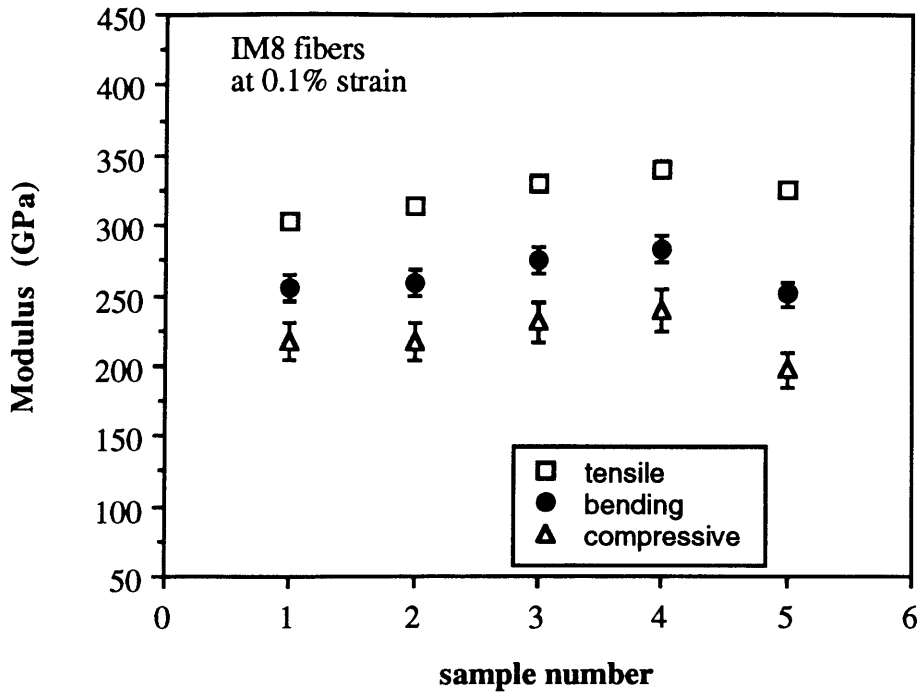

Figure 3.59. IM8 fiber bending and compressive modulii are already noticeably less than the tensile modulus at 0.1% bending strain.

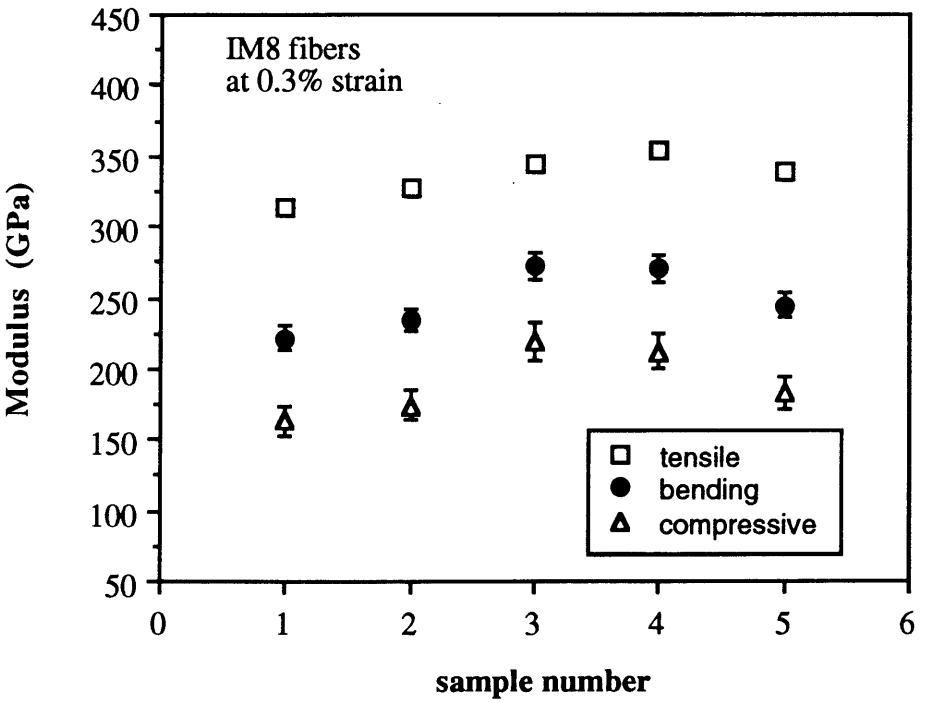

Figure 3.60. IM8 bending and compressive modulii deviate further from the tensile modulus at 0.3% bending strain, decreasing to approximately 75% and 60% of the tensile modulus.

HMS4 fibers have the highest tensile modulus of the PAN- based fibers tested in this study. The load deflection curve, shown in Figure 3.61, is smooth, with slight downward curvature. The bending stress- strain curve, Figures 3.62, matches the tensile stress-strain curve up to approximately 0.25% strain (Figure 3.63). At 0.1% bending strain, only the tensile and bending modulii are calculated (Figure 3.64, Table 3.12) because the fiber behavior is isotropic. At 0.4% bending strain, the average bending and compressive modulii are 78% and 62% of the average tensile modulus (Figure 3.65).

Table 3.12. Average tensile, bending and compressive modulii of seven HMS4 fibers at 0.1% and 0.4% bending strain.

Modulus	0.1% bending strain	0.4% bending strain
Tensile (GPa)	330.1 ±7.7	368.2 ±10.4
(Msi)	47.9 ±1.1	53.4 ±1.5
Bending (GPa)	332.5 ±13.2	286.0 ±10.1
(Msi)	48.2 ±1.9	41.5 ±1.5
Compressive (GPa)		227.8 ±13.9
(Msi)		33.0 ±2.0

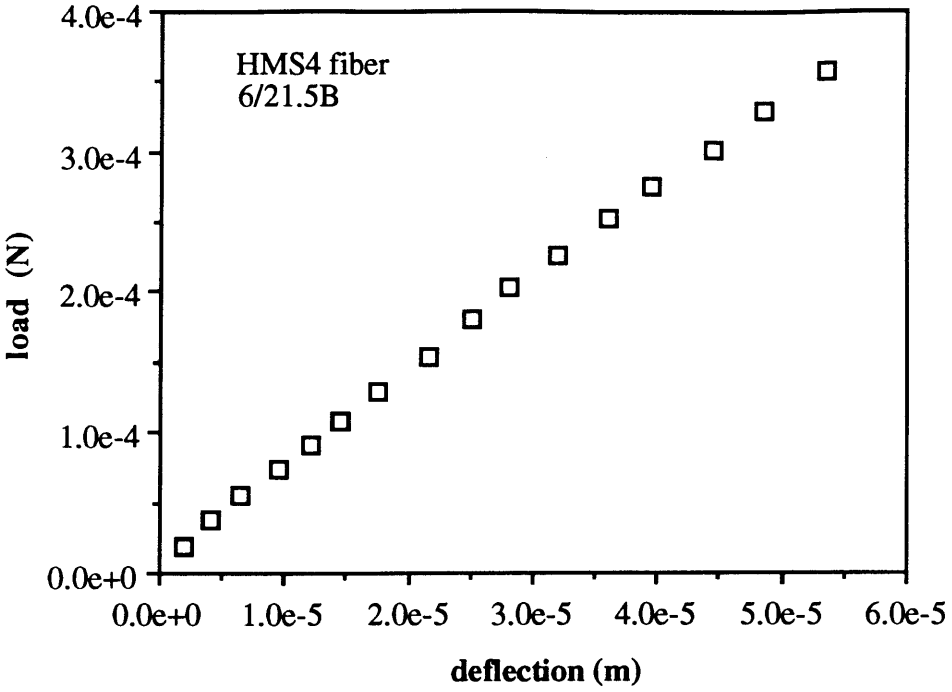

Figure 3.61. HMS4 fiber load- deflection curve. Fiber diameter is 7.16 μm. Test span is 666 μm, midspan is 90 μm.

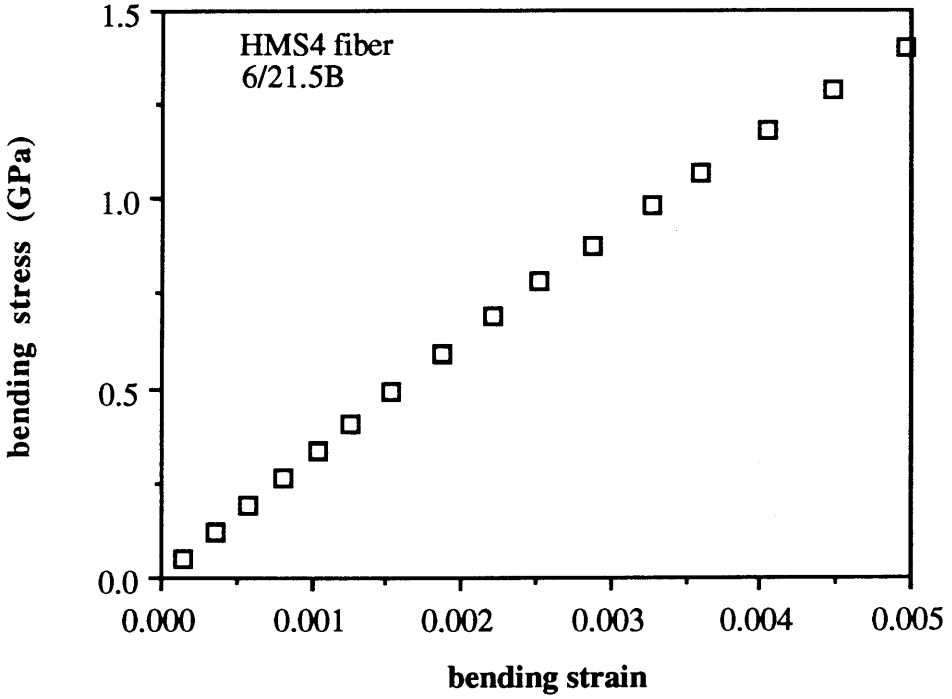

Figure 3.62. Bending stress- strain curve for typical HMS4 fiber, described in Figure 3.61.

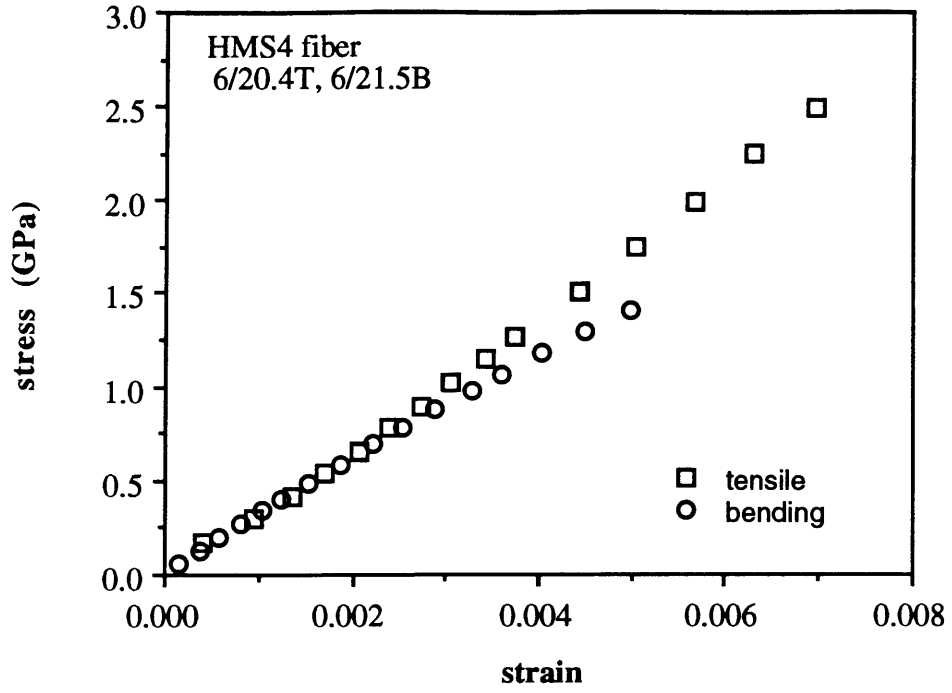

Figure 3.63. Tensile and bending stress- strain curves overlap until approximately 0.25% strain.

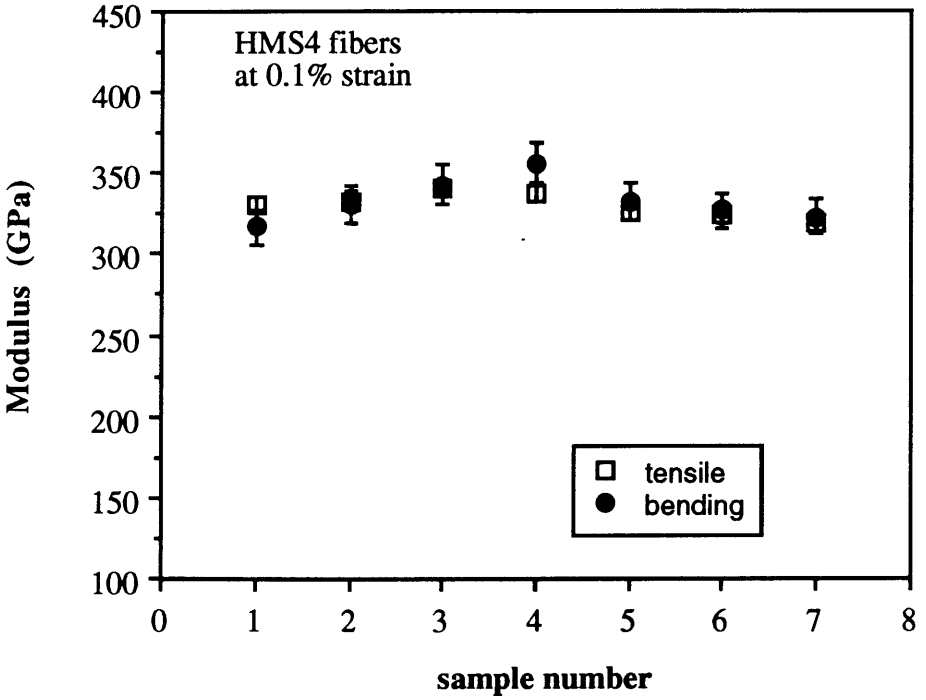

Figure 3.64. At low strains, the stress- strain behavior of HMS4 is isotropic.

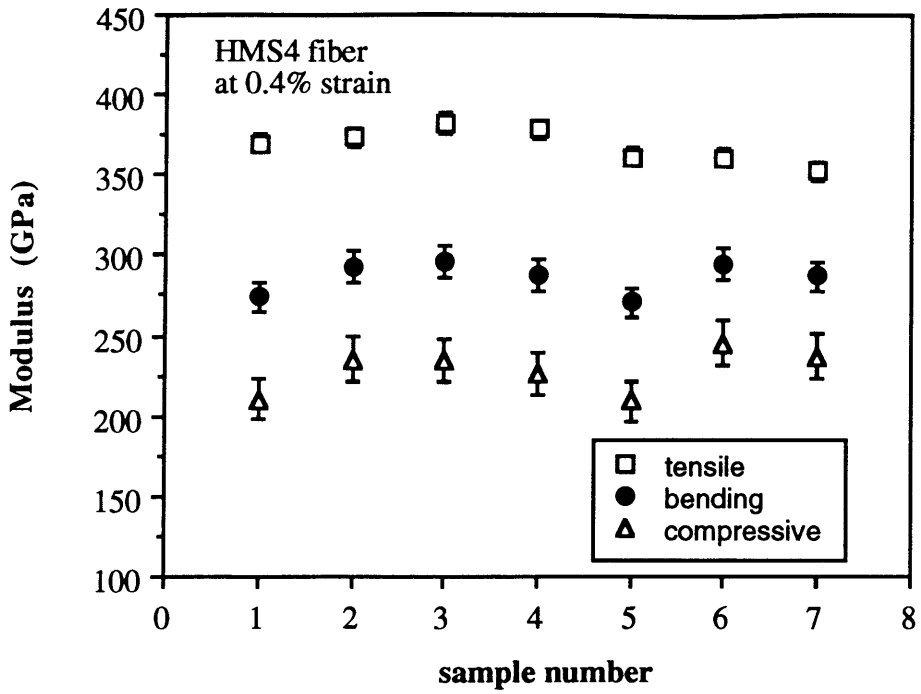

Figure 3.65. By 0.4% bending strain, the bending and compressive modulii are noticeably less than the tensile modulus.

Pitch-based

The mechanical properties of pitch- based carbon fibers are elastic and a strong function of strain. The load- deflection behavior of a straight section of P25 HT is shown in Figure 3.66 and converted to bending stress and strain in Figure 3.67. In tension and in bending the modulus is similar to approximately 0.2% strain. (See Figure 3.68.) The tensile, bending and compressive modulii of nine P25 samples are presented in Figure 3.69 and 3.70 for 0.1% and 0.6% bending strain. The average values, as well as the average values at 0.4% bending strain are given in Table 3.13.

Table 3.13. Average tensile, bending and compressive modulii of nine P25 HT fibers at 0.1%, 0.4% and 0.6% bending strain.

Modulus	0.1% bending strain	0.4% bending strain	0.6% bending strain
Tensile (GPa)	117.1 ±9.6	127.2 ±9.7	132.9 ±10.5
(Msi)	17.0 ±1.4	18.4 ±1.4	19.3 ±1.5
Bending (GPa)	112.2 ±17.2	100.1 ±15.8	93.8 ±14.5
(Msi)	16.3 ±2.5	14.5 ±2.3	13.6 ±2.1
Compressive (GPa)	110.2 ±32.5	81.8 ±23.2	70.2 ±18.8
(Msi)	16.0 ±4.7	11.9 ±3.4	10.2 ±2.7

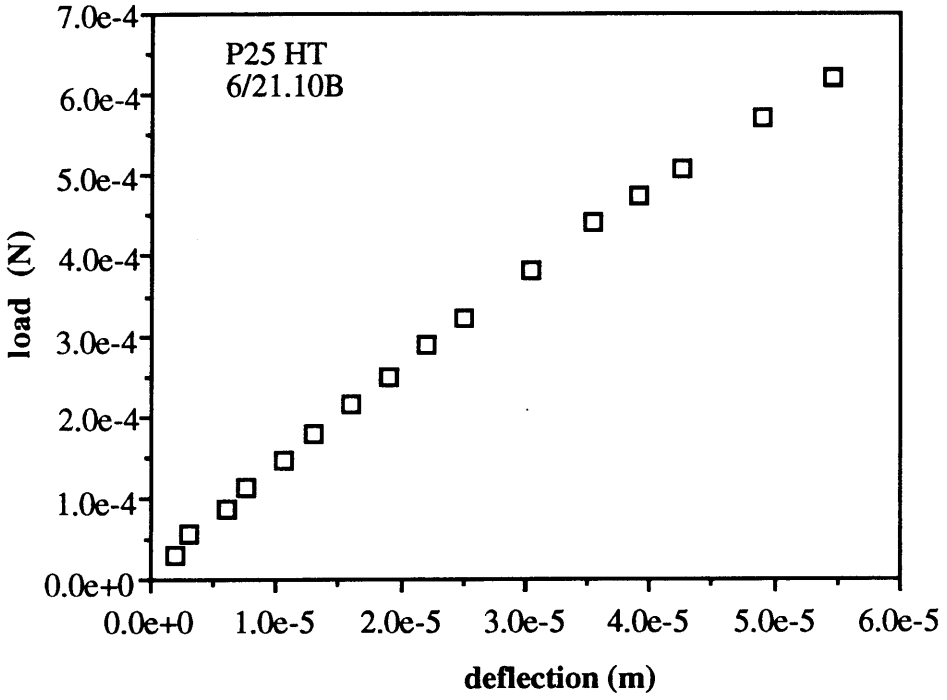

Figure 3.66. Load-deflection curve of a straight section of an 11.1 μm diameter P25 HT fiber. Test span is 666 μm, midspan is 90 μm.

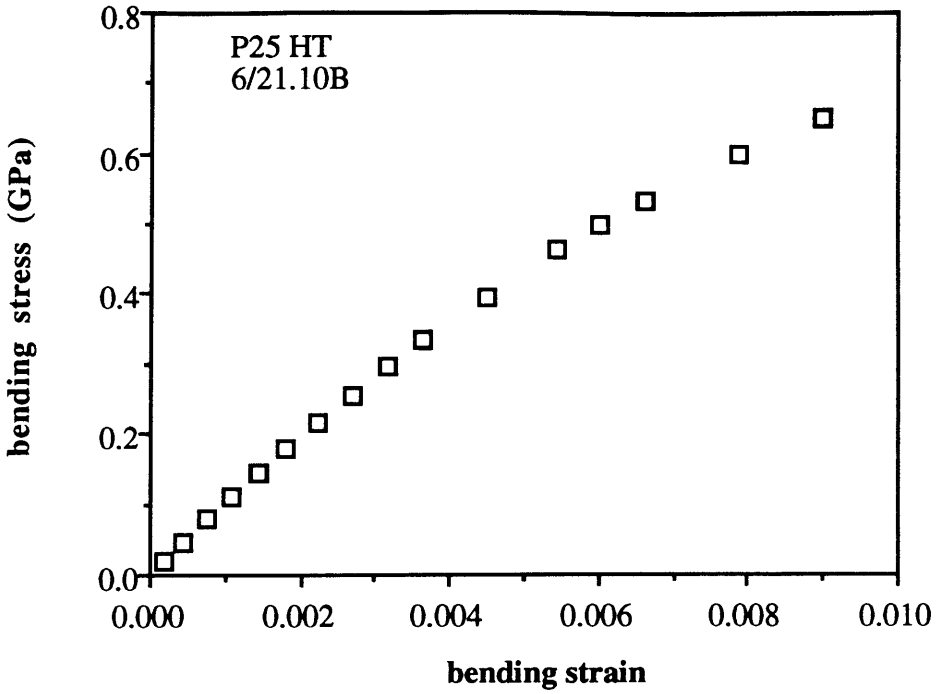

Figure 3.67. P25 HT fiber from Figure 3.66 softens with increased bending strain. No damge to fiber is observed during test.

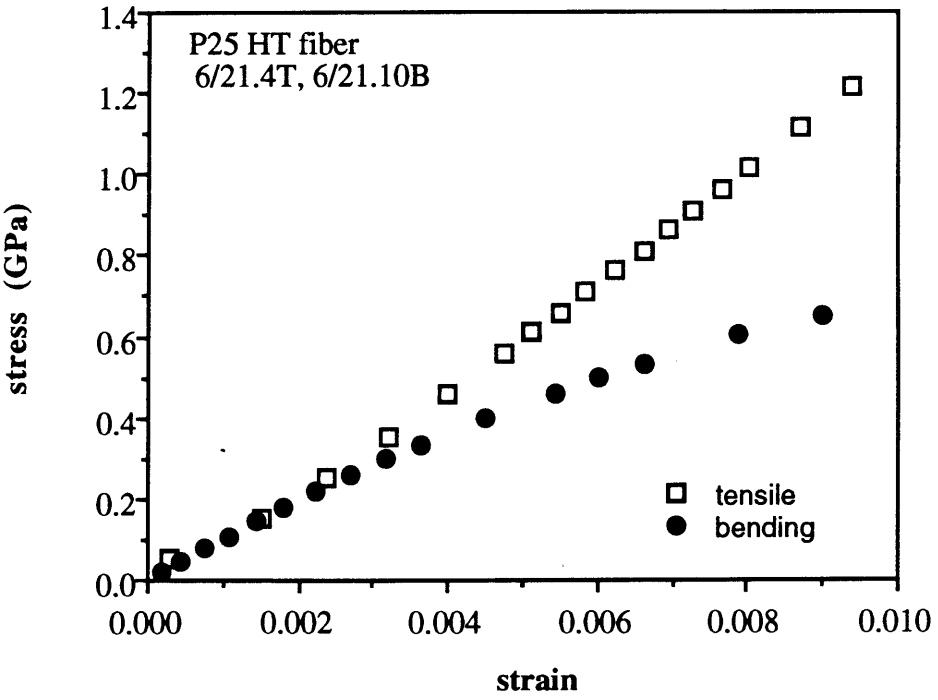

Figure 3.68. Tensile and bending stress- strain curves for P25 fiber overlap, but the curvature is opposite. A significant difference between the tensile and bending modulii is apparent by 0.4% strain.

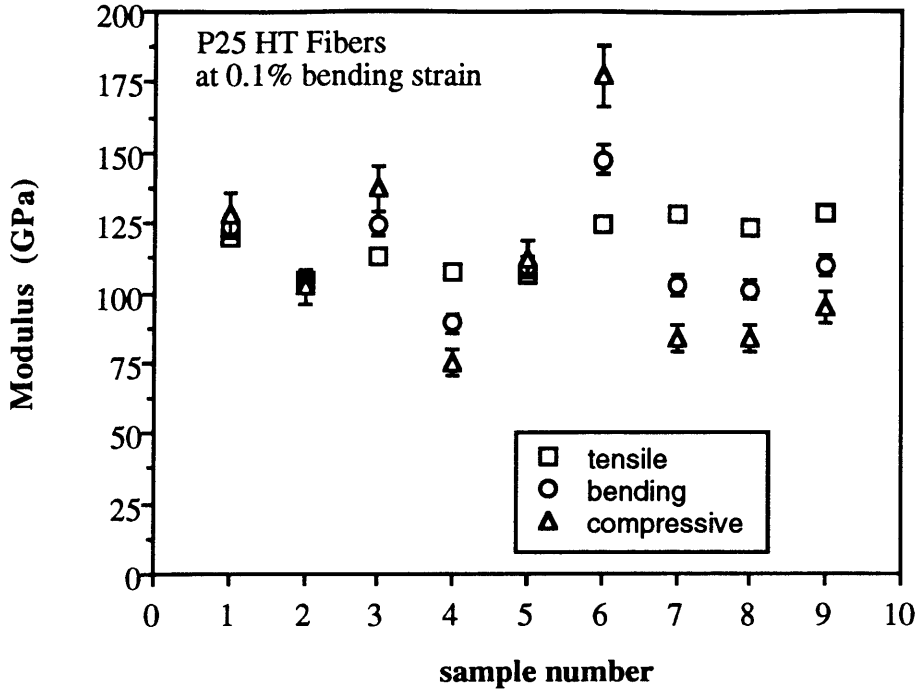

Figure 3.69. Modulii of P25 fibers in tension, bending and compression do not differ significantly at 0.1% bending strain.

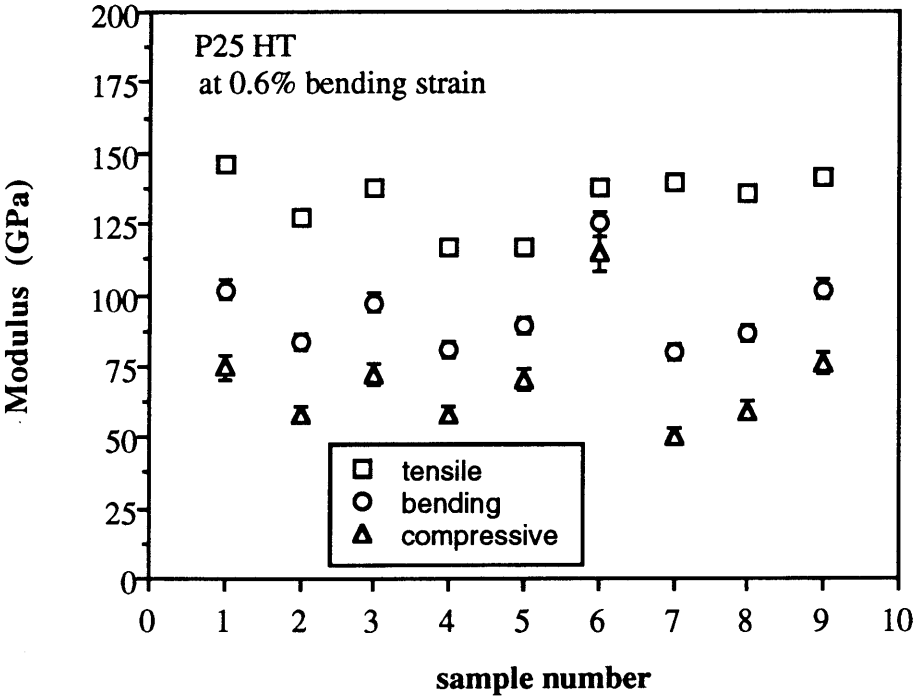

Figure 3.70. The bending and compressive modulii of P25 fibers has dropped to approximately 70% and 55% of the tensile modulus at 0.6% bending strain.

The P55s fibers also show significant strain dependence. The load-deflection and bending stress-strain curves for are typical fiber a shown in Figures 3.71 and 3.72. Although the fiber reaches 0.8% bending strain, tensile stress-strain information is only available to 0.2% strain (Figure 3.73) for this and the two other samples from FITT test 7/21.2T. The tensile breaking strain in the other four samples was slightly more than 0.1% in the FITT test. The average tensile, bending and compressive modulii are calculated at 0.1% bending strain (Figure 3.74) for all seven samples and at 0.2% bending strain for the last three samples (Table 3.14).

Table 3.14. Average tensile, bending and compressive modulii of P55s fibers at 0.1% bending strain (seven samples) and at 0.2% bending strain (three samples).

Modulus	0.1% bending strain	0.2% bending strain
Tensile (GPa)	462.8 ±39.0	451.1 ±7.6
(Msi)	67.1 ±5.6	65.4 ±1.1
Bending (GPa)	349.4 ±55.5	268.5 ±15.4
(Msi)	50.7 ±8.0	38.9 ±2.2
Compressive (GPa)	273.3 ±59.4	174.4 ±15.2
(Msi)	39.6 ±8.6	25.3 ±2.2

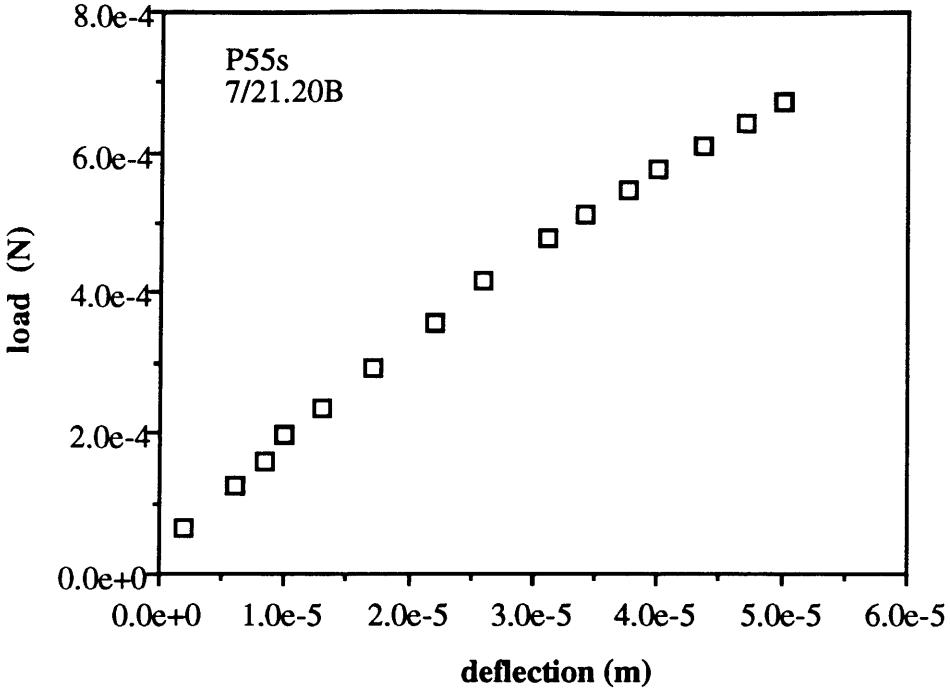

Figure 3.71. Typical load- deflection behavior of 8.87 μm diameter P55 fiber. No visually apparent physical change corresponds to the observed strain- softening.

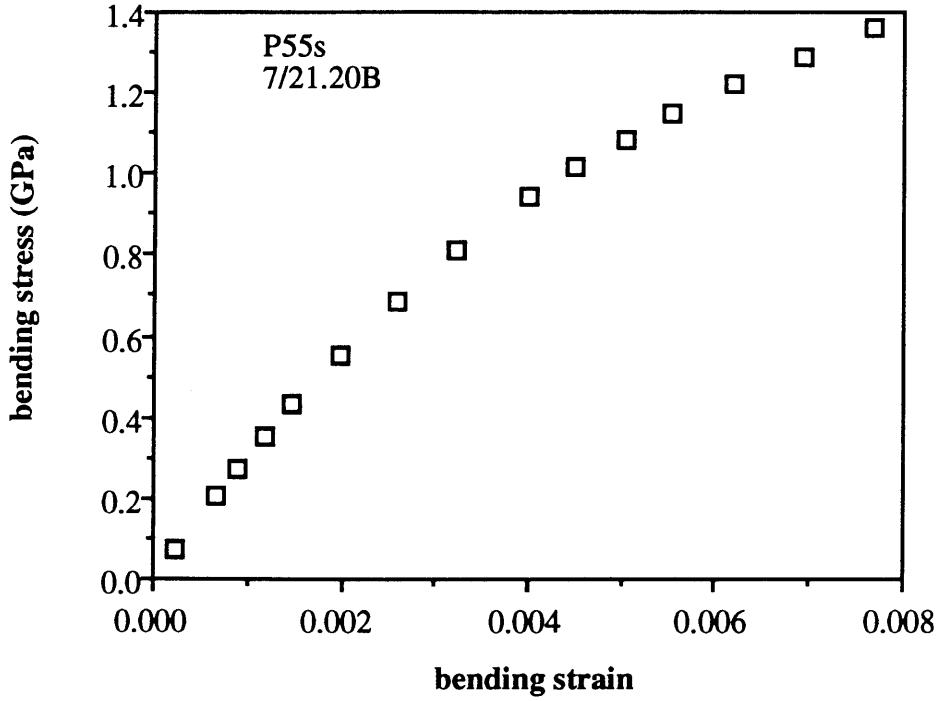

Figure 3.72. Bending stress- strain curve of P55 fiber described in Figure 3.71. Bending strain reaches 0.8%, at which point fiber bending stress has exceeded the reported compressive strength of 0.89 GPa, but is less than the tensile strength of 1.90 GPa.

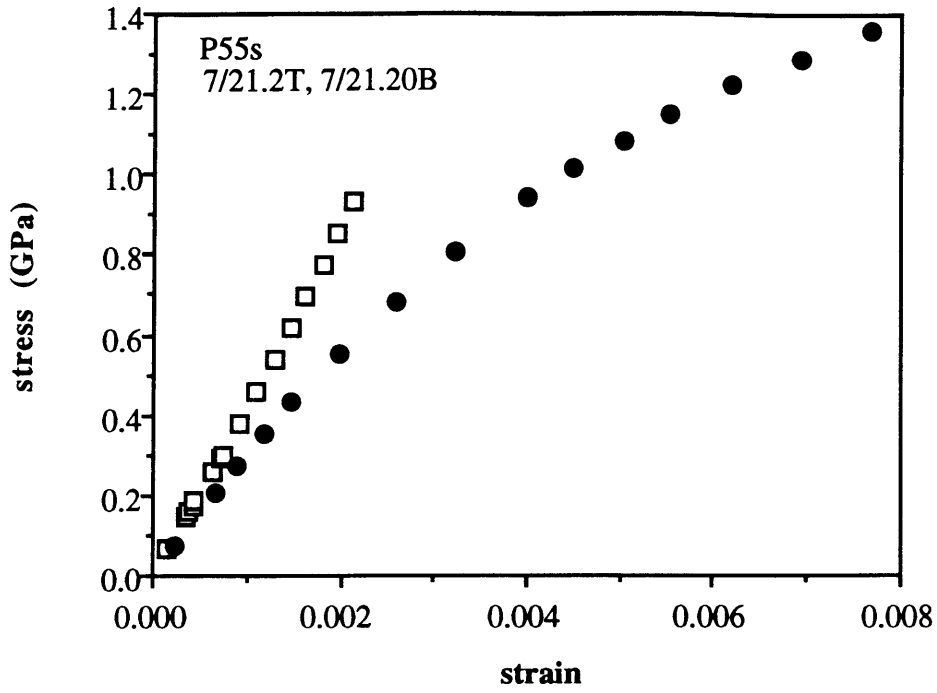

Figure 3.73. Tensile and bending stress-strain curves for P55 fiber. Premature fracture in the tensile test prevents calculation of compressive properties above approximately 0.2% strain.

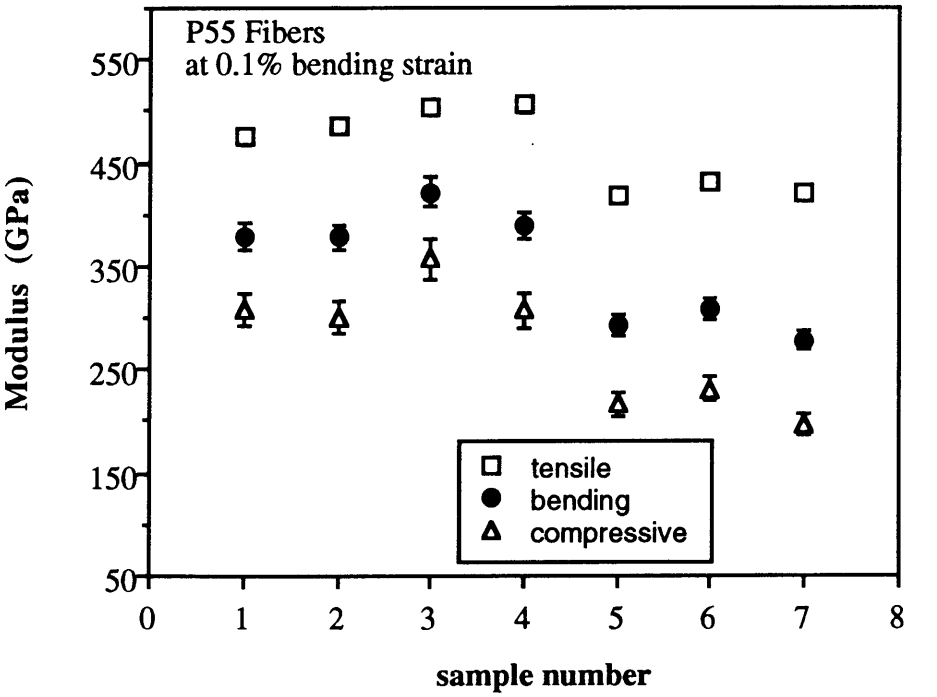

Figure 3.74. P55 fiber tensile, bending and compressive modulii at 0.1% bending strain. Anisotropy is visible: the bending and compressive modulii are approximately 75% and 60% of the tensile modulii of the seven samples.

The P75 fibers show the most nonlinearity of all the fibers tested. A typical load-deflection curve and the corresponding bending stress-strain curve are shown in Figures 3.75 and 3.76. In addition, the deviation from isotropic behavior is evident at a low strain level (Figure 3.77). The average tensile, bending and compressive modulii from tests on five samples at 0.1%, 0.2% and 0.35% bending strain are presented in Table 3.15. The compressive properties cannot be calculated at higher strains because tensile stress-strain information is not available for all of the fibers; they broke at low strain levels in the FITT mode. Test results at 0.1% and 0.35% bending strain are shown in Figures 3.78 and 3.79.

Table 3.15. Average tensile, bending and compressive modulii of seven P75 fibers at 0.1%, 0.2% and 0.35% bending strain.

Modulus	0.1% bending strain	0.2% bending strain	0.35% bending strain
Tensile (GPa)	499.8 ±13.6	524.1 ±18.9	572.6 ±33.1
(Msi)	72.5 ±2.0	76.0 ±2.7	83.0 ±4.8
Bending (GPa)	347.9 ±25.2	308.4 ±19.8	259.1 ±14.1
(Msi)	50.5 ±3.7	44.7 ±2.9	37.6 ±2.0
Compressive (GPa)	254.1 ±29.5	197.2 ±18.2	142.2 ±10.8
(Msi)	36.9 ±4.3	28.6 ±2.6	20.6 ±1.6

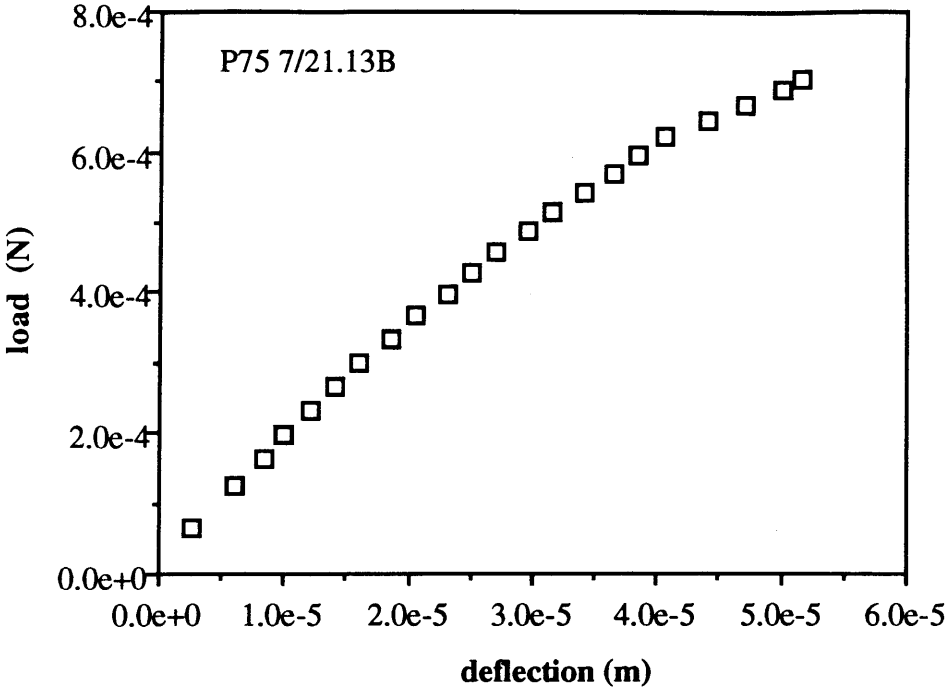

Figure 3.75. Load deflection curve of P75 fiber with a diameter of 9.06 μm. Test span is 666 μm, midspan is 90 μm.

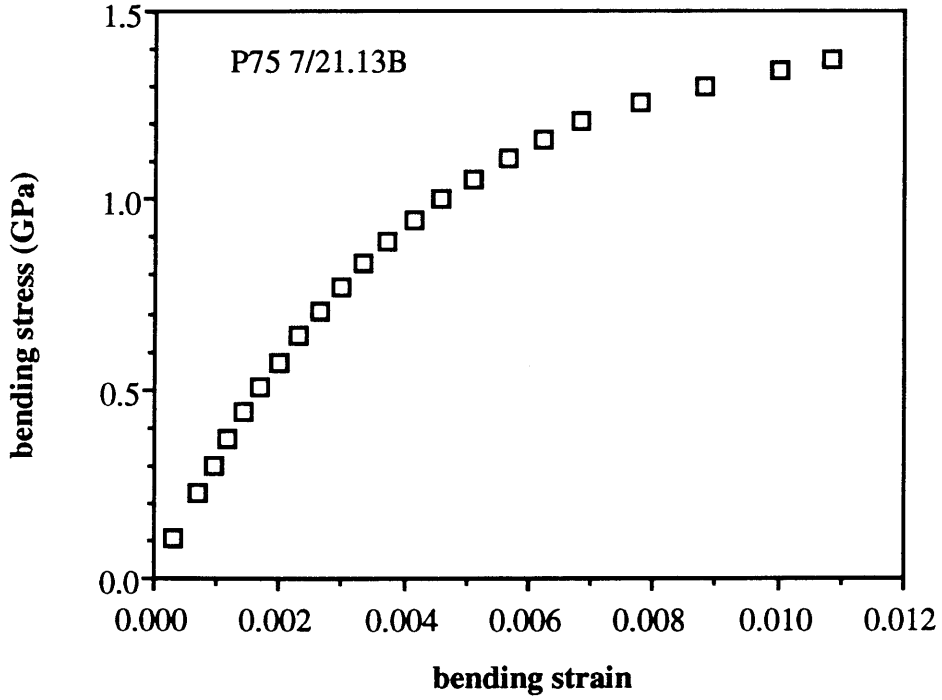

Figure 3.76. Bending stress- stain curve for P75 fiber described in Figure 3.75. No visible changes in fiber accompany strain softening.

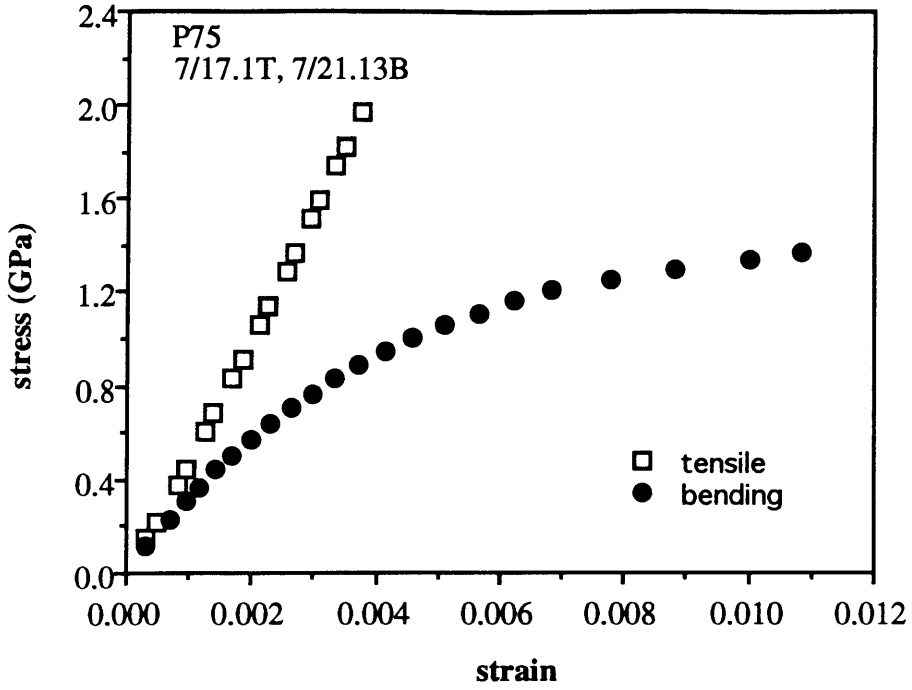

Figure 3.77. Tensile and bending stress-strain curves for a typical P75 fiber. Deviation from isotropy is immediate. Fiber bending stress exceeds reported compresssive failure stress, but fiber compressive stress does not.

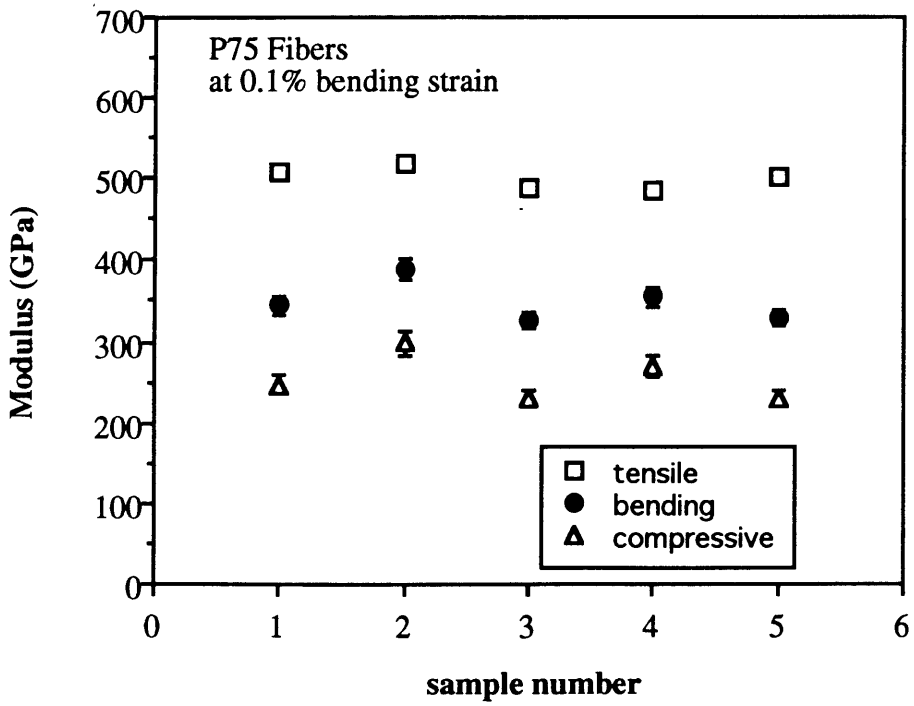

Figure 3.78. At 0.1% bending strain, the bending and compressive modulii are approximately 70% and 50% of the tensile modulii for the five samples tested.

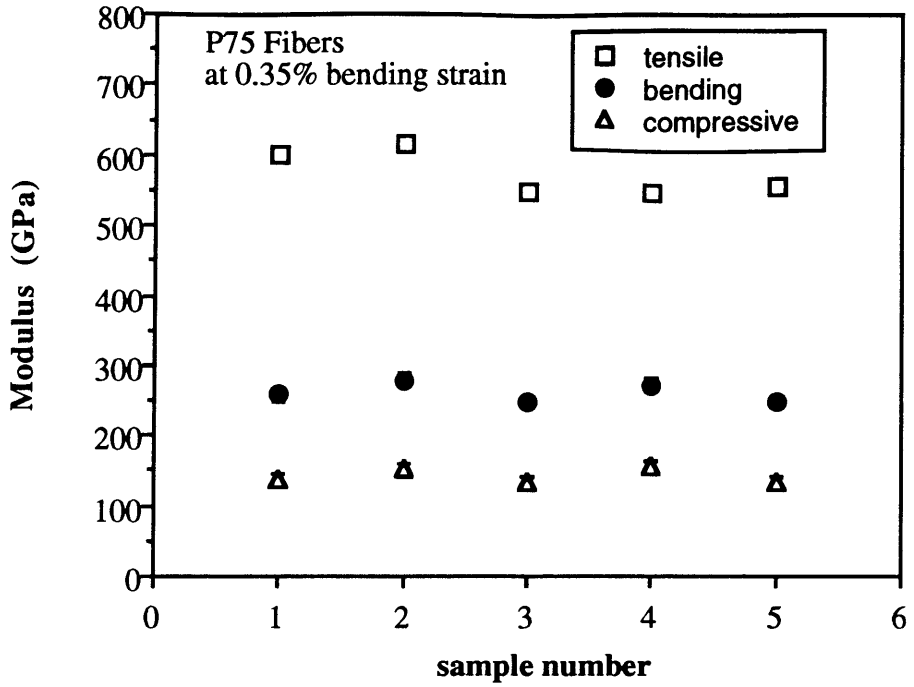

Figure 3.79. The tensile and bending stress-strain curves have diverged considerably by 0.35% bending strain, giving a bending modulus approximately 45% of the tensile modulus and a compressive modulus only 25% of the tensile modulus.

3.5. Discussion

In the Micro-Flex test, the fiber experiences tension and compression on opposite sides of the neutral axis. The neutral axis defines a strain-free surface from which the strain, either tensile or compressive, increases linearly to a maximum at the fiber surface. In axially anisotropic fibers, the difference between the tensile and compressive modulii causes a shift in the fiber neutral axis. This means the compressive and tensile strains will differ from the bending strain by a factor of $(1 \pm k)$, where k is the fractional shift distance defined in Equation 3.11. Figure 3.80 shows the increase in the shift factor with decreasing ratio of compressive to tensile modulus. The difference in strain is important in the calculation of the compressive modulus from the bending and tensile modulii and it causes the shift in strain values at which the various modulii are reported; see Figure 3.85.

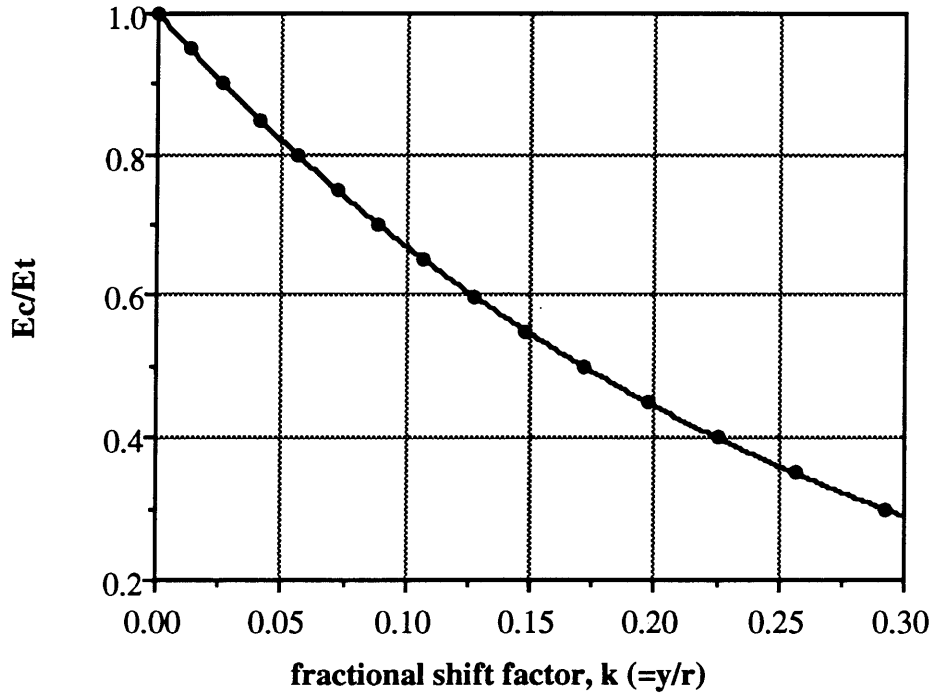

Figure 3.80. Neutral axis shift distance relative to fiber radius increases as the ratio of compressive modulus to tensile modulus decreases. The neutral axis shift causes a difference between the tensile and compressive strains at a given bending strain.

3.5.1 Kevlar Fibers

The bending stress-strain curves of representative Kevlar 119, 29, 129, 49 and 149 fibers are compared in Figure 3.81. The bending curves scale according to the tensile modulus increase, with the exception of Kevlar 149 which starts out in order but then crosses the Kevlar 49 curve because of greater softening.

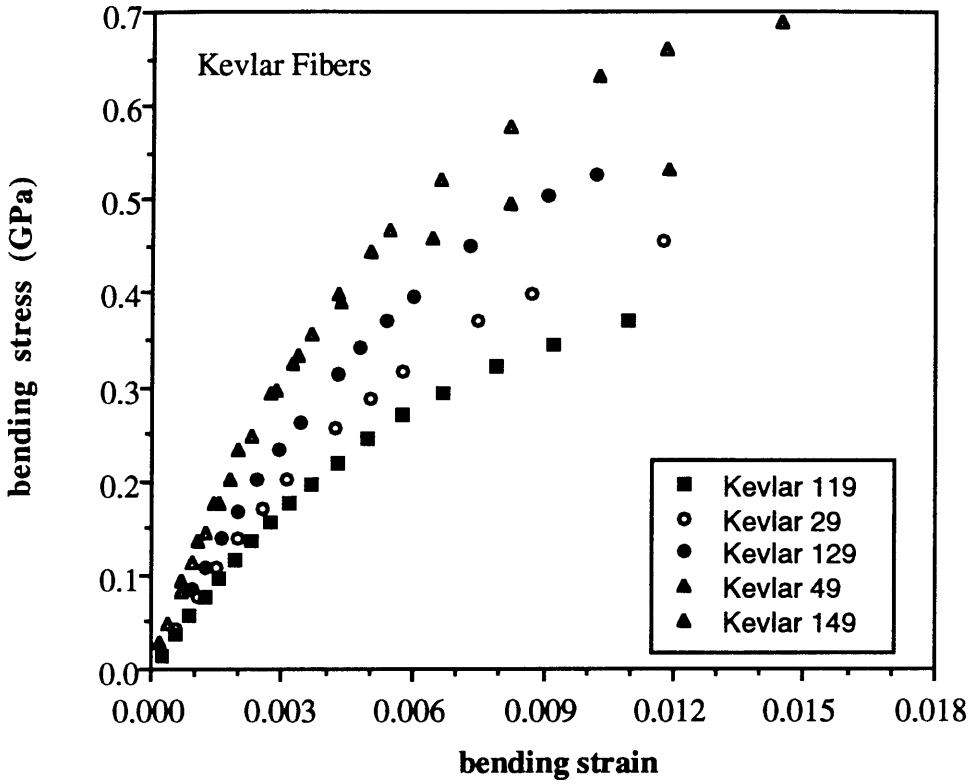

Figure 3.81. The bending stress- strain curves for Kevlar fibers, listed in order of increasing tensile modulus. Behavior scales with modulus, except Kevlar 149, which shows a greater loss in load- carrying ability above approximately 0.5% strain.

The average tensile, bending and compressive modulii for the five types of Kevlar at 0.15% bending strain are shown in Figure 3.82. The stress- strain curve must be continuous at the origin, 0% strain, which means the fiber modulus will be the same whether measured in tension, bending or compression; axial anisotropy develops only as increasing strain affects the microstructural orientation. At low strains the stiffnesses are similar in the lower modulus fibers but the modulii of the most highly oriented fiber,

Kevlar 149, have already diverged. At the compressive failure strain (Figure 3.83), the difference between the three kinds of modulus is greater because the tensile modulus has increased while the bending stiffness has decreased, leading to an even greater decrease in the compressive modulus.

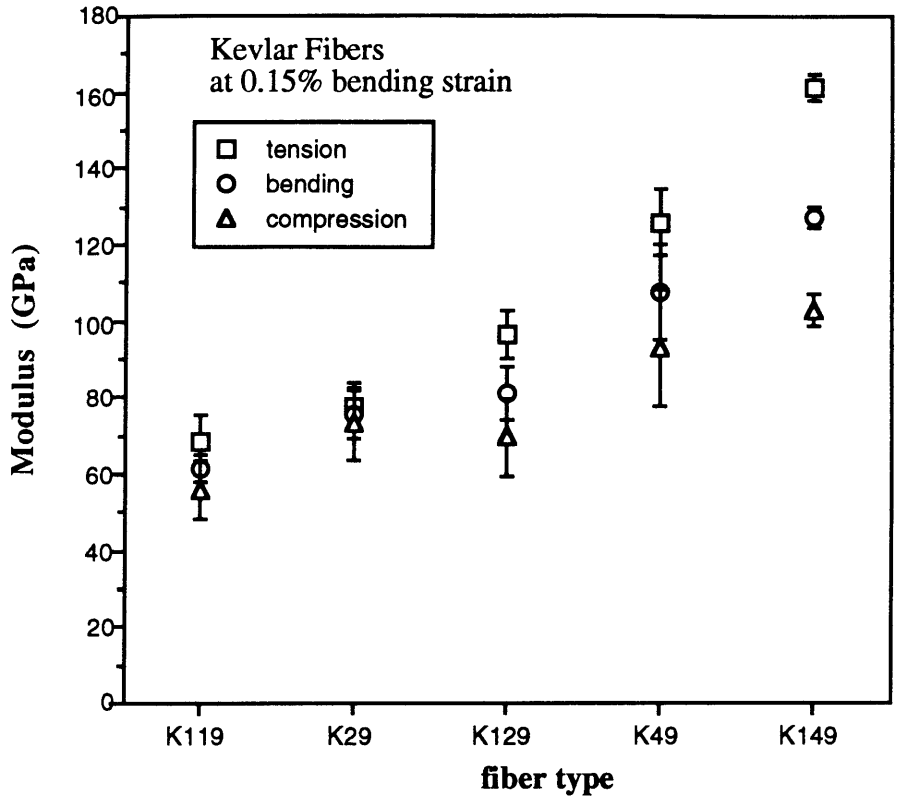

Figure 3.82. Kevlar fiber average modulus in tension, bending and compression, by fiber type at 0.15% bending strain. Error bars are the standard deviation of the collected data. Kevlar 119 and 29 modulii are nearly equal, while the tensile and compressive modulii of the higher modulus fibers, especially Kevlar 149, begin to diverge.

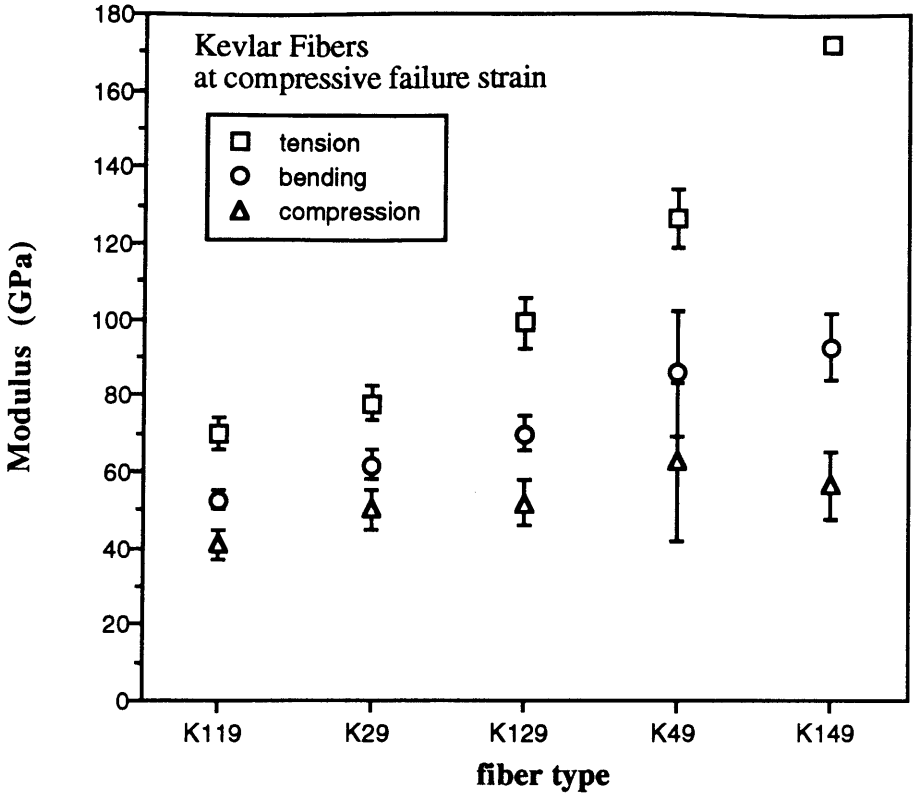

Figure 3.83. Differences between tensile, compressive and bending modulii for Kevlar fibers is significant at the compressive failure strain. Average modulus in tension and bending increase between types, compressive modulus is approximately constant. Error bars are the standard deviation of the collected data.

Often, nonlinearity in the Kevlar load- deflection curve begins before kinks are observed. This can be attributed to two factors. The kink bands observed actually are clusters of many small bands[7] which coalesce into features large enough to be seen with the light microscope. Second, the pleated sheet structure reported by Dobb *et al.*[1] is a fundamental source of strain softening under compression. Kevlar 149 does not exhibit the pleated sheet structure; instead the axial split which wraps around the fiber reduces the fiber resistance to deformation in bending and compression, lowering both modulii.

The bending strain at which kinks are observed is approximately 0.4% for the three lower modulus Kevlars, 119, 29 and 129. Visible kinks do not develop until approximately 0.5% bending strain in Kevlar 49, and they are not observed at any point during Kevlar 149 testing. However, the load- carrying ability of Kevlar 149 levels off

abruptly after approximately 0.4% bending strain where the axial split deforms, and this is defined at the failure point. Kevlar average compressive strengths are shown in Figure 3.84:

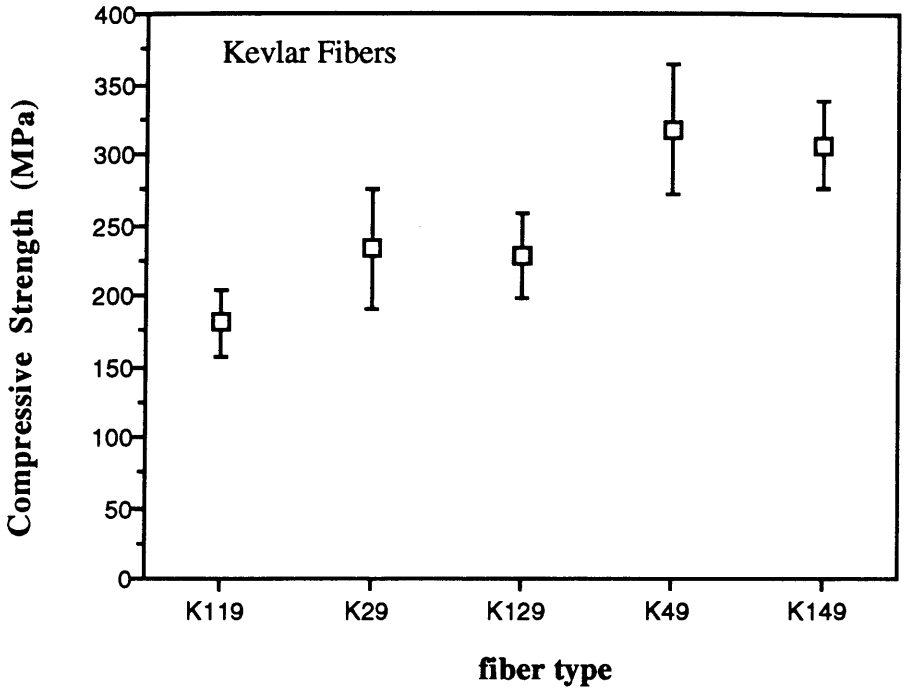

Figure 3.84. Average compressive strength of Kevlar fibers from bending tests. Error bars are standard deviation of the data. Tensile strengths are on the order of 2.75 GPa.

The standard deviation in the Kevlar 49 results is larger than the others because of varying fiber quality. Visual preselection was used to avoid testing prekinked and otherwise damaged fibers. The Kevlar 49 fiber has a water finish, which makes it more prone to damage from handling which can be difficult to see in the light microscope. Although the Kevlar 149 also has a water finish, scatter in the results is the least of the five fiber types since the degree and type of damage is most consistent: the helical split is always present.

Figures 3.85- 3.89 show tensile, bending and compressive modulii as a function of the corresponding strain for the five fibers. Each point was calculated individually, based on the FITT and Micro-Flex data, then the results were fit with first-, second- and fourth-order polynomial expression to describe the tensile, bending and compressive modulus

change with the corresponding strain: $a + bx + cx^2 + dx^3 + ex^4$. The coefficients of these equations are given in Table 3.16 and using them, the tensile, bending and compressive modulii can be calculated at any strain. In Table 3.17, the modulii at zero strain and the percent change in modulii between zero and 0.3% strain are listed.

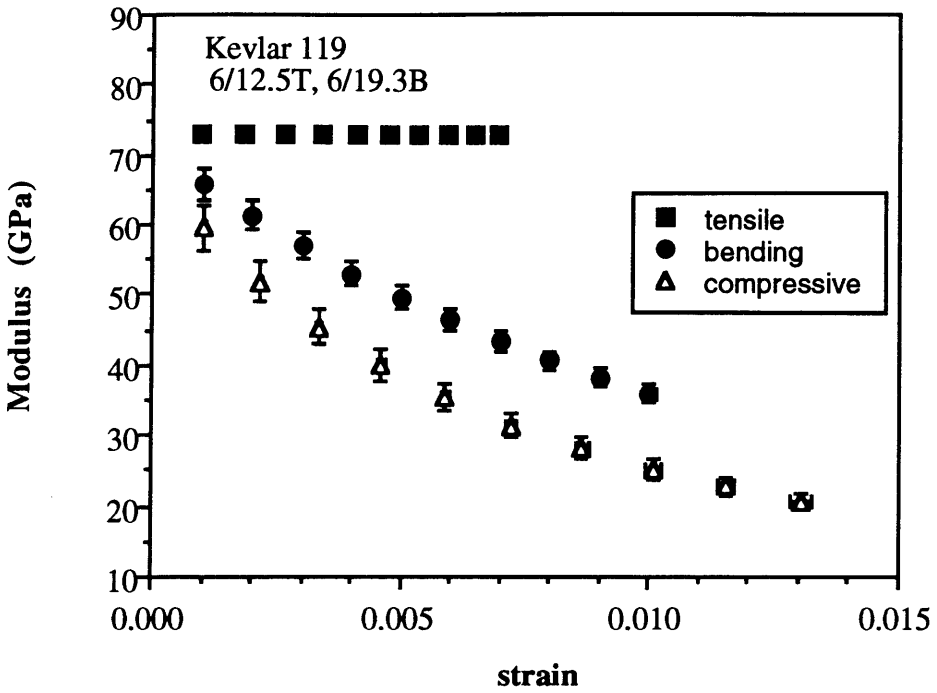

Figure 3.85. Tensile modulus of Kevlar 119 fiber remains constant while bending modulus decreases, indicating a decreasing compressive modulus. Kink bends are visible at approximately 0.5% compressive strain.

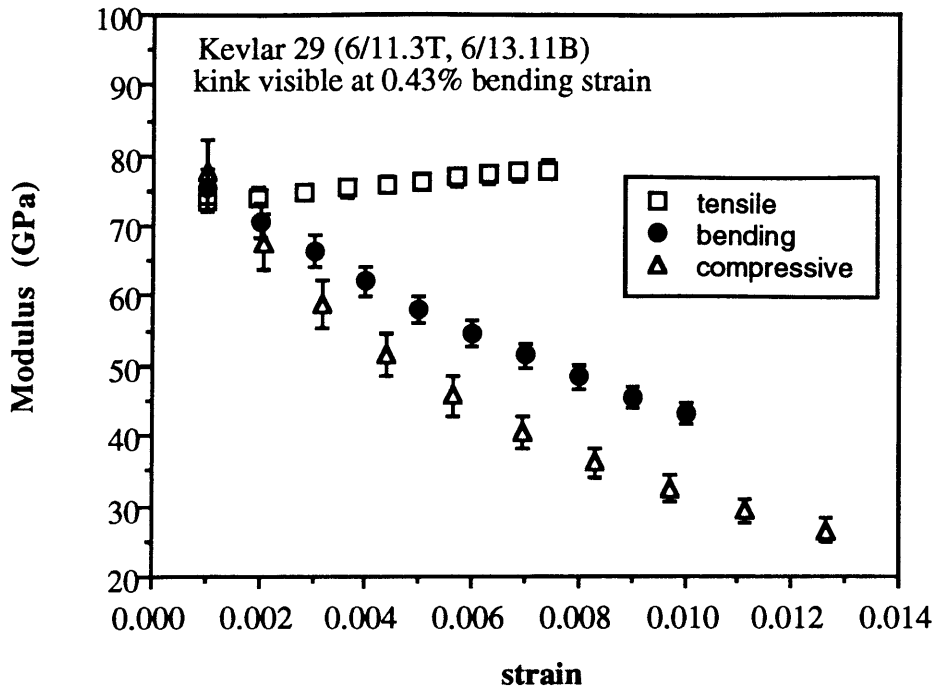

Figure 3.86. Kevlar 29 fiber behavior: tensile and compressive modulii diverge rapidly with increasing strain. Compressive failure occurs at approximately 0.5% strain.

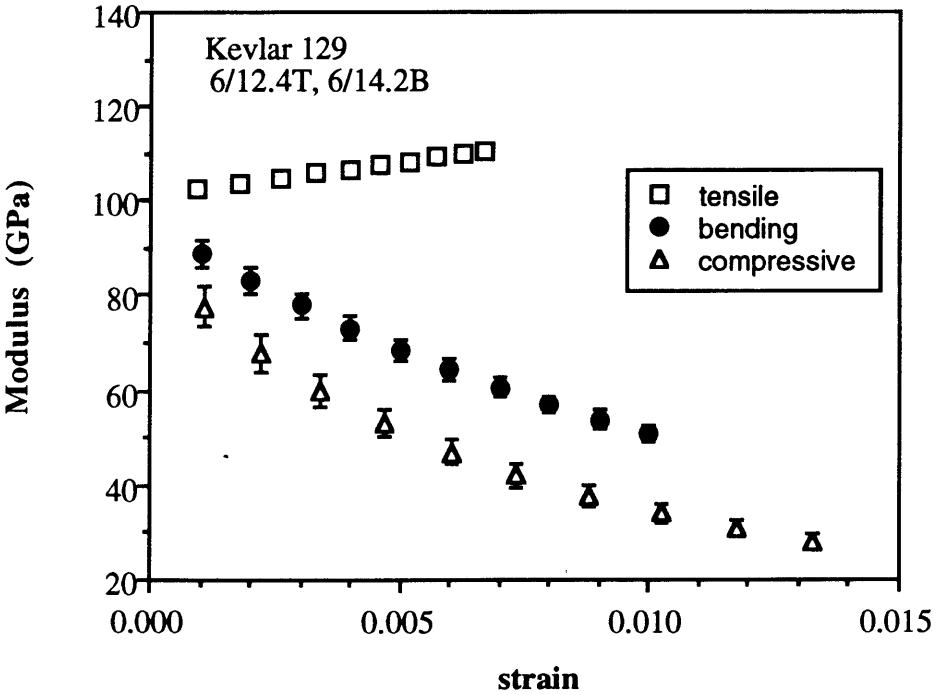

Figure 3.87. Kevlar 129 tensile and compressive modulii diverge at very low strains, even though kink bands are not visible until approximately 0.45% strain.

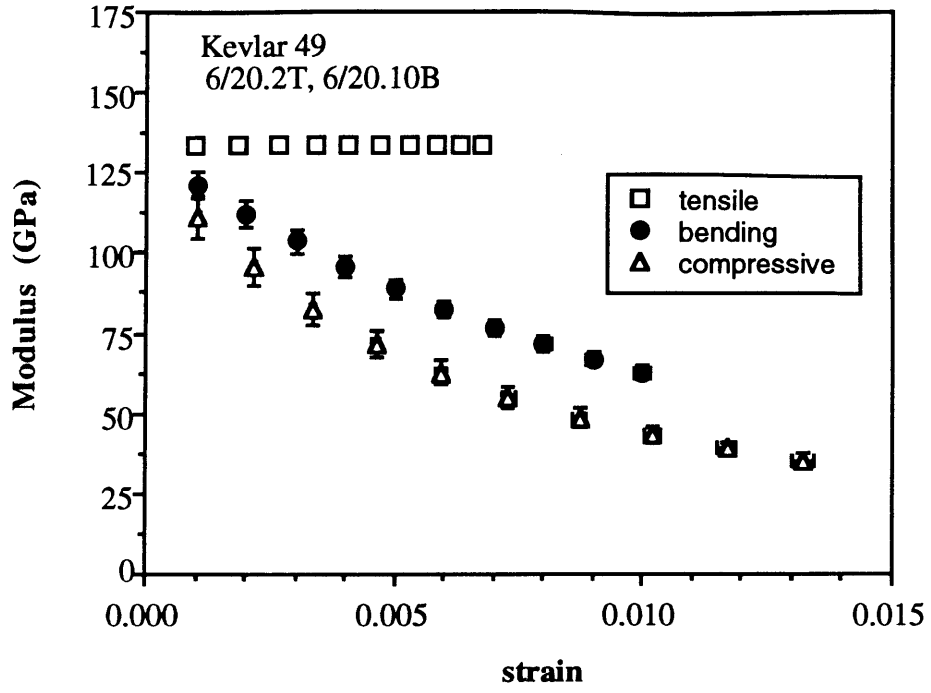

Figure 3.88. This Kevlar 49 fiber fails at 0.8% strain, but the tensile and compressive modulii diverge much earlier.

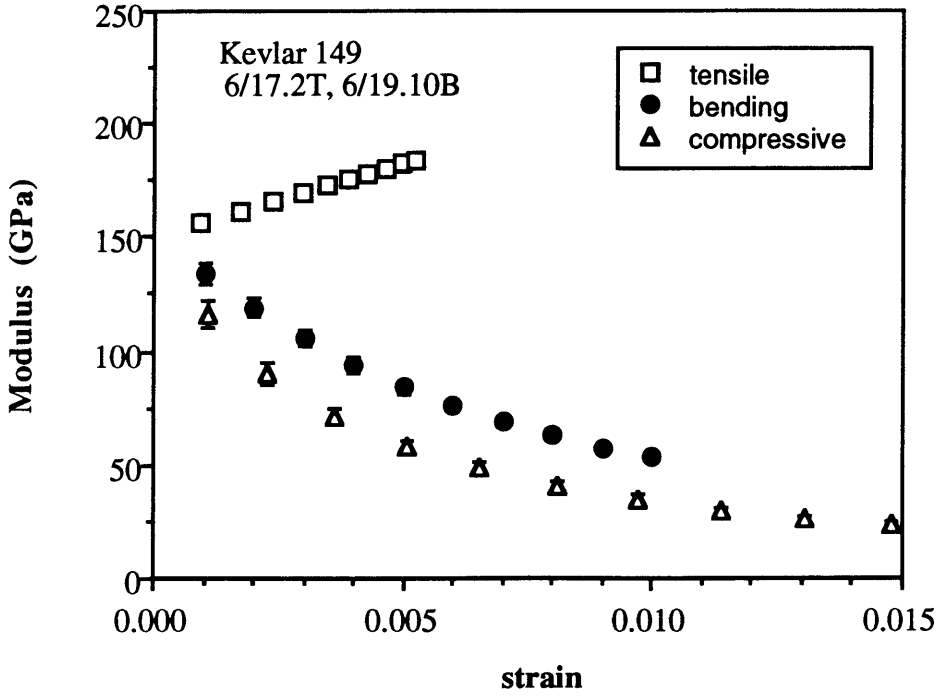

Figure 3.89. Kevlar 149 exhibits the most strain-dependent behavior of the Kevlar family because of the highly oriented microstructure.

Table 3.16. Coefficients of the modulus- strain equations for tension (T), bending (B) and compression (C) of Kevlar fibers. Modulus in GPa, strain in m/m.

fiber Kevlar	stress	a GPa	b GPa/(m/m)	c GPa/(m/m)^2	d GPa/(m/m)^3	e GPa/(m/m)^4
119	T	73				
	B	70.5	-4.93E+03	1.48E+05		
	C	68.3	-9.15E+03	8.36E+05	-4.57E+07	1.07E+09
29	T	72.6	7.40E+02	3.34E+03		
	B	80.5	-5.22E+03	1.48E+05		
	C	89.4	-1.30E+04	1.30E+06	-7.60E+07	1.85E+09
129	T	101.2	1.40E+03			
	B	94.7	-6.10E+03	1.73E+05		
	C	88.5	1.13E+04	9.95E+05	-5.24E+07	1.17E+09
49	T	133.3				
	B	130.9	-1.01E+04	3.29E+05		
	C	129.2	-1.93E+04	1.90E+06	-1.10E+08	2.65E+09
149	T	150.4	6.40E+03			
	B	149.1	-1.64E+04	6.92E+05		
	C	145.5	-3.13E+04	3.78E+06	-2.31E+08	5.48E+09

Table 3.17. Percent change in Kevlar modulus from zero strain to 0.15% and 0.4% strain.

Kevlar	second strain	Tension	Bending	Compression
119	0.15%	0.0%	-10.0%	-17.6%
	0.4%	0.0%	-24.6%	-37.9%
29	0.15%	1.5%	-9.3%	-18.9%
	0.4%	4.2%	-23.0%	-39.9%
129	0.15%	2.1%	-9.3%	-16.8%
	0.4%	5.5%	-22.8%	-36.4%
49	0.15%	0.0%	-11.0%	-19.3%
	0.4%	0.0%	-26.9%	-40.9%
149	0.15%	6.4%	-15.5%	-27.0%
	0.4%	17.0%	-36.7%	-53.7%

3.5.2 Carbon Fibers

PAN- based

The bending stress-strain curves for PAN- based carbon fibers (Figure 3.90) show a more gradual change with strain than the other fibers because the residual PAN ribbon network is more tightly intertwined than the fibrillar structure of Kevlar or the sheet structure of pitch- based carbon.. Small fiber diameters (6-7 μm for AS4 and HMS4, 4-5μm for IM7 and IM8) limited the maximum measurable strain for the test, preventing the measurement of bending failure stress.

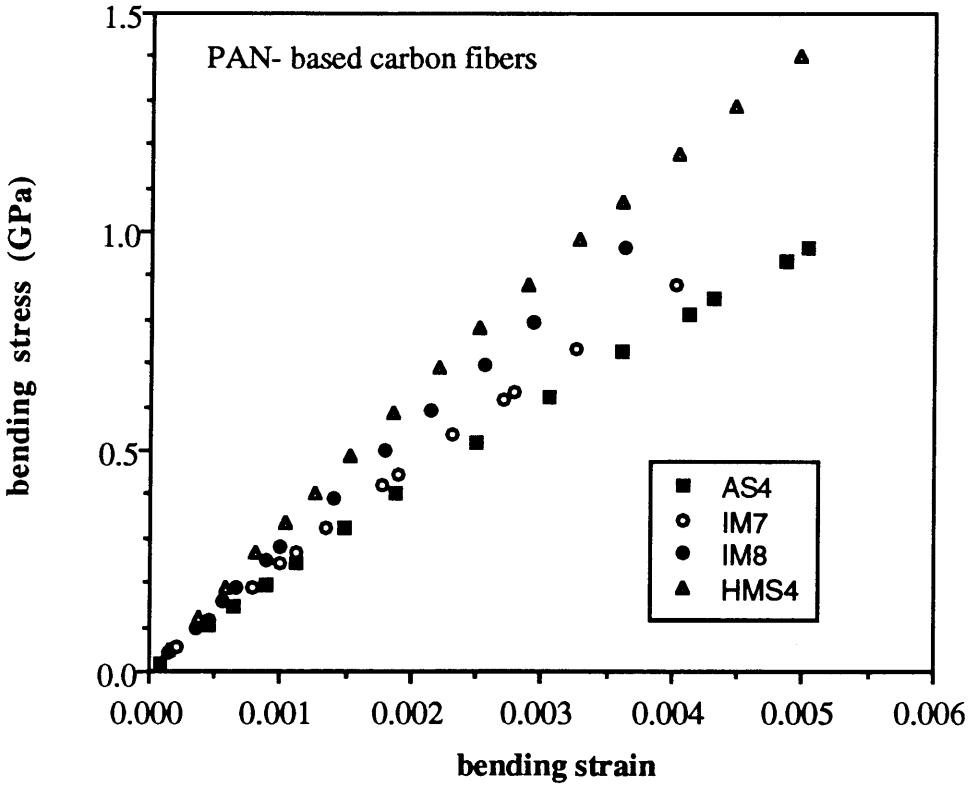

Figure 3.90. Bending stress-strain curves for representative PAN-based carbon fibers. Strain softening is apparent, but not as pronounced as in Kevlar and pitch- based carbon fibers.

The average tensile, bending and compressive modulii of the PAN- based AS4, IM7, IM8 and HMS4 fibers at 0.1% bending strain are shown in Figure 3.91. The behavior should be nearly equal at this point, as in the AS4 and HMS4 fibers. However,

the tensile and compressive modulii of the IM7 and IM8 fibers differ by more than the standard deviation of the data.

Anisotropy in all of the fibers does appear at higher strains: Figure 3.92 shows the average tensile, bending and compressive modulii at 0.4% bending strain in the AS4 and HMS4 fiber and 0.3% bending strain in the IM7 and IM8 fibers. The early appearance of anisotropic behavior in the intermediate modulus fiber may be due to the small fiber diameter. Keeping the initial deflection in the Micro-Flex test to a minimum is difficult for fibers with such low bending stiffnesses, so the measured bending strain could be higher than the actual bending strain.

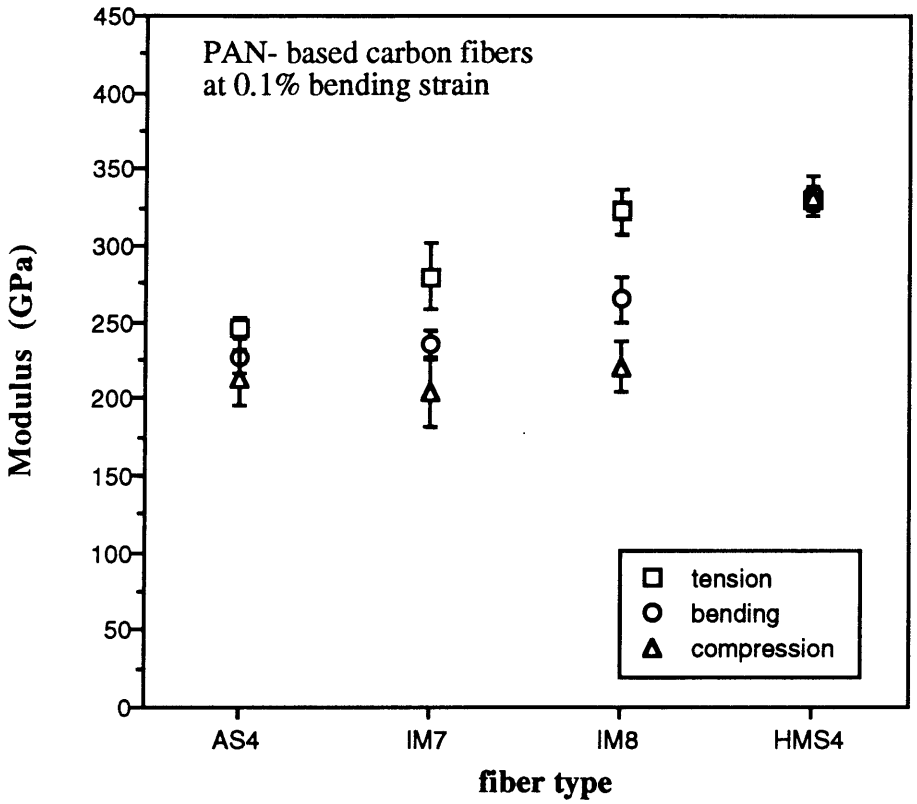

Figure 3.91. Average tensile, bending and compressive modulii of PAN- based carbon fibers at 0.1% bending strain. Error bars indicate the standard deviation of the data. AS4 and HMS4 modulii are nearly equal, but the tensile and compressive modulii of the intermediate modulus IM7 and IM8 have diverged.

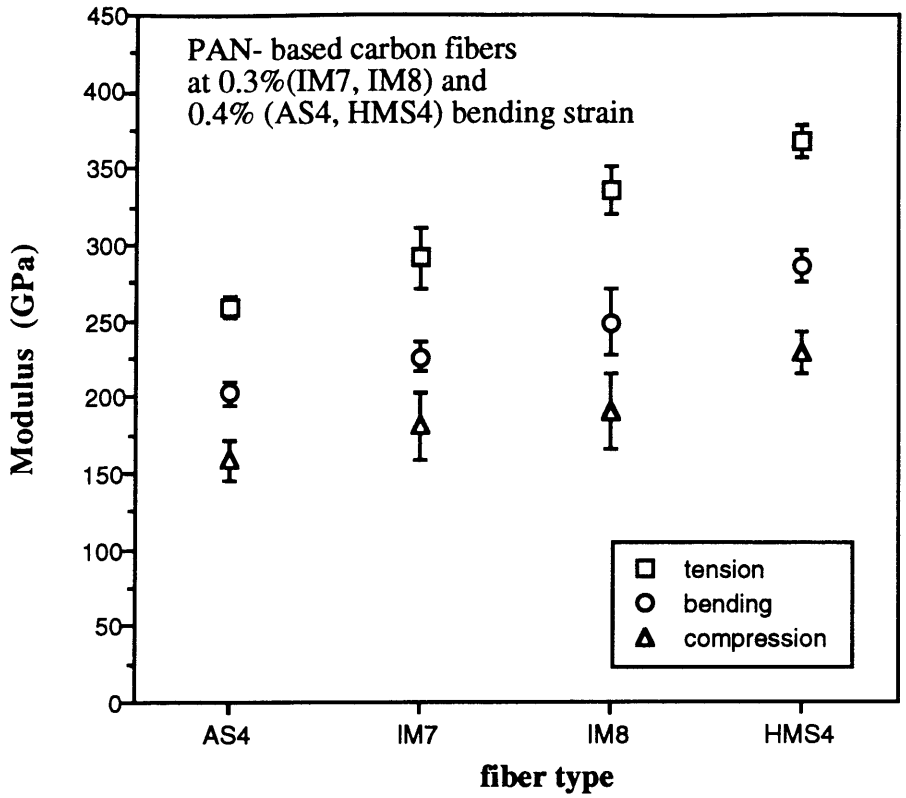

Figure 3.92. Compressive modulii of PAN- based fibers at 0.3% and 0.4% bending strain are significantly less than the measured tensile modulii.

The modulii of the PAN based fibers in tension, bending and compression as a function of strain are shown in Figures 3.93- 3.96. The intermediate modulus fiber data do not intersect at zero strain, suggesting that the bending modulus curve, and therefore the compressive modulus curve, is shifted to a lower strain. These individually calculated points from FITT and Micro-Flex data were fit with polynomial expressions to describe the change in modulus with strain in tension, bending and compression. The coefficients listed in Table 3.18 refer to equations of the form: $a + bx + cx^2 + dx^3 + ex^4$. The first coefficient, the "a" term, is the zero- strain modulus. In Table 3.19, the percent increase in modulus over the zero-strain value is listed for two strains, 0.1% and 0.4%. In the first 0.4% tensile strain, the modulus of the standard and intermediate modulus fibers increases by less than 10%, while a 0.4% compressive strain causes a drop of approximately 20% in the compressive modulus. The high modulus HMS4 fiber (presumably) has the most

highly oriented network structure, which is reflected in the increased degree of nonlinearity: a 0.4% tensile strain causes an increase in the tensile modulus of almost 20%, while a 0.4% compressive strain causes a decrease in the compressive modulus of 33%.

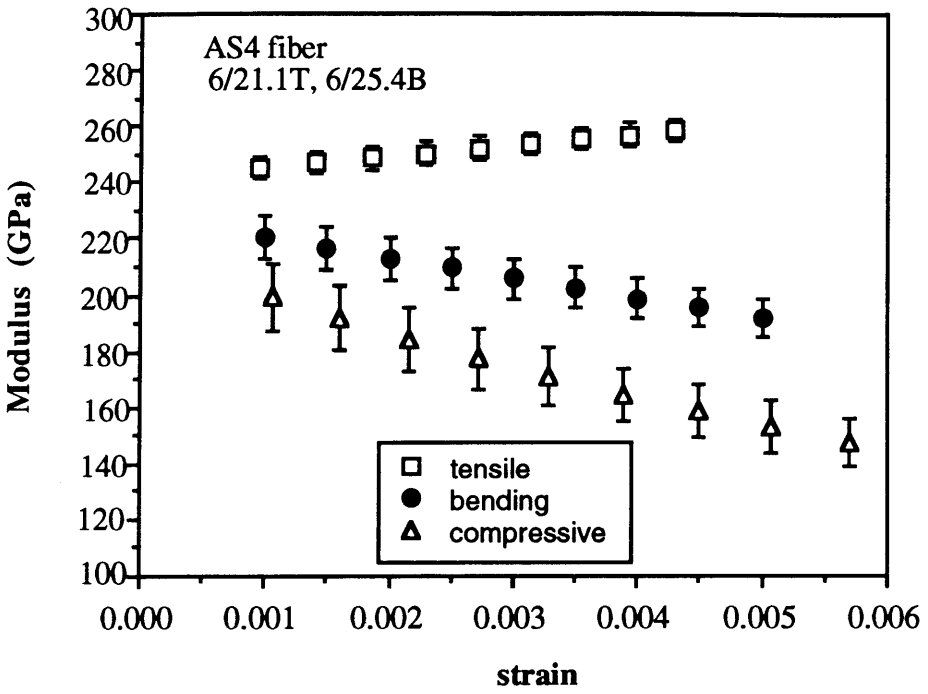

Figure 3.93. Tensile, bending and compressive modulii of an AS4 fiber diverge at very low strains. The error bars indicate the standard error of the measurement.

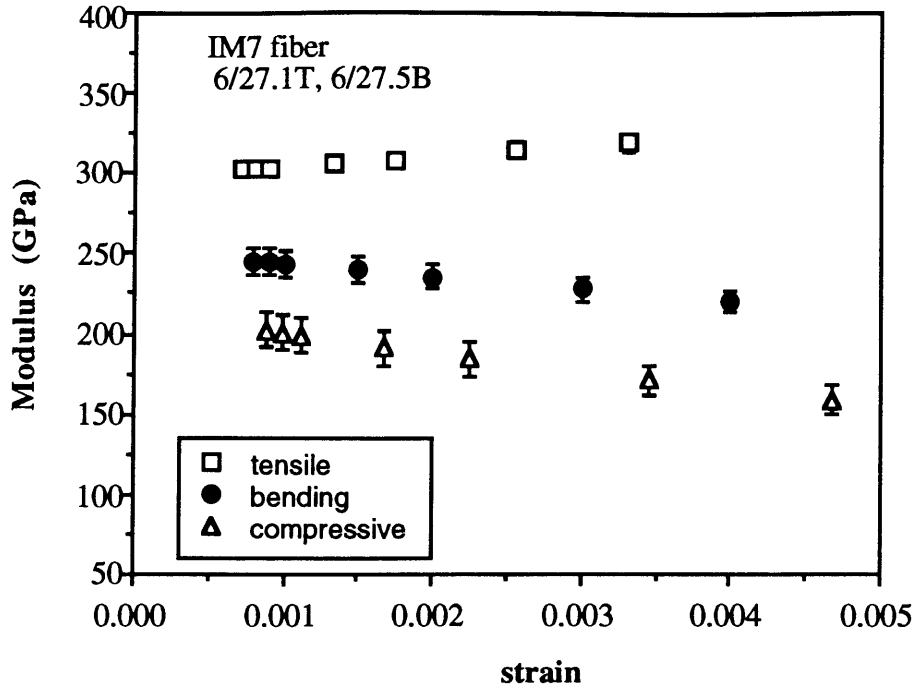

Figure 3.94. IM7 fiber modulii do not appear to converge at zero strain. The small fiber size may be responsible for a slight offset in the bending and therfore compressive stress strain curves.

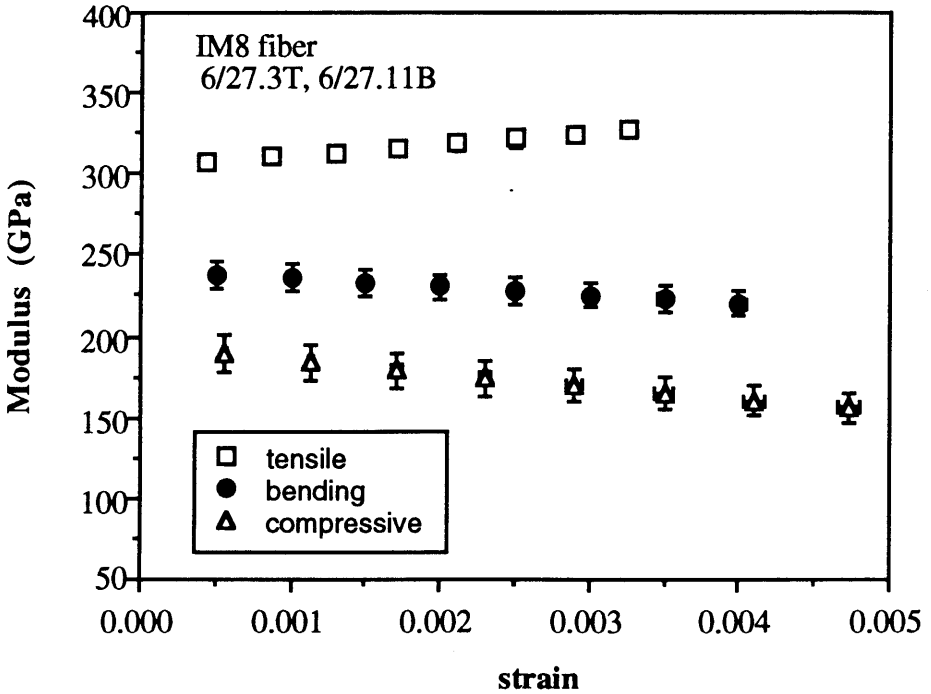

Figure 3.95. Similar to the IM7 fiber, the modulii of this IM8 fiber do not converge at zero strain.

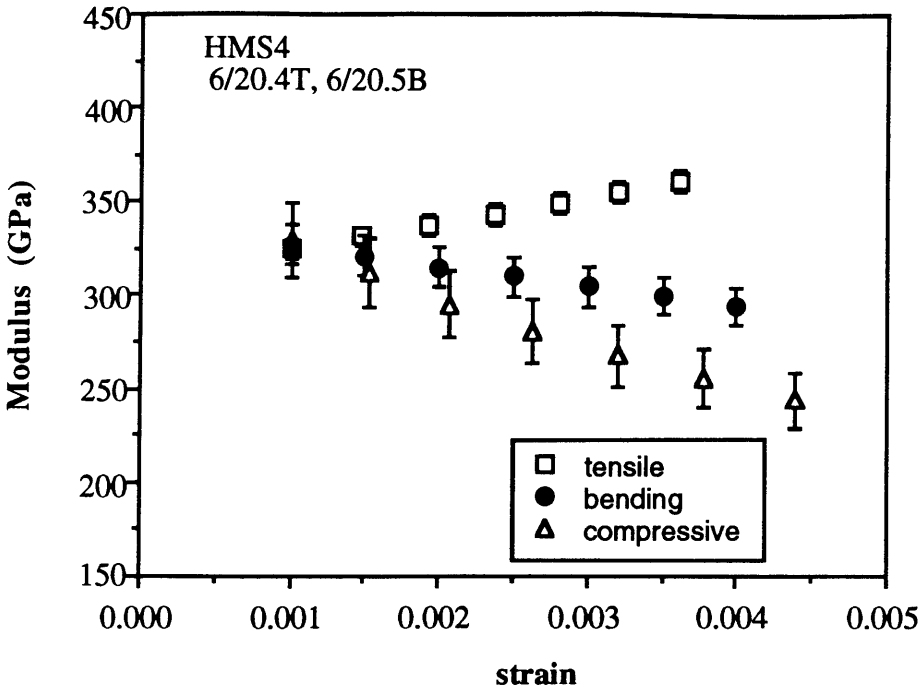

Figure 3.96. The tensile and compressive modulii converge at low strains. The increasing tensile modulus is more than compensated by the decreasing compressive modulus, causing a decrease in the bending modulus as strain increases.

Table 3.18. Coefficients of the modulus- strain equations for tension (T), bending (B) and compression (C) of Hercules PAN- based carbon fibers. Modulus in GPa, strain in m/m.

fiber	stress	a	b	c	d	e
		GPa	GPa/(m/m)	GPa/(m/m)^2	GPa/(m/m)^3	GPa/(m/m)^4
AS4	T	241.1	4.03E+03			
	B	228.3	-7.87E+03	1.34E+05		
	C	214.1	-1.38E+04	-4.84E+05	2.87E+08	-2.38E+10
IM7	T	296.9	6.36E+03			
	B	251.5	-8.68E+03	1.55E+05		
	C	215.3	-1.65E+04	1.30E+06	-9.62E+07	3.82E+09
IM8	T	303.5	7.15E+03			
	B	241	-5.56E+03	7.14E+04		
	C	195.3	-1.06E+04	6.30E+05	-2.27E+07	-1.48E+09
HMS4	T	310.8	1.38E+04			
	B	338.6	-1.19E+04	2.05E+05		
	C	372	-5.10E+04	9.34E+06	-1.45E+09	1.04E+11

Table 3.19. Percent change in PAN- based carbon fiber modulus from zero strain to 0.1% and 0.4% strain.

Fiber	second strain	Tension	Bending	Compression
AS4	0.1%	2%	-3%	-7%
	0.4%	7%	-13%	-24%
IM7	0.1%	2%	-3%	-7%
	0.3%	9%	-13%	-23%
IM8	0.1%	2%	-2%	-5%
	0.3%	9%	-9%	-18%
HMS4	0.1%	4%	-3%	-12%
	0.4%	18%	-13%	-33%

Pitch- based

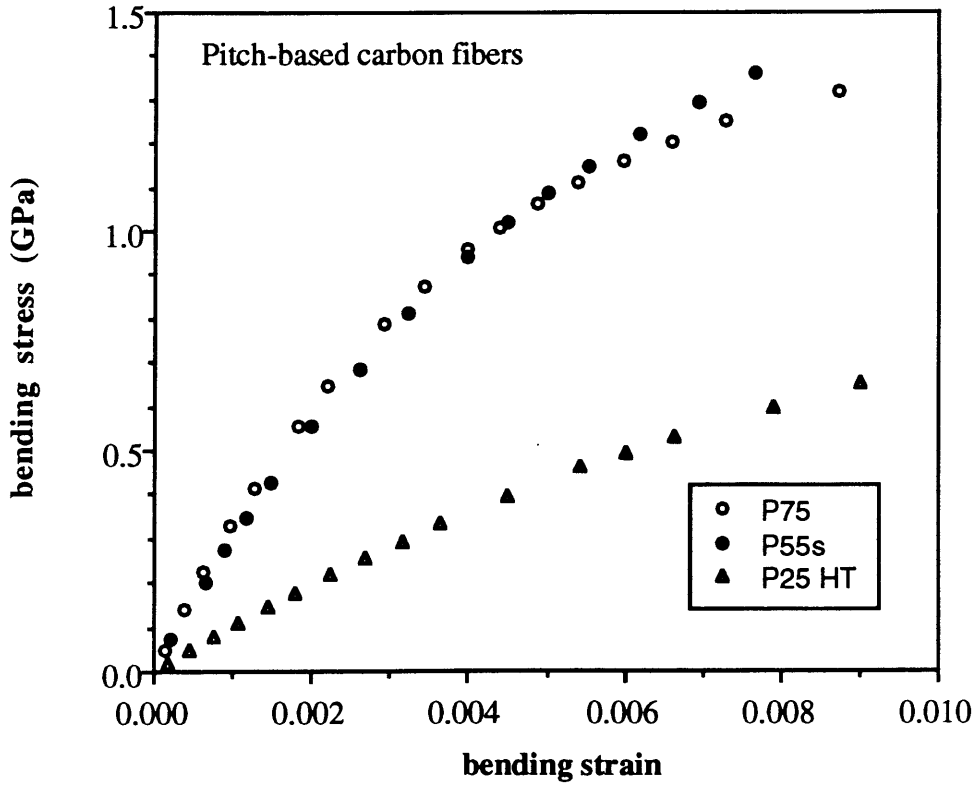

Figure 3.97. Bending stress-strain curves of pitch- based carbon fibers. Significant nonlinearity is present, but no fiber damge is apparent.

The sheet-like structure of the pitch- based carbon fiber is the source of its highly nonlinear mechanical behavior. Wide Angle X-Ray studies[6] show the graphite crystallite size perpendicular to the basal plane increases from 2.6 nm for P25 to 12.4 nm and 14.6 nm for P55 and P75 respectively. The P75 exhibits three dimensional crystalline order

while the P55 may and the P25 does not, although all show the sheet morphology. These physical features are reflected in the nonlinear bending stress-strain curves shown in Figure 3.97.

The curvature is much greater than the PAN- based fiber and resembles the Kevlar behavior. However, the major source of strain softening in the Kevlar fibers is the formation of tiny kink bands which eventually grow larger and cause compressive failure. This damage is irreversible: a fiber which has been tested to compressive failure is permanently deformed after the test. Pitch- based carbon fibers do not show any signs of failure within the limits of the Micro-Flex test, and the bending stress strain curves are reversible.

The loading and unloading curves for a single P75 fiber are shown in Figure 3.98. (The physical challenge of unloading the fiber is much greater than for loading the fiber, accounting for the minimal offset at the origin. If the weights are not removed in a slow and steady manner, the fiber may move slightly in the vertical direction, slightly changing the focus and increasing the error in the deflection measurement.) The Figure illustrates the nonlinear but elastic behavior of pitch-based fibers during Micro-Flex testing.

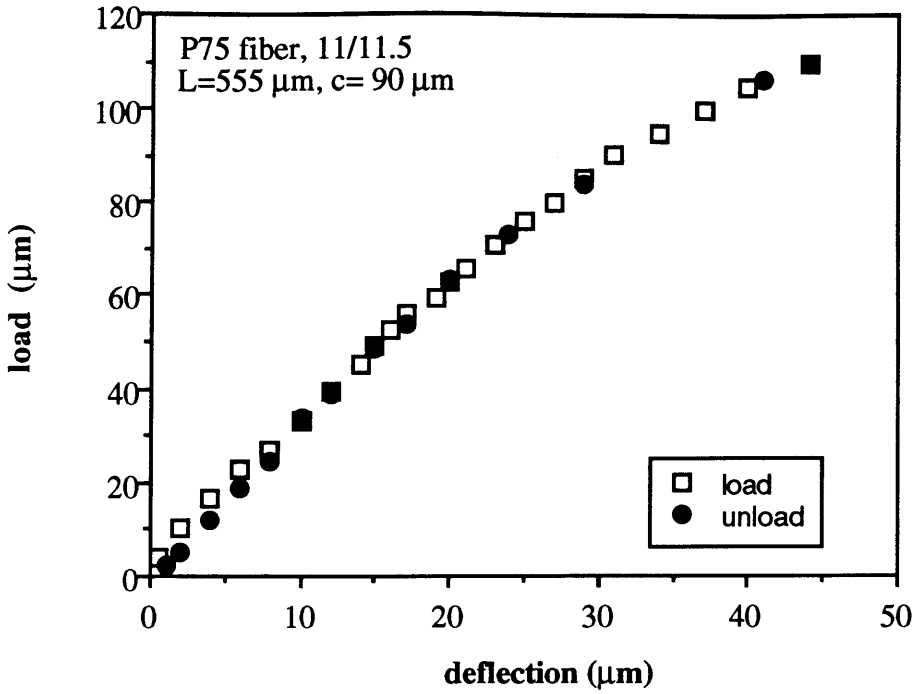

Figure 3.98. Loading and unloading curves for a P75 fiber. Behavior is nonlinear and elastic.

Figures 3.99 and 3.100 show the average tensile, bending and compressive modulii of P25, P55 and P75 fibers and the standard deviation of the data. At 0.1% bending strain, the P25 is isotropic, but the P55 and P75 already show significant differences between the tensile and compressive modulii. At higher bending strains, 0.6% for P25 and 0.2% for P55 and P75, the tensile modulii of all three fibers is much higher than the corresponding compressive modulii. The scatter in the P55 results at 0.2% bending strain is lower than at 0.1% bending strain because fewer samples have the required tensile information at this strain to calculate the compressive modulus.

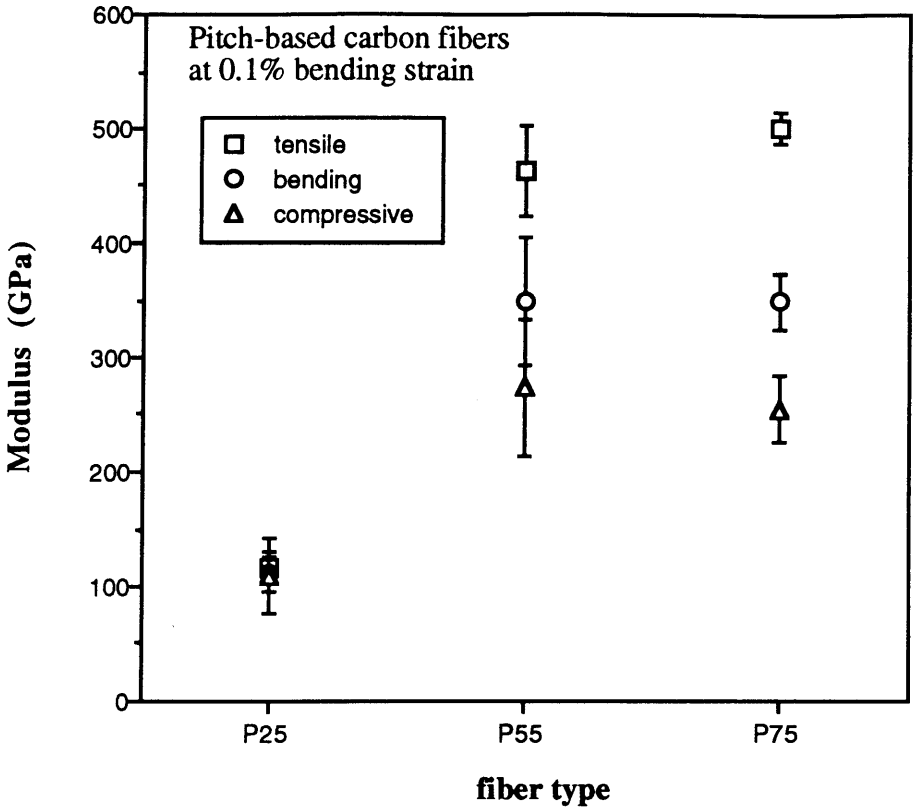

Figure 3.99. Average tensile, bending and compressive modulii of pitch- based carbon fibers at 0.1% bending strain. P25 is still in the isotropic range. The higher modulus P55 and P75 already exhibit anisotropy in the axial modulii.

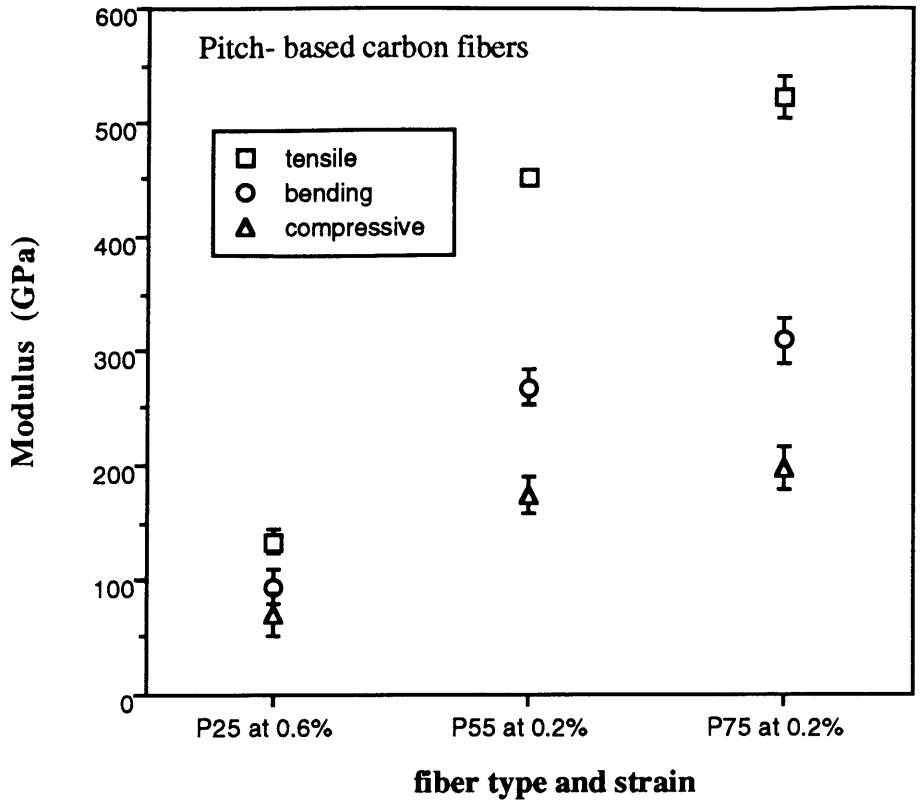

Figure 3.100. At higher bending strains, which are indicated on the x- axis for each fiber type, the tensile modulus of the pitch- based carbon fibers is twice as much as the compressive modulus.

Strain dependence of the tensile, bending and compressive modulii for the three types of pitch- based fiber is described by Figures 3.101-3.103. The divergence from isotropy is rapid in all three cases. The modulus vs. strain behavior is fit by polynomial regression, and the coefficients are listed in Table 3.20. The increase in modulus relative to the zero strain modulus, the coefficient "a" in Table 3.20, at low (0.1%) and intermediate (0.4% for P25 and 0.2% for P55 and P75) strains is listed in Table 3.21 for the three fibers in tension, bending and compression. The magnitude of the change in compression is 40-60% larger than in tension because the weak interaction between graphitic sheets in the fiber plays a more significant role in compression than in tension.

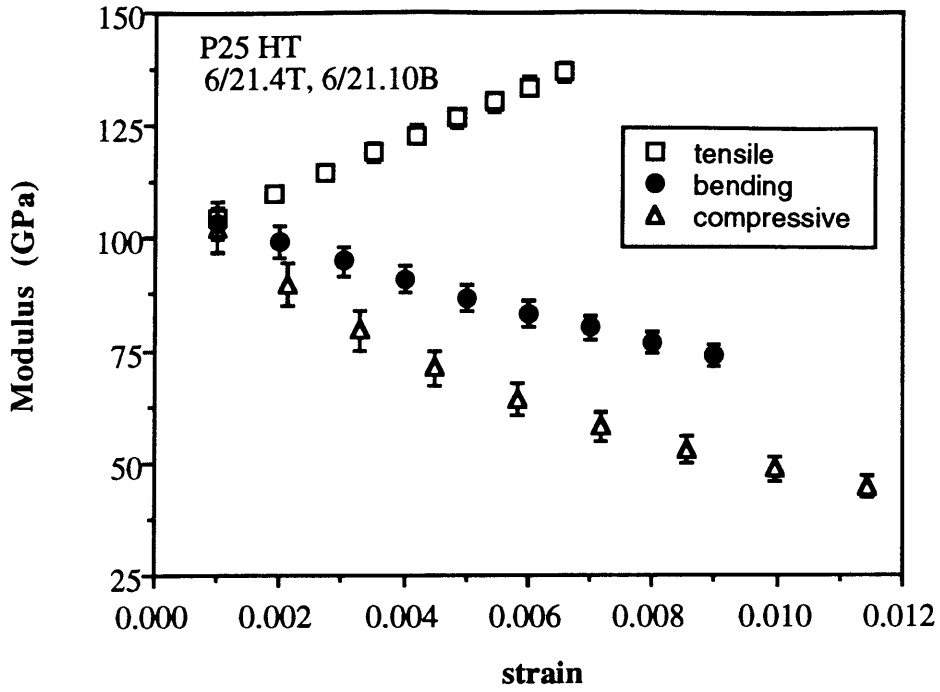

Figure 3.101. P25 is isotropic at low strains, but the tensile modulus increases while the compressive modulul decreases with strain.

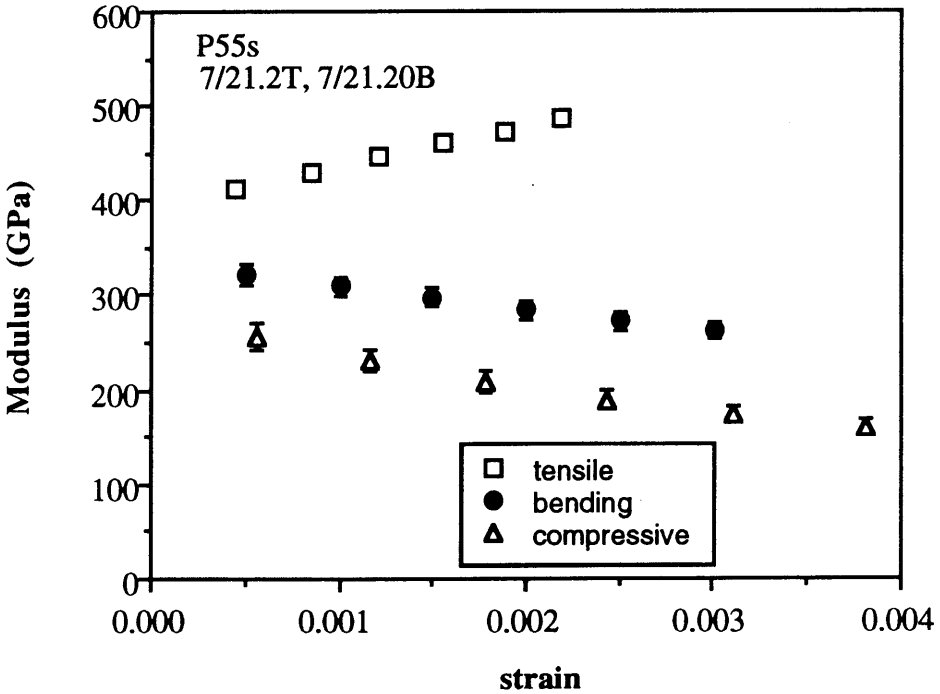

Figure 3.102. The tensile and compressive modulii of P55 fibers diverge at very low strains.

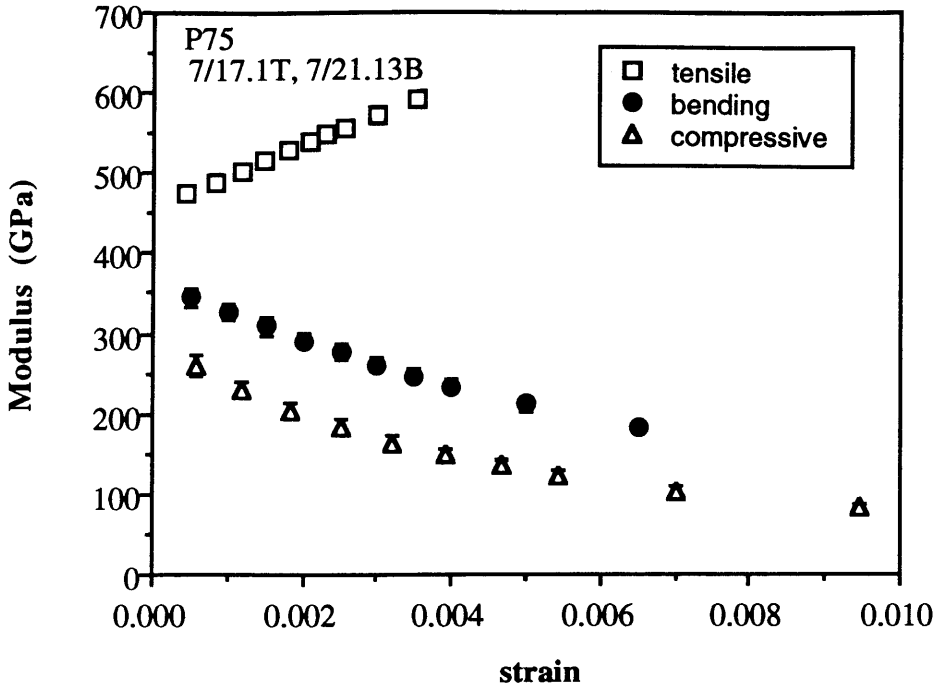

Figure 3.103. P75 is the most higly oriented of the pitch based fibers and shows the most nonlinear behavior. Significant anisotropy develops immeditely as the graphite sheets respond by orienting with applied tensile strain and away from applied compressive strain.

Table 3.20. Coefficients of the modulus- strain equations for tension (T), bending (B) and compression (C) of pitch- based carbon fibers. Modulus in GPa, strain in m/m.

fiber	stress	a	b	c	d	e
		GPa	GPa/(m/m)	GPa/(m/m)^2	GPa/(m/m)^3	GPa/(m/m)^4
P25	T	98.7	5.79E+03			
	B	108	-4.73E+03	9.89E+04		
	C	116.8	-1.63E+04	1.86E+06	-1.28E+08	3.63E+09
P55	T	395.7	4.10E+04			
	B	336.3	-2.87E+04	1.17E+06		
	C	284.9	-5.40E+04	5.92E+06	3.10E+08	-1.10E+11
P75	T	458.5	3.77E+04			
	B	363.7	-4.04E+04	1.93E+06		
	C	291.7	-6.28E+04	9.44E+06	-8.19E+08	2.90E+10

Table 3.21. Percent change in pitch- based carbon fiber modulus from zero strain to 0.1% and 0.4% (P25) or 0.2% (P55, P75) strains.

fiber type	second strain	Tension	Bending	Compression
P25	0.1%	6%	-4%	-12%
	0.4%	23%	-16%	-37%
P55	0.1%	10%	-8%	-17%
	0.2%	21%	-16%	-29%
P75	0.1%	8%	-11%	-19%
	0.2%	16%	-20%	-32%

3.6. Conclusion

The mechanical properties of high performance fibers directly reflect the fiber microstructure. In general, fiber behavior is isotropic at very low strains when the microstructure, either polymeric fibrils, the PAN ribbon- structure, or graphitic sheets, is in the as- processed condition. With the application of compressive strain, microstructural units which are oriented slightly off axis are forced away from the highest- modulus perfectly- aligned condition, causing a decrease in the observed compressive modulus. The strain softening in compression is more pronounced than the strain stiffening in tension as the microstructural units are brought into more perfect alignment with the latter. The bending behavior of these fibers, therefore, is dominated by the compressive softening, giving the bending and tensile stress strain curves distinctly different shapes.

Of the fibers in this study, the Kevlar ones are weakest in compression, followed by the pitch- and PAN- based carbon fibers. Weak lateral interaction between fibrils and between graphite sheets are responsible for both the nonlinear and anisotropic behavior of Kevlar and pitch- based fibers under axial strain. The interwoven ribbon network of the PAN- based fibers is less affected by applied strain, although the more open structure under compression has a lower modulus than in tension.

4. Summary

4.1. Nonlinear stress- strain behavior of high performance fibers

The axial mechanical behavior of the three types of fibers in this study, Kevlar aramid, PAN- based carbon and pitch- based carbon, is distinctly different from the glass fibers which were used as a control. The oriented microstructures characteristic of these fibers are responsible for a modulus which increases with tensile strain and decreases with compressive strain. Glass fibers do not have an oriented microstructure so the stress-strain curve is linear and the modulus measured in tension and bending is the same. Kevlar fibers have a hierarchical fibrillar structure developed during processing. In addition, all but Kevlar 149 exhibit a radially arranged pleated sheet morphology which respond to the applied strain. In tension, the pleats open, gradually offering more resistance as the pleat angles are stretched. Since the pleated structure is absent in Kevlar 149, the tensile modulus is larger than the other fibers initially and increases more rapidly with strain: the stress acts directly on the crystallites which are axially oriented.

The network ribbon structure of the PAN- based carbon fibers has good lateral connectivity. The open structure tightens and further orients the crystallites under tension, giving a continuous increase in tensile modulus with increasing strain. The network interpenetration prevents significant slip in compression, but the modulus decreases from the opening of the void structure. High modulus HMS4 fibers exhibit the greatest nonlinearity, due to a more perfectly aligned ribbon structure, than the standard modulus AS4 and intermediate modulus IM7 and IM8 fibers. The lower the degree of ribbon intertwining in the HMS4 is responsible for its higher initial modulus. Reduced lateral connectivity explains the greater strain sensitivity which is caused by crystallite rotation.

The sheet -like structure of the pitch- based fibers gives them the most nonlinear behavior. The relatively low modulus P25 fiber exhibits behavior in tension and compression similar in shape and magnitude to Kevlar 149 at low strains. The change in

compressive modulus with strain is less in P25 at higher strains because the fiber does not fail in a fashion similar to Kevlar. The higher modulus P55 and P75 fibers exhibit the most nonlinearity of all the fibers tested. The tensile modulus increases rapidly with strain as the graphite sheets orient further under stress and the fibers soften considerably under compression. Deformation is reversible in the strain range examined because the inter-sheet forces are low.

4.2. Axial anisotropy in high performance fibers

The stress-strain curves of high performance fibers are continuous at the origin so the modulii in tension, bending and compression are approximately the same at zero strain. The difference between the tensile and compressive modulii increases as the strain increases in the strain range in which the fibers are used. The tensile and compressive behaviors are not mirror images: the compressive modulus decreases more rapidly than the tensile modulus increases, reducing the ratio of compressive to tensile modulus with increasing strain.

Compressive failure occurs before tensile failure because of lateral connectivity and microstructural stability. This is true of the three types of fibers tested, but only the Kevlar fibres failed within the limits of the tests. Inter-fibrillar forces are weak, providing easy regions of separation within the fiber and the pleat angle is approximately $\pm 6°$ from the fiber axis, so buckling and collapse under compressive forces is possible. Kink bands develop, permanently softening the material. In Kevlar 149, kink bands are not visible during testing: the compressive strength is more strongly affected by the helical split due to processing which wraps around the fiber axis and it evident on the surface.

Generally, the compressive properties of high performance fibers suffer as the tensile properties are improved. Thus, the nonlinearity of fiber stress-strain behavior, as well as the anisotropy between axial modulii and strengths due to the oriented microstructure, should be considered when designing with these materials. A better

understanding of material behavior will permit more efficient design and use of these high performance fibers.

4.3. Single Fiber test methods

Single fiber testing is preferable to composite testing because of the reduced and more readily quantifiable errors and the smaller sample requirements. Methods for measuring the stress-strain response of a fiber in tension exist, but attempts to measure the response in compression have met with little success. This thesis introduces two single fiber test methods which, when performed sequentially, yield stress-strain behavior in tension, bending and compression.

The Fiber Incremental Tensile Tester provides tensile stress-strain data for single fibers without the need to adjust for system compliance. Test execution and data analysis are straightforward and result in an estimated error of ±1.6%. The FITT fixtures could be modified by increasing the screw neck size to test more brittle fibers. If preferred, the secant modulus can be calculated instead of the tangent modulus. The measured results are neither consistently higher nor lower than the modulus values for the tested fibers reported by others, which lends confidence to the validity of this method. In fact, however, the measured values are different, because the strain effects are more precisely determined.

The Micro-Flex test is a simple way to observe single fiber compressive properties directly. The system is inexpensive to build and is extremely versatile. The fixtures can be machined to the dimensions necessary to achieve a specific strain range in fibers with various diameters and the load-deflection data collection system can be modified to accommodate existing equipment. Obviously, care is required in calculating the compressive properties of strain dependent fibers, but the propagated error can be kept to ±6%. Although it requires an isolated environment, the FITT/ Micro-Flex sequence is ideal for assessing the tensile, bending and compressive properties of commercially available and experimental high performance fibers. This information is useful for material development and selection and for a more efficient product design.

Appendix A: Error Analysis

While the single fiber tests are simple in concept, small errors in preparation and execution can lead to large errors in the measured properties. This analysis quantifies the contributions of error from the slope of the load- deflection curve, the fiber radius and the test span measurements, the tensile modulus and apparatus misalignment. Once the standard error for each step in the test, $S(x_i)$, is determined, the propagation is calculated according to Equation A.1. The analysis indicates that the standard error in the compressive modulus and strength determinations are approximately ± 6%.

$$S(y) = \sqrt{\sum \left(\frac{\partial y}{\partial x_i}\right)^2 (S(x_i))^2} \qquad (A.1)$$

A1. Tensile modulus error

The fiber tensile modulus can vary depending on the method of measurement. In fibers which continue to orient and stiffen under tension, the modulus changes with strain, so a single reported value is insufficient in the Micro-Flex calculations. Tensile stress-strain behavior is measured with the Fiber Incremental Tensile Tester, and the tangent modulus is calculated according to Equation A.2, where m_T is the tangent of the load-extension data, L_0 is the gage length and r is the fiber radius.

$$E_T = \frac{m_T L_0}{2\pi r^2} \qquad (A.2)$$

The derivatives of this expression with respect to the test variables are given in Equation group A.3, and the standard error is determined by Equation A.4. The uncertainty in gage length measurement contributes approximately 0.02%- 0.03% error to the measured tensile modulus. The slope repeatability, as described in Chapter 2, is on the order of ±0.6%. Radius variation of 0.1 micron in a typical radius of 3- 6 microns leads to an error of up to ±1% , so the radius is the dominant source of error. The tensile modulus measured with the FITT test has a standard error of 1.6%.

$$\frac{\partial E_T}{\partial m_T} = \frac{E_T}{m_T} \qquad \frac{\partial E_T}{\partial L_0} = \frac{E_T}{L_0} \qquad \frac{\partial E_T}{\partial r} = \frac{-2E_T}{r} \tag{A.3}$$

$$S(E_T) = \sqrt{\left(\frac{\partial E_T}{\partial m_T}\right)^2 (S(m_T))^2 + \left(\frac{\partial E_T}{\partial L_0}\right)^2 (S(L_0))^2 + \left(\frac{\partial E_T}{\partial r}\right)^2 (S(r))^2} \tag{A.4}$$

A2. Bending stiffness error

The bending stiffness, Equation A.5, is a function of the slope of the load-deflection data, the test span and the test midspan. The change in bending stiffness with each variable is given by the Equation group A.6. The standard error in bending stiffness is calculated with Equation A.7, and is of the order of ±1.5%.

$$EI = mG \tag{A.5}$$

$$\frac{\partial EI}{\partial m} = G \qquad \frac{\partial EI}{\partial L} = m\frac{2L^2 - c^2}{32} \qquad \frac{\partial EI}{\partial c} = m\frac{c^2 - 2Lc}{32} \tag{A.6}$$

$$S(EI) = \sqrt{\left(\frac{\partial EI}{\partial m}\right)^2 (S(m))^2 + \left(\frac{\partial EI}{\partial L}\right)^2 (S(L))^2 + \left(\frac{\partial EI}{\partial c}\right)^2 (S(c))^2} \tag{A.7}$$

A2.1. Slope precision

The slope of the load- deflection curve is used to calculate the bending stiffness. The quality of the fit is indicated by the correlation coefficient, R^2, where a perfect fit corresponds to R^2 = 1.000. The standard error in the slope from regression depends on the quality of the fit and the number of load- deflection pairs used to calculate the equation, but it remains approximately 1- 2%. The standard deviation of the slopes from repeated testing of a single fiber is of the order of 1%, which is less than the error in the equation, so the standard error assigned to the slope of the load- deflection curve is ± 1%.

A2.2. Test span and midspan

The geometric factor relating slope to bending stiffness is a function of both span, L, and midspan, c. The Micro-Flex fixtures were measured both at 0° and 45° tilt in the

SEM at approximately 100 x magnification. Because the measurement cursors are calibrated with the focus, the accuracy of measurement depends on the focus and alignment of the fixture columns. Based on repeated measurements, the test spans of 666 μm and 542 μm are correct to within ±5 μm, while the 90 μm midspan is correct to within ±2 microns.

If the fiber is not completely horizontal, the distances increase by a factor equal to the secant of the angle with the horizontal. This angle is checked visually, and is always less than 8°. The dimension increase due to a non- horizontal fiber is within the error of the dimension measurements themselves.

A2.3. Effect of Misalignment

Fixture misalignments above approximately 3% are immediately apparent in the Micro-Flex test. The error translates to a negligible increase in the geometric factor. Column alignment is checked before testing, and the fiber curvature checked during testing. If the load probe is off- center, the fiber will curve more noticeably at one load column, and in Kevlar fibers kinking will occur preferentially at this site because the maximum compressive stress in the fiber increases.

A3. Compressive modulus error

The compressive modulus is calculated using Equation A.8 with the tensile modulus, E_T, from the FITT test and the bending stiffness, EI, from the Micro-Flex test. The error in the compressive modulus is larger than in the tensile modulus and bending stiffness because of the neutral axis shift, which affects the calculation of the centroidal moments of inertia of the whole fiber, I_F, and the tensile sector, I_T. The derivatives of the compressive modulus are given in Equation group A.9, and the expression for standard error in Equation A.10.

$$E_c = \frac{(EI) - E_T I_T}{I_F - I_T} \tag{A.8}$$

$$\frac{\partial E_C}{\partial EI} = \frac{1}{(I_F - I_T)} \tag{A.9a}$$

$$\frac{\partial E_C}{\partial I_F} = \frac{-EI + E_T I_T}{(I_F - I_T)^2} \qquad \frac{\partial E_C}{\partial I_T} = \frac{-I_F + I_T + EI - E_T I_T}{(I_F - I_T)^2} \tag{A.9b}$$

$$\frac{\partial E_C}{\partial E_T} = \frac{(I_F - I_T)\left(-I_T - E_T \frac{\partial I_T}{\partial E_T}\right) - [EI - E_T I_T]\frac{\partial}{\partial E_T}(I_F - I_T)}{(I_F - I_T)^2} \tag{A.9c}$$

$$S(E_C) = \sqrt{\left(\frac{\partial E_C}{\partial EI}\right)^2 (S(EI))^2 + \left(\frac{\partial E_C}{\partial E_T}\right)^2 (S(E_T))^2 + \left(\frac{\partial E_C}{\partial I_T}\right)^2 (S(I_T))^2 + \left(\frac{\partial E_C}{\partial I_F}\right)^2 (S(I_F))^2} \tag{A.10}$$

A3.1. Effect of Bending Stiffness

The change in compressive modulus with bending stiffness is given by Equation A.9a. The error in the compressive modulus from this source as described in section 2 is less than ±2.5% and depends on the fiber size and the ratio of compressive to tensile modulus.

A3.2. Effect of tensile modulus, Et

Figure A.1 is a graph of compressive modulus vs. bending stiffness for a Kevlar 49 fiber of radius 6.0 μm. The tensile modulus is reported by duPont to be 18 Msi, which is represented by the middle curve. Increasing or decreasing that value by 10% yields the flanking curves. Generally, the ratio of tensile to compressive modulus ranges from 1.3 to 2.0 . This area is marked on the graph. If the measured bending stiffness is 10^{-10} N*m^2, a typical value, the difference between the high and low compressive modulii is 17.4% compared to the result calculated from the reported tensile modulus. The variation is not symmetric, however. If the tensile modulus is 10% lower than reported, the compressive modulus is 9.6% higher than calculated. If the tensile modulus is 10% higher than reported, the compressive modulus is 7.8% lower. In this study, the tensile modulus error was ±1.6%, thus the large spreads in compressive modulii were not encountered.

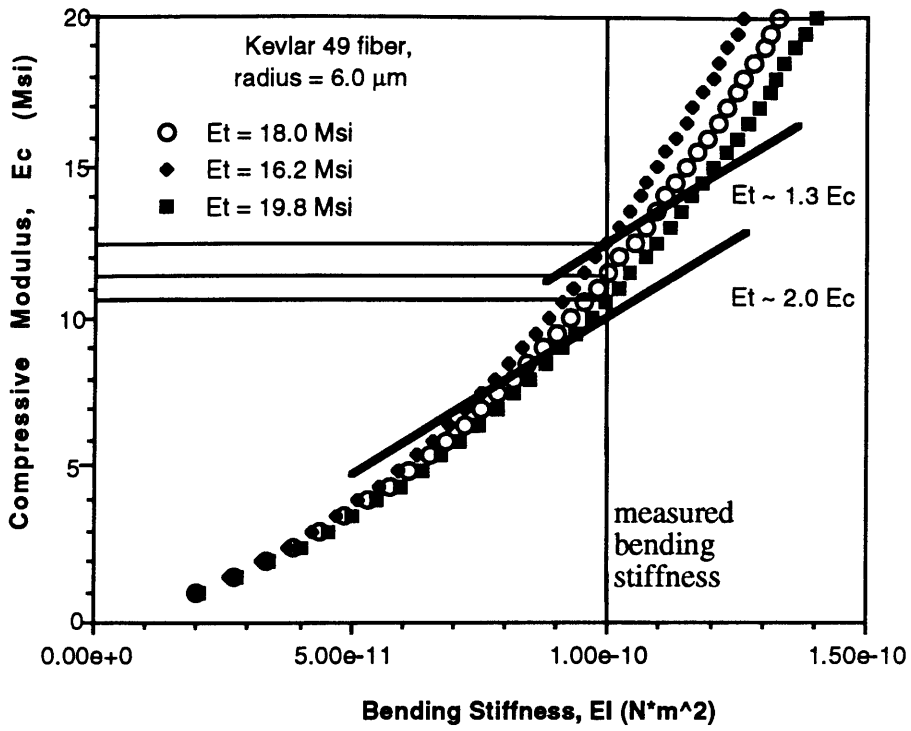

Figure A.1. Compressive modulus as a function of bending stiffness. Reported tensile modulus is 18.0 Msi. Filled curves are for variation of 10% from reported value. For these fibers, the ratio of Et to Ec is usually 1.3 to 2.0, so a typical measured EI is 10^(-10) N*m^2.

A3.3. Effect of neutral axis shift

The asymmetry in the compressive modulus calculated from the bending stiffness for varying tensile modulii, cited in Section A3.2, is due to the shift in the fiber neutral axis, defined in Equation A.11. The derivative of the shift with respect to the tensile modulus is given in Equation A.12. The shift factor and the fiber radius determine the centroidal moments of inertia for the whole fiber (Equation A.13) and tensile sector (Equation A.16), so the geometric contribution to bending stiffness is no longer easily separated from the material contribution. The derivatives with respect to radius and tensile modulus are given in Equation groups A.14 and A.17, and the standard errors are given by Equations A.15 and A.18.

$$k = \frac{\sqrt{E_T/E_C} - 1}{\sqrt{E_T/E_C} + 1} \tag{A.11}$$

$$\frac{\partial k}{\partial E_T} = \frac{\sqrt{E_T/E_C}}{E_T\left(\sqrt{E_T/E_C} + 1\right)^2} \tag{A.12}$$

$$I_F = \pi r^4 (0.25 + k^2) \tag{A.13}$$

$$\frac{\partial I_F}{\partial r} = \frac{4I_F}{r} \qquad \frac{\partial I_F}{\partial E_T} = 2\pi r^4 k \frac{\partial k}{\partial E_T} \tag{A.14}$$

$$S(I_F) = \sqrt{\left(\frac{\partial I_F}{\partial E_T}\right)^2 (S(E_T))^2 + \left(\frac{\partial I_F}{\partial r}\right)^2 (S(r))^2} \tag{A.15}$$

$$I_T = r^4\left[\frac{a}{2}\left(0.25 + k^2\right) - \frac{5}{6}k\left(1 - k^2\right)^{1.5}\right] \tag{A.16}$$

where $\quad a = \alpha - k\left(1 - k^2\right)^{0.5}$

$$\frac{\partial I_T}{\partial r} = \frac{4I_T}{r} \tag{A.17a}$$

$$\frac{\partial I_T}{\partial E_T} = r^4\left[ak - \left(0.5 + 3.5k^2\right)\left(1 - k^2\right)^{0.5} - \frac{5}{6}\left(1 - k^2\right)^{1.5}\right]\frac{\partial k}{\partial E_T} \tag{A.17b}$$

$$S(I_T) = \sqrt{\left(\frac{\partial I_T}{\partial E_T}\right)^2 (S(E_T))^2 + \left(\frac{\partial I_T}{\partial r}\right)^2 (S(r))^2} \tag{A.18}$$

A3.4. Effect of variation in radius, r

The compressive modulus dependence on fiber radius is very strong, especially at higher values of bending stiffness. Figure A.2 is similar to figure A.1, but there the reported tensile modulus of 18 Msi is held constant and the fiber radius is changed ± 0.1 μm from 6.0 μm. For a typical bending stiffness of 10^{-10} N*m^2, the difference between the high and low compressive modulii is 24.3%: [E_C(5.9μm)-E_C(6.1μm)]/E_C(6.0μm).

Again, the variation is not symmetric because the shift factor, k, is the shift distance relative to the fiber radius, and the fourth power of the radius is used to calculate fiber moments of inertia. Decreasing the radius by 1.7% increases the calculated compressive modulus by 13.0%, while increasing the radius by 1.7% decreases the calculated compressive modulus by 11.3%.

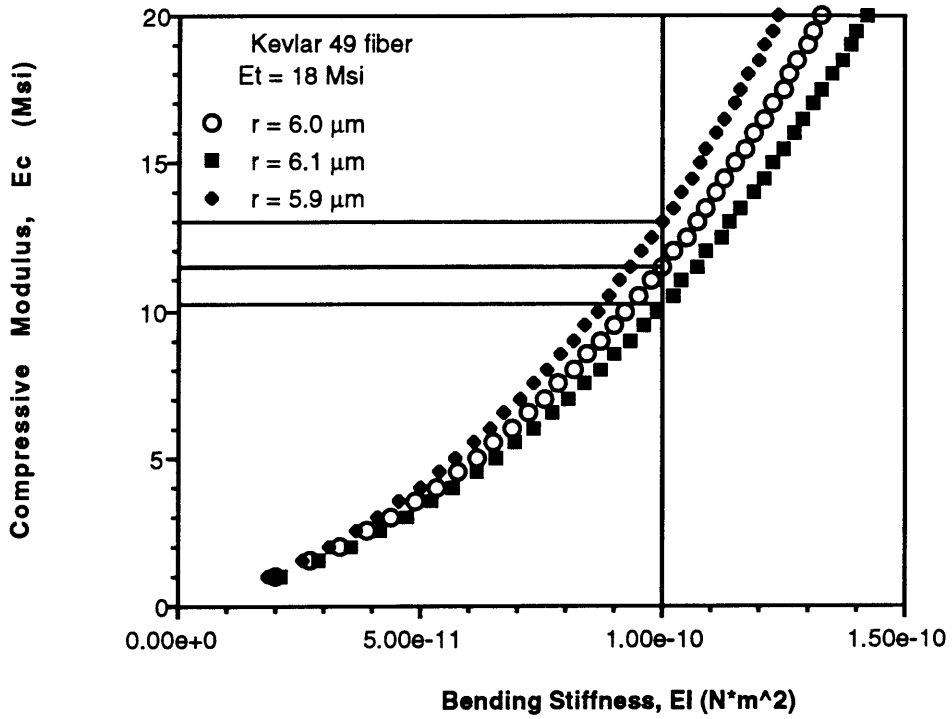

Figure A.2. Compressive modulus as a function of bending stiffness for Kevlar 49 fibers (tensile modulus = 18 Msi). Bending stiffness is chosen as in Figure A.1. Radius variation of 1.7% yield large variation in the calculated compressive modulus.

A4. Conclusion

The sources of error which have been identified are the tensile modulus, bending stiffness and fiber radius. Of the three, the bending stiffness is the most precisely measured and contributes the least to compressive modulus error. Both the tensile modulus and the fiber radius strongly affect the calculated compressive properties and they should be measured with the greatest care. By keeping the total error in the fiber radius to less than 1.6% the error in the FITT- measured tensile modulus is ±1.6% and the error in the compressive modulus is ±6%.

Appendix B: FITT data plots

B1. Glass Fibers

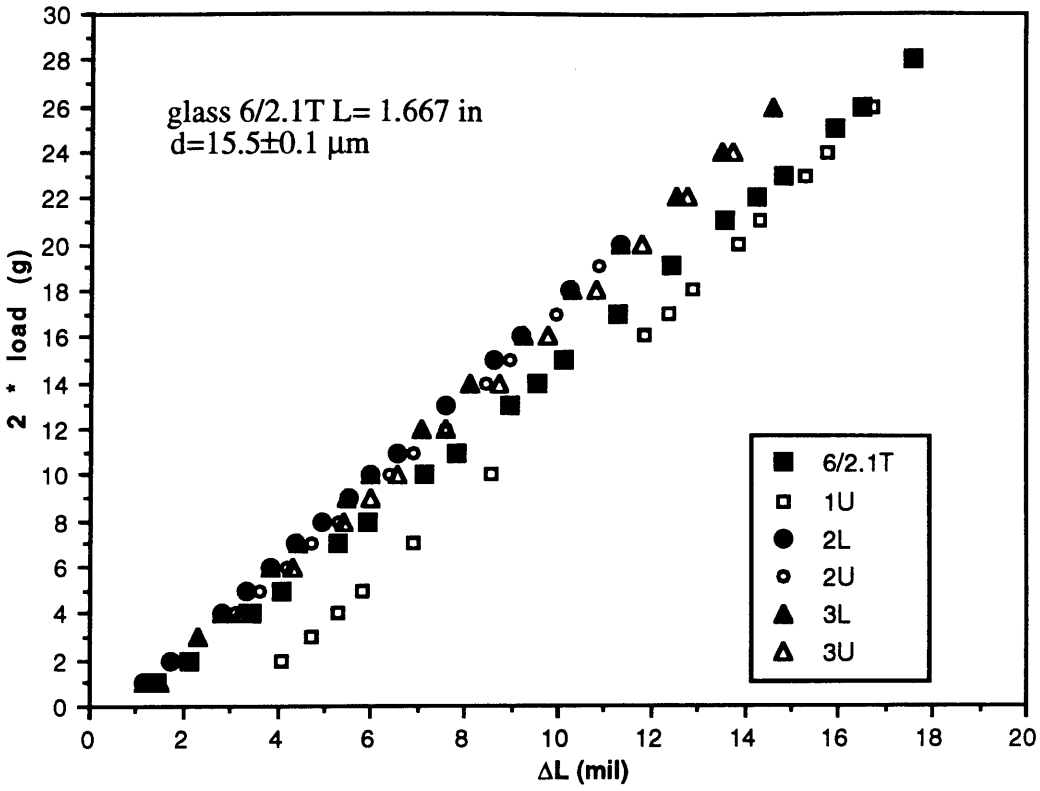

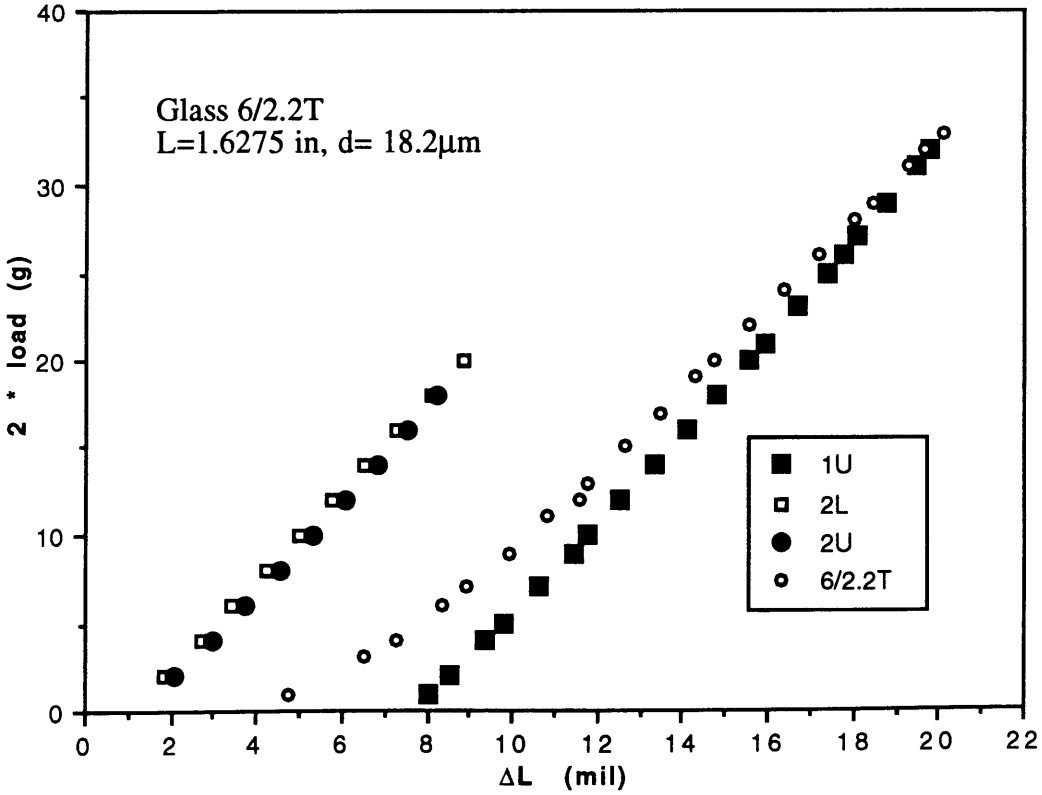

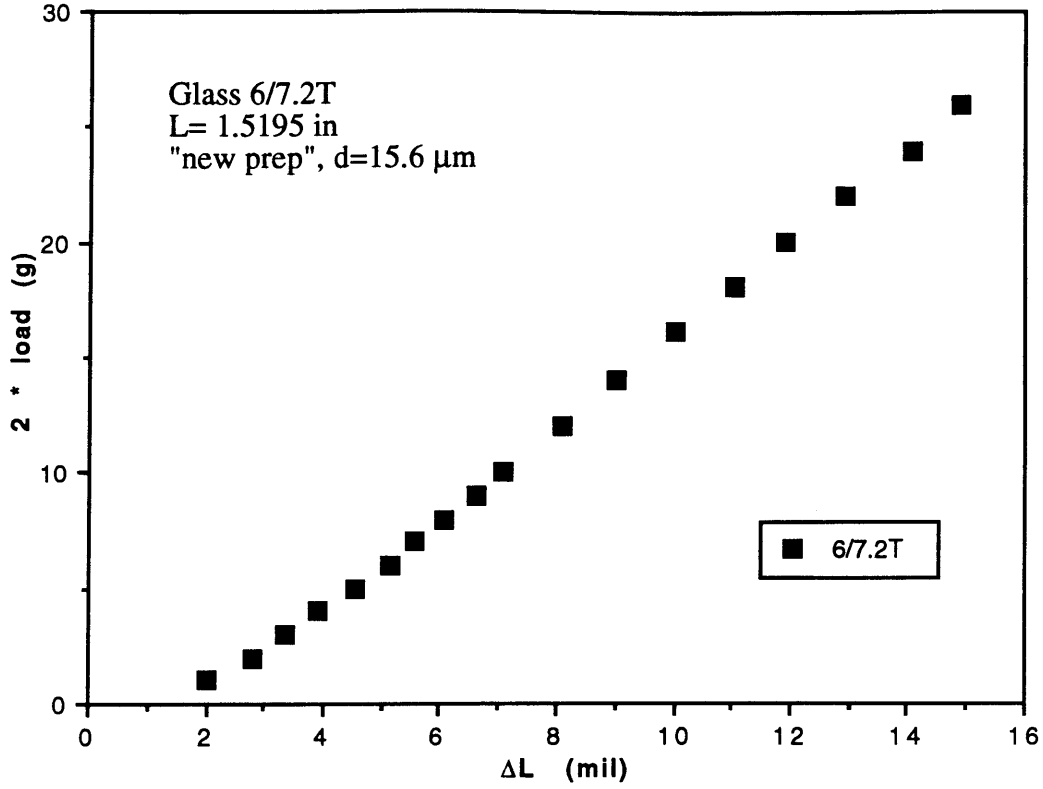
Glass 6/7.2T
L= 1.5195 in
"new prep", d=15.6 µm
2 * load (g)
ΔL (mil)
6/7.2T
0
10
20
30
0
2
4
6
8
10
12
14
16

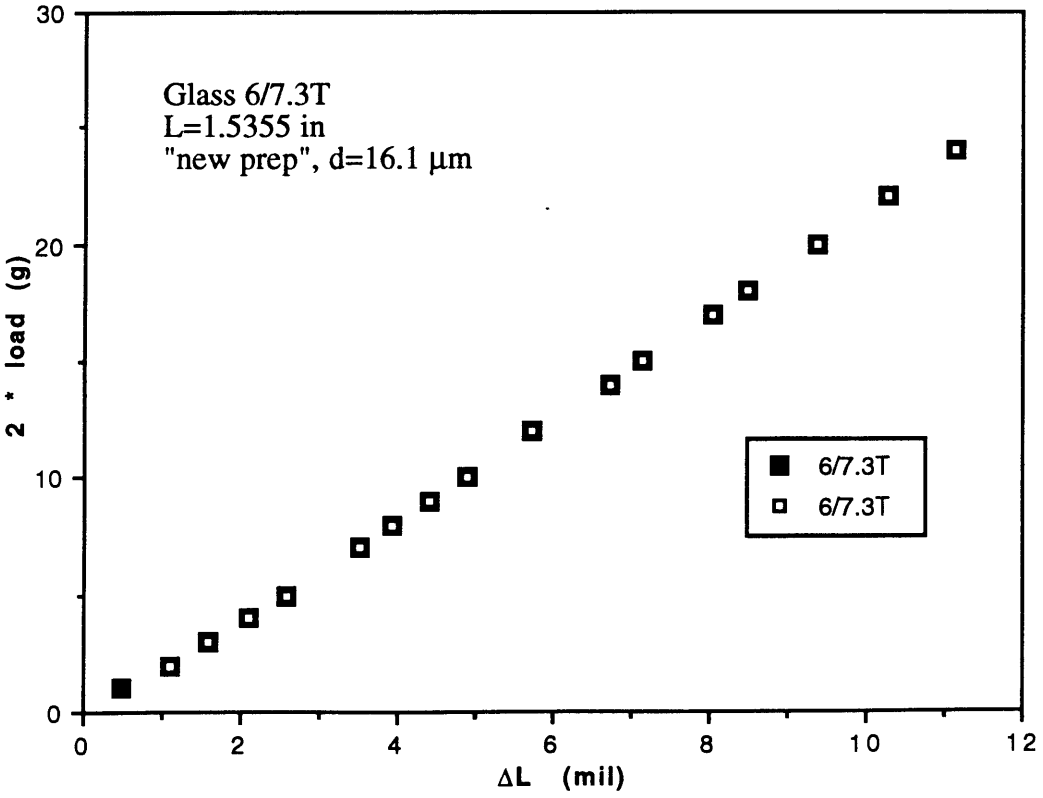
Glass 6/7.3T
L=1.5355 in
"new prep", d=16.1 µm
2 * load (g)
ΔL (mil)
6/7.3T
6/7.3T
0
10
20
30
0
2
4
6
8
10
12

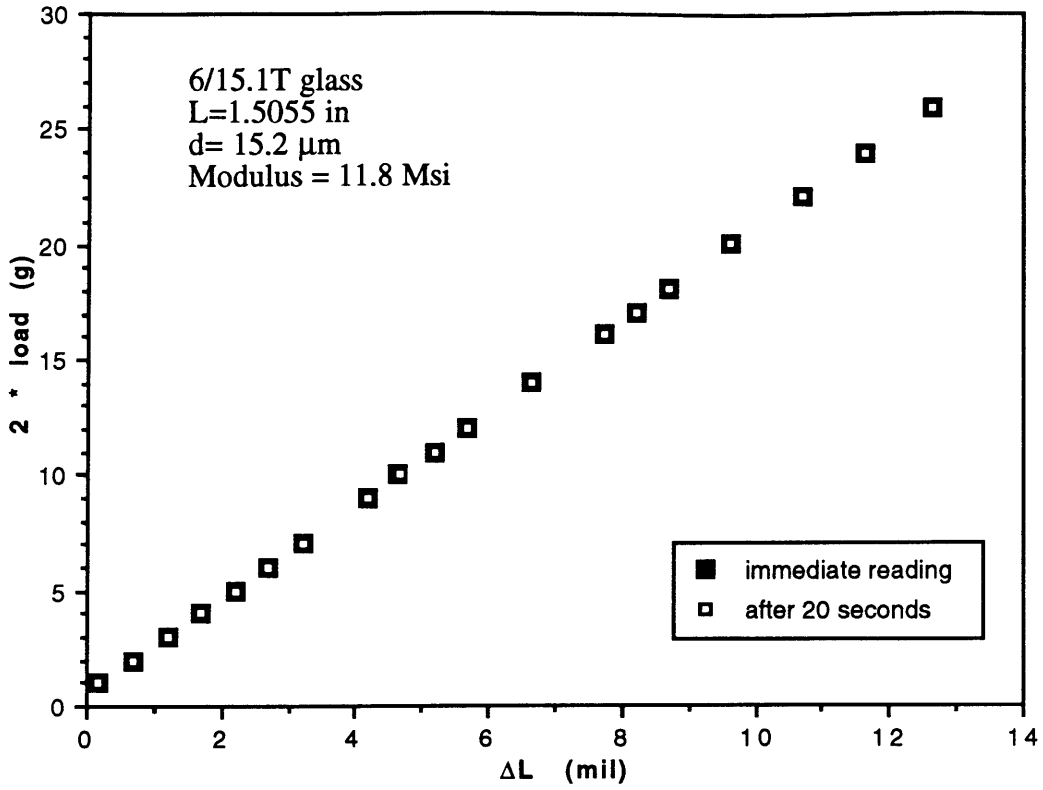
6/15.1T glass
L=1.5055 in
d= 15.2 μm
Modulus = 11.8 Msi
immediate reading
after 20 seconds
2 * load (g)
ΔL (mil)
0
5
10
15
20
25
30
0
2
4
6
8
10
12
14

B2. Kevlar 119 Fibers

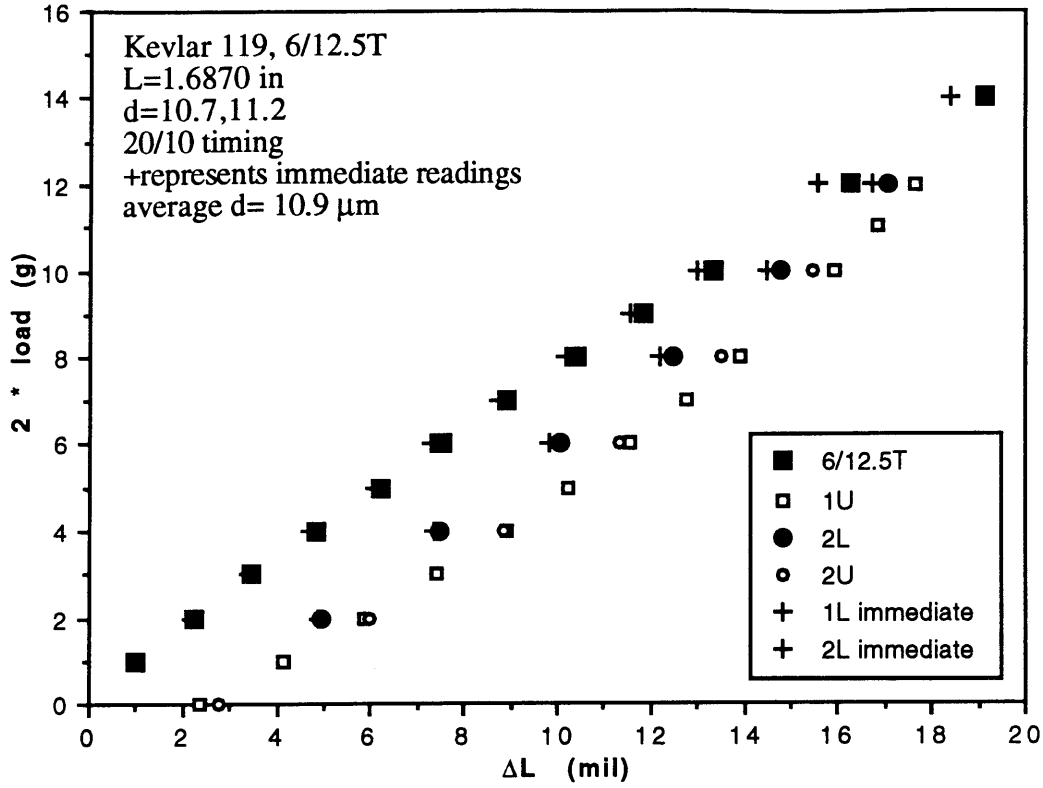

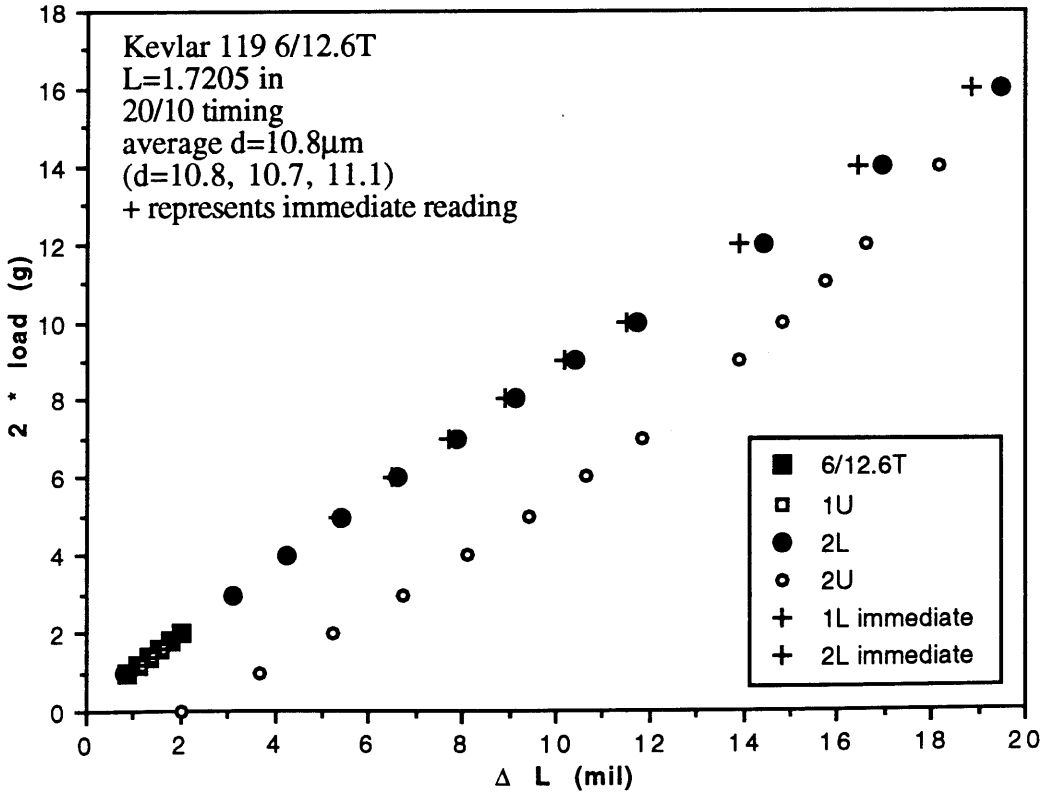

B3. Kevlar 29 Fibers

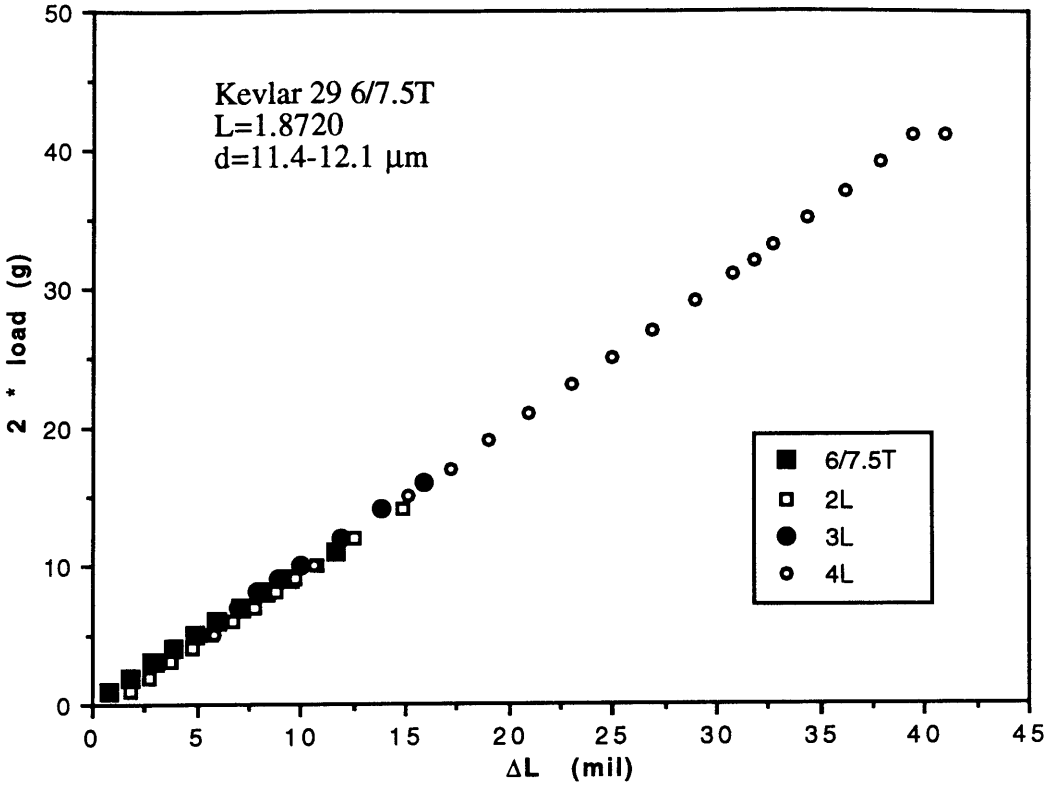

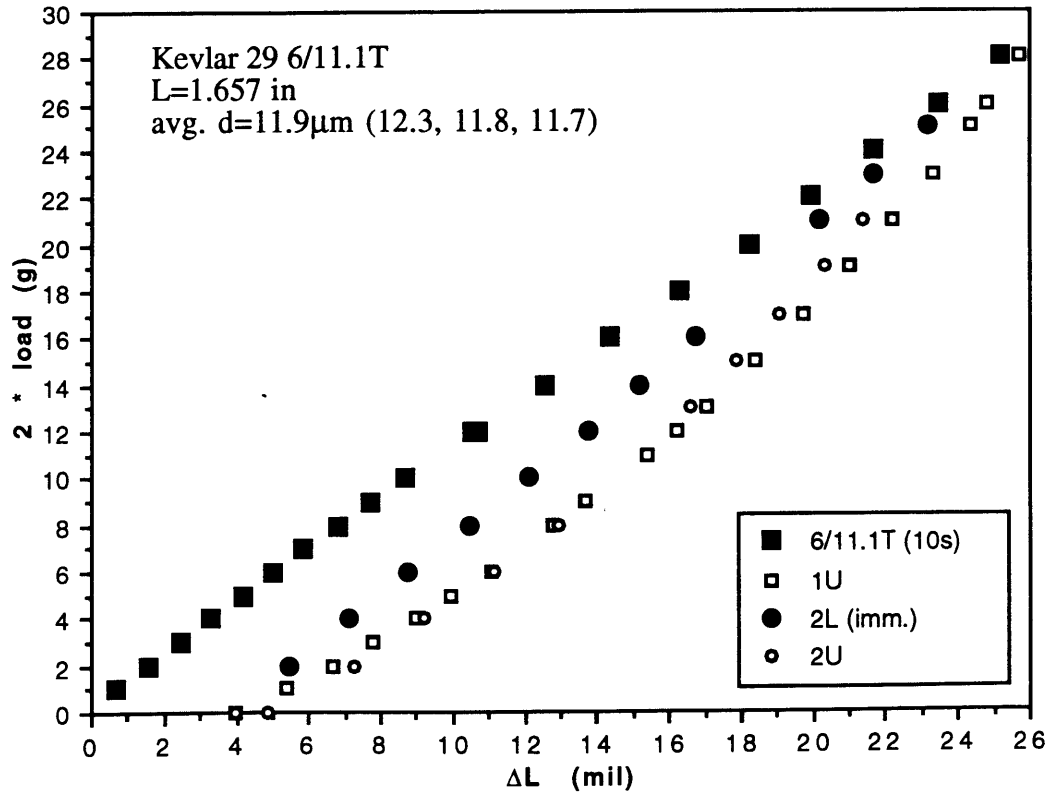

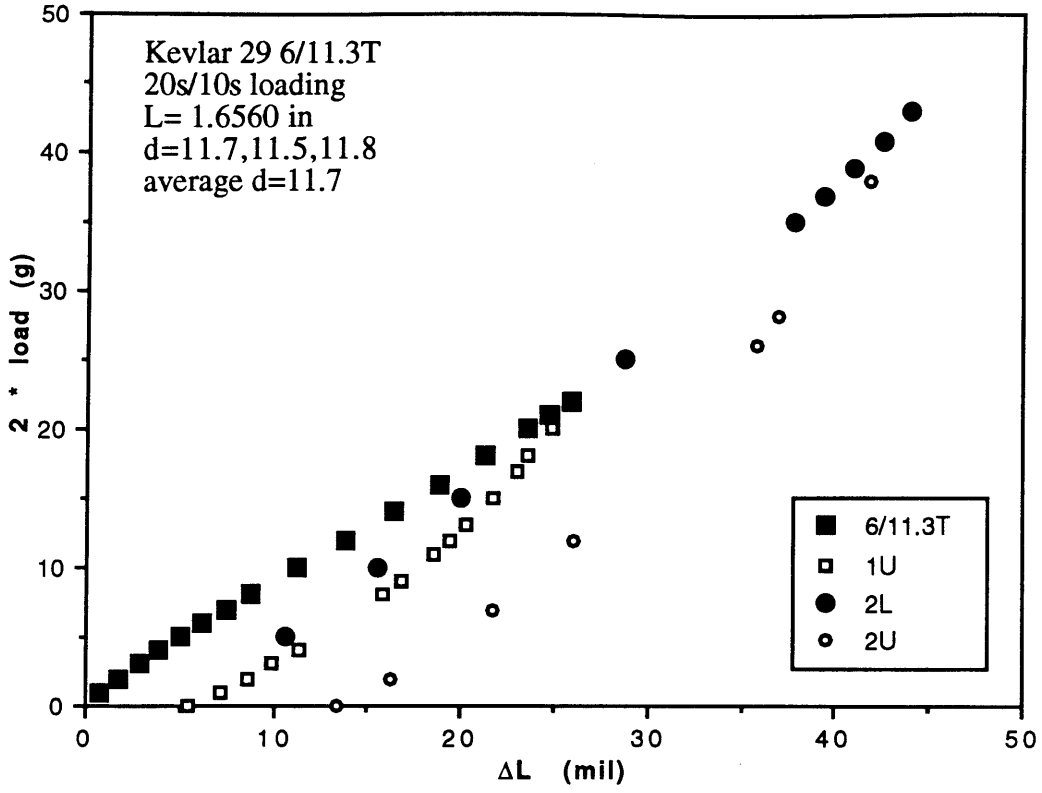
Kevlar 29 6/11.3T
20s/10s loading
L= 1.6560 in
d=11.7,11.5,11.8
average d=11.7
2 * load (g)
ΔL (mil)
6/11.3T
1U
2L
2U

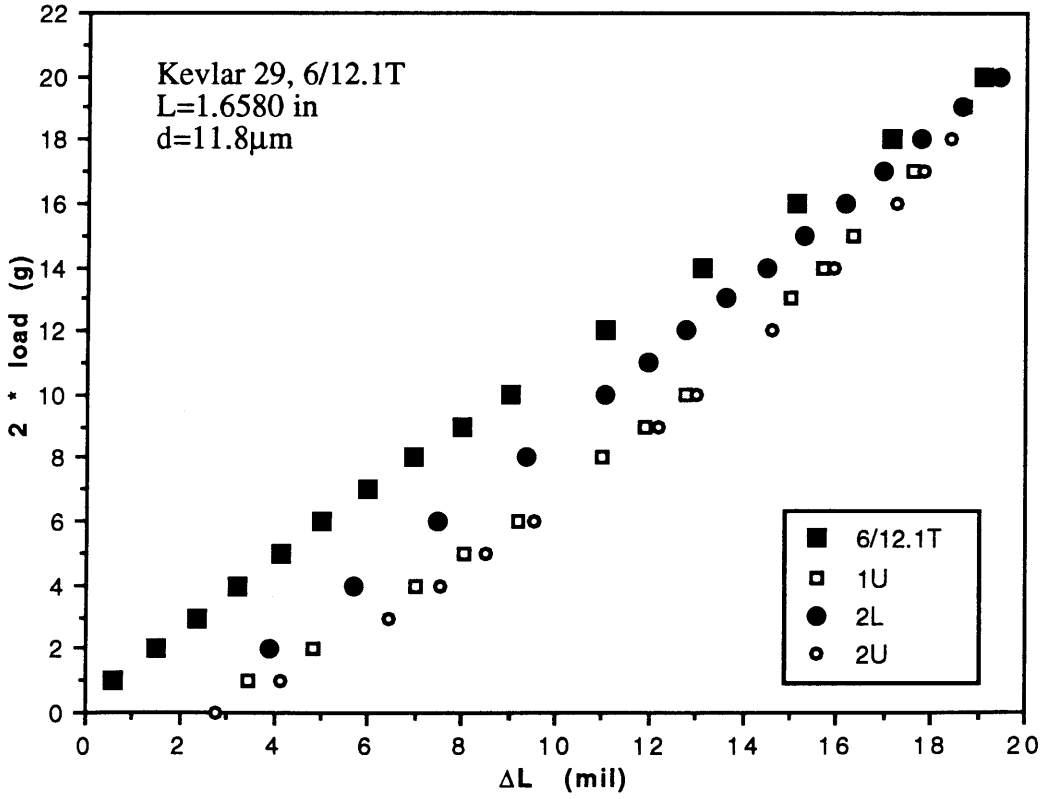
Kevlar 29, 6/12.1T
L=1.6580 in
d=11.8μm
2 * load (g)
ΔL (mil)
6/12.1T
1U
2L
2U

B4. Kevlar 129 Fibers

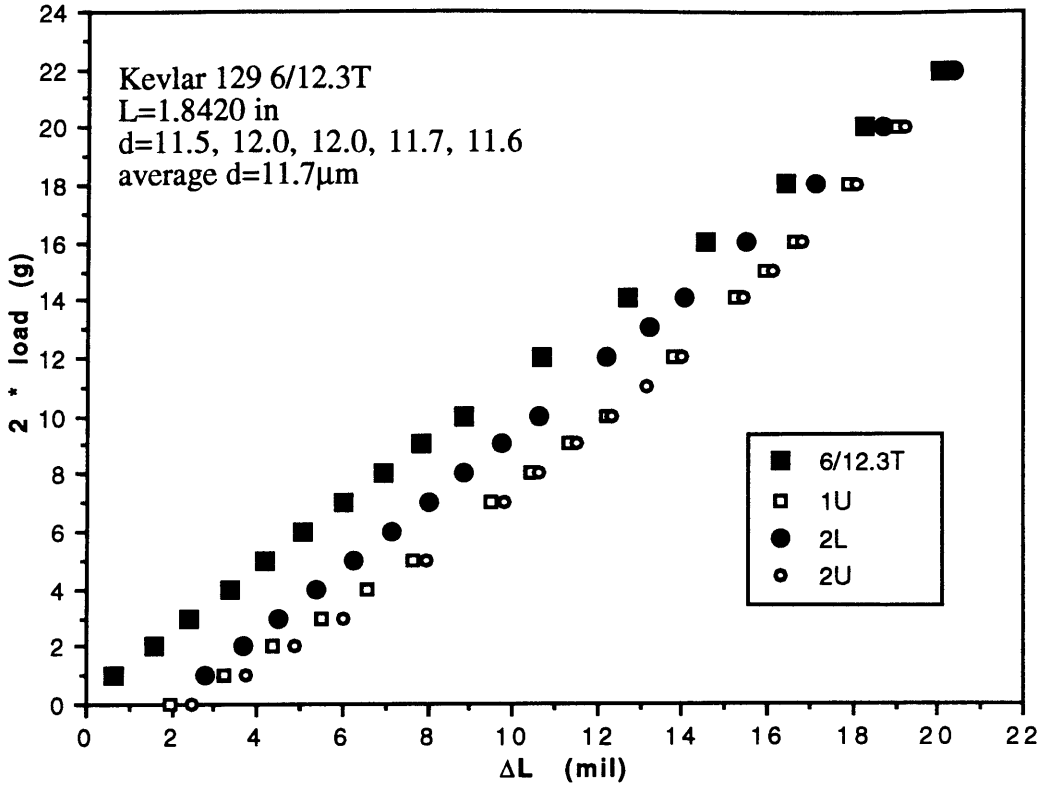

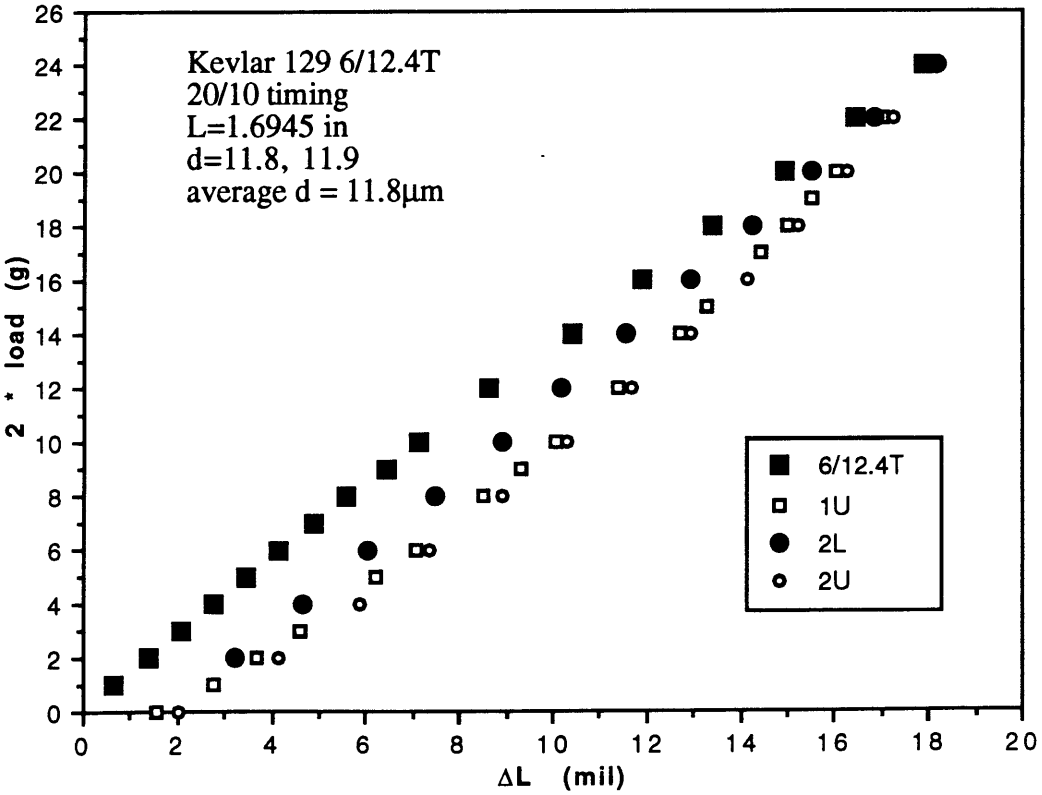

B5. Kevlar 49 Fibers

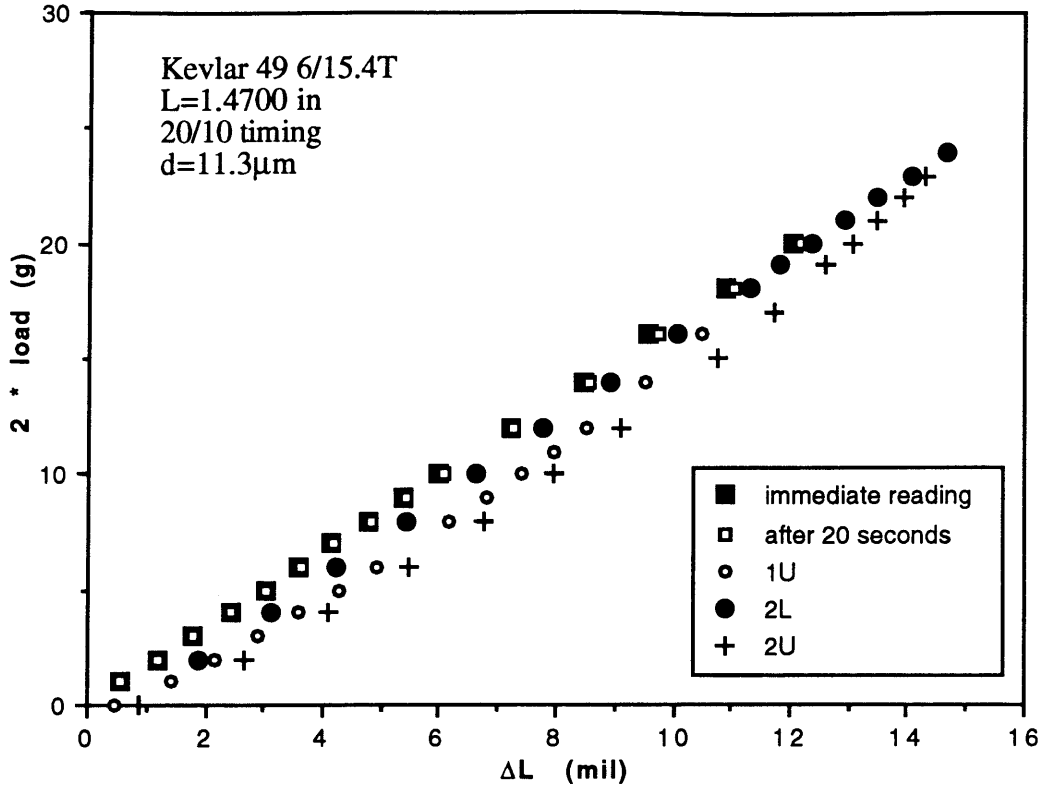

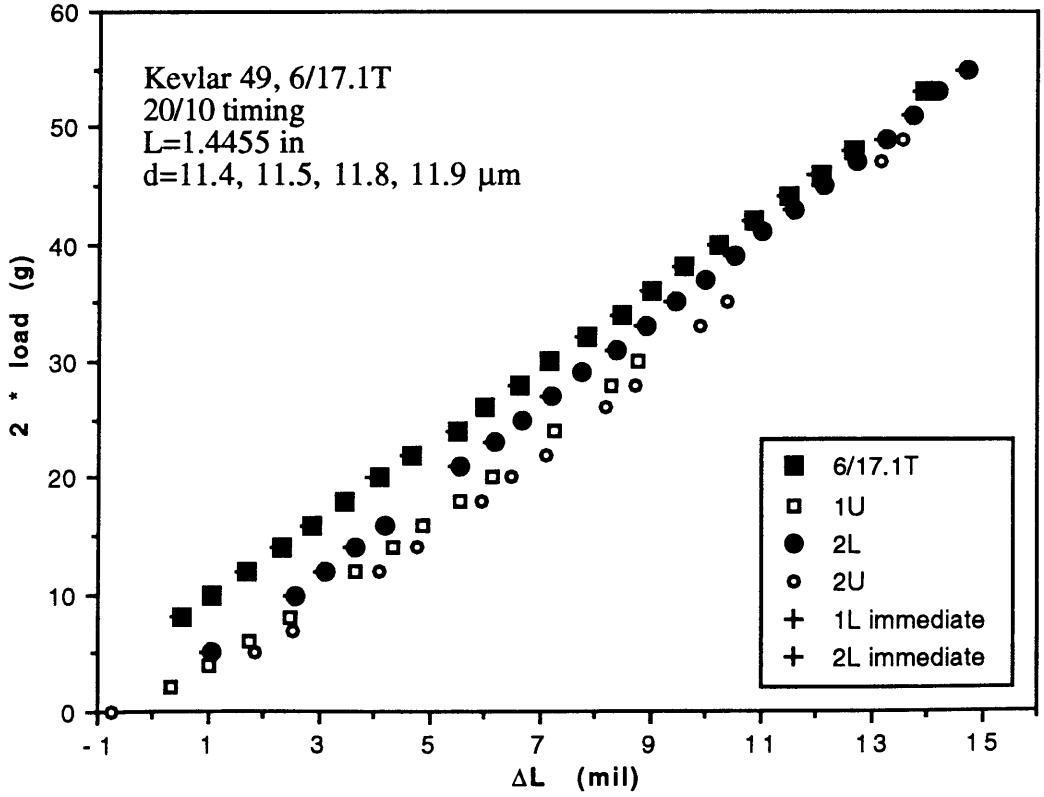

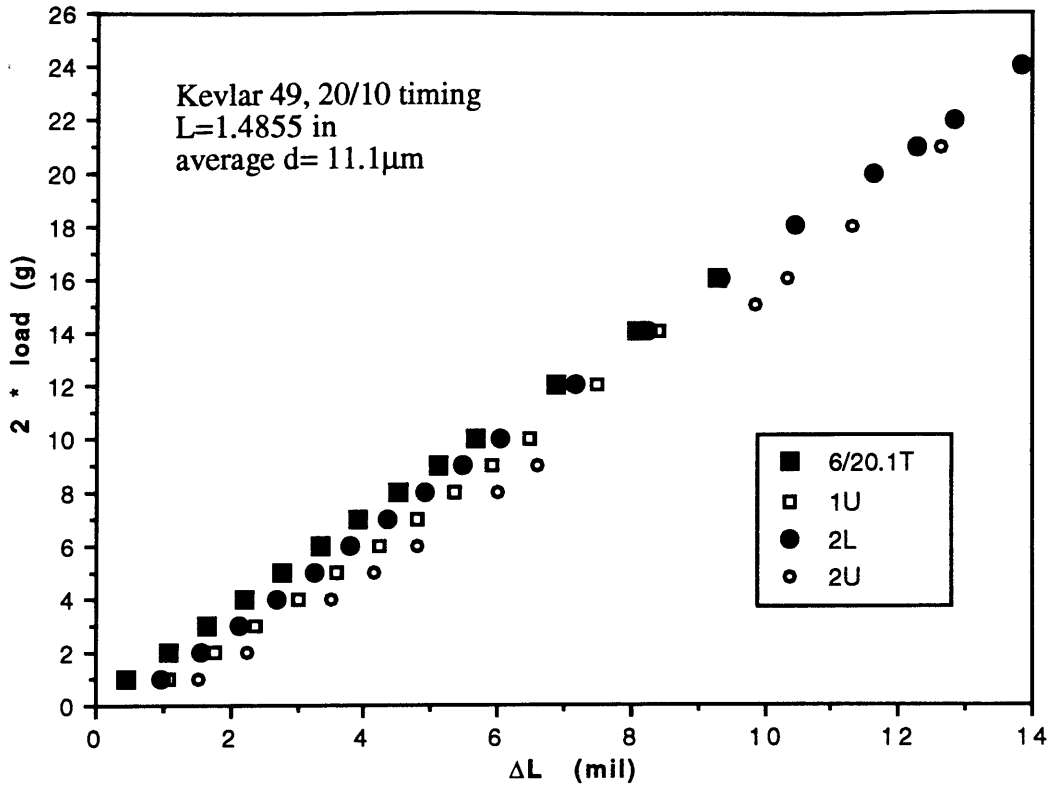
Kevlar 49, 20/10 timing
L=1.4855 in
average d= 11.1μm
2 * load (g)
ΔL (mil)
6/20.1T
1U
2L
2U

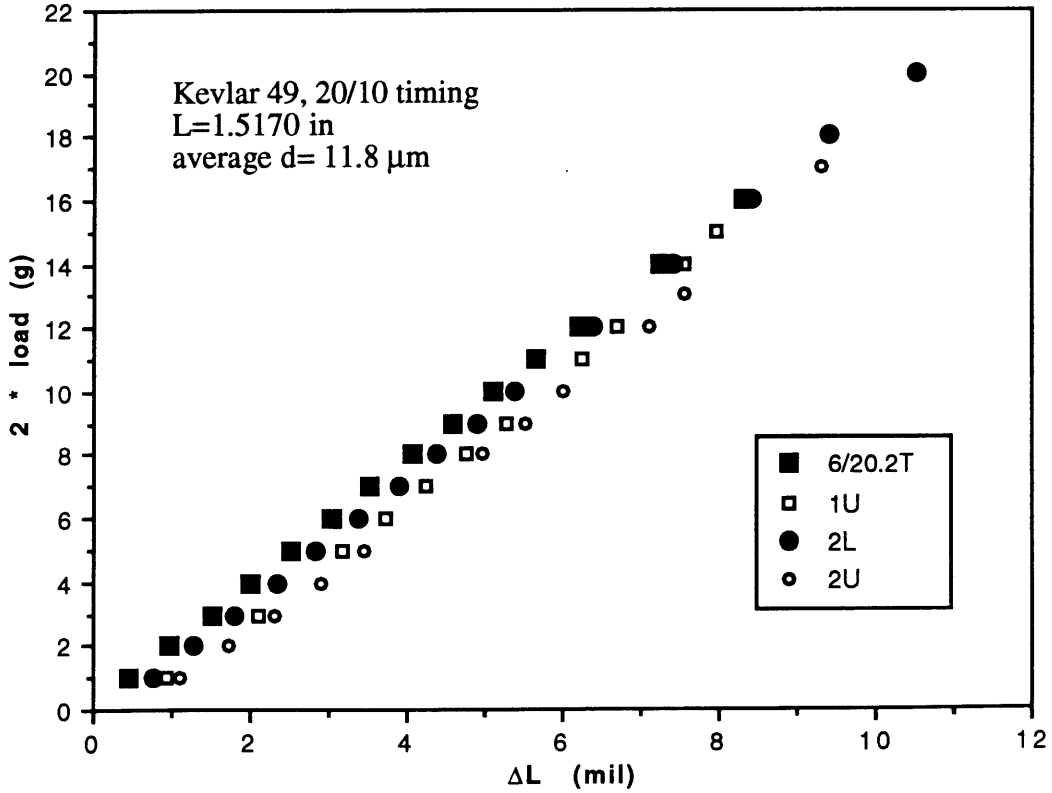
Kevlar 49, 20/10 timing
L=1.5170 in
average d= 11.8 μm
2 * load (g)
ΔL (mil)
6/20.2T
1U
2L
2U

B6. Kevlar 149 Fibers

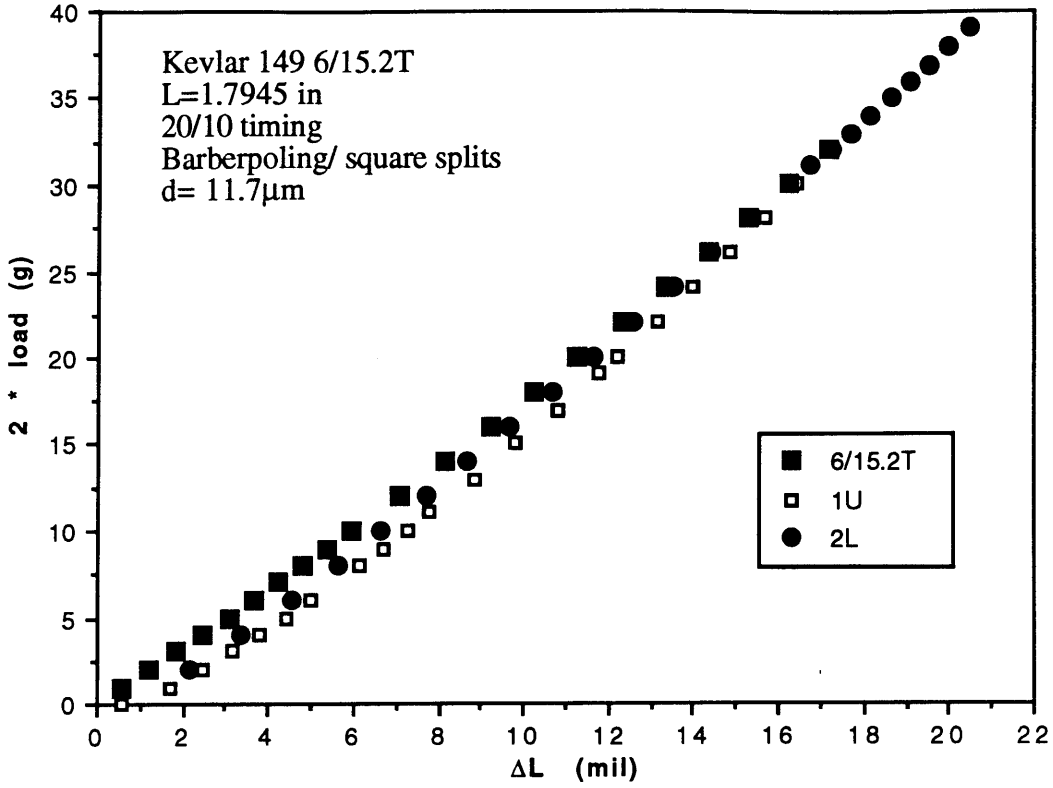

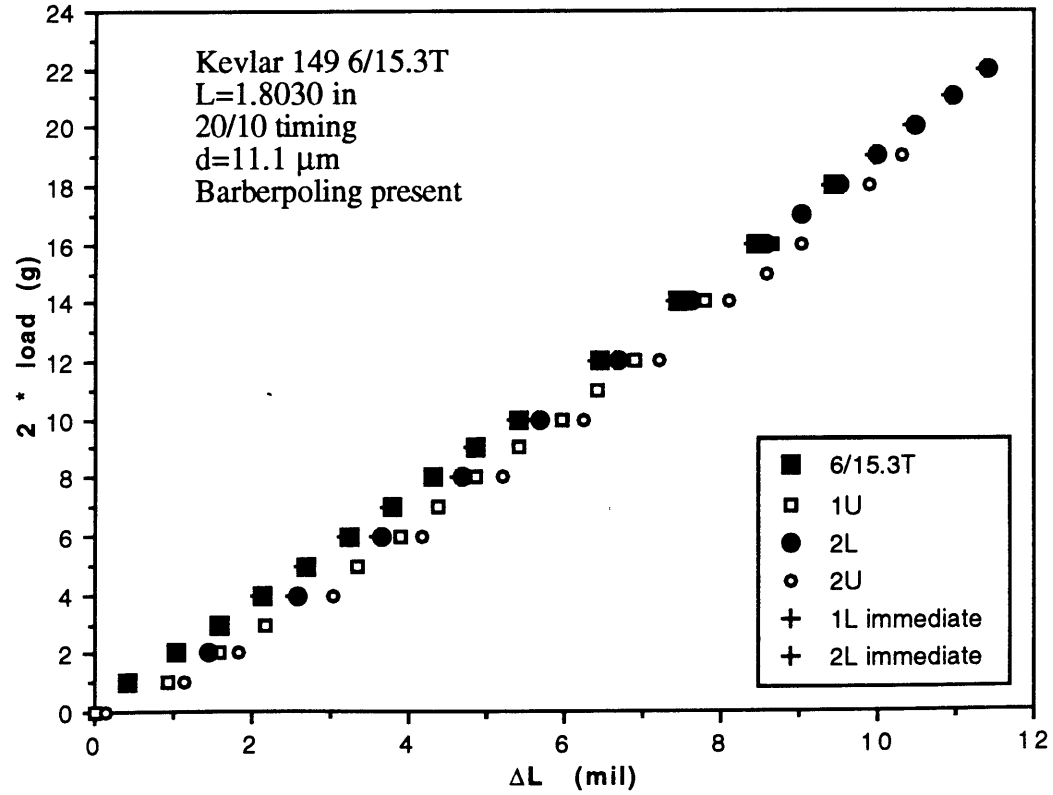

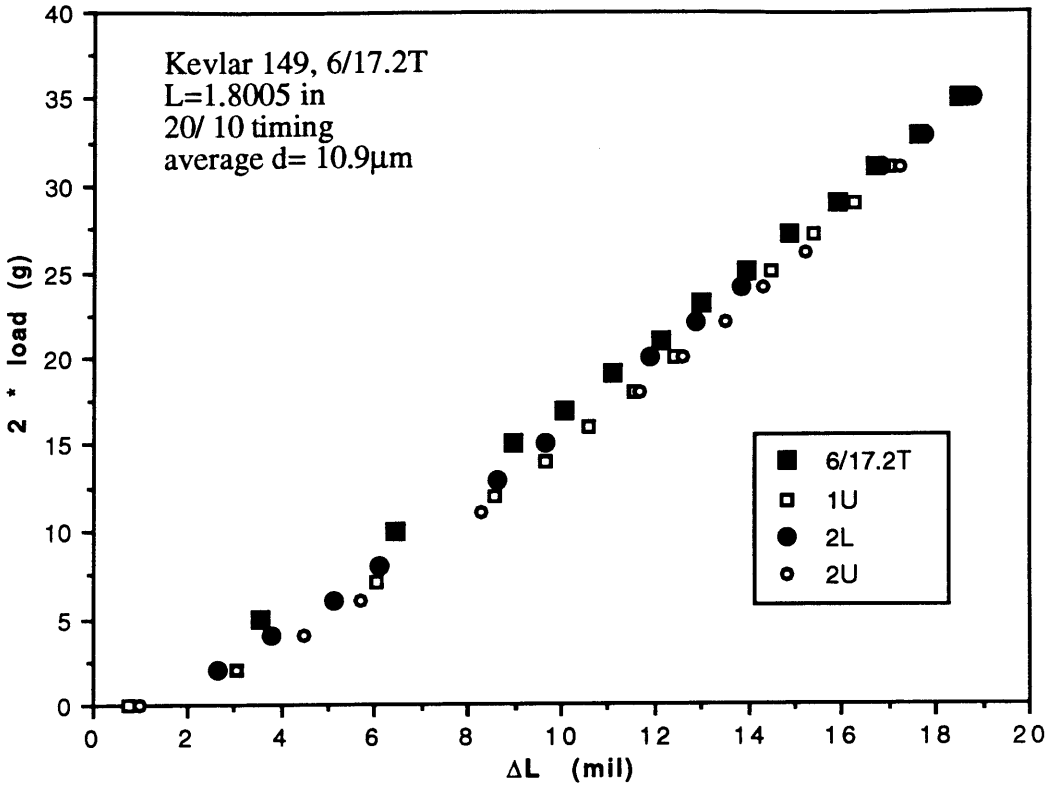
Kevlar 149, 6/17.2T
L=1.8005 in
20/ 10 timing
average d= 10.9µm
2 * load (g)
ΔL (mil)
6/17.2T
1U
2L
2U
0
5
10
15
20
25
30
35
40
0
2
4
6
8
10
12
14
16
18
20

B7. AS4 Fibers

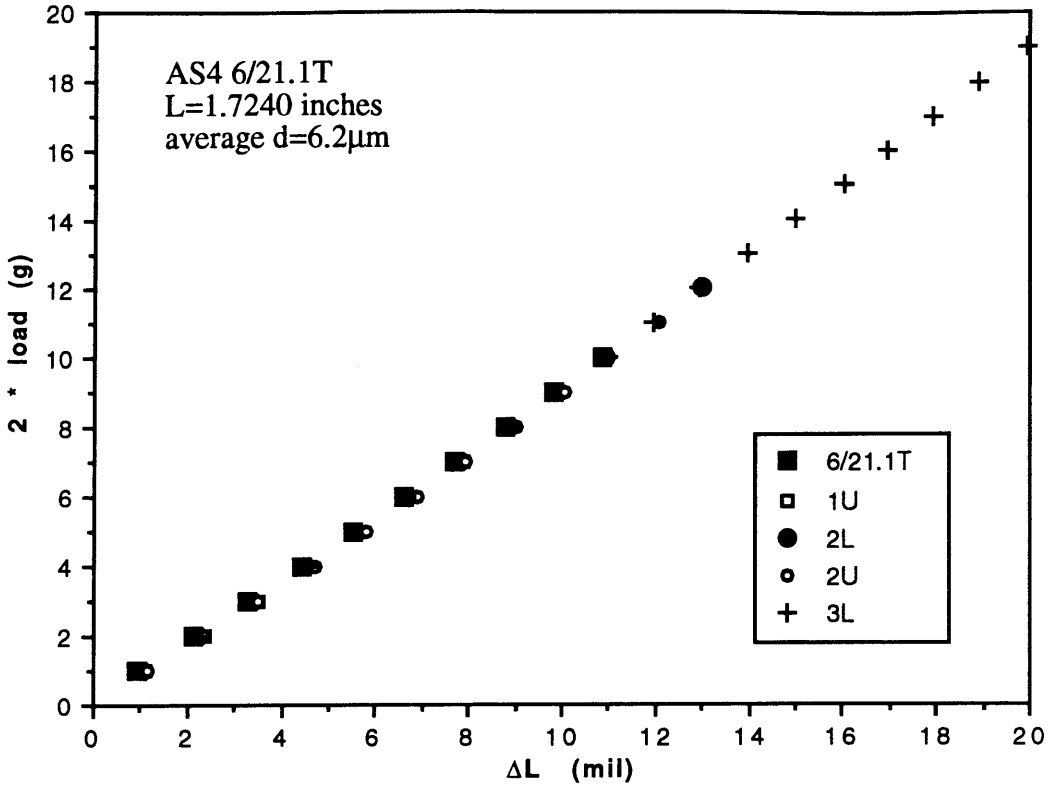

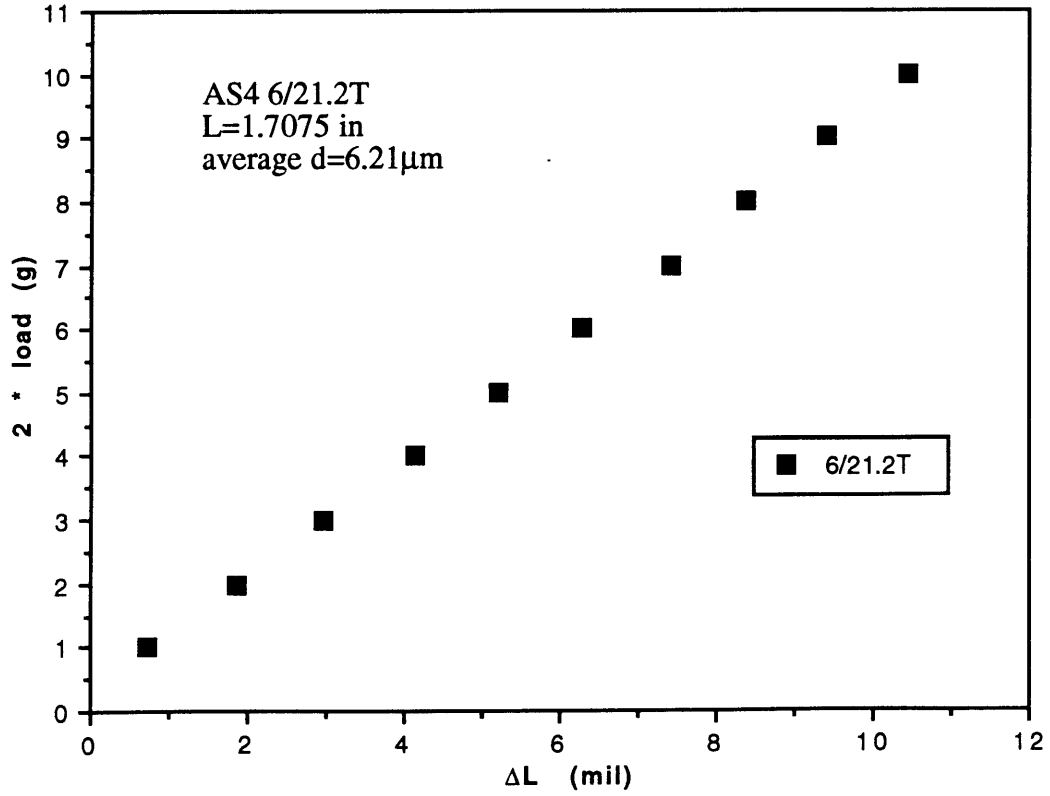

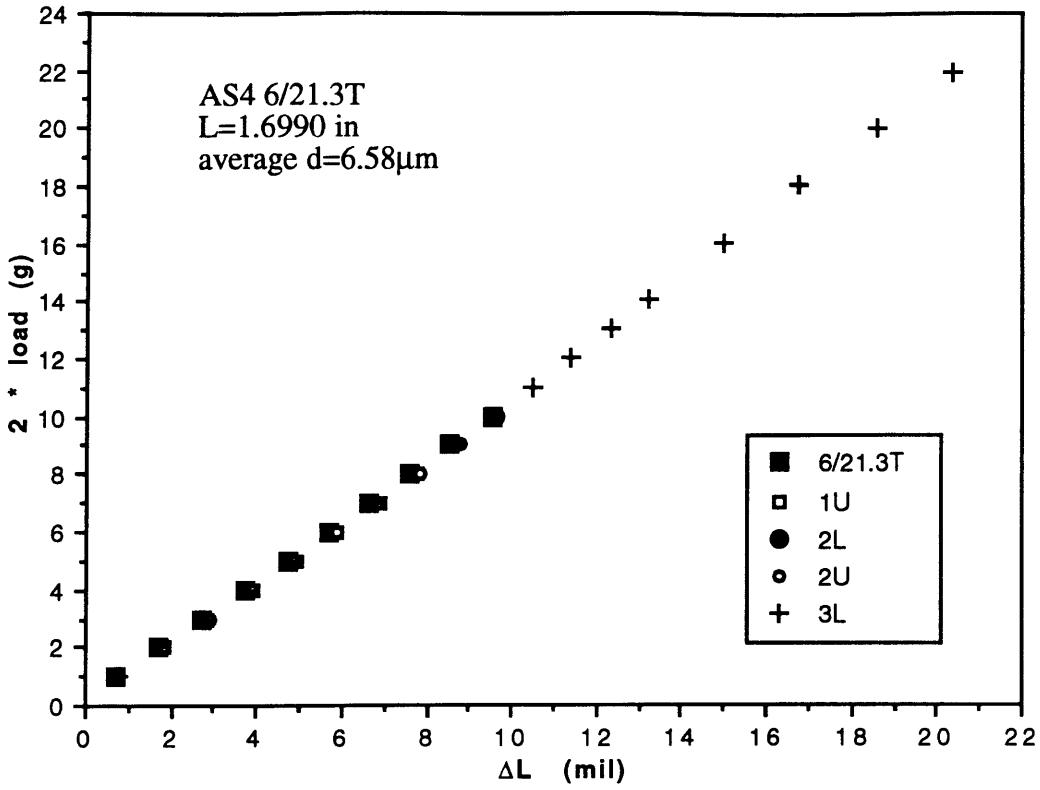
AS4 6/21.3T
L=1.6990 in
average d=6.58μm
2 * load (g)
ΔL (mil)
6/21.3T
1U
2L
2U
3L

B8. IM7 Fibers

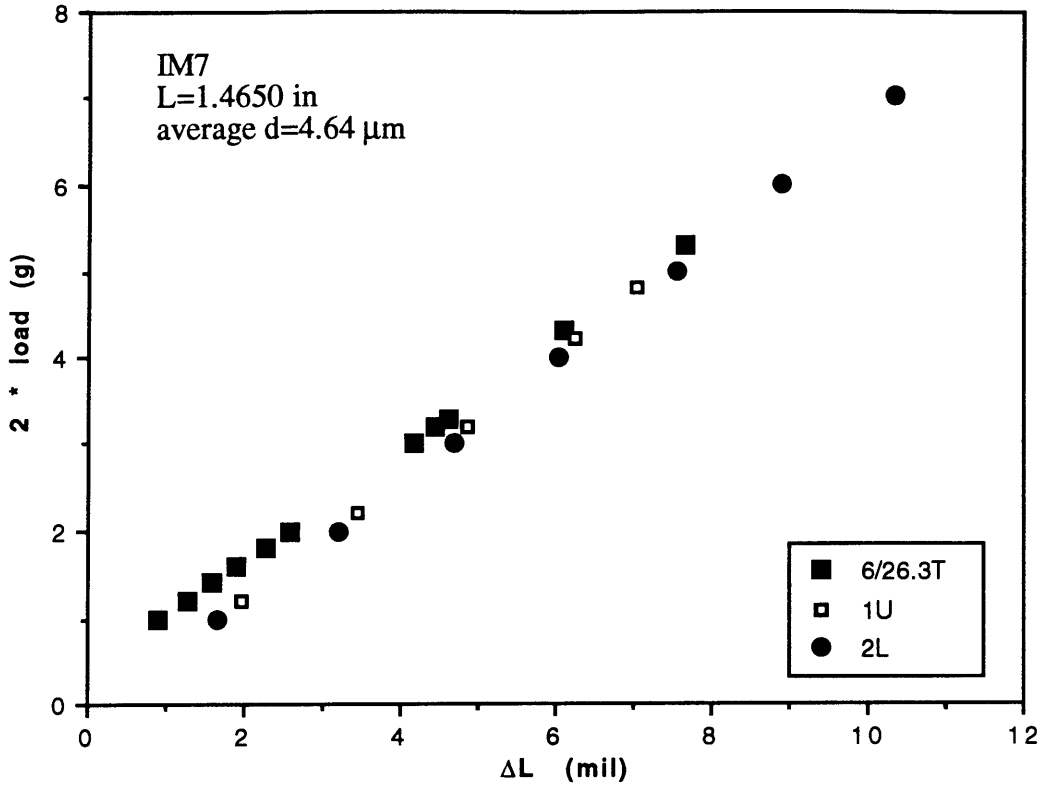

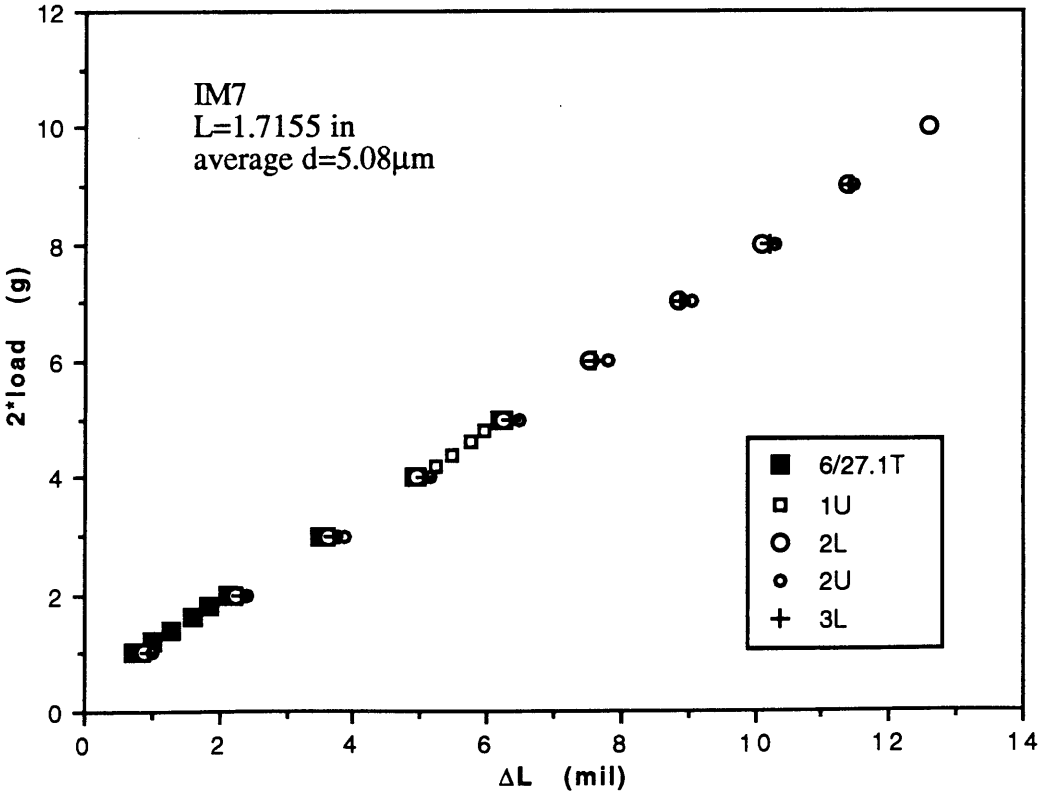

B9. IM8 Fibers

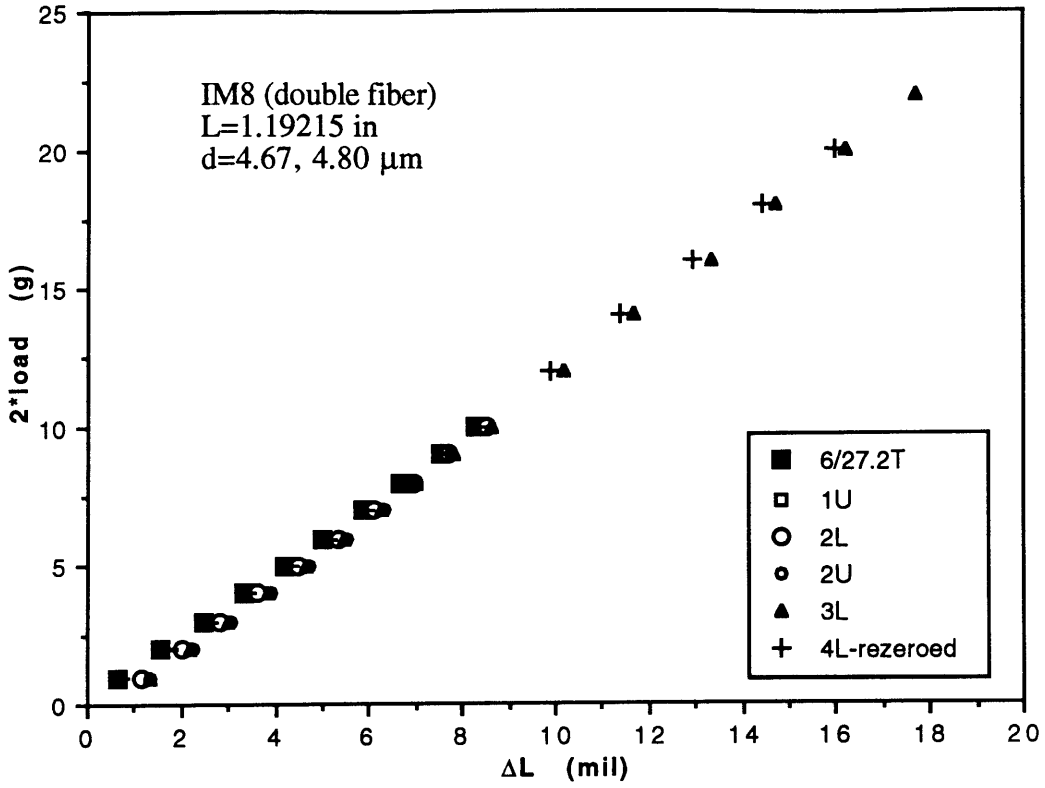

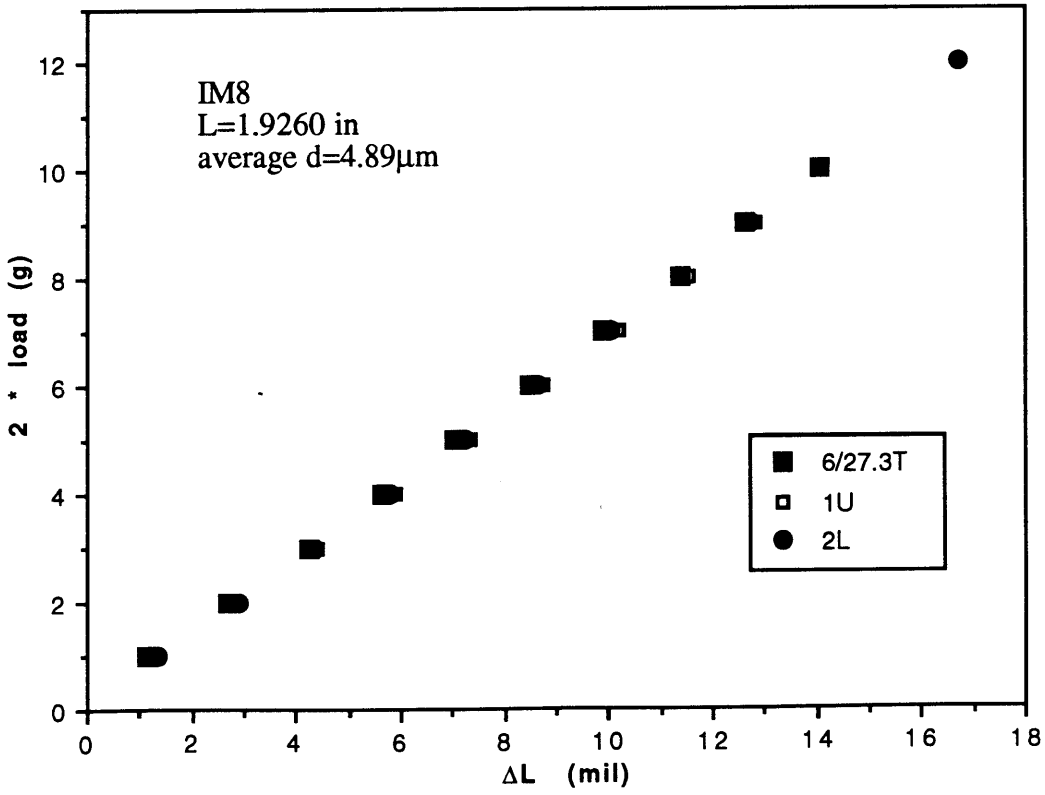

B10. HMS4 Fibers

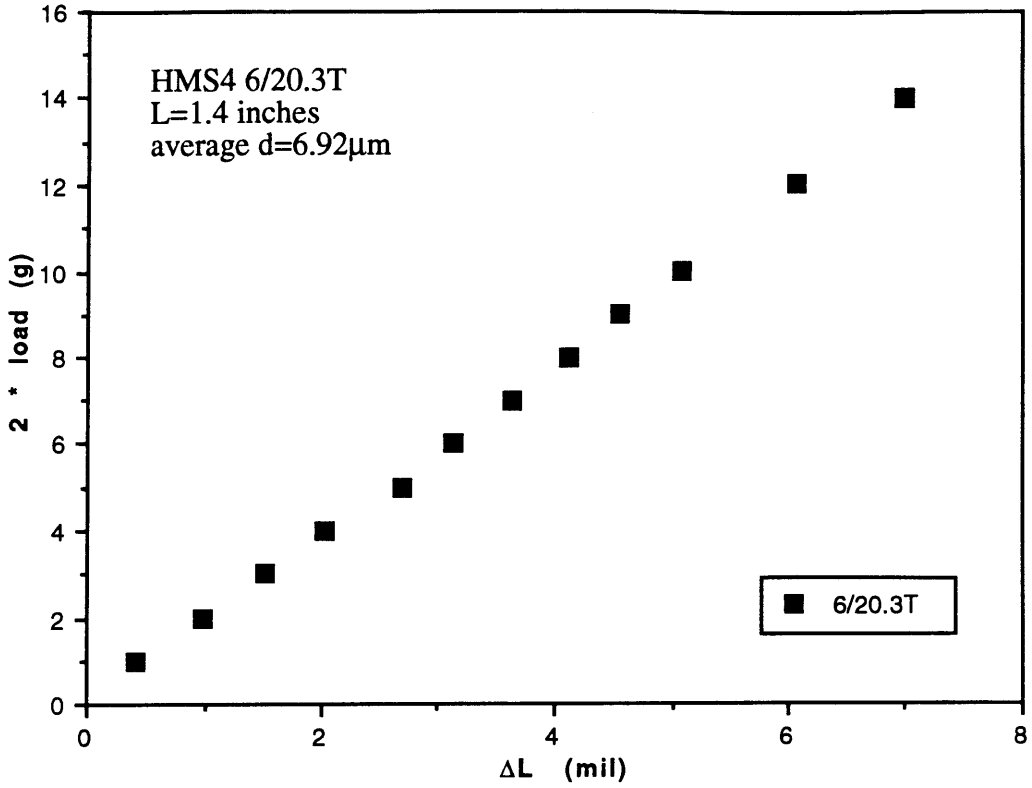

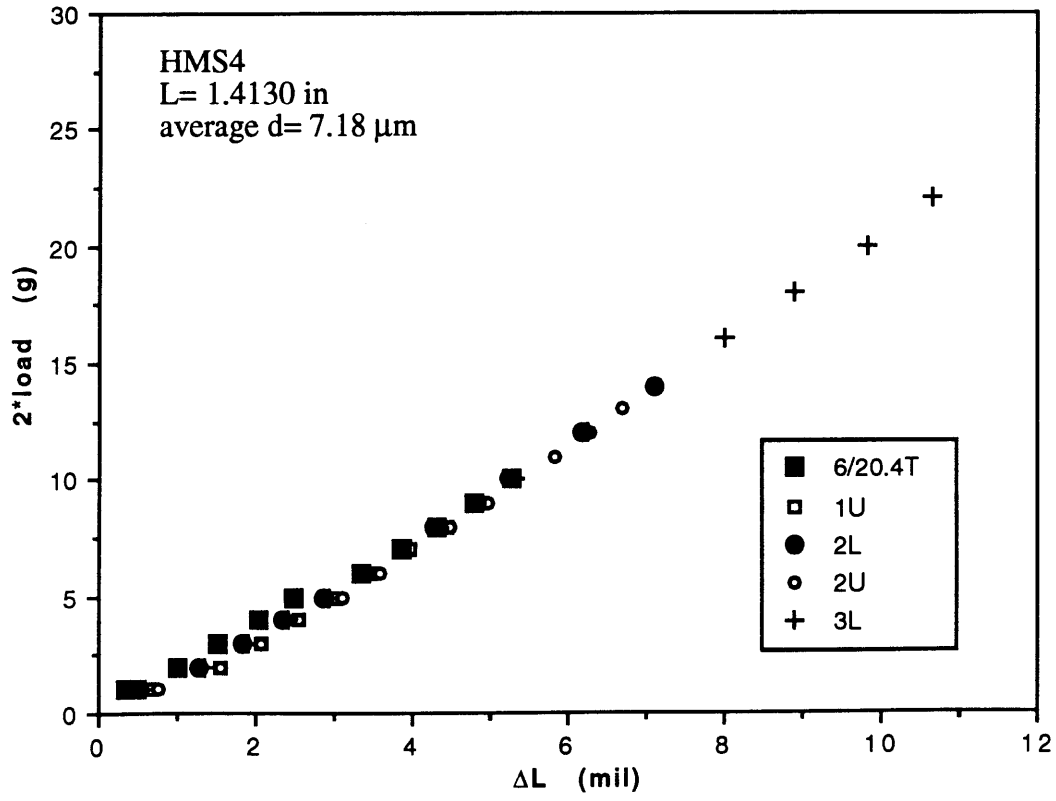

B11. P25 HT Fibers

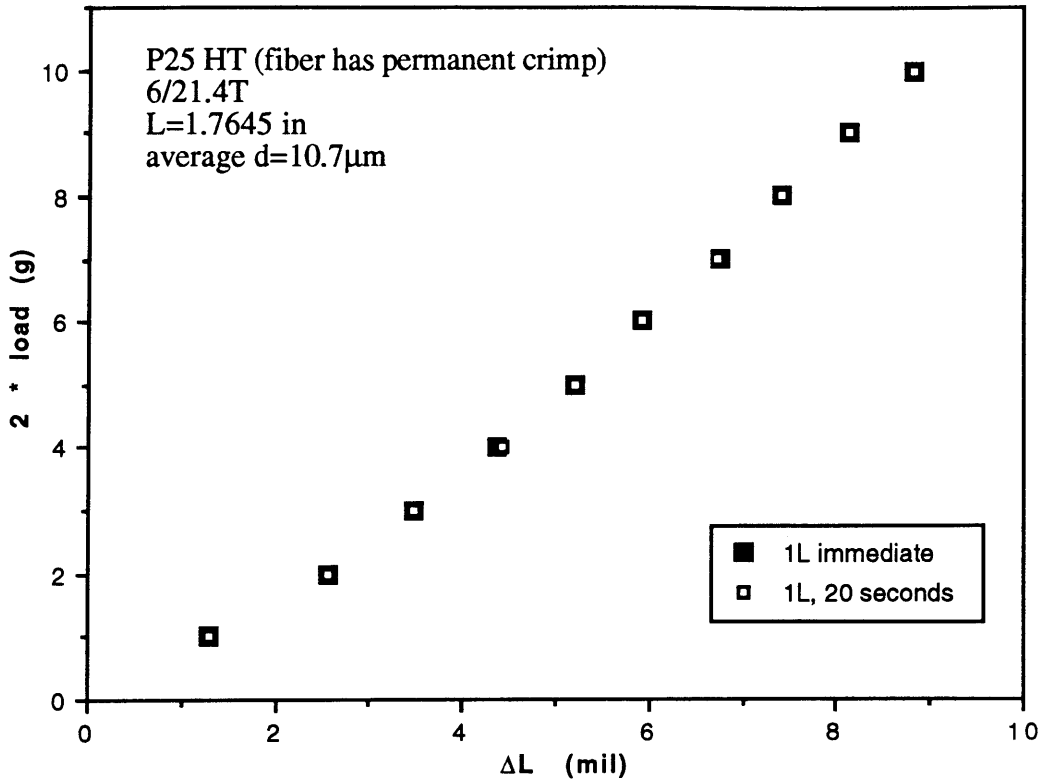

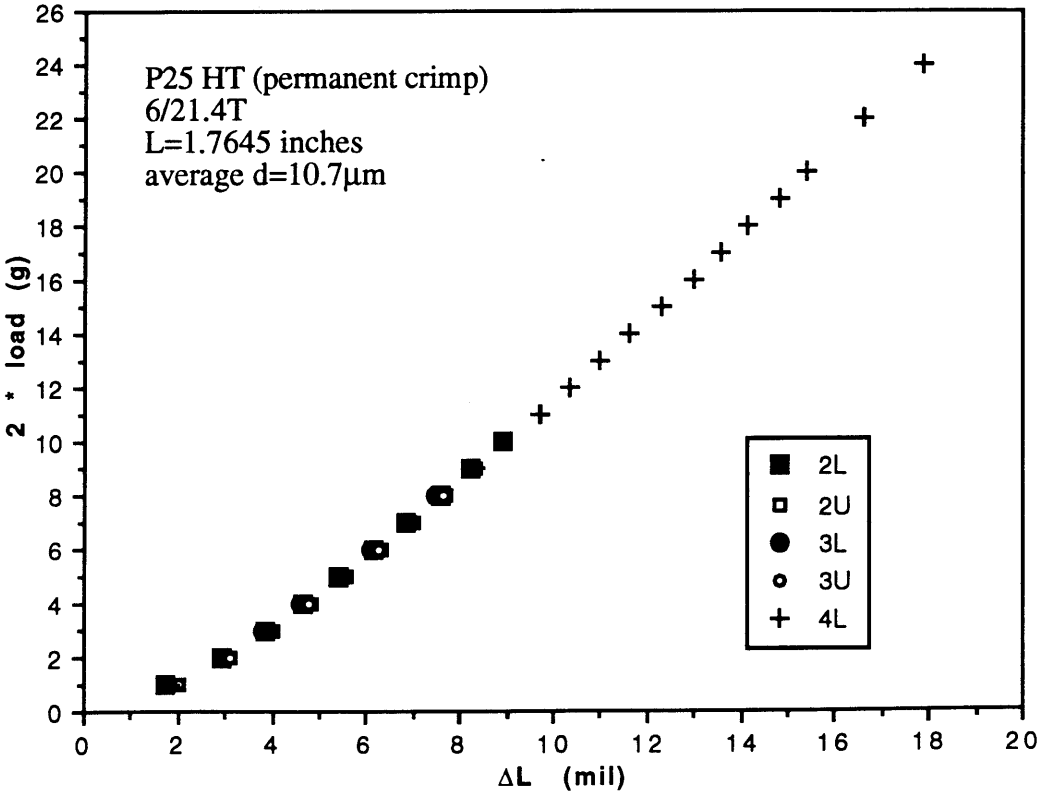

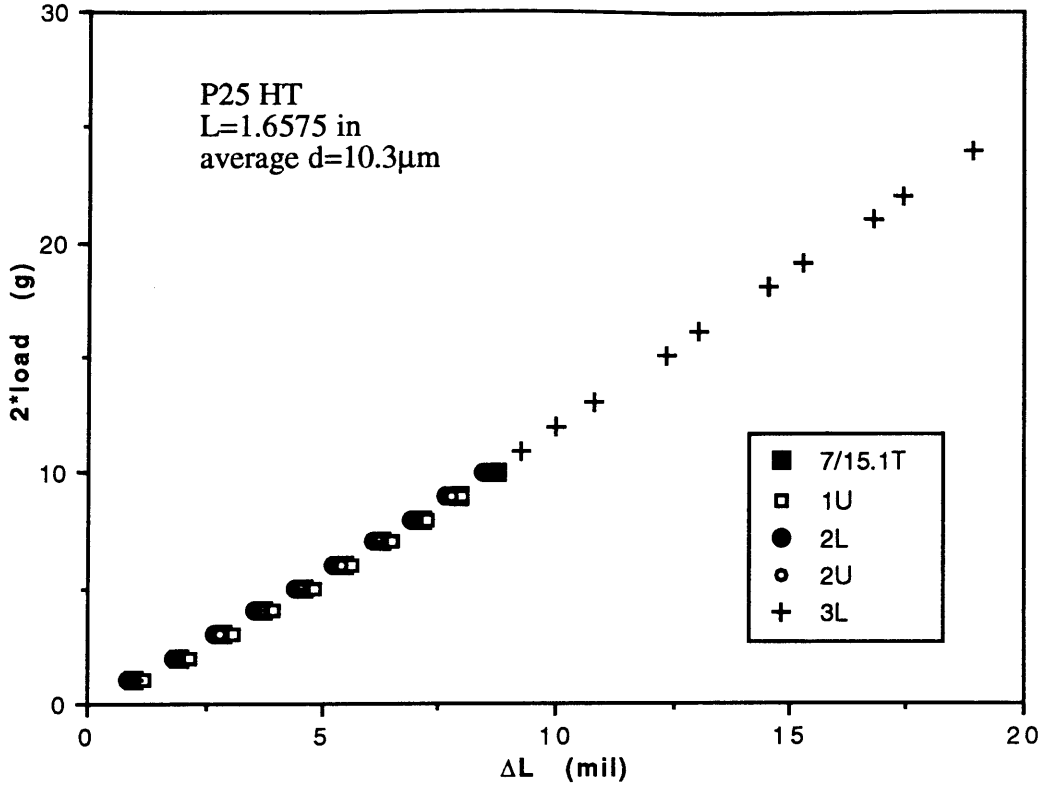
P25 HT
L=1.6575 in
average d=10.3µm
2*load (g)
ΔL (mil)
7/15.1T
1U
2L
2U
3L
0
10
20
30
0
5
10
15
20

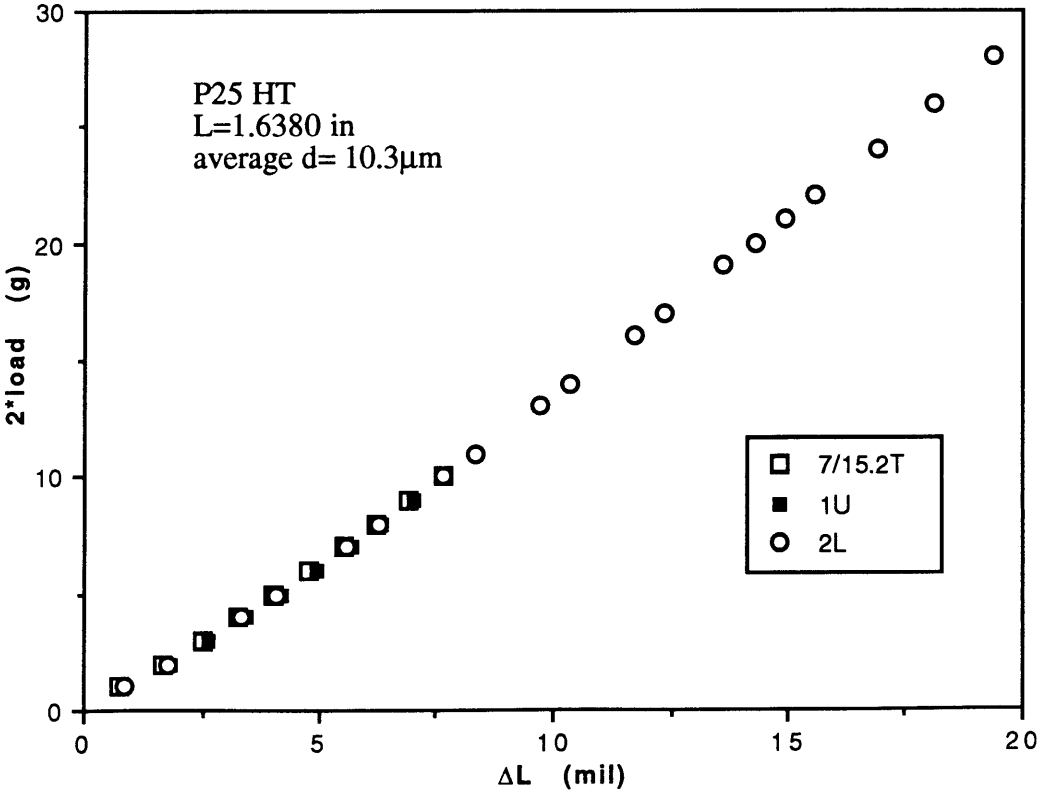
P25 HT
L=1.6380 in
average d= 10.3µm
2*load (g)
ΔL (mil)
7/15.2T
1U
2L
0
10
20
30
0
5
10
15
20

B12. P55s Fibers

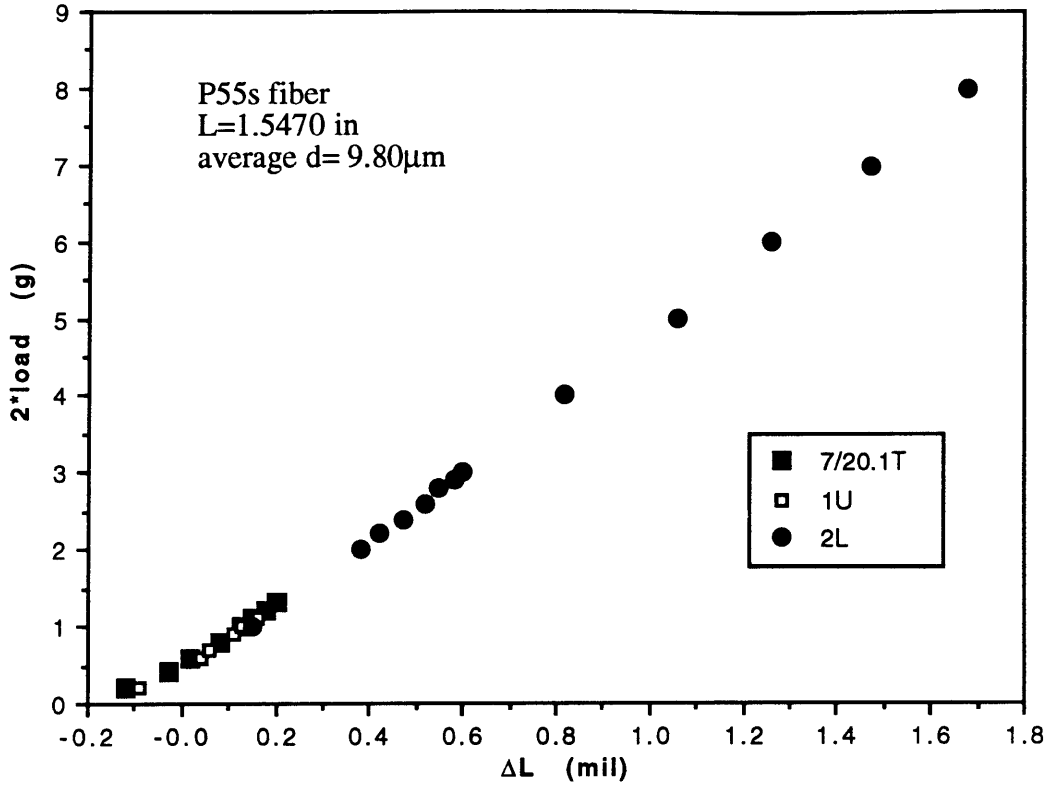

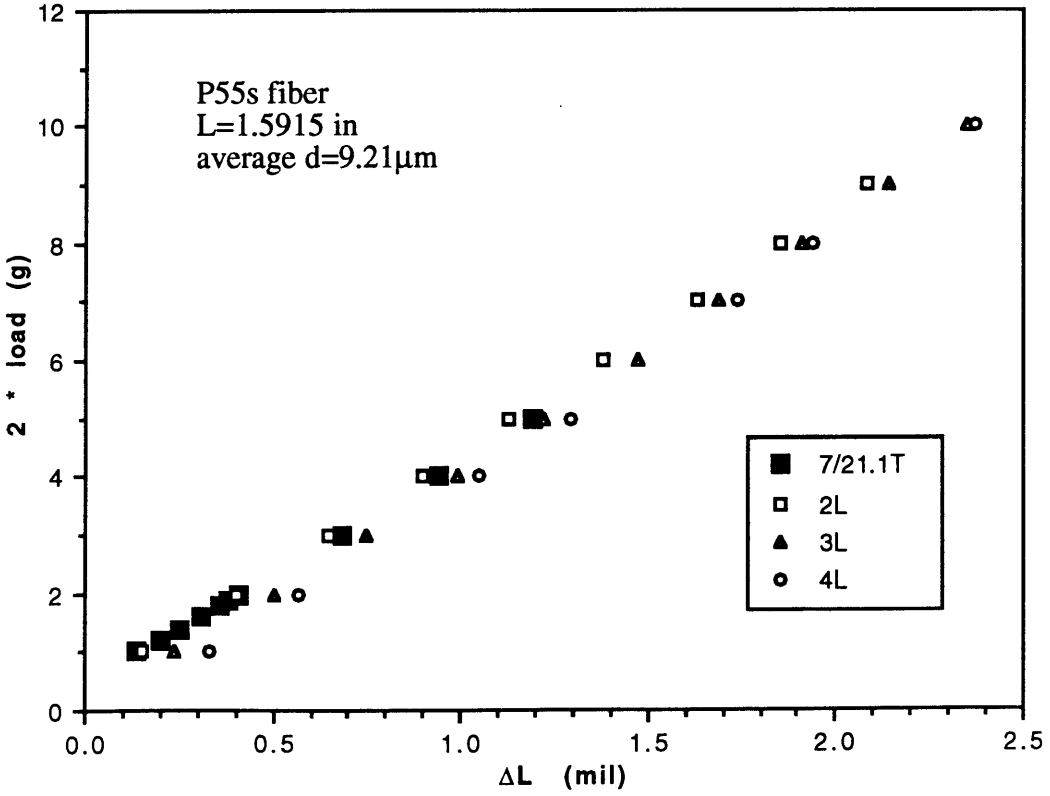

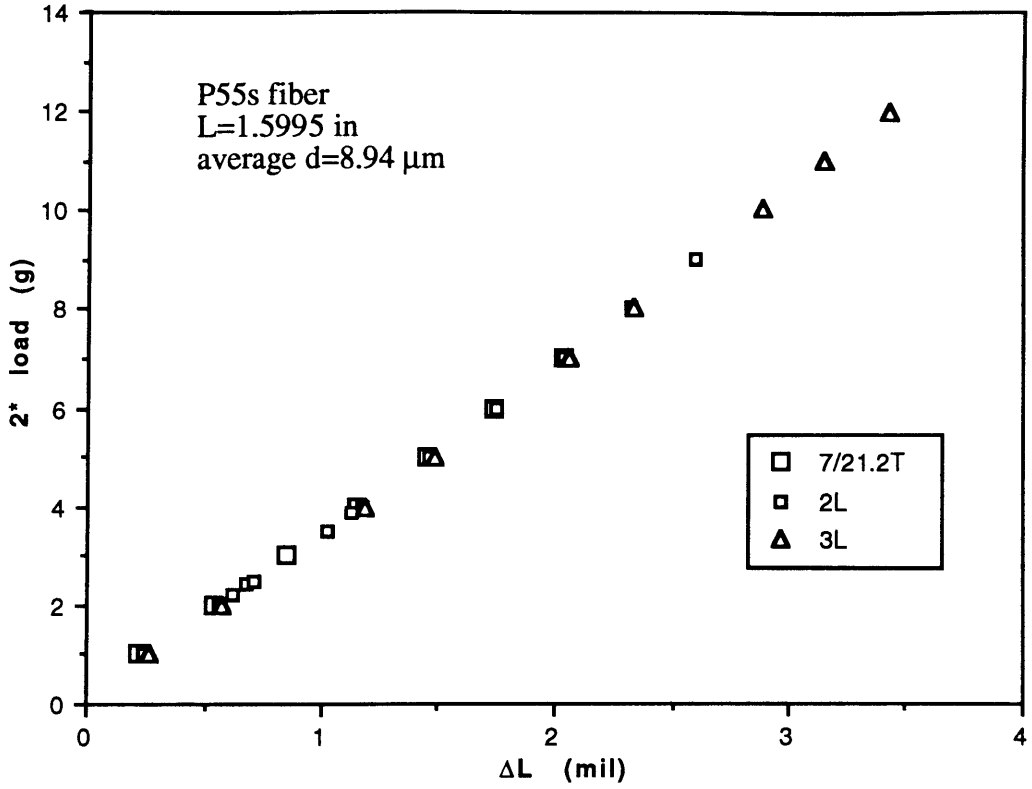
P55s fiber
L=1.5995 in
average d=8.94 μm
2* load (g)
ΔL (mil)
7/21.2T
2L
3L
0
2
4
6
8
10
12
14
0
1
2
3
4

B13. P75 Fibers

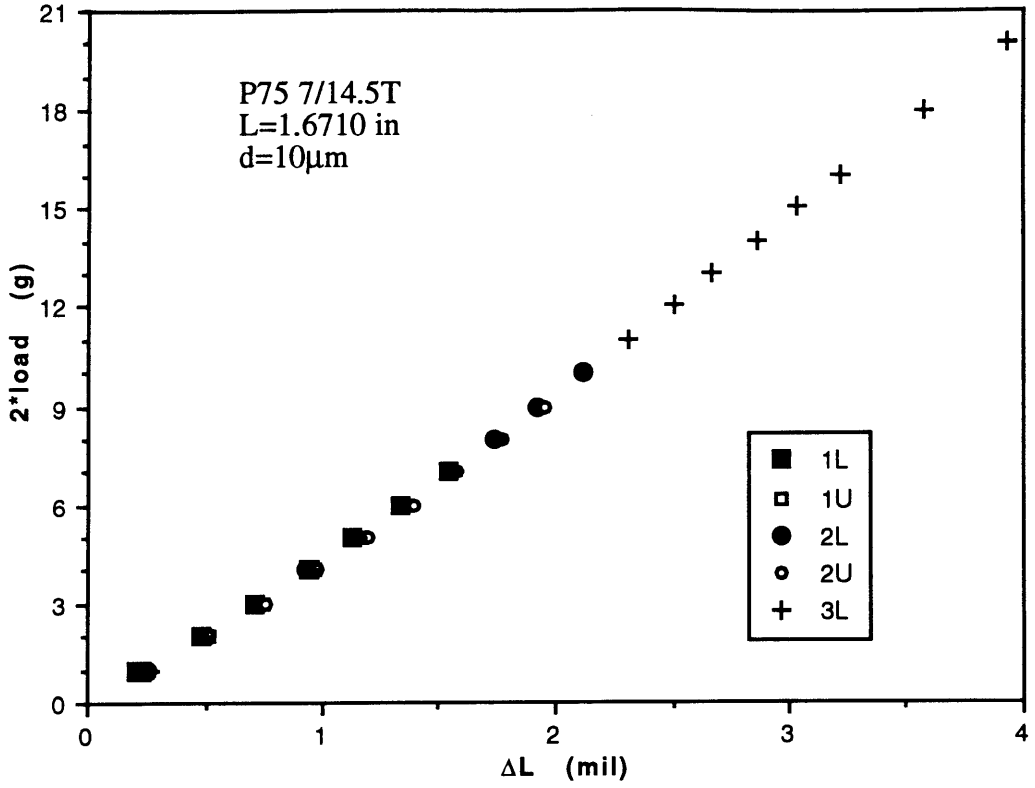

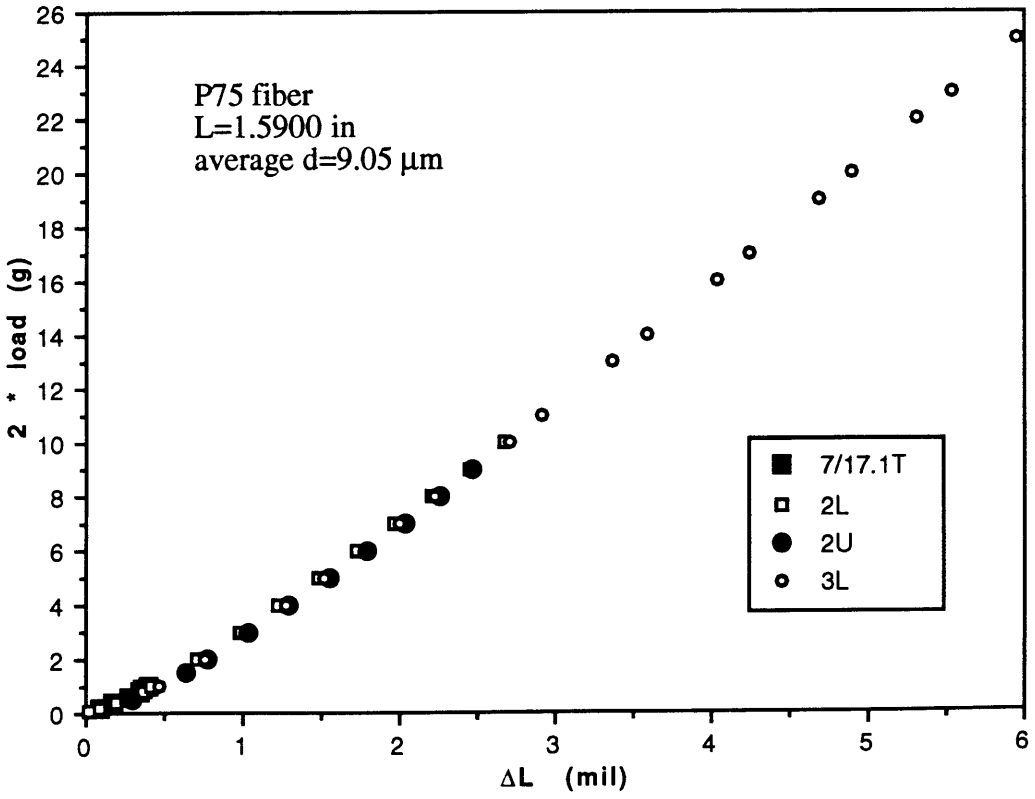

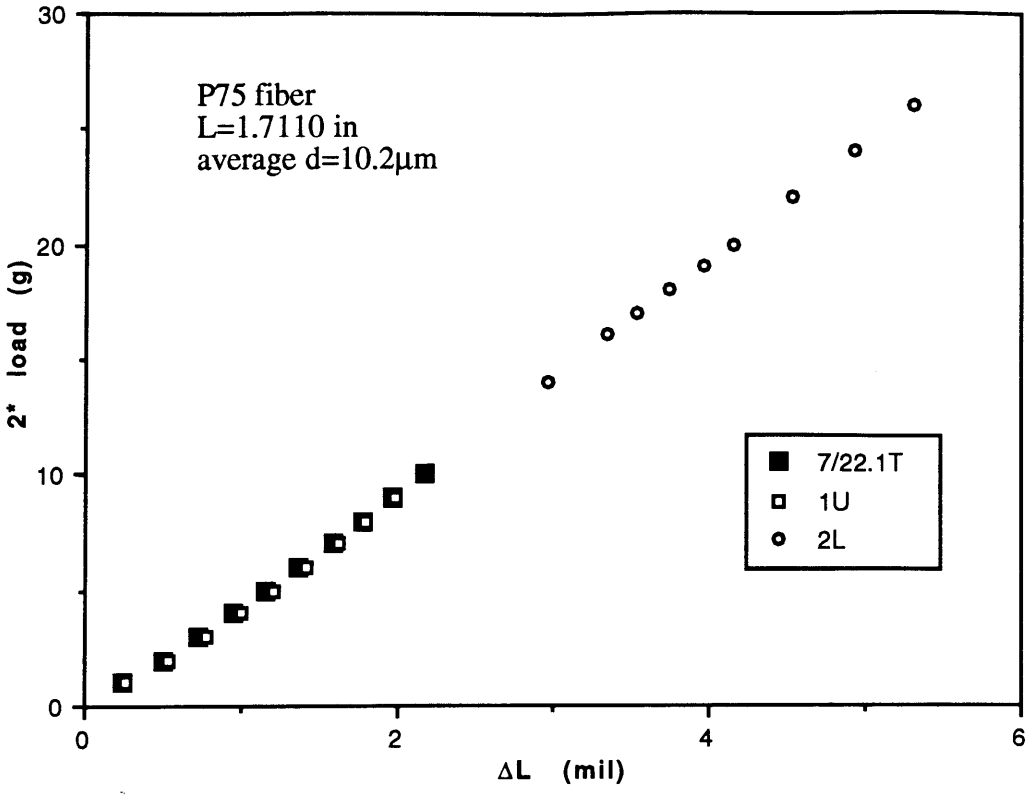
P75 fiber
L=1.7110 in
average d=10.2μm
2* load (g)
ΔL (mil)
7/22.1T
1U
2L
0
10
20
30
0
2
4
6

Appendix C: Micro- Flex plots and data tables

C1. Glass Fibers

FITT- test

sample	diameter (μm)	mt (g/mil)	Lo (in)	**Et (GPa)**	**Et (Msi)**
6/2.1T	15.50	1.6775	1.6670	72.7	10.5
	15.60	1.6775	1.6670	71.7	10.4
	15.40	1.6775	1.6670	73.6	10.7
	15.40	1.6775	1.6670	73.6	10.7
	15.70	1.6775	1.6670	70.8	10.3
6/2.2T	18.10	2.3095	1.6275	71.6	10.4
6/7.2T	15.60	1.9799	1.5195	77.2	11.2
	15.60	1.9799	1.5195	77.2	11.2
	15.60	1.9799	1.5195	77.2	11.2
	15.60	1.9799	1.5195	77.2	11.2
6/7.3T	16.10	2.1900	1.5355	81.0	11.7
	16.10	2.1900	1.5355	81.0	11.7
6/15.1T	15.20	2.0044	1.5055	81.5	11.8
	15.30	2.0044	1.5055	80.5	11.7
	15.30	2.0044	1.5055	80.5	11.7
			average:	**76.5**	**11.1**
			std. dev:	3.9	0.6

span (m)	midspan (m)
6.66E-4	9.00E-5
5.42E-4	

Micro-Flex test

sample	mB (mg/μm)	b (mg)	P (mg)	P* (mg)	(EI)f (N*m^2)	**Eb (GPa)**	**Eb (Msi)**	Eb/Et
6/2.1B	3.5490	-9.2	186.5	195.7	2.09E-10	73.6	10.7	1.01
6/2.2B	3.9265	-10.4	190.0	200.4	2.31E-10	79.4	11.5	1.11
6/2.3B	3.3674	-0.7	190.0	190.7	1.98E-10	71.7	10.4	0.97
6/5.2B	3.3579	2.0	160.0	158.0	1.97E-10	71.5	10.4	0.97
7/21.2	3.5527	4.0	184.8	180.8	2.09E-10	70.0	10.2	0.99
6/2.4B	6.5525	11.3	350.0	338.7	3.85E-10	73.1	10.6	1.02
6/7.3B	3.7715	3.6	210.0	206.4	2.22E-10	76.2	11.1	0.99
6/7.5B	3.8629	3.4	200.0	196.6	2.27E-10	78.1	11.3	1.01
6/13.1B	3.9022	2.7	190.0	187.3	2.29E-10	78.9	11.4	1.02
6/13.2B	3.6777	4.2	180.0	175.8	2.16E-10	74.4	10.8	0.96
6/7.6B	4.4100	7.0	210.0	203.0	2.59E-10	78.6	11.4	0.97
6/7.7B	4.3898	7.0	220.0	213.0	2.58E-10	78.2	11.3	0.97
6/19.1B	3.6170	2.6	180.0	177.4	2.13E-10	81.1	11.8	0.99
6/25.1B*	6.8440	1.4	260.0	258.6	2.14E-10	81.6	11.8	1.01
6/25.2B*	6.6667	6.6	280.0	273.4	2.08E-10	79.5	11.5	0.99
average:						**76.4**	**11.1**	1.00
std. dev:						3.7	0.5	

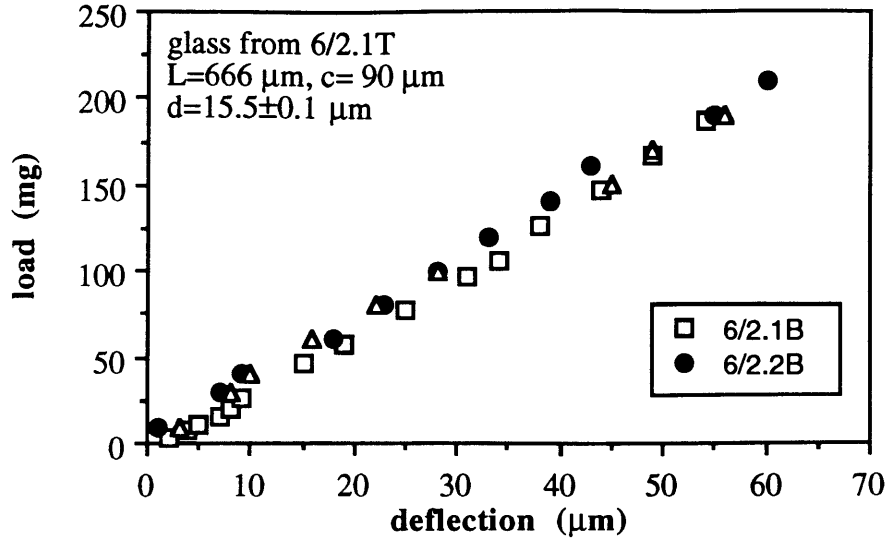
glass from 6/2.1T
L=666 μm, c= 90 μm
d=15.5±0.1 μm
6/2.1B
6/2.2B
load (mg)
deflection (μm)
0
50
100
150
200
250
0
10
20
30
40
50
60
70

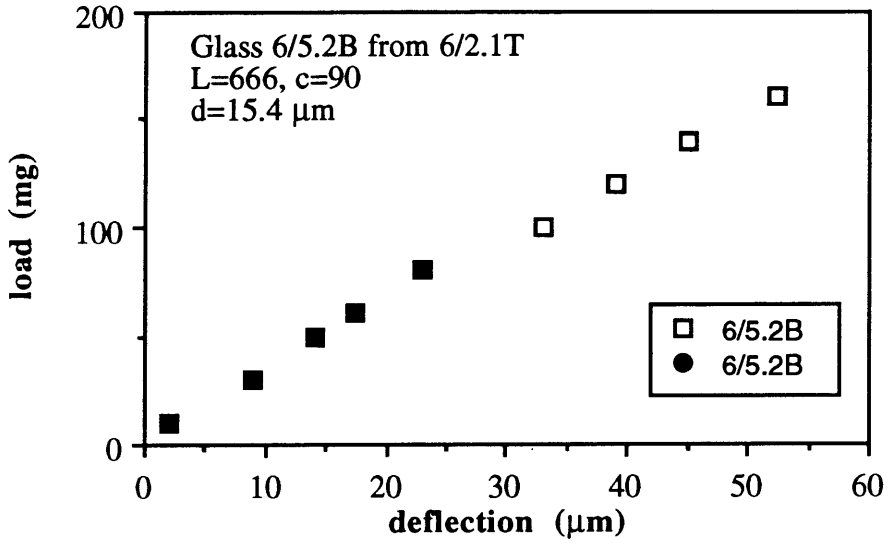
Glass 6/5.2B from 6/2.1T
L=666, c=90
d=15.4 μm
6/5.2B
6/5.2B
load (mg)
deflection (μm)
0
100
200
0
10
20
30
40
50
60

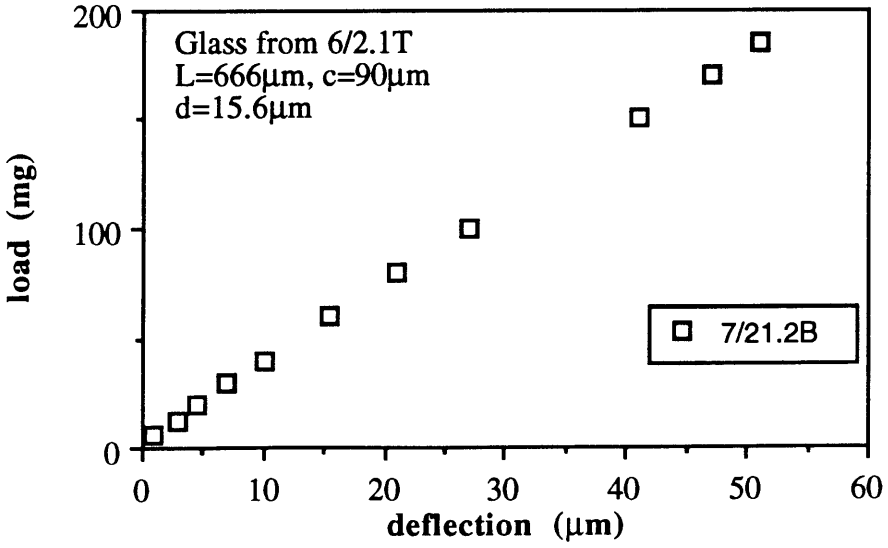
Glass from 6/2.1T
L=666μm, c=90μm
d=15.6μm
7/21.2B
load (mg)
deflection (μm)
0
100
200
0
10
20
30
40
50
60

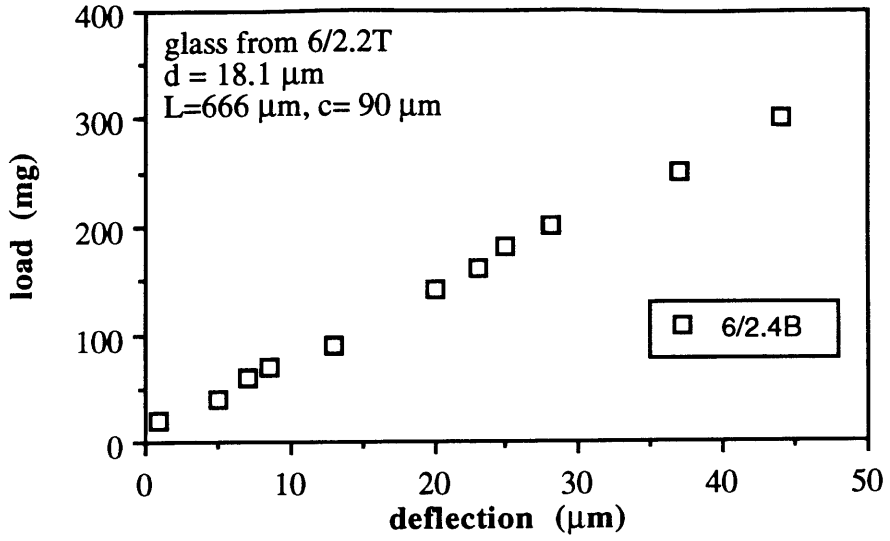
glass from 6/2.2T
d = 18.1 μm
L=666 μm, c= 90 μm
6/2.4B
load (mg)
deflection (μm)
0
100
200
300
400
0
10
20
30
40
50

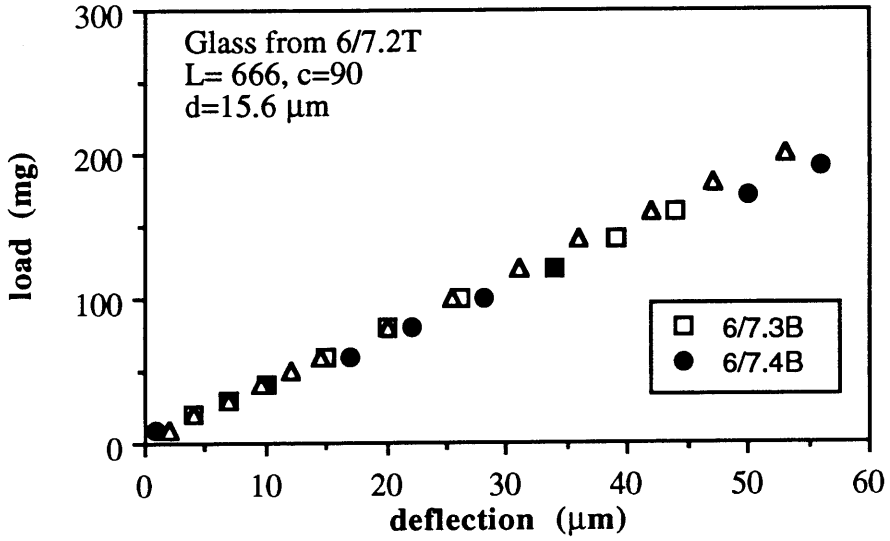
Glass from 6/7.2T
L= 666, c=90
d=15.6 μm
6/7.3B
6/7.4B
load (mg)
deflection (μm)
0
100
200
300
0
10
20
30
40
50
60

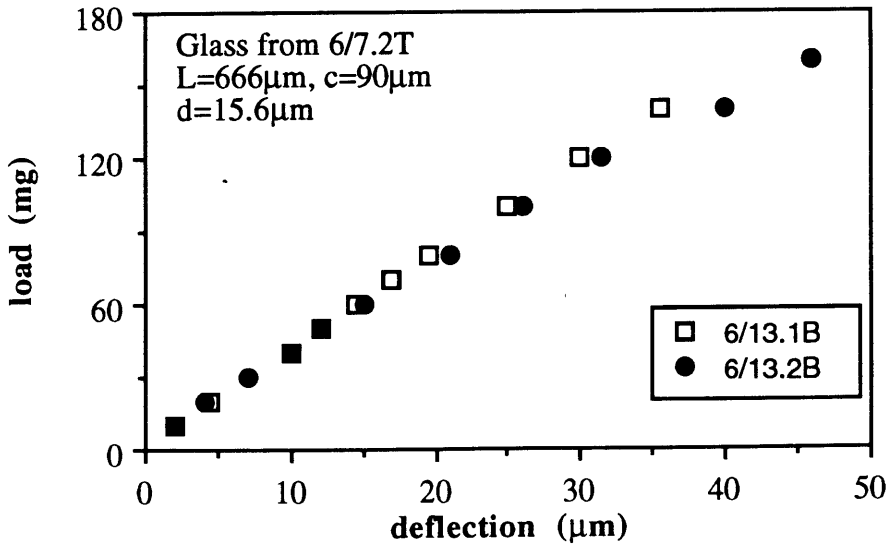
Glass from 6/7.2T
L=666μm, c=90μm
d=15.6μm
6/13.1B
6/13.2B
load (mg)
deflection (μm)
0
60
120
180
0
10
20
30
40
50

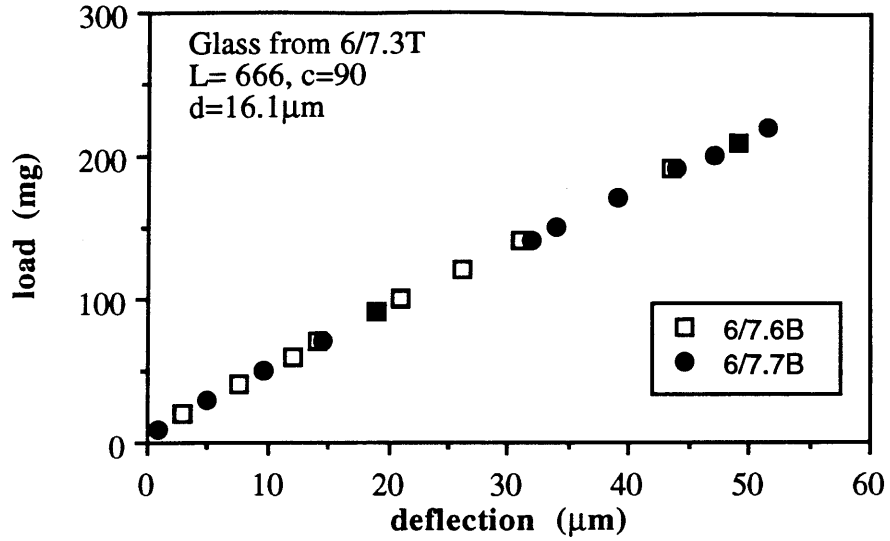
Glass from 6/7.3T
L= 666, c=90
d=16.1μm
6/7.6B
6/7.7B
load (mg)
deflection (μm)
0
100
200
300
0
10
20
30
40
50
60

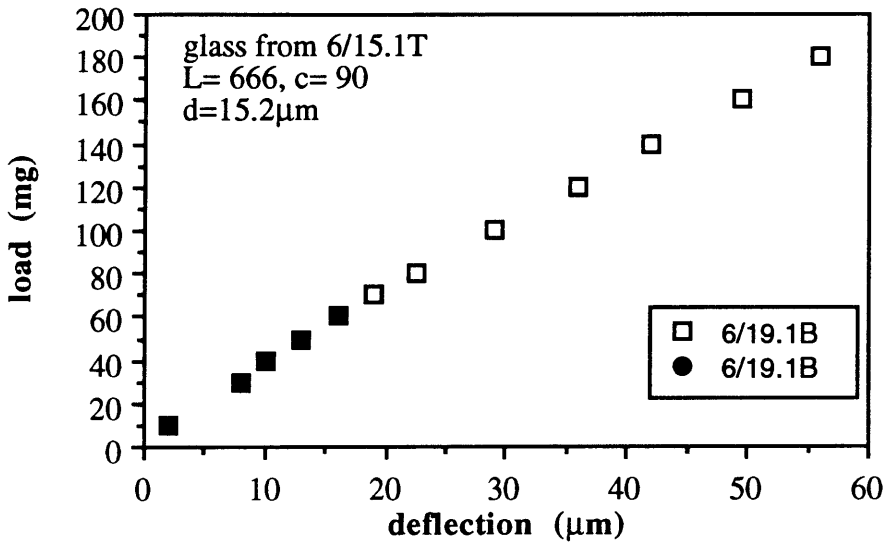
glass from 6/15.1T
L= 666, c= 90
d=15.2μm
6/19.1B
6/19.1B
load (mg)
deflection (μm)
0
20
40
60
80
100
120
140
160
180
200
0
10
20
30
40
50
60

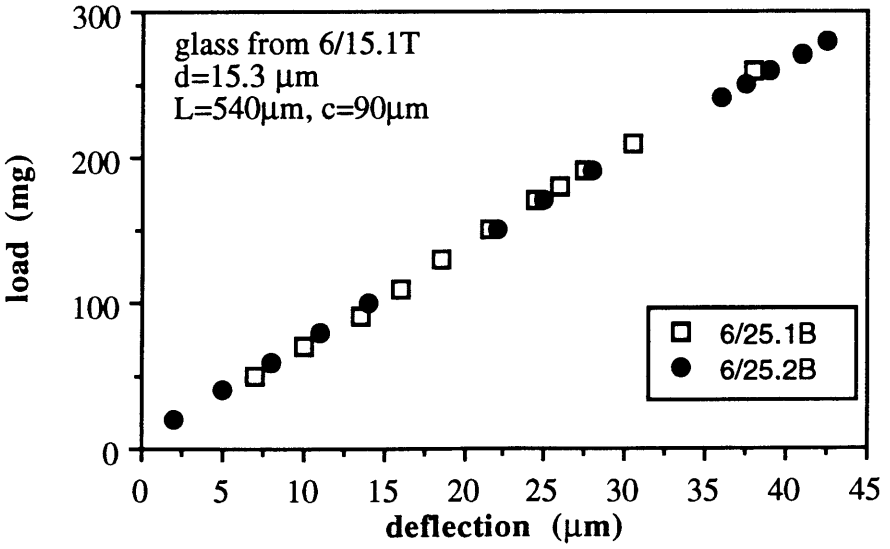
glass from 6/15.1T
d=15.3 μm
L=540μm, c=90μm
6/25.1B
6/25.2B
load (mg)
deflection (μm)
0
100
200
300
0
5
10
15
20
25
30
35
40
45

C2. Kevlar 119 Fibers

FITT- test

sample	diamtr. (μm)	mt (g/mil)	Lo (in)	**Et** (GPa)	**Et** (Msi)
6/12.5T	10.7	0.824	1.6870	75.8	10.99
	11.2	0.824	1.6870	69.2	10.03
	11.1	0.824	1.6870	70.4	10.22
	10.9	0.824	1.6870	73.0	10.59
6/12.6T	10.8	0.799	1.7205	73.6	10.67
	11.1	0.799	1.7205	69.6	10.10
average				**71.9**	**10.4**
st.dev.				2.6	0.4

span= 666μm

midspan= 90μm

Micro-Flex test

sample	mB (mg/μ)	b (mg)	x	x^2	P * (mg)	defl. μm	(EI)f (N*m^2)	**Eb** (GPa)	**Eb** (Msi)	Eb/Et
6/14.6Bk	0.544	0.8	0.6782	-2.85e-3	15.2	23.5	3.20E-11	49.7	7.2	0.66
6/14.7B	0.666	0.4	0.8337	-3.42e-3	18.8	24.5	3.92E-11	50.7	7.4	0.73
6/19.2Bk	0.708	0.4	0.9121	-3.92e-3	21.5	26	4.16E-11	55.9	8.1	0.79
6/19.3Bk	0.611	0.4	0.8310	-4.00e-3	20.2	27.5	3.59E-11	51.8	7.5	0.71
6/14.3B	0.605	-0.1	0.8057	-3.46e-3	20.4	29	3.56E-11	53.3	7.7	0.72
6/14.5Bk	0.685	1.1	0.8067	-2.89e-3	16.8	21	4.03E-11	54.0	7.8	0.78
average								**52.6**	**7.6**	
st. dev.								2.3	0.3	

Compressive Properties

sample	**Ec** **(GPa)**	**Ec** **(Msi)**	Ec/Et	shift factor	UCS (MPa)	UCS (ksi)	c-strain (%)	t-strn %	fail b-strn
6/14.6Bk	34.6	**5.02**	0.46	0.19	147.9	21.5	0.43%	0.29%	0.36%
6/14.7B	38.5	**5.59**	0.56	0.15	167.4	24.3	0.43%	0.32%	0.38%
6/19.2Bk	45.2	**6.56**	0.64	0.11	202.9	29.4	0.45%	0.36%	0.40%
6/19.3Bk	38.3	**5.56**	0.52	0.16	192.7	28.0	0.50%	0.36%	0.43%
6/14.3B	39.9	**5.79**	0.54	0.15	201.1	29.2	0.50%	0.37%	0.44%
6/14.5Bk	42.9	**6.22**	0.62	0.12	156.8	22.7	0.37%	0.29%	0.33%
average	**39.9**	**5.8**	0.56		**178**	**25.8**			
st. dev.	3.7	0.5			23.8	3.5			

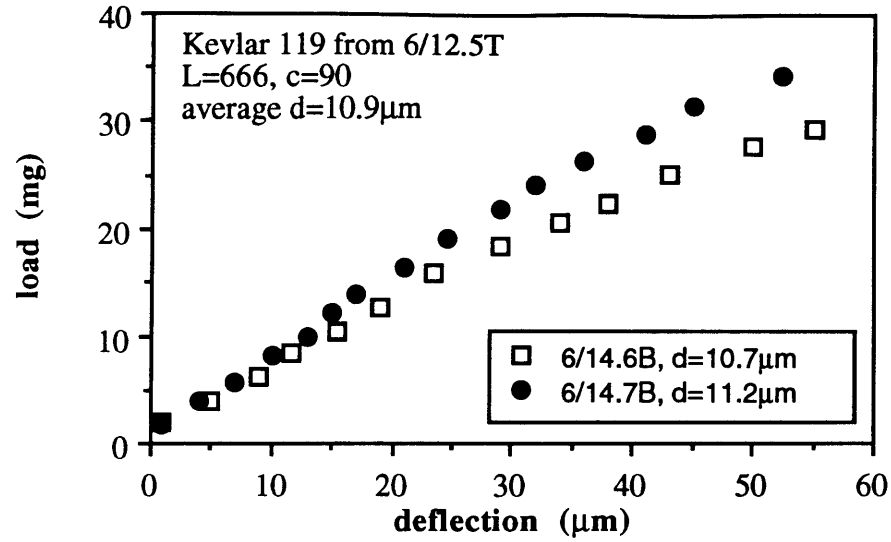
Kevlar 119 from 6/12.5T
L=666, c=90
average d=10.9μm
6/14.6B, d=10.7μm
6/14.7B, d=11.2μm
load (mg)
deflection (μm)
0
10
20
30
40
50
60

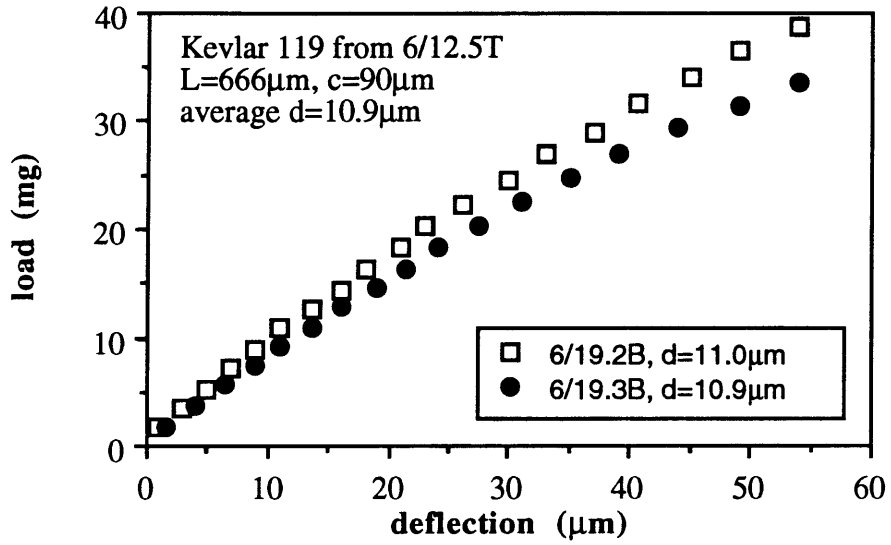
Kevlar 119 from 6/12.5T
L=666μm, c=90μm
average d=10.9μm
6/19.2B, d=11.0μm
6/19.3B, d=10.9μm
load (mg)
deflection (μm)
0
10
20
30
40
50
60

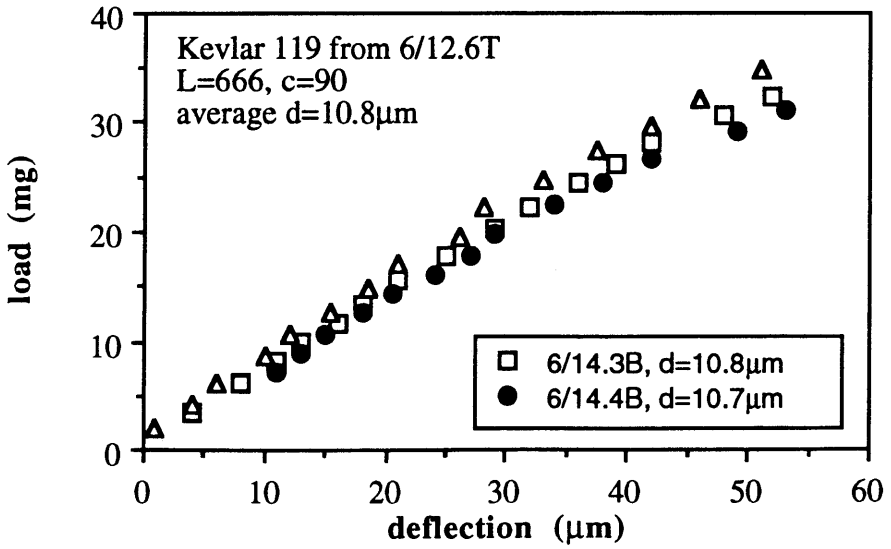
Kevlar 119 from 6/12.6T
L=666, c=90
average d=10.8μm
6/14.3B, d=10.8μm
6/14.4B, d=10.7μm
load (mg)
deflection (μm)
0
10
20
30
40
50
60

C3. Kevlar 29 Fibers

FITT- test sample	diamtr. (μm)	mt (g/mil)	Lo (in)	Et (GPa)	Et (Msi)	ΔL	strain
6/7.5T	12.2	0.992	1.872	77.9	11.29	7.45	0.40%
	12.1	0.988	1.872	78.8	11.43	6.5	0.35%
	11.4	0.984	1.872	88.5	12.83	5.65	0.30%
	12.1	0.980	1.872	78.2	11.34	4.65	0.25%
6/11.1T	12.3	1.173	1.657	80.2	11.63	7.12	0.43%
	11.8	1.153	1.657	85.6	12.42	5.98	0.36%
	11.7	1.176	1.657	88.9	12.89	7.28	0.44%
6/11.3T	11.7	1.008	1.656	76.1	11.04	5.25	0.32%
	11.5	1.019	1.656	79.7	11.55	7.15	0.43%
	11.8	1.015	1.656	75.4	10.93	6.45	0.39%
6/12.1T	11.9	1.102	1.658	80.6	11.69	5.55	0.33%
	11.8	1.117	1.658	83.0	12.04	7	0.42%
			avg.	**81.1**	**11.8**		
Micro-Flex test			st.dev.	4.5	0.7		

span=	666μ
midspn=	90μm

sample	mB (mg/μ)	b (mg)	x	x^2	P * (mg)	∂	(EI)f (N*m^2)	**Eb** (GPa)	**Eb** (Msi)	Eb/Et
6/7.8Bk	1.133	1.0	1.800	-1.45e-2	34.7	23	6.66e-11	61.2	8.9	0.79
6/9.1B	1.170	1.4	1.507	-7.65e-3	30.9	22	6.88e-11	65.4	9.5	0.83
6/9.4Bk	0.886	1.7	1.209	-7.88e-3	23.2	20.5	5.21e-11	62.8	9.1	0.71
6/9.5Bk	1.036	0.8	1.296	-7.64e-3	20.6	17	6.09e-11	57.9	8.4	0.74
6/13.3B	1.026	0.4	1.560	-9.53e-3	36.6	28	6.03e-11	53.7	7.8	0.67
6/13.4B	1.057	0.8	1.556	-1.08e-2	30.9	23	6.21e-11	65.3	9.5	0.76
6/13.5B	1.034	1.0	1.491	-7.88e-3	37.6	29	6.08e-11	66.0	9.6	0.74
6/13.9Bk	0.938	0.6	1.172	-5.32e-3	23.8	22	5.51e-11	59.9	8.7	0.79
6/13.10B	0.926	1.1	1.321	-7.05e-3	32.6	28	5.44e-11	63.4	9.2	0.80
6/13.11Bk	0.980	1.0	1.297	-6.21e-3	30.0	25.5	5.76e-11	60.5	8.8	0.80
6/13.12B	0.973	0.8	1.203	-4.79e-3	26.9	24	5.72e-11	58.1	8.4	0.72
6/13.13Bk	0.988	1.0	1.402	-7.38e-3	34.5	28	5.81e-11	61.0	8.9	0.74
							average	**61.3**	**8.9**	
Compressive Properties							st. dev.	3.6	0.5	

sample	**Ec** (GPa)	**Ec** (Msi)	Ec/Et	shift factor	UCS (MPa)	UCS (ksi)	c-strn	t-strn	fail b-strn
6/7.8Bk	49.2	7.13	0.63	0.11	246.2	35.7	0.50%	0.40%	0.45%
6/9.1B	54.6	7.92	0.69	0.09	228.4	33.1	0.42%	0.35%	0.38%
6/9.4Bk	46.4	6.73	0.52	0.16	192.8	28.0	0.42%	0.30%	0.36%
6/9.5Bk	44.3	6.42	0.57	0.14	146.2	21.2	0.33%	0.25%	0.29%
6/13.3B	38.0	5.51	0.47	0.18	237.2	34.4	0.62%	0.43%	0.53%
6/13.4B	51.2	7.42	0.60	0.13	238.7	34.6	0.47%	0.36%	0.41%
6/13.5B	50.7	7.35	0.57	0.14	295.3	42.8	0.58%	0.44%	0.51%
6/13.9Bk	48.1	6.98	0.63	0.11	191.3	27.8	0.40%	0.32%	0.36%
6/13.10B	51.4	7.46	0.65	0.11	277.0	40.2	0.54%	0.43%	0.49%
6/13.11Bk	49.5	7.18	0.66	0.10	237.5	34.5	0.48%	0.39%	0.43%
6/13.12B	43.5	6.31	0.54	0.15	198.3	28.8	0.46%	0.33%	0.40%
6/13.13Bk	46.3	6.72	0.56	0.14	262.2	38.0	0.57%	0.42%	0.49%
average	**47.8**	**6.9**	**0.59**		**229.3**	**33.3**			**0.42%**
st. dev.	4.4	0.6			41.4	6.0			0.07%

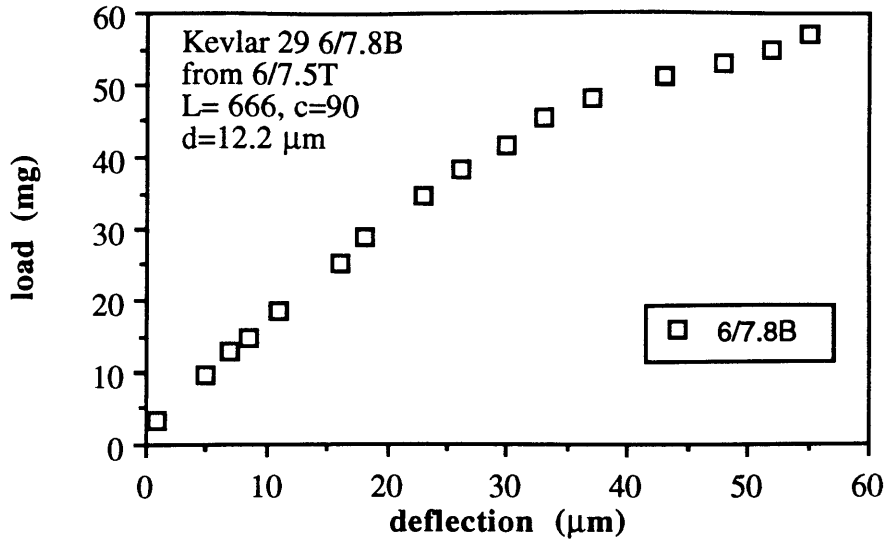
Kevlar 29 6/7.8B
from 6/7.5T
L= 666, c=90
d=12.2 μm
6/7.8B
load (mg)
deflection (μm)
0
10
20
30
40
50
60

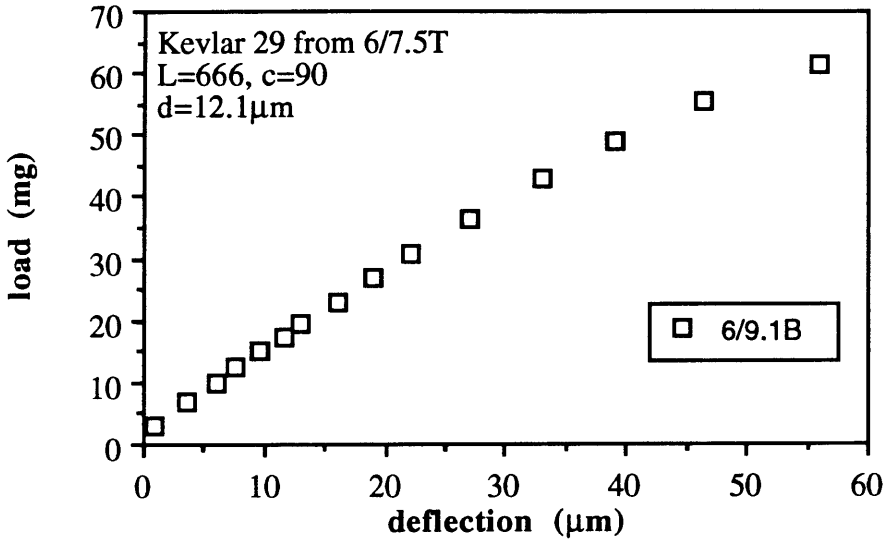
Kevlar 29 from 6/7.5T
L=666, c=90
d=12.1μm
6/9.1B
load (mg)
deflection (μm)
0
10
20
30
40
50
60
70

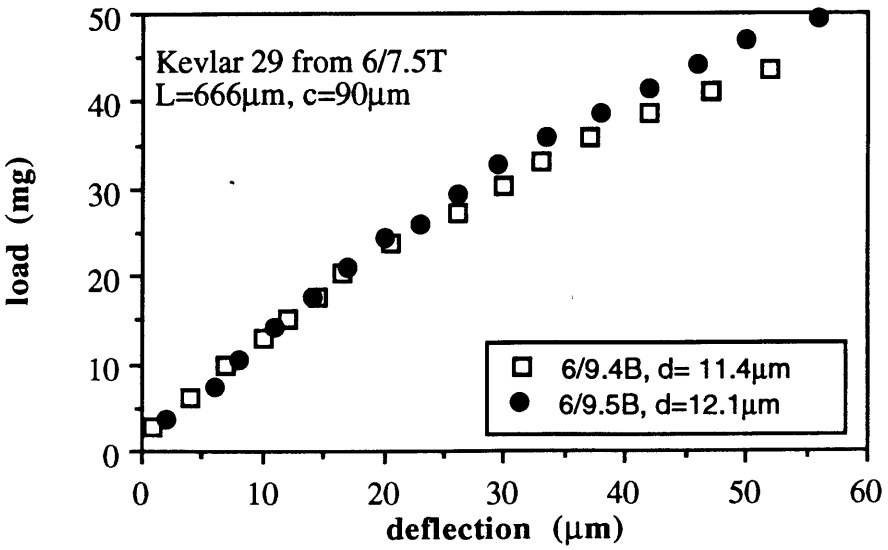
Kevlar 29 from 6/7.5T
L=666μm, c=90μm
6/9.4B, d= 11.4μm
6/9.5B, d=12.1μm
load (mg)
deflection (μm)
0
10
20
30
40
50
60

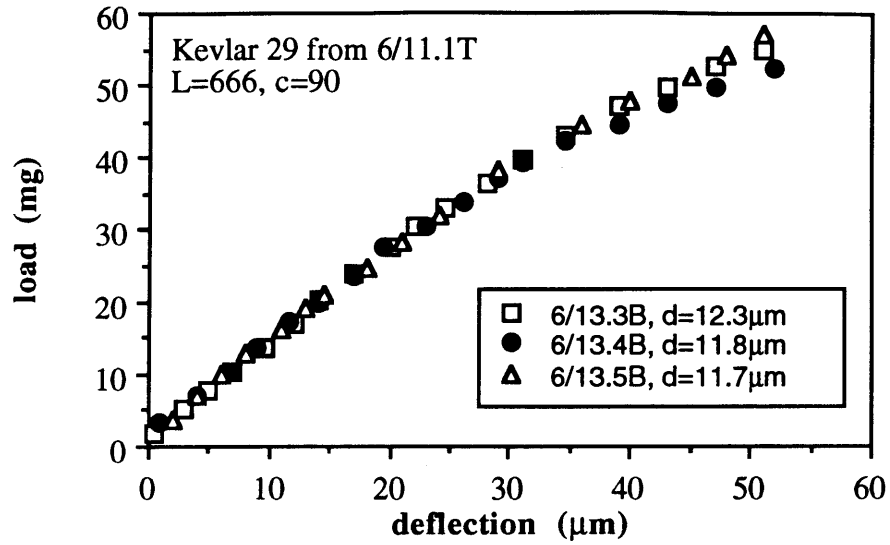
Kevlar 29 from 6/11.1T
L=666, c=90
6/13.3B, d=12.3μm
6/13.4B, d=11.8μm
6/13.5B, d=11.7μm
load (mg)
deflection (μm)
0
10
20
30
40
50
60

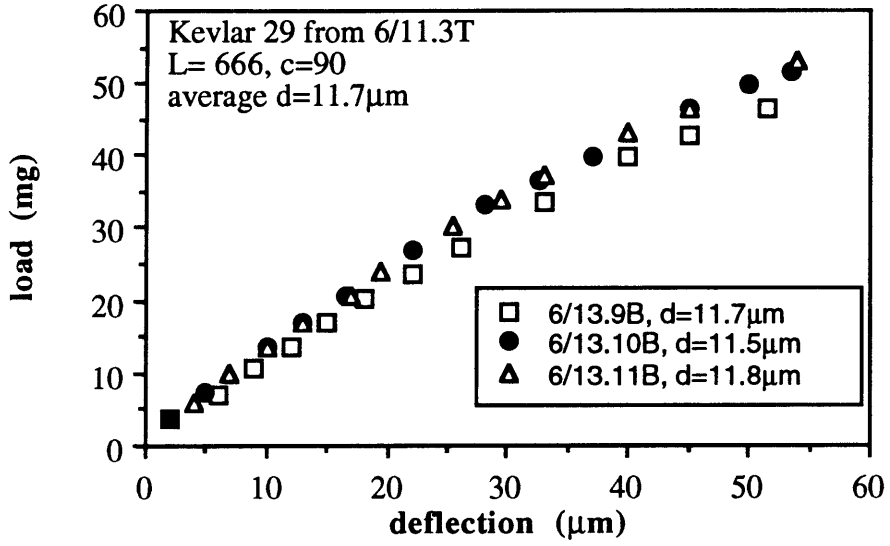
Kevlar 29 from 6/11.3T
L= 666, c=90
average d=11.7μm
6/13.9B, d=11.7μm
6/13.10B, d=11.5μm
6/13.11B, d=11.8μm
load (mg)
deflection (μm)
0
10
20
30
40
50
60

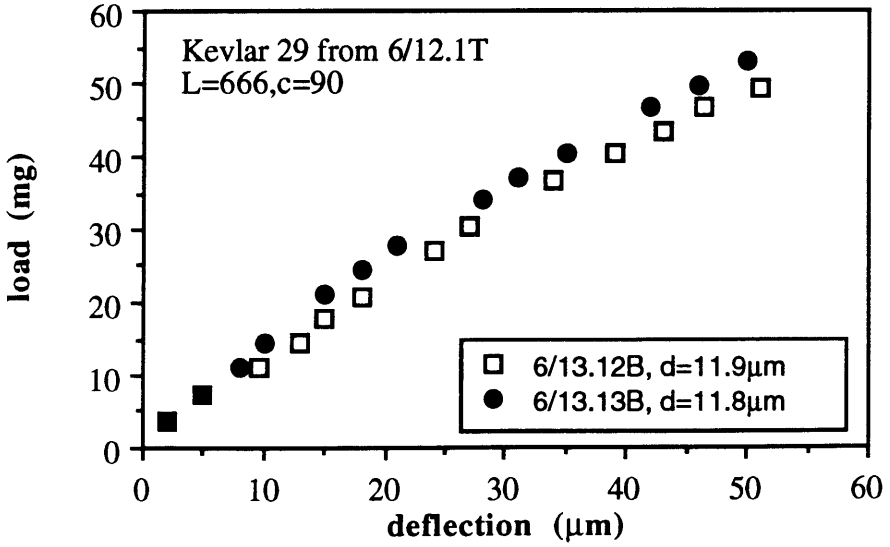
Kevlar 29 from 6/12.1T
L=666,c=90
6/13.12B, d=11.9μm
6/13.13B, d=11.8μm
load (mg)
deflection (μm)
0
10
20
30
40
50
60

C4. Kevlar 129 Fibers

FITT- test

sample june	diam. (μm)	mt (g/mil)	Lo (in)	**Et** (GPa)	**Et** (Msi)	ΔL	strain
6/12.3T	11.5	1.137	1.842	98.8	14.34	6.15	0.33%
	12.0	1.131	1.842	90.3	13.10	5.6	0.30%
	11.7	1.138	1.842	95.6	13.87	6.3	0.34%
	11.6	1.122	1.842	95.9	13.91	4.8	0.26%
6/12.4T	11.8	1.418	1.695	107.7	15.63	5.8	0.34%
	11.9	1.415	1.695	105.7	15.33	5.5	0.32%
average				**99.0**	**14.4**		
st.dev.				6.6	1.0		span (m)
							6.66E-4
							midspan (m)
							9.00E-5

Micro-Flex test

sample	mB (mg/μ)	b (mg)	x	x^2	P * (mg)	defl. μm	(EI)f (N*m^2)	**Eb** (GPa)	**Eb** (Msi)	Eb/Et
6/13.15B	1.085	1.8	1.392	-6.66e-3	30.3	23	6.38e-11	74.3	10.8	0.75
6/13.16Bk	1.259	-0.1	1.584	-7.73e-3	29.8	21	7.40e-11	72.7	10.5	0.81
6/13.17Bk	1.041	0.4	1.371	-6.60e-3	30.6	25	6.12e-11	66.5	9.6	0.70
6/13.18Bk	0.954	1.6	1.101	-3.69e-3	22.2	20	5.61e-11	63.1	9.1	0.66
6/14.1B	1.133	0.5	1.458	-6.25e-3	34.2	26	6.66e-11	70.0	10.1	0.65
6/14.2Bk	1.230	-3.5	1.623	-7.56e-3	33.6	26	7.23e-11	73.4	10.7	0.69
average								**70.0**	**10.2**	
st. dev.								4.4	0.6	

Compressive Properties

sample	**Ec** (GPa)	**Ec** (Msi)	Ec/Et	shift factor	**UCS** (MPa)	**UCS** (ksi)	c-strn	t-strn	fail b-strn
6/13.15B	57.5	8.34	0.58	0.13	251.5	36.5	0.44%	0.33%	0.39%
6/13.16Bk	59.6	8.64	0.66	0.10	223.9	32.5	0.38%	0.31%	0.34%
6/13.17Bk	48.4	7.02	0.51	0.17	233.3	33.8	0.48%	0.34%	0.41%
6/13.18Bk	44.0	6.38	0.46	0.19	169.8	24.6	0.39%	0.26%	0.32%
6/14.1B	48.4	7.02	0.45	0.20	247.9	36.0	0.51%	0.34%	0.43%
6/14.2Bk	53.4	7.75	0.51	0.17	243.9	35.4	0.46%	0.32%	0.39%
average	**51.9**	**7.5**	0.53		**228.4**	**33.1**			
st. dev.	6.0	0.9			30.4	4.4			

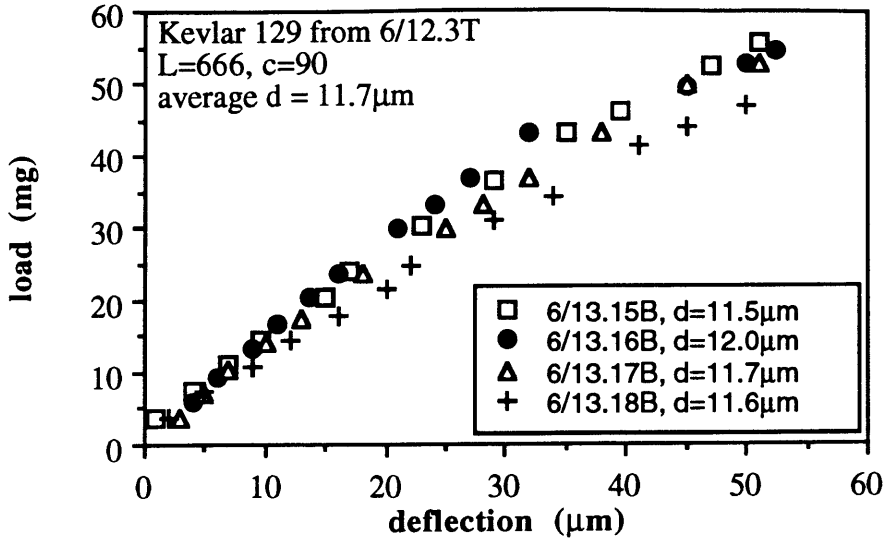
Kevlar 129 from 6/12.3T
L=666, c=90
average d = 11.7μm
6/13.15B, d=11.5μm
6/13.16B, d=12.0μm
6/13.17B, d=11.7μm
6/13.18B, d=11.6μm
load (mg)
deflection (μm)
0
10
20
30
40
50
60

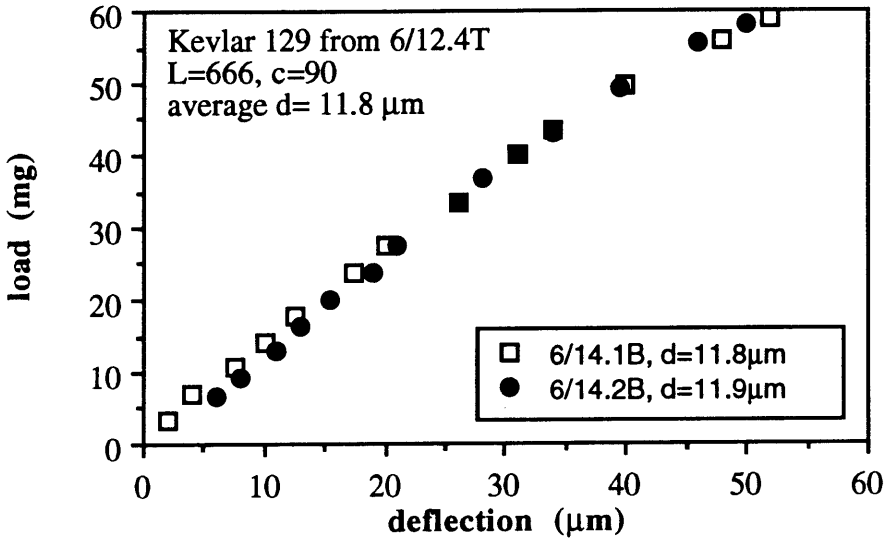
Kevlar 129 from 6/12.4T
L=666, c=90
average d= 11.8 μm
6/14.1B, d=11.8μm
6/14.2B, d=11.9μm
load (mg)
deflection (μm)
0
10
20
30
40
50
60

C5. Kevlar 49 Fibers

FITT- test

sample	diamtr. (μm)	mt (g/mil)	Lo (in)	**Et** (GPa)	**Et** (Msi)
6/15.4	11.3	1.727	1.470	124.1	18.00
6/17.1T	11.5	3.652	1.446	124.6	18.07
2L	11.8	3.652	1.446	118.4	17.17
	11.9	3.652	1.446	116.4	16.88
	11.4	3.652	1.446	126.8	18.39
6/20.1T	11.1	1.785	1.486	134.4	19.49
1L	10.8	1.785	1.486	141.9	20.59
	11.2	1.785	1.486	132.0	19.14
6/20.2T	11.9	1.960	1.517	131.1	19.01
2L	11.8	1.960	1.517	133.3	19.33
	11.9	1.960	1.517	131.1	19.01
			avg.	**128.5**	**18.6**
			st.dev.	7.4	1.1

span= 666μm
midspn= 90μm

Micro-Flex test

sample	mB (mg/μ)	b (mg)	x	x^2	P * (mg)	defl. μm	(El)f (N*m^2)	**Eb** (GPa)	**Eb** (Msi)	Eb/Et
6/20.1Bk	1.253	1.8	1.453	-5.87e-3	24.8	17	7.37e-11	85.8	12.4	0.69
6/20.2BK	1.425	4.3	1.593	-7.31e-3	21.7	11.5	8.38e-11	88.0	12.8	0.74
6/20.3B	1.147	1.2	1.598	-6.44e-3	49.2	35	6.74e-11	68.5	9.9	0.59
6/20.4B	1.065	5.6	1.741	-8.66e-3	60.3	39	6.26e-11	75.5	11.0	0.60
6/20.5Bk	1.048	0.9	1.409	-5.72e-3	39.6	31.5	6.16e-11	82.7	12.0	0.62
6/20.6Bk	1.266	2.1	1.492	-5.95e-3	28.3	19	7.44e-11	111.4	16.2	0.78
6/20.8Bk	1.248	2.1	2.021	-8.99e-3	72.4	43	7.33e-11	74.5	10.8	0.57
6/20.10Bk	1.275	0.6	2.125	-1.23e-2	59.3	34.5	7.50e-11	78.8	11.4	0.59
6/20.11Bk	1.519	0.1	2.139	-1.29e-2	44.0	24	8.93e-11	90.7	13.2	0.69
							average	**84.0**	**12.2**	
							st. dev.	12.5	1.8	

Compressive Properties

sample	**Ec** (GPa)	**Ec** (Msi)	Ec/Et	shift factor	**UCS** (MPa)	**UCS** (ksi)	c-strn	t-strn	fail b-strn
6/20.1Bk	62.0	8.99	0.50	0.17	198.8	28.8	0.32%	0.23%	0.27%
6/20.2BK	67.5	9.79	0.57	0.14	165.7	24.0	0.25%	0.19%	0.22%
6/20.3B	44.2	6.41	0.38	0.24	335.6	48.7	0.76%	0.47%	0.61%
6/20.4B	49.2	7.14	0.39	0.23	470.3	68.2	0.96%	0.60%	0.78%
6/20.5Bk	55.0	7.98	0.41	0.22	338.0	49.0	0.61%	0.39%	0.50%
6/20.6Bk	89.3	12.95	0.63	0.12	288.9	41.9	0.32%	0.26%	0.29%
6/20.8Bk	47.0	6.81	0.36	0.25	487.1	70.7	1.04%	0.62%	0.83%
6/20.10Bk	51.0	7.39	0.38	0.24	414.8	60.2	0.81%	0.50%	0.66%
6/20.11Bk	65.8	9.54	0.50	0.17	318.9	46.3	0.48%	0.34%	0.41%
average	**59.0**	**8.6**	0.46		**335.3**	**48.6**			
st. dev.	14.1	2.0			110.4	16.0			

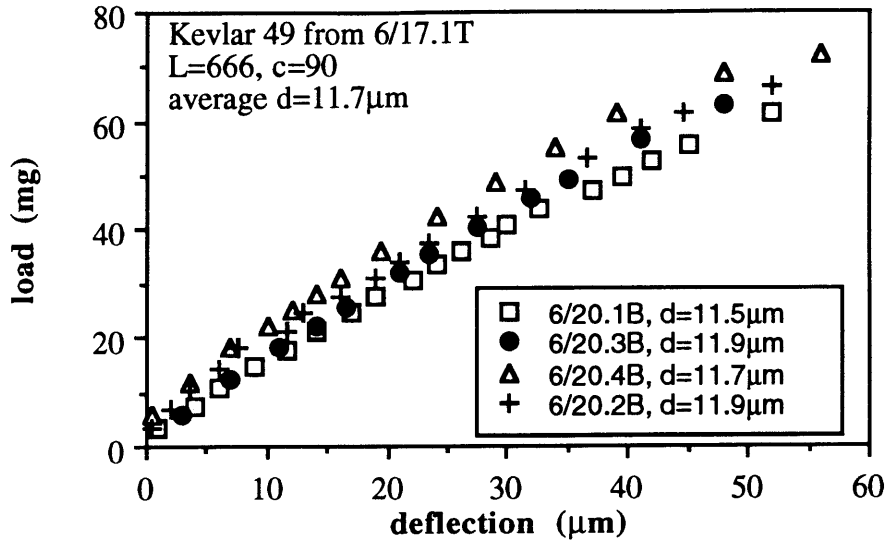
Kevlar 49 from 6/17.1T
L=666, c=90
average d=11.7μm
6/20.1B, d=11.5μm
6/20.3B, d=11.9μm
6/20.4B, d=11.7μm
6/20.2B, d=11.9μm
load (mg)
deflection (μm)
0
20
40
60
80
0
10
20
30
40
50
60

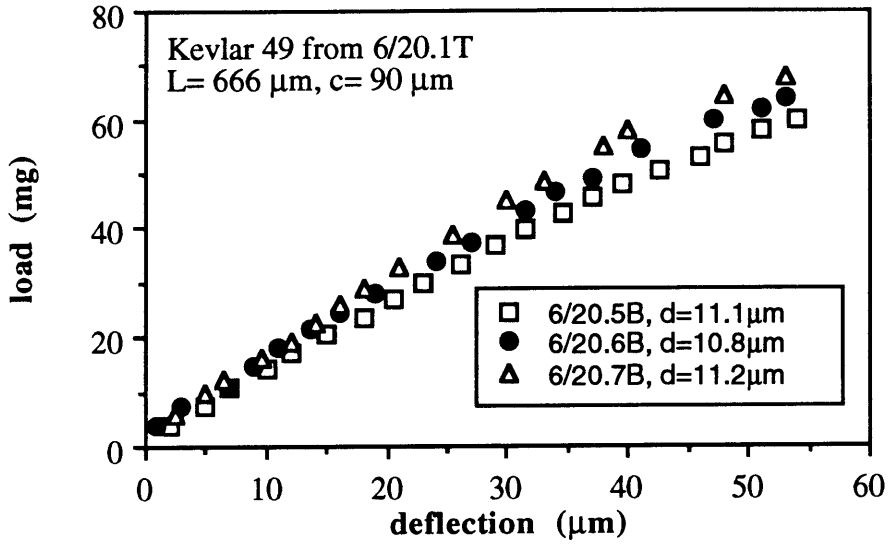
Kevlar 49 from 6/20.1T
L= 666 μm, c= 90 μm
6/20.5B, d=11.1μm
6/20.6B, d=10.8μm
6/20.7B, d=11.2μm
load (mg)
deflection (μm)
0
20
40
60
80
0
10
20
30
40
50
60

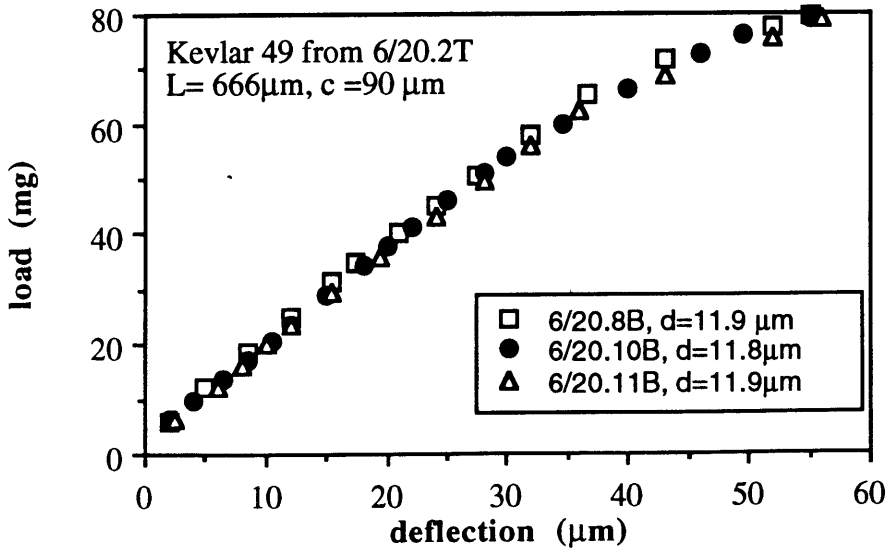
Kevlar 49 from 6/20.2T
L= 666μm, c =90 μm
6/20.8B, d=11.9 μm
6/20.10B, d=11.8μm
6/20.11B, d=11.9μm
load (mg)
deflection (μm)
0
20
40
60
80
0
10
20
30
40
50
60

C6. Kevlar 149 Fibers

FITT- test

sample june	diamtr. (μm)	mt (g/mil)	Lo (in)	**Et** (GPa)	**Et** (Msi)	ΔL	strain
6/15.2T	10.6	1.745	1.795	174.0	25.23	4.95	0.276%
	10.7	1.727	1.795	169.0	24.51	4.4	0.245%
	10.6	1.737	1.795	173.2	25.11	4.7	0.262%
6/15.3T	11.5	1.996	1.803	169.9	24.64	5.85	0.324%
	11.4	2.017	1.803	174.7	25.34	6.4	0.355%
6/17.2T	10.9	1.800	1.801	170.3	24.69	5.6	0.311%
	10.8	1.816	1.801	175.0	25.39	6.04	0.335%
	11.0	1.860	1.801	172.8	25.06	7.2	0.400%
average				**172.3**	**25.0**		
st.dev.				2.3	0.3		

span= 666μm
midspn.=90μm

Micro-Flex test

sample	mB (mg/μ)	b (mg)	x	x^2	P * (mg)	defl. μm	(EI)f (N*m^2)	**Eb** (GPa)	**Eb** (Msi)	Eb/Et
6/19.4B	1.080	1.7	1.623	-1.26e-2	30.8	21.5	6.35e-11	102.5	14.9	0.59
6/19.5B	1.126	0.6	1.665	-1.38e-2	27.8	19.5	6.62e-11	102.9	14.9	0.61
6/19.6B	1.065	0.8	1.612	-1.30e-2	28.9	21	6.26e-11	101.0	14.6	0.58
6/19.8B	1.302	2.8	2.161	-1.87e-2	42.6	23	7.65e-11	89.1	12.9	0.52
6/19.9B	1.142	1.4	2.026	-1.64e-2	44.2	27	6.71e-11	81.0	11.7	0.46
6/19.10B	1.065	1.0	1.780	-1.49e-2	35.1	24	6.26e-11	90.4	13.1	0.53
6/19.11B	0.987	1.6	1.756	-1.51e-2	36.6	25.5	5.80e-11	86.8	12.6	0.50
6/19.12B	1.048	2.3	1.831	-1.30e-2	45.5	30	6.16e-11	85.7	12.4	0.50
average								**92.4**	**13.4**	
st. dev.								8.5	1.2	

Compressive Properties

sample	**Ec** (GPa)	**Ec** (Msi)	Ec/Et	shift factor	**UCS** (MPa)	**UCS** (ksi)	c-strn	t-strn	no kinks b-strn
6/19.4B	66.1	9.59	0.38	0.24	296.6	43.0	0.45%	0.28%	0.36%
6/19.5B	68.0	9.86	0.40	0.22	264.2	38.3	0.39%	0.25%	0.32%
6/19.6B	64.8	9.40	0.37	0.24	278.0	40.3	0.43%	0.26%	0.35%
6/19.8B	53.4	7.74	0.31	0.28	309.4	44.9	0.58%	0.32%	0.45%
6/19.9B	45.0	6.52	0.26	0.33	315.9	45.8	0.70%	0.36%	0.53%
6/19.10B	54.5	7.90	0.32	0.28	300.5	43.6	0.55%	0.31%	0.43%
6/19.11B	50.2	7.28	0.29	0.30	314.4	45.6	0.63%	0.34%	0.48%
6/19.12B	49.6	7.19	0.29	0.30	370.2	53.7	0.75%	0.40%	0.57%
average	**56.4**	**8.2**	0.33		**306.2**	**44.4**			
st. dev.	8.7	1.3			31.5	4.6			

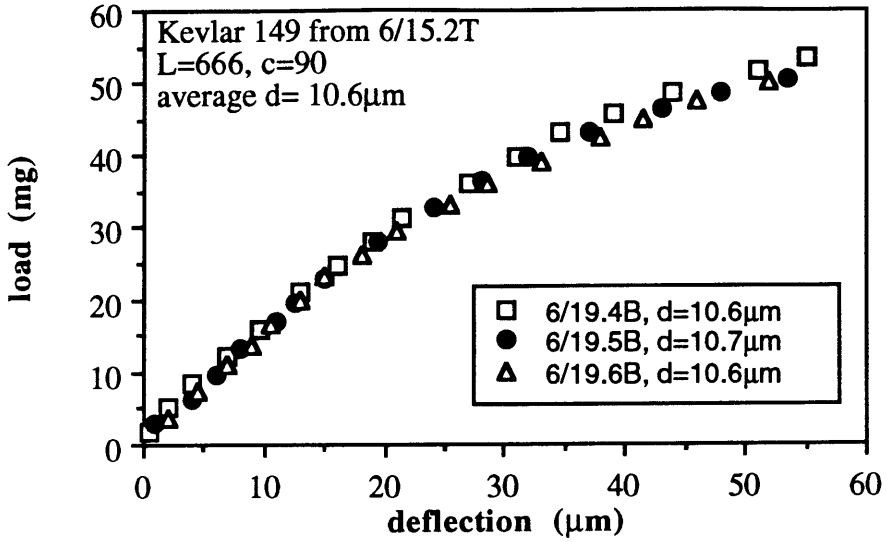
Kevlar 149 from 6/15.2T
L=666, c=90
average d= 10.6μm
6/19.4B, d=10.6μm
6/19.5B, d=10.7μm
6/19.6B, d=10.6μm
load (mg)
deflection (μm)
0
10
20
30
40
50
60

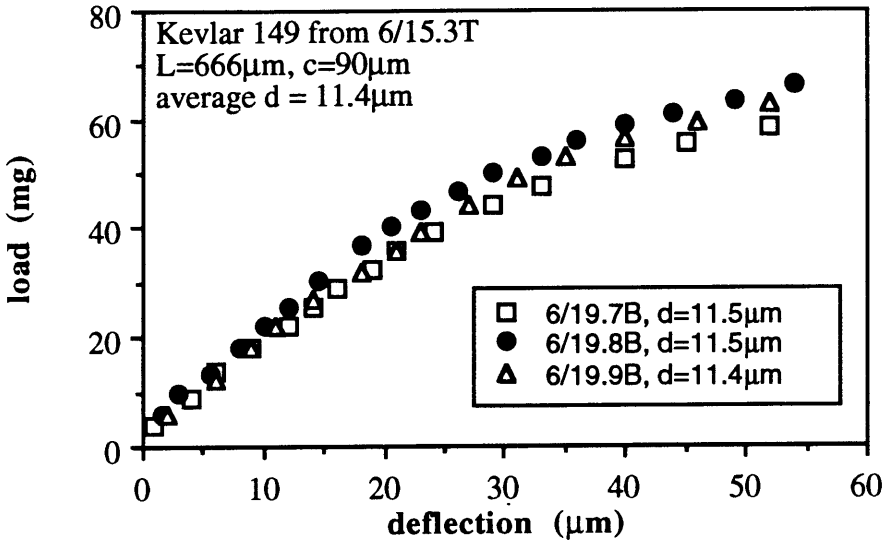
Kevlar 149 from 6/15.3T
L=666μm, c=90μm
average d = 11.4μm
6/19.7B, d=11.5μm
6/19.8B, d=11.5μm
6/19.9B, d=11.4μm
load (mg)
deflection (μm)
0
10
20
30
40
50
60
80

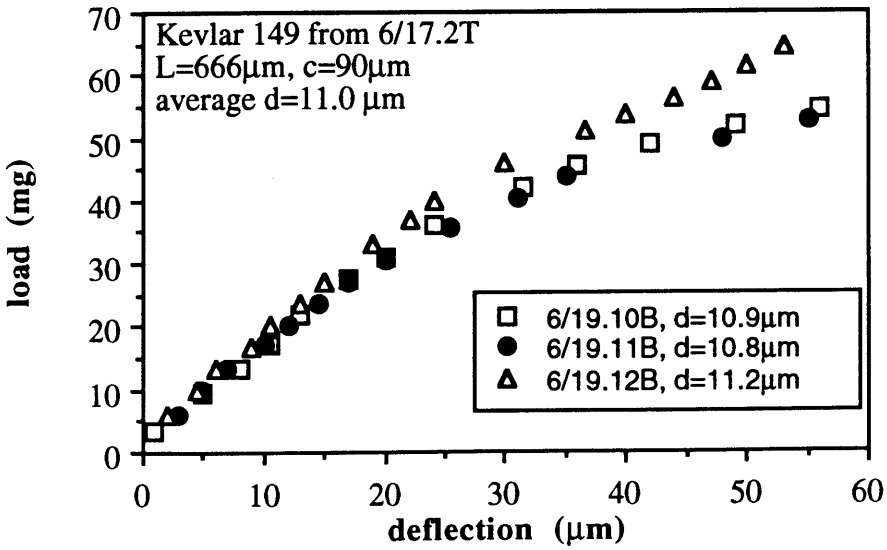
Kevlar 149 from 6/17.2T
L=666μm, c=90μm
average d=11.0 μm
6/19.10B, d=10.9μm
6/19.11B, d=10.8μm
6/19.12B, d=11.2μm
load (mg)
deflection (μm)
0
10
20
30
40
50
60
70

C7. AS4 Fibers

FITT- test

sample june	diamtr. (μm)	mT (g/mil)	x	x^2	Lo (in)	**Et (GPa)**	**Et (Msi)**	ΔL	strain
6/21.1T	6.20	0.9211	0.8721	4.23e-3	1.7240	257.9	37.41	5.8	0.34%
	6.20	0.9241	0.8721	4.23e-3	1.7240	258.7	37.53	6.15	0.36%
	6.24	0.9235	0.8721	4.23e-3	1.7240	255.3	37.02	6.08	0.35%
	6.04	0.9228	0.8721	4.23e-3	1.7240	272.3	39.49	6	0.35%
6/21.2T	6.31	0.9345	0.8517	6.68e-3	1.7075	250.2	36.29	6.2	0.36%
	6.19	0.9326	0.8517	6.68e-3	1.7075	259.5	37.63	6.06	0.35%
	6.12	0.9301	0.8517	6.68e-3	1.7075	264.7	38.39	5.87	0.34%
6/21.3T	6.53	1.0366	0.9801	4.63e-3	1.6990	257.9	37.40	6.1	0.36%
	6.63	1.0374	0.9801	4.63e-3	1.6990	250.3	36.31	6.18	0.36%
	6.54	1.0359	0.9801	4.63e-3	1.6990	256.9	37.26	6.02	0.35%
					average	**258.4**	**37.5**		
					st.dev.	6.5	0.9		

Micro-Flex test

span=666μm
(*span=542μm)
midspn=90μm

sample	mB (mg/μ)	b (mg)	x	x^2	P * (mg)	defl. μm	(EI)f (N*m^2)	**Eb (GPa)**	**Eb (Msi)**	Eb/Et
6/21.7B*	0.2248	0.8	0.2857	-6.89e-4	12.1	44.2	1.32e-11	182.1	26.4	0.71
6/25.3B	0.4808	0.4	0.5833	-1.59e-3	17.5	32.15	1.50e-11	207.2	30.1	0.80
6/25.4B	0.4737	0.7	0.5409	-1.04e-3	17.1	32.4	1.48e-11	199.0	28.9	0.78
6/25.5B	0.4314	0.5	0.5534	-1.92e-3	16.1	31.7	1.35e-11	206.4	29.9	0.76
6/25.6B	0.5107	0.9	0.5494	-5.90e-4	18.3	32.8	1.60e-11	205.1	29.8	0.82
6/25.7B	0.4704	0.8	0.5620	-1.44e-3	17.2	31.7	1.47e-11	204.0	29.6	0.79
6/25.8B	0.4308	0.6	0.5080	-1.18e-3	15.9	32.6	1.35e-11	195.6	28.4	0.74
6/25.9B	0.5971	1.1	0.6862	-1.46e-3	20.6	30.45	1.87e-11	209.1	30.3	0.81
6/25.10B	0.6307	0.7	0.6550	-3.75e-4	21.5	32.3	1.97e-11	207.9	30.1	0.83
6/25.11B	0.5784	0.3	0.6584	-1.26e-3	20.0	31.8	1.81e-11	201.3	29.2	0.78
							average	**201.8**	**29.3**	
							st. dev.	8.1	1.2	

Compressive Properties

sample	**Ec** (GPa)	**Ec** (Msi)	Ec/Et	shift factor	**c-stress** (MPa)	(ksi)	**c-strn**	t-strn	bending strain
6/21.7B*	134.2	**19.46**	0.52	0.16	624.1	90.5	0.47%	0.34%	0.40%
6/25.3B	168.9	**24.50**	0.65	0.11	747.7	108.4	0.44%	0.36%	0.40%
6/25.4B	158.7	**23.02**	0.62	0.12	710.1	103.0	0.45%	0.35%	0.40%
6/25.5B	161.0	**23.35**	0.59	0.13	727.7	105.5	0.45%	0.35%	0.40%
6/25.6B	170.6	**24.74**	0.68	0.10	748.3	108.5	0.44%	0.36%	0.40%
6/25.7B	163.8	**23.75**	0.63	0.11	730.7	106.0	0.45%	0.35%	0.40%
6/25.8B	149.3	**21.66**	0.56	0.14	683.0	99.1	0.46%	0.34%	0.40%
6/25.9B	172.2	**24.98**	0.67	0.10	758.4	110.0	0.44%	0.36%	0.40%
6/25.10B	174.9	**25.36**	0.70	0.09	761.8	110.5	0.44%	0.36%	0.40%
6/25.11B	161.2	**23.38**	0.63	0.12	719.9	104.4	0.45%	0.35%	0.40%
average	**158.1**	**22.9**	0.61		**710.2**	**103.0**			
st. dev.	12.7	1.8			44.2	6.4			

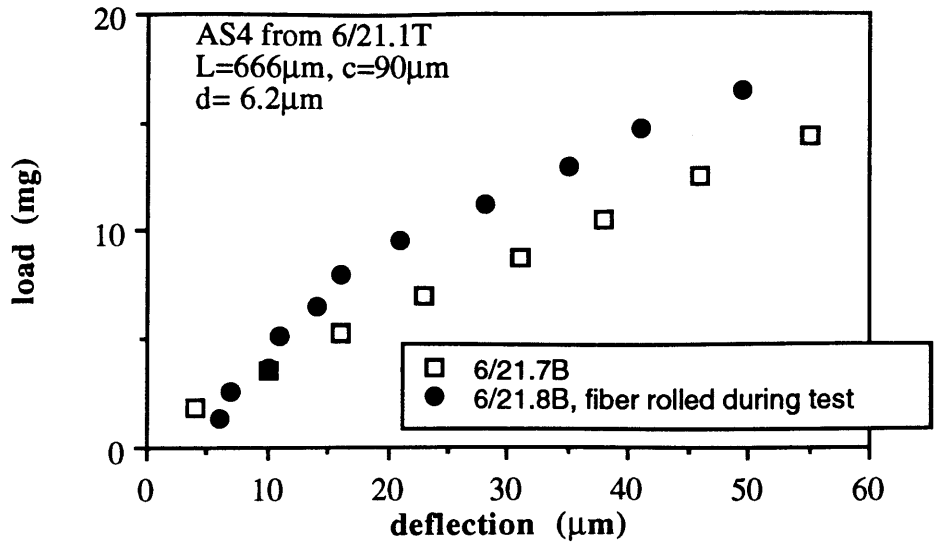
AS4 from 6/21.1T
L=666μm, c=90μm
d= 6.2μm
6/21.7B
6/21.8B, fiber rolled during test
load (mg)
deflection (μm)
0
10
20
30
40
50
60

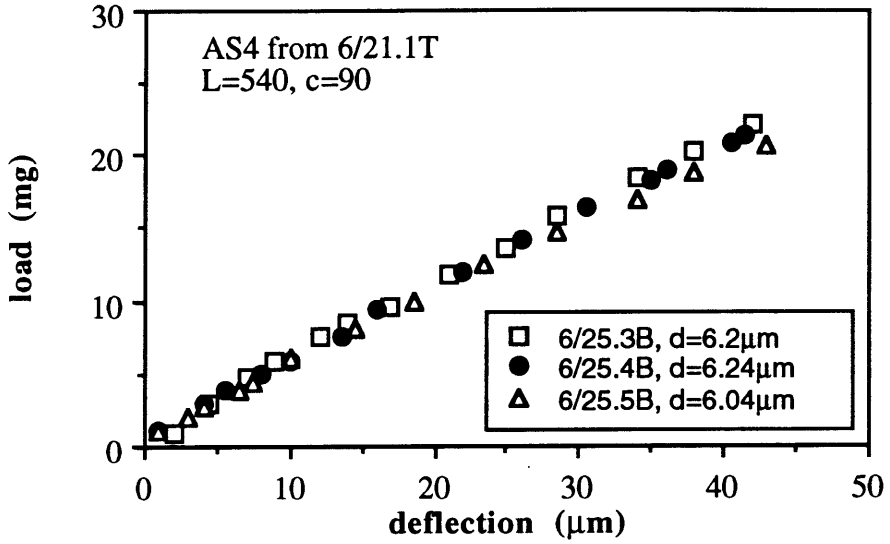
AS4 from 6/21.1T
L=540, c=90
6/25.3B, d=6.2μm
6/25.4B, d=6.24μm
6/25.5B, d=6.04μm
load (mg)
deflection (μm)
0
10
20
30
40
50

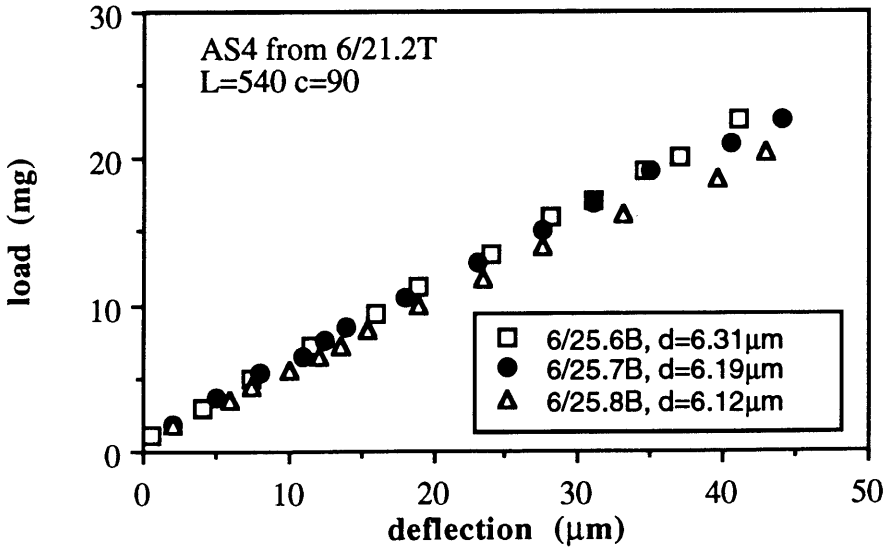
AS4 from 6/21.2T
L=540 c=90
6/25.6B, d=6.31μm
6/25.7B, d=6.19μm
6/25.8B, d=6.12μm
load (mg)
deflection (μm)
0
10
20
30
40
50

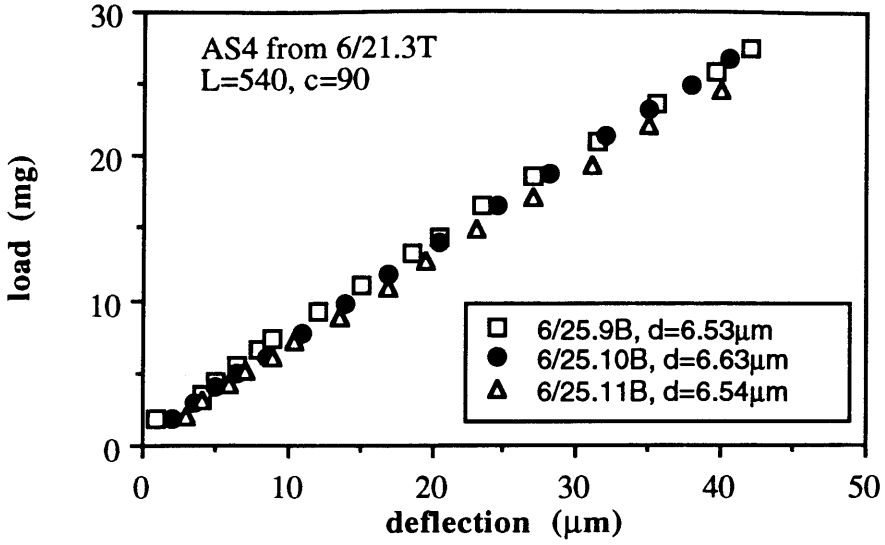
AS4 from 6/21.3T
L=540, c=90
load (mg)
deflection (μm)
6/25.9B, d=6.53μm
6/25.10B, d=6.63μm
6/25.11B, d=6.54μm
0
10
20
30
40
50

C8. IM7 Fibers

FITT- test

sample	diamtr. (μm)	mT (g/mil)	x	x^2	Lo (in)	**Et** (GPa)	**Et** (Msi)	ΔL	strain
6/26.3T	4.65	0.6408	0.5949	5.60e-3	1.4650	271.1	39.31	4.1	0.28%
	4.63	0.6407	0.5949	5.60e-3	1.4650	273.4	39.65	4.09	0.28%
	4.63	0.6390	0.5949	5.60e-3	1.4650	272.6	39.54	3.94	0.27%
6/27.1T	5.13	0.7481	0.7098	4.42e-3	1.7155	304.5	44.16	4.34	0.25%
	5.06	0.7484	0.7098	4.42e-3	1.7155	313.1	45.40	4.37	0.25%
	5.08	0.7477	0.7098	4.42e-3	1.7155	310.3	45.01	4.29	0.25%
				average:		**290.8**	**42.2**		
				std. dev:		20.4	3.0		

Micro-Flex test

span= 542μm
midspn=90μm

sample	mB (mg/μ)	b (mg)	x	x^2	P * (mg)	defl. μm	(EI)f (N*m^2)	**Eb** (GPa)	**Eb** (Msi)	Eb/Et
6/27.1B	0.1736	-0.1	0.1749	-1.72e-5	6.3	36.8	5.43e-12	236.4	34.3	0.87
6/27.2B	0.1710	0.3	0.1801	-1.34e-4	6.3	33.9	5.35e-12	237.0	34.4	0.87
6/27.3B	0.1585	0.0	0.1716	-1.86e-4	5.8	35.1	4.95e-12	219.6	31.9	0.81
6/27.4B	0.2354	0.0	0.2429	-1.16e-4	7.8	32.5	7.36e-12	216.4	31.4	0.71
6/27.5B	0.2335	0.0	0.2589	-4.01e-4	7.8	31.7	7.30e-12	226.8	32.9	0.72
6/27.6B	0.2278	0.3	0.2591	-5.23e-4	7.6	29.9	7.12e-12	217.8	31.6	0.70
							average	**225.7**	**32.7**	
							st. dev.	9.3	1.3	

Compressive Properties

sample	**Ec** (GPa)	**Ec** (Msi)	Ec/Et	shift factor	c stress (MPa)	(ksi)	c-strn	t-strn	b-strn
6/27.1B	207.7	**30.12**	0.77	0.07	663.7	96.3	0.32%	0.28%	0.30%
6/27.2B	207.1	**30.04**	0.76	0.07	664.3	96.4	0.32%	0.28%	0.30%
6/27.3B	180.0	**26.10**	0.66	0.10	595.6	86.4	0.33%	0.27%	0.30%
6/27.4B	160.2	**23.24**	0.53	0.16	557.7	80.9	0.35%	0.25%	0.30%
6/27.5B	170.4	**24.72**	0.54	0.15	588.0	85.3	0.35%	0.25%	0.30%
6/27.6B	159.7	**23.16**	0.51	0.16	557.1	80.8	0.35%	0.25%	0.30%
average	**180.8**	**26.2**	0.63		**604.4**	**87.7**			
st. dev.	21.9	3.2			48.7	7.1			

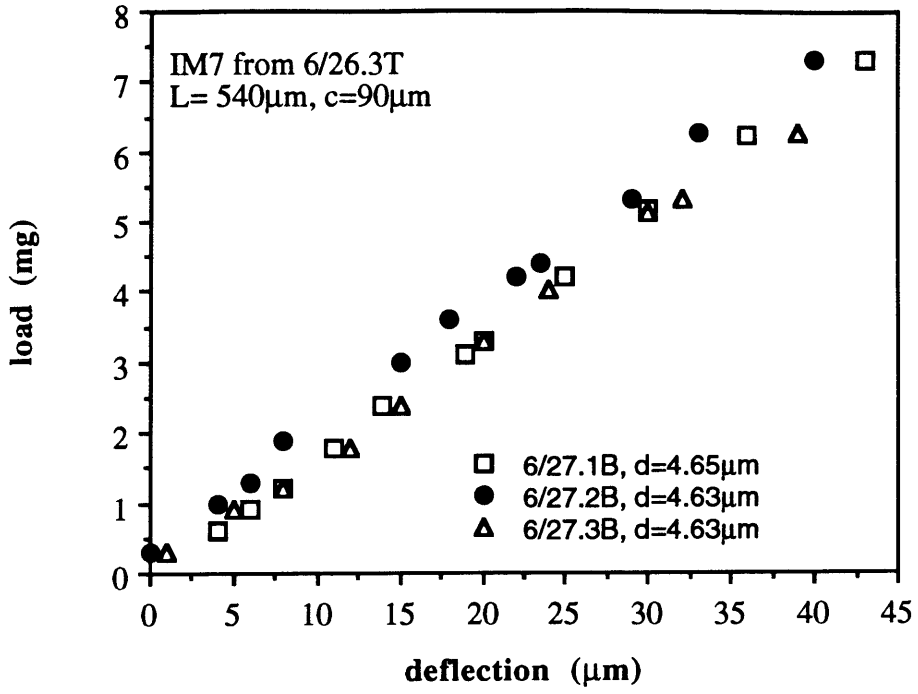
IM7 from 6/26.3T
L= 540µm, c=90µm
load (mg)
deflection (µm)
6/27.1B, d=4.65µm
6/27.2B, d=4.63µm
6/27.3B, d=4.63µm
0
1
2
3
4
5
6
7
8
0
5
10
15
20
25
30
35
40
45

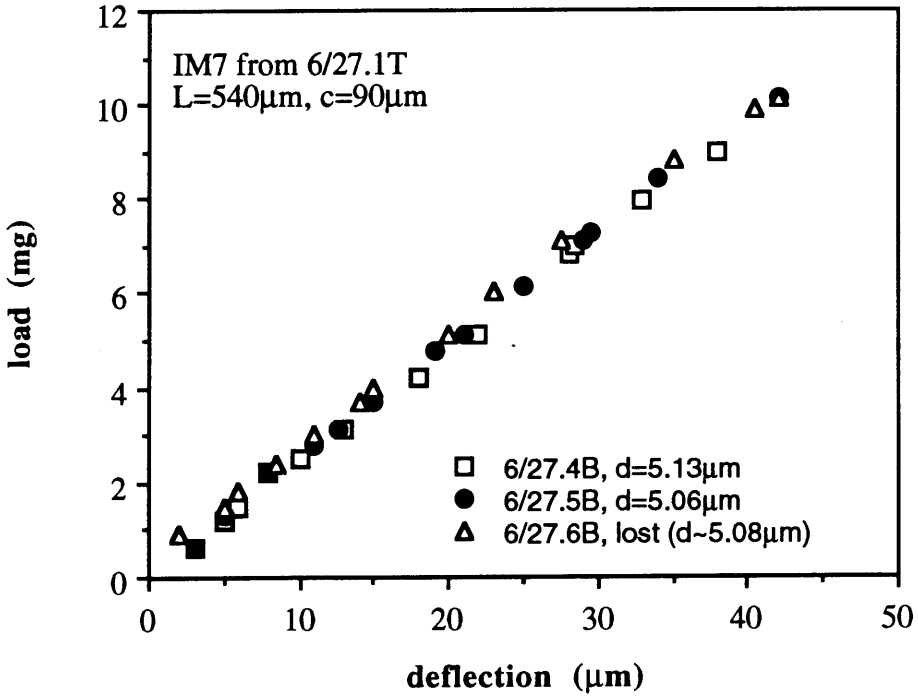
IM7 from 6/27.1T
L=540µm, c=90µm
load (mg)
deflection (µm)
6/27.4B, d=5.13µm
6/27.5B, d=5.06µm
6/27.6B, lost (d~5.08µm)
0
2
4
6
8
10
12
0
10
20
30
40
50

C9. IM8 Fibers

FITT- test

sample	diamtr. (μm)	mT (g/mil)	x	x^2	Lo (in)	**Et** (GPa)	**Et** (Msi)	ΔL	strain
6/27.2T	4.80	1.201	1.124	7.97e-3	1.9320	314.4	45.59	4.85	0.25%
	4.71	1.202	1.124	7.97e-3	1.9320	326.7	47.38	4.9	0.25%
6/27.3T	4.90	0.687	0.646	3.95e-3	1.9260	343.9	49.87	5.12	0.27%
	4.83	0.686	0.646	3.95e-3	1.9260	353.6	51.29	5.05	0.26%
	4.94	0.685	0.646	3.95e-3	1.9260	337.5	48.95	4.92	0.26%
average:						**335.2**	**48.6**		
std. dev:						15.2	2.2		

Micro-Flex test

sample	mB (mg/μ)	b (mg)	x	x^2	P * (mg)	defl. μm	(EI)f (N*m^2)	**Eb** (GPa)	**Eb** (Msi)	Eb/Et
6/27.7B	0.1847	0.0	0.2274	-6.76e-4	6.5	31.6	5.77e-12	221.5	32.1	0.70
6/27.8B	0.1807	0.5	0.2079	-4.40e-4	6.5	30.9	5.65e-12	233.9	33.9	0.72
6/27.10B	0.2461	0.1	0.2505	-6.47e-5	8.5	33.8	7.69e-12	271.9	39.4	0.79
6/27.11B	0.2308	0.3	0.2475	-2.56e-4	8.1	32.6	7.21e-12	270.0	39.2	0.76
6/27.12B	0.2278	0.1	0.2369	-1.36e-4	7.8	33.2	7.12e-12	243.6	35.3	0.72
average:								**248.2**	**36.0**	**0.74**
std dev								22.2	3.2	

Compressive Properties

span= 542μm
midspn= 90μm

sample	**Ec** (GPa)	**Ec** (Msi)	Ec/Et	shift factor	c stress (MPa)	(ksi)	c-strn	t-strn	b-strn
6/27.7B	162.9	**23.6**	0.52	0.16	568.3	82.4	0.35%	0.25%	0.30%
6/27.8B	174.1	**25.3**	0.53	0.16	604.8	87.7	0.35%	0.25%	0.30%
6/27.10B	219.3	**31.8**	0.64	0.11	730.9	106.0	0.33%	0.27%	0.30%
6/27.11B	211.6	**30.7**	0.60	0.13	716.6	103.9	0.34%	0.26%	0.30%
6/27.12B	182.6	**26.5**	0.54	0.15	631.9	91.6	0.35%	0.25%	0.30%
average	**190.1**	**27.6**	0.57		650.5	94.3			
st. dev.	24.3	3.5			70.8	10.3			

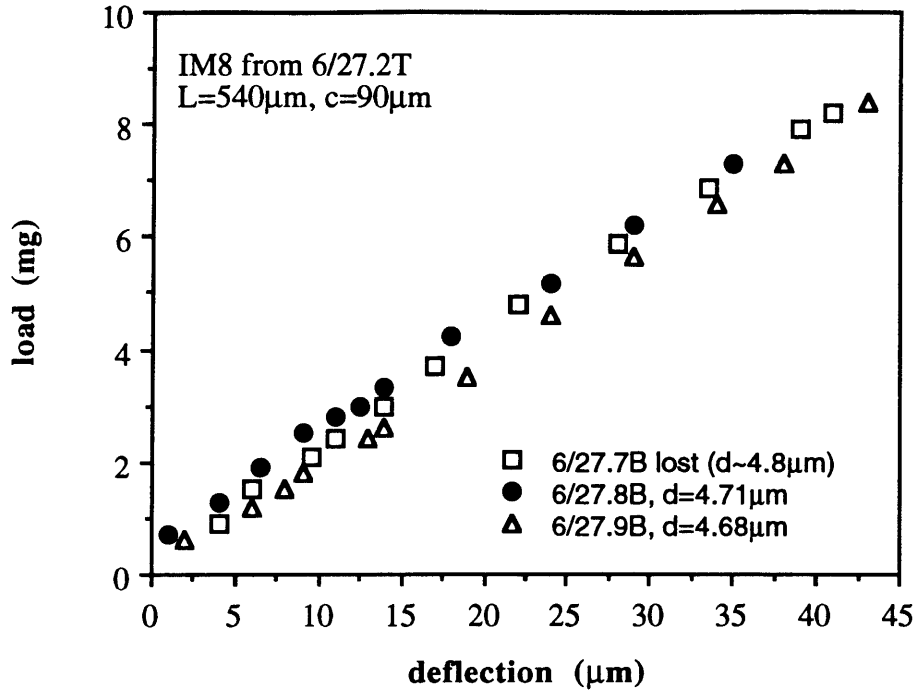
IM8 from 6/27.2T
L=540μm, c=90μm
load (mg)
deflection (μm)
6/27.7B lost (d~4.8μm)
6/27.8B, d=4.71μm
6/27.9B, d=4.68μm
0
2
4
6
8
10
0
5
10
15
20
25
30
35
40
45

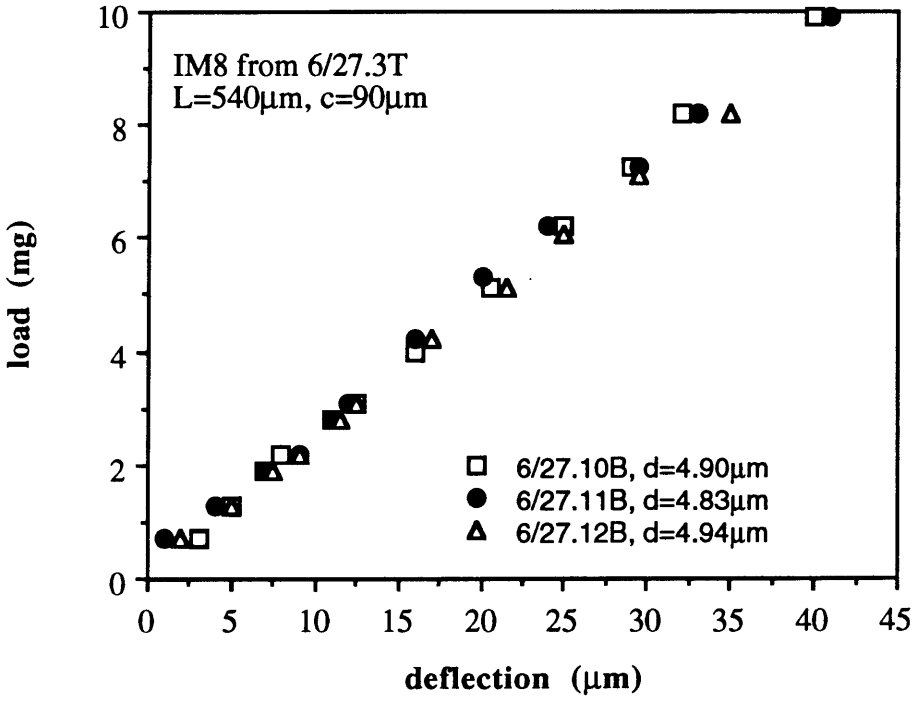
IM8 from 6/27.3T
L=540μm, c=90μm
load (mg)
deflection (μm)
6/27.10B, d=4.90μm
6/27.11B, d=4.83μm
6/27.12B, d=4.94μm
0
2
4
6
8
10
0
5
10
15
20
25
30
35
40
45

C10. HMS4 Fibers

FITT- test

sample june	diamtr. (μm)	mt (g/mil)	Lo (in)	**Et (GPa)**	**Et (Msi)**	ΔL	strain
6/20.3T	6.97	2.054	1.40	369.5	53.6	4.8	0.34%
	6.95	2.063	1.40	373.4	54.2	4.95	0.35%
	6.87	2.062	1.40	381.8	55.4	4.93	0.35%
	6.90	2.060	1.40	378.2	54.9	4.9	0.35%
6/20.4T	7.14	2.084	1.4130	360.6	52.3	4.9	0.35%
	7.16	2.095	1.4130	360.5	52.3	5.1	0.36%
	7.23	2.095	1.4130	353.6	51.3	5.1	0.36%
average				**368.2**	**53.4**		
st.dev.				10.4	1.5		

Micro-Flex test

span=666μm
midspn=90μm

sample	mB (mg/μ)	b (mg)	x	x^2	P * (mg)	defl. μm	(EI)f (N*m^2)	**Eb (GPa)**	**Eb (Msi)**	Eb/Et
6/20.12B	0.5394	1.0	0.6510	-1.34e-3	25.8	41.6	3.17e-11	273.7	39.7	0.74
6/21.1B	0.5714	0.6	0.6674	-1.11e-3	27.4	43.2	3.36e-11	293.2	42.5	0.79
6/21.2B	0.5499	-0.2	0.6716	-1.38e-3	26.7	44	3.23e-11	295.6	42.9	0.77
6/21.3B	0.5454	0.2	0.7231	-2.16e-3	26.3	41.2	3.21e-11	288.1	41.8	0.76
6/21.4B	0.5868	-1.6	0.7820	-2.31e-3	27.4	42.3	3.45e-11	270.4	39.2	0.75
6/21.5B	0.6455	0.7	0.7412	-1.13e-3	30.0	42.3	3.79e-11	294.1	42.7	0.82
6/21.6B	0.6546	2.6	0.7577	-1.32e-3	30.1	39	3.85e-11	286.8	41.6	0.81
average								**286.0**	**41.5**	
st. dev.								10.1	1.5	

Compressive Properties

sample	**Ec (GPa)**	**Ec (Msi)**	Ec/Et	shift factor	c stress (MPa)	(ksi)	c-strn	t-strn	b-strn
6/20.12B	209.6	**30.4**	0.57	0.14	956.1	138.7	0.46%	0.34%	0.40%
6/21.1B	235.1	**34.1**	0.63	0.12	1048.0	152.0	0.45%	0.35%	0.40%
6/21.2B	234.4	**34.0**	0.61	0.12	1052.3	152.6	0.45%	0.35%	0.40%
6/21.3B	225.5	**32.7**	0.60	0.13	1018.3	147.7	0.45%	0.35%	0.40%
6/21.4B	208.9	**30.3**	0.58	0.14	948.4	137.6	0.45%	0.35%	0.40%
6/21.5B	244.8	**35.5**	0.68	0.10	1073.9	155.8	0.44%	0.36%	0.40%
6/21.6B	236.5	**34.3**	0.67	0.10	1040.5	150.9	0.44%	0.36%	0.40%
average	**227.8**	**33.0**	0.62		1019.6	147.9			
st. dev.	13.9	2.0			48.9	7.1			

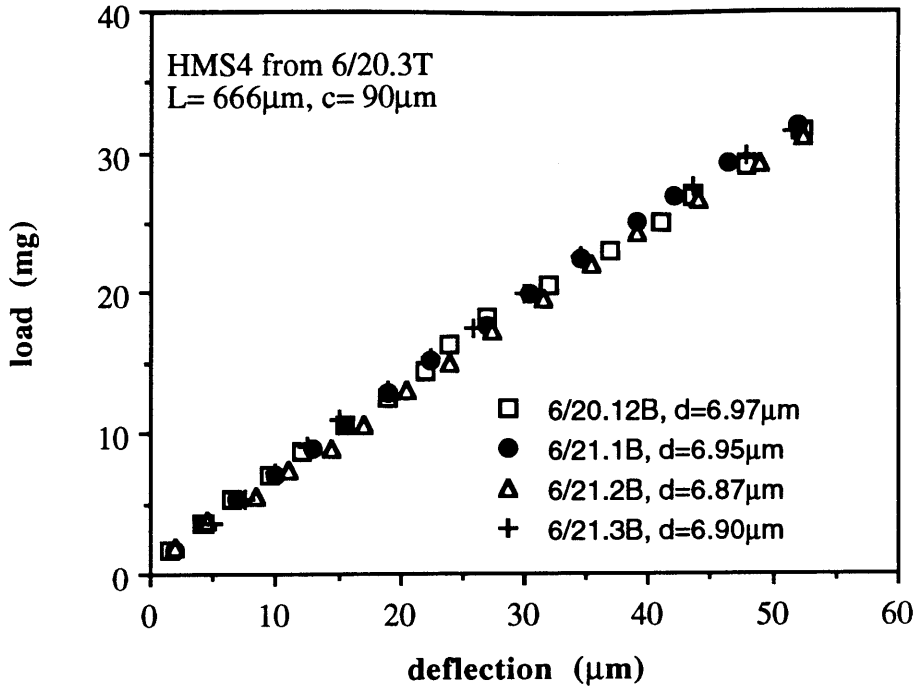
HMS4 from 6/20.3T
L= 666μm, c= 90μm
6/20.12B, d=6.97μm
6/21.1B, d=6.95μm
6/21.2B, d=6.87μm
6/21.3B, d=6.90μm
load (mg)
deflection (μm)
0
10
20
30
40
50
60

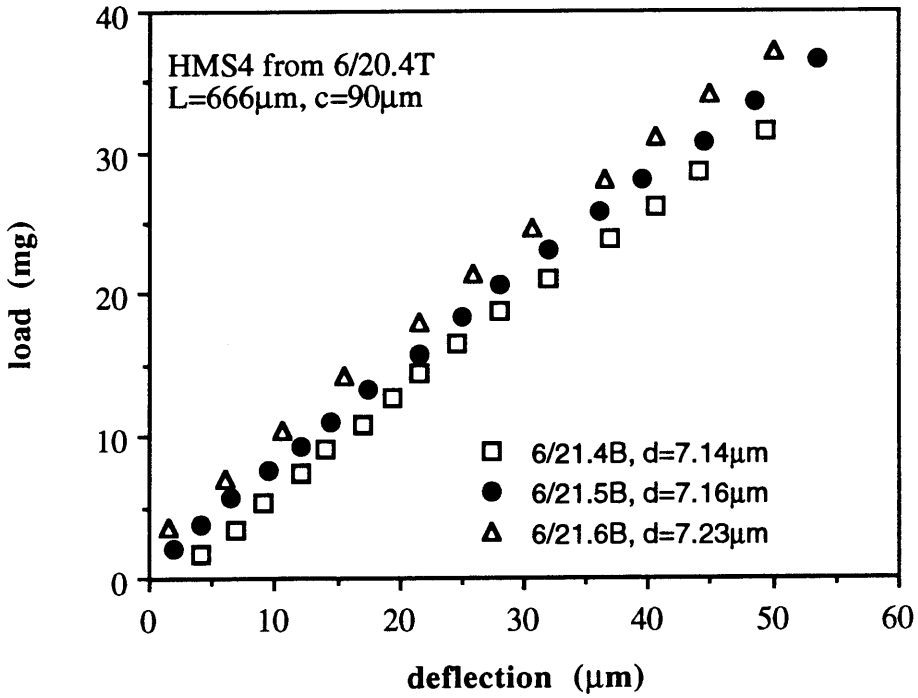
HMS4 from 6/20.4T
L=666μm, c=90μm
6/21.4B, d=7.14μm
6/21.5B, d=7.16μm
6/21.6B, d=7.23μm
load (mg)
deflection (μm)
0
10
20
30
40
50
60

C11. P25 HT Fibers

FITT- test

sample	diamtr. (μm)	mt (g/mil)	x	x^2	Lo (in)	Et (GPa)	Et (Msi)	ΔL	strain
6/21.4	10.40	1.4284	1.1046	1.84E-02	1.7645	145.5	21.1	8.82	0.50%
	11.10	1.4167	1.1046	1.84E-02	1.7645	126.7	18.4	8.5	0.48%
	10.70	1.4295	1.1046	1.84E-02	1.7645	137.5	19.9	8.85	0.50%
7/15.1T	10.58	1.2609	1.1314	7.90E-03	1.6575	116.6	16.9	8.2	0.49%
	10.60	1.2680	1.1314	7.90E-03	1.6575	116.8	16.9	8.65	0.52%
	9.83	1.2814	1.1314	7.90E-03	1.6575	137.2	19.9	9.5	0.57%
7/15.2T	10.20	1.4209	1.2739	9.93E-03	1.6380	139.7	20.3	7.4	0.45%
	10.40	1.4288	1.2739	9.93E-03	1.6380	135.1	19.6	7.8	0.48%
	10.20	1.4387	1.2739	9.93E-03	1.6380	141.4	20.5	8.3	0.51%
					avg.	**132.9**	**19.3**		
					st. dev.	10.5	1.5		

Micro-Flex test

sample	mB (mg/μ)	b (mg)	x	x^2	P * (mg)	defl. μm	(EI)f (N*m^2)	Eb (GPa)	Eb (Msi)	Eb/Et
6/21.9B	0.99	0.6	1.2502	-3.05E-03	47.7	42	5.84E-11	101.7	14.8	0.70
6/21.10B	1.05	1.2	1.3638	-4.07E-03	47.4	38.2	6.19E-11	83.0	12.0	0.66
6/21.11B	1.06	1.8	1.4198	-4.62E-03	49.7	38.55	6.25E-11	97.1	14.1	0.71
7/21.3B	0.84	1.0	0.9451	-1.21E-03	39.7	43.3	4.94E-11	80.3	11.6	0.69
7/21.4B	0.94	0.8	1.1958	-3.14E-03	44.3	40.7	5.52E-11	89.1	12.9	0.76
7/21.5B	0.98	0.7	1.1838	-2.30E-03	49.5	45.25	5.73E-11	125.1	18.1	0.91
7/21.6B	0.72	1.8	0.8258	-1.19E-03	35.4	43.35	4.25E-11	79.9	11.6	0.57
7/21.7B	0.84	0.6	1.0128	-2.00E-03	40.4	42.9	4.94E-11	86.1	12.5	0.64
7/21.8B	0.92	0.8	1.0078	-9.68E-04	45.0	45.9	5.40E-11	101.6	14.7	0.72
average:								**93.8**	**13.6**	**0.71**
std dev								14.5	2.1	

Compressive Properties

sample	Ec (GPa)	Ec (Msi)	Ec/Et	shift factor	UCS (MPa)	UCS (ksi)	c-strain	t-strn	b-strn
6/21.9B	74.5	**10.8**	0.51	0.17	520.8	75.5	0.70%	0.50%	0.60%
6/21.10B	57.9	**8.4**	0.46	0.19	414.5	60.1	0.72%	0.48%	0.60%
6/21.11B	71.7	**10.4**	0.52	0.16	500.0	72.5	0.70%	0.50%	0.60%
7/21.3B	57.9	**8.4**	0.50	0.17	407.5	59.1	0.70%	0.50%	0.60%
7/21.4B	70.3	**10.2**	0.60	0.13	474.9	68.9	0.68%	0.52%	0.60%
7/21.5B	114.5	**16.6**	0.83	0.05	717.8	104.1	0.63%	0.57%	0.60%
7/21.6B	51.0	**7.4**	0.37	0.25	381.5	55.3	0.75%	0.45%	0.60%
7/21.7B	59.3	**8.6**	0.44	0.20	427.6	62.0	0.72%	0.48%	0.60%
7/21.8B	75.8	**11.0**	0.54	0.15	525.6	76.2	0.69%	0.51%	0.60%
average	**70.3**	**10.2**	0.53		**485.6**	**70.4**			
st. dev.	18.7	2.7			101.5	14.7			

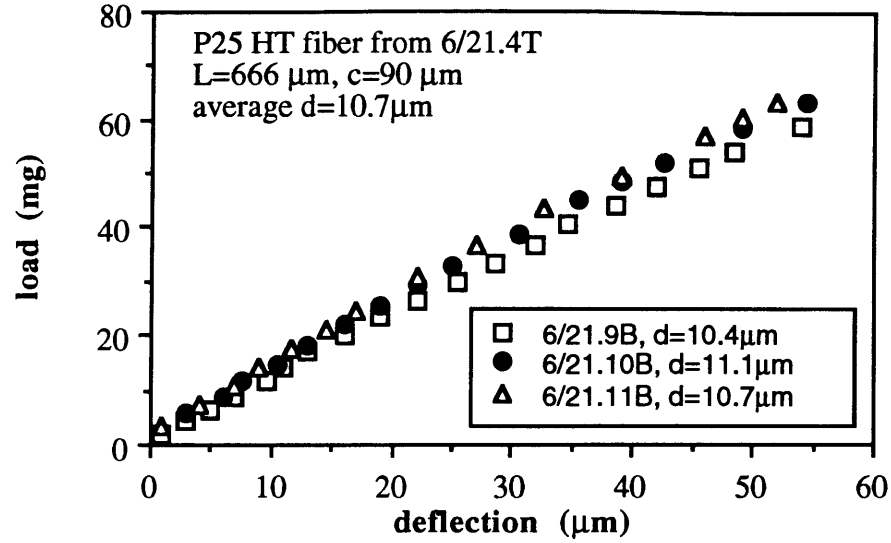
P25 HT fiber from 6/21.4T
L=666 μm, c=90 μm
average d=10.7μm
6/21.9B, d=10.4μm
6/21.10B, d=11.1μm
6/21.11B, d=10.7μm
load (mg)
deflection (μm)
0
20
40
60
80
0
10
20
30
40
50
60

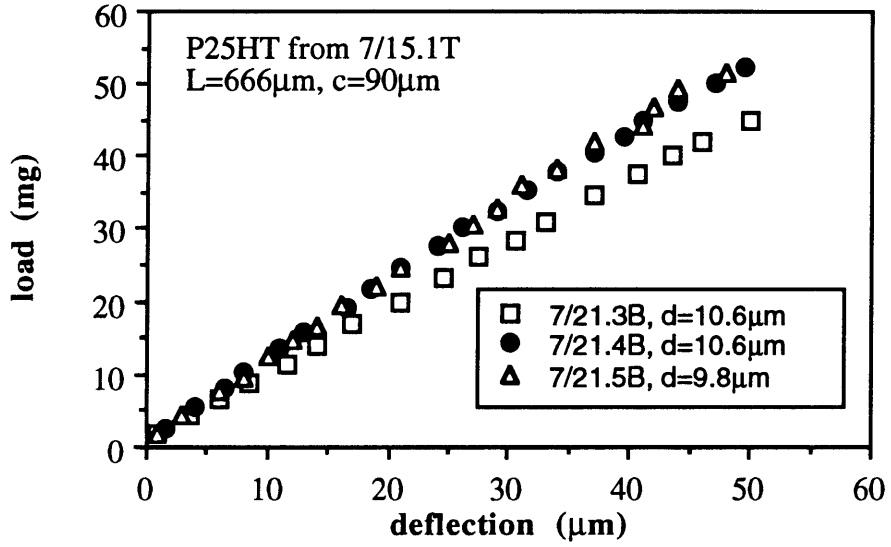
P25HT from 7/15.1T
L=666μm, c=90μm
7/21.3B, d=10.6μm
7/21.4B, d=10.6μm
7/21.5B, d=9.8μm
load (mg)
deflection (μm)
0
10
20
30
40
50
60
0
10
20
30
40
50
60

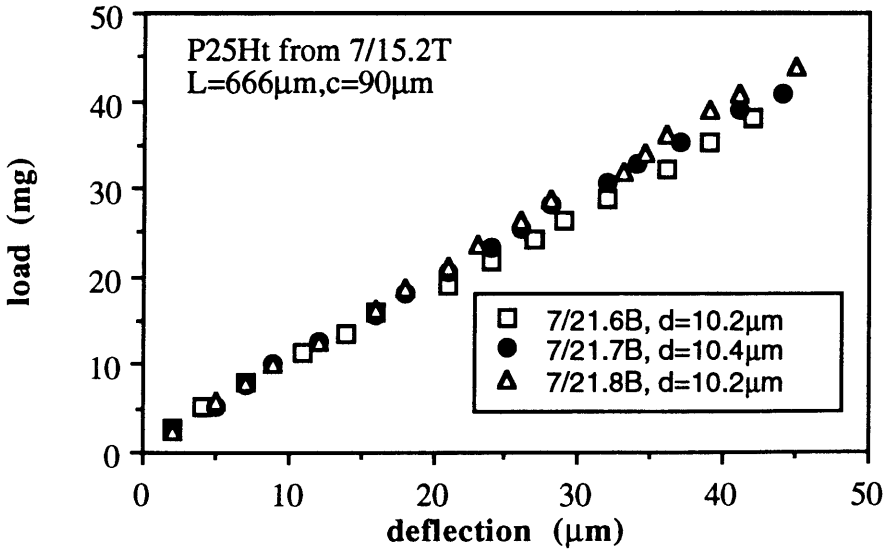
P25Ht from 7/15.2T
L=666μm,c=90μm
7/21.6B, d=10.2μm
7/21.7B, d=10.4μm
7/21.8B, d=10.2μm
load (mg)
deflection (μm)
0
10
20
30
40
50
0
10
20
30
40
50

C12. P55s Fibers

FITT- test

sample	diamtr. (μm)	mT (g/mil)	x	x^2	Lo (in)	**Et** (GPa)	**Et** (Msi)	ΔL	strain
7/20.1T	9.79	4.714	4.24	0.174	1.5470	475.1	68.9	1.35	0.09%
	9.68	4.714	4.24	0.174	1.5470	485.9	70.5	1.35	0.09%
7/21.1T	9.24	4.325	3.78	0.189	1.5915	503.3	73.0	1.45	0.09%
	9.19	4.306	3.78	0.189	1.5915	506.6	73.5	1.4	0.09%
7/21.2T	9.00	3.390	3.12	0.101	1.5995	417.9	60.6	1.35	0.08%
	8.87	3.392	3.12	0.101	1.5995	430.5	62.4	1.36	0.09%
	8.96	3.380	3.12	0.101	1.5995	420.4	61.0	1.3	0.08%
					average:	**462.8**	**67.1**		
					std. dev:	39.0	5.6		

Micro-Flex test

span= 666μm
midspn= 90μm

sample	mB (mg/μ)	b (mg)	x	x^2	P * (mg)	defl. μm	(EI)f (N*m^2)	**Eb** (GPa)	**Eb** (Msi)	Eb/Et
7/21.10B	2.91	-0.7	3.264	-0.022	24.6	8.2	1.71E-10	378.9	55.0	0.80
7/21.16B	2.77	2.3	2.980	-0.014	23.8	7.5	1.63E-10	377.2	54.7	0.78
7/21.17B	2.56	1.1	2.883	-0.020	23.2	8.1	1.51E-10	421.3	61.1	0.84
7/21.18B	2.32	1.1	2.562	-0.015	21.1	8.2	1.36E-10	389.6	56.5	0.77
7/21.19B	1.61	1.7	1.735	-0.008	14.9	7.9	9.44E-11	293.1	42.5	0.70
7/21.20B	1.60	3.0	1.712	-0.008	15.0	7.25	9.38E-11	308.7	44.8	0.72
7/21.21B	1.49	0.0	1.638	-0.008	13.9	8.9	8.77E-11	277.2	40.2	0.66
average:								**349.4**	**50.7**	**0.75**
std dev								55.5	8.0	

Compressive Properties

sample	**Ec** (GPa)	**Ec** (Msi)	Ec/Et	shift factor	**c-stress** (MPa)	(ksi)	**c-strain**	t-strn	b-strn
7/21.10B	308.2	**44.7**	0.65	0.11	339.8	49.3	0.11%	0.09%	0.10%
7/21.16B	299.9	**43.5**	0.62	0.12	336.8	48.8	0.11%	0.09%	0.10%
7/21.17B	356.5	**51.7**	0.71	0.09	388.1	56.3	0.11%	0.09%	0.10%
7/21.18B	306.8	**44.5**	0.61	0.12	346.7	50.3	0.11%	0.09%	0.10%
7/21.19B	215.8	**31.3**	0.52	0.16	251.9	36.5	0.12%	0.08%	0.10%
7/21.20B	231.0	**33.5**	0.54	0.15	266.8	38.7	0.12%	0.08%	0.10%
7/21.21B	195.1	**28.3**	0.46	0.19	233.2	33.8	0.12%	0.08%	0.10%
average	**273.3**	**39.6**	0.59		**309.0**	**44.8**			
st. dev.	59.4	8.6			58.0	8.4			

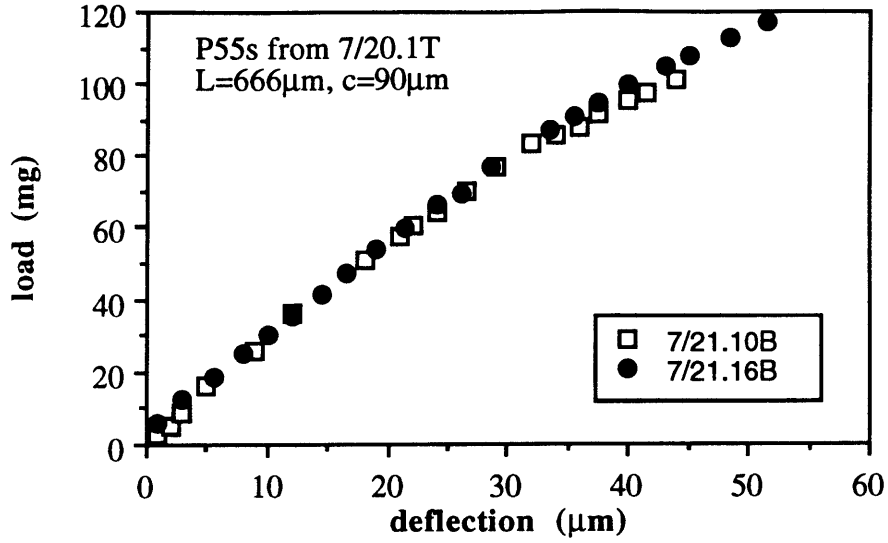
P55s from 7/20.1T
L=666μm, c=90μm
load (mg)
deflection (μm)
7/21.10B
7/21.16B
0
20
40
60
80
100
120
0
10
20
30
40
50
60

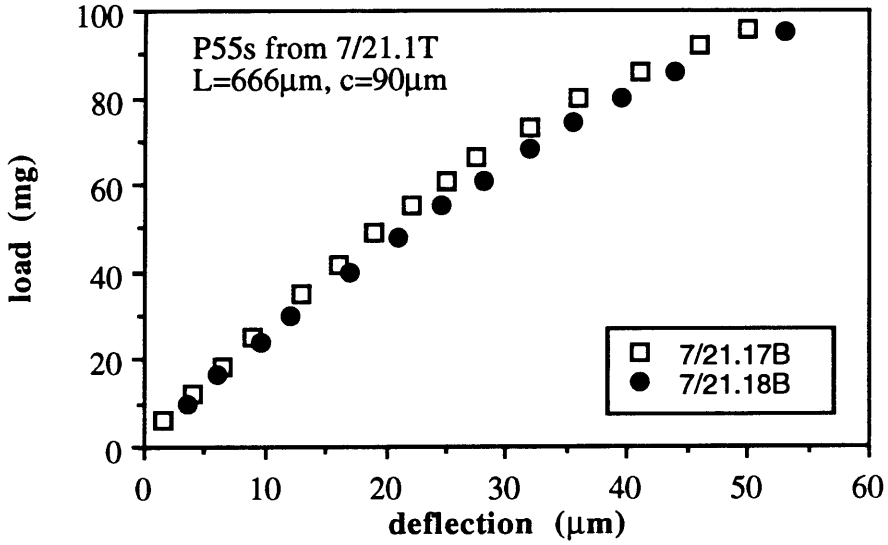
P55s from 7/21.1T
L=666μm, c=90μm
load (mg)
deflection (μm)
7/21.17B
7/21.18B
0
20
40
60
80
100
0
10
20
30
40
50
60

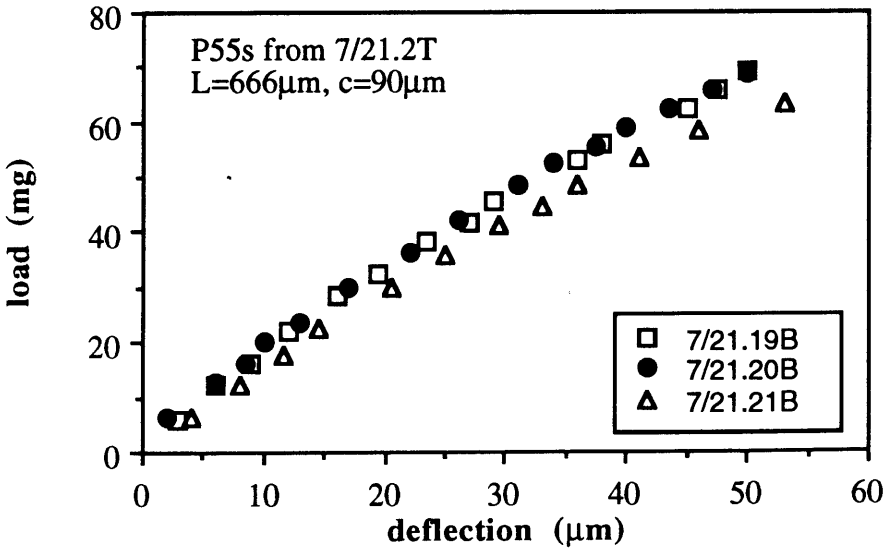
P55s from 7/21.2T
L=666μm, c=90μm
load (mg)
deflection (μm)
7/21.19B
7/21.20B
7/21.21B
0
20
40
60
80
0
10
20
30
40
50
60

C13. P75 Fibers

FITT- test

sample	diamtr. (μm)	mT (g/mil)	x	x^2	Lo (in)	Et (GPa)	Et (Msi)	ΔL	strain
7/14.5T	10.10	5.866	4.431	0.190	1.671	599.9	87.0	3.78	0.23%
	10.00	5.904	4.431	0.190	1.671	615.9	89.3	3.88	0.23%
7/17.1	9.06	4.513	3.792	0.098	1.590	545.8	79.2	3.69	0.23%
	9.11	4.551	3.792	0.098	1.590	544.3	78.9	3.88	0.24%
	8.96	4.504	3.792	0.098	1.590	556.9	80.8	3.64	0.23%
					avg.	**572.6**	**83.0**		
					st. dev.	33.1	4.8		

span= 666μm
midspn=90μm

Micro-Flex test

sample	mB (mg/μ)	b (mg)	x	x^2	P * (mg)		(EI)f (N*m^2)	**Eb** (GPa)	**Eb** (Msi)	Eb/Et
7/21.11B	2.232	2.8	3.337	-0.025	64.3	22.1	1.31E-10	256.8	37.3	0.43
7/21.12B	2.315	3.1	3.676	-0.032	67.5	21.5	1.36E-10	277.2	40.2	0.45
7/21.13B	1.385	0.9	2.041	-0.013	44.6	25.5	8.14E-11	246.1	35.7	0.45
7/21.14B	1.551	0.7	2.271	-0.014	49.6	25.6	9.12E-11	269.6	39.1	0.50
7/21.15B	1.322	1.5	1.974	-0.013	42.9	25.15	7.77E-11	245.6	35.6	0.44
average:								**259.1**	**37.6**	**0.45**
std dev								14.1	2.0	

Compressive Properties

sample	**Ec** (GPa)	**Ec** (Msi)	Ec/Et	shift factor	**c-stress** (MPa)	(ksi)	**c-strain**	t-strn	b-strn
7/21.11B	136.5	**19.8**	0.23	0.35	646.5	93.8	0.47%	0.23%	0.35%
7/21.12B	151.7	**22.0**	0.25	0.34	710.2	103.0	0.47%	0.23%	0.35%
7/21.13B	134.4	**19.5**	0.25	0.34	629.7	91.3	0.47%	0.23%	0.35%
7/21.14B	155.8	**22.6**	0.29	0.30	710.7	103.1	0.46%	0.24%	0.35%
7/21.15B	132.4	**19.2**	0.24	0.34	622.4	90.3	0.47%	0.23%	0.35%
average	**142.2**	**20.6**	0.25		**663.9**	**96.3**			
st. dev.	10.8	1.6			43.4	6.3			

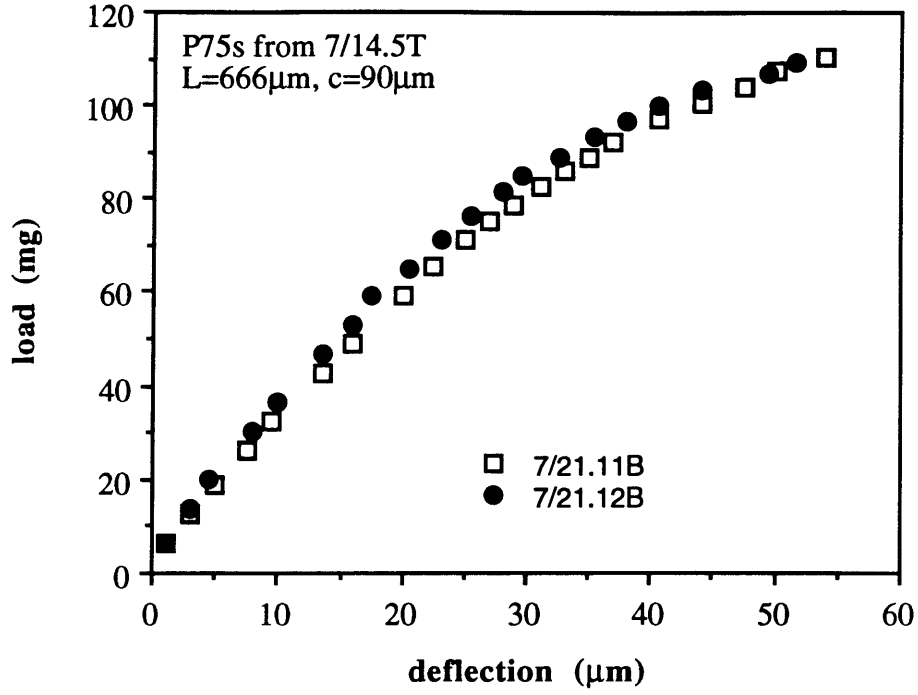
P75s from 7/14.5T
L=666μm, c=90μm
load (mg)
deflection (μm)
7/21.11B
7/21.12B
0
20
40
60
80
100
120
0
10
20
30
40
50
60

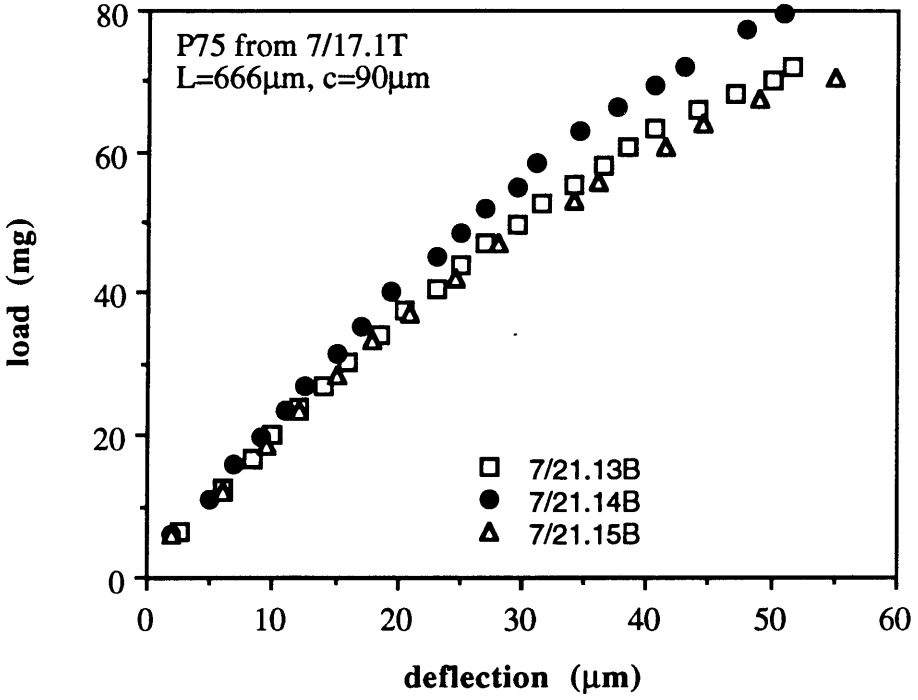
P75 from 7/17.1T
L=666μm, c=90μm
load (mg)
deflection (μm)
7/21.13B
7/21.14B
7/21.15B
0
20
40
60
80
0
10
20
30
40
50
60

Bibliography

[1] Dobb, MG; Johnson, DJ; Saville, BP. "Supramolecular Structure of a High- Modulus Polyaromatic Fiber (Kevlar 49)" *J. Polym. Sci. Polym. Phys. Ed.* **15** (1977) 2201.

[2] Sawyer, LC; Jaffe, M. "The structure of thermotropic copolyesters" *J. Mat. Sci.* **21** (1986) 1897- 1913.

[3] Lin, SS. "Recent Developments of Carbon Fiber in Japan" *SAMPE Journal* **28** (1992) 9-19.

[4] Vezie, DL; Adams WW. "High resolution scanning electron microscopy of PAN-based and pitch-based carbon fibers" *J. Mat. Sci.*, **9** (1990) 883.

[5] Johnson, DJ; Dyson, HM. "Structure of high strength carbon fibers" Carbon '88, McEnaney and Mays, ed., U. of Newcastle upon Tyne (1988) 383.

[6] Kumar, S; Anderson, DP; Crasto, AS. "Carbon fibre compressive strength and its dependence on structure and morphology" *J. Mater. Sci.* **28** (1993) 423-39.

[7] Vezie, DL. "Ultrastructural Studies of the Mechanism of Compressive Deformation in Rigid Rod Polymers" Ph.D. Thesis, MIT June 1993.

[8] Harper JP; Heumann, TO. "Elastic properties and failure mechanisms in hybrid composites with differing resin matrices" *Diss. Abstr. Int. B* **49** (1988) 1889.

[9] Crasto, AS; Kim, RY. "Nonlinear stress- strain behavior of advanced fibers and composites" *36th International SAMPE Symp.* (1991) 1649-63.

[10] Kumar, S; Adams, WW; Helminiak, TE. "Uniaxial Compressive Strength of High Modulus Fibers in Composites" *J. Reinf. Plast. and Comp.* **7** (1988) 108-119.

[11] Riggs, DM; Shuford, RJ; and Lewis, RW. "Graphite Fibers and Composites" in Handbook of Composites, G. Lubin, ed. Van Nostrand Reinhold, New York, 1982, p236-237.

[12] Greenwood, JH; Rose, PG "Compressive behaviour of Kevlar 49 fibres and composites" *J. Mat. Sci.* **9** (1974) 1809-1814.

[13] Fisher, S; Marom, G. "A Complete Elastic- Plastic Analysis of Aramid Fibre Composites" *Fibre Sci. and Tech.* **20** (1984) 91-98.

[14] Kumar, S; Helminiak, TE. "Compressive Strength of High Performance Fibers" in The Materials Science and Engineering of Rigid-Rod Polymers. WW Adams, RK Eby and DE McLemore eds. *Mat. Res. Soc. Symp. Proc.* **134** (1989)

[15] Piggott, MR; Harris, B. "Compression strength of carbon, glass and Kevlar-49 fibre reinforced polyester resins" *J. Mat. Sci.*, **15** (1980) 2523-38.

[16] Chamis, CC. "Mechanics of Composite Materials: Past, Present, and Future" *J. Comp. Tech. and Res.* **11** (1989) 3- 14.

[17] Mrse, A; Piggott, MR. "Relation between fibre divagation and compressive properties of fibre composites" *35th International SAMPE Symp.*, April 1990, 2236.

[18] Swift, DG. "Elastic moduli of fibrous composites containing misaligned fibres" *J. Phys. D: Appl. Phys.* **8** (1975) 223-40.

[19] Klunziger, PE; Macturk, KS; Eby, RK and Adams, WW. "Nonlinear Elasticity of High Performance Fibers" *Polym. Preprints* **32** (1991) 187-88.

[20] Curtis, GJ; Milne, JM; Reynolds, WN. "Non- Hookean Behaviour of Strong Carbon Fibres" *Nature* **220** (1968) 1024.

[21] Gill, RM. Carbon Fibers in Composite Materials. The Plastics Institute, London, 1972, 59.

[22] Hughes, JDH. "The evaluation of current carbon fibres" *J. Appl. Phys. D: Appl. Phys.* **20** (1987) 276.

[23] Banisaukas, JJ. "SACMA recommended carbon fiber test method and lot acceptance procedures" *35th International SAMPE Symp.*, April 1990, 1840.

[24] Arsenovic, P; Jiang, H; Eby RK; Adams WW; and Liu, JM. "Nonlinear Elasticity in Carbon Fibers" Carbon '88 McEnaney and Mays, ed., U. of Newcastle upon Tyne (1988) 485.

[25] Kawabata, S. "Measurements of Anisotropic Mechanical Property and Thermal Conductivity of Single Fiber for Several High Performance Fibers" *Proc. Jpn- US Conf on Comp. Mater., 4th,* (1988) 253-62.

[26] Allen, SR; Roche, EJ. "Deformation Behaviour of Kevlar® aramid fibers" *Polym.* **30** (1989)996-1003.

[27] ASTM D 3379-75 "Standard Test Method for Tensile Strength and Young's Modulus for High- Modulus Single- Filament Materials" vol. 15.03, 1991, 127.

[28] Jouquet, G; Schill, R. "Mechanical properties of carbon fibres and their composites" *Carbon Fibers; their composites and applications*, ICFC Proceedings, The Plastics Institute (1971) 113.

[29] Schoppee, MM; Skelton, J. "Bending Limits of Some High-Modulus Fibers" *Text. Res. J.* **44** (1974) 968-75.

[30] Jones, WR; Johnson, JW. "Intrinsic strength and non-Hookean behaviour of carbon fibers" *Carbon*, **9** (1971) 645.

[31] Macturk, KS; Eby, RK; Adams WW. "Characterization of compressive properties of high-performance polymer fibres with a new microcompression apparatus" *Polymer*, **32** (1991) 1782.

[32] Kumar, S. "Structure and Properties of High Performance Polymeric and Carbon Fibers- An Overview" *SAMPE Quarterly* (1989) 3-8.

[33] Fawaz, SA; Palazotto, AN; Wang, CS. "Axial tensile and compressive properties of high - performance polymeric fibres" *Polym.* **33** (1992) 100-105.

[34] Sittig, M., ed. Carbon and Graphite Fibers: Manufacture and Application. Noyes Data Corp., Park Ridge, NJ, 1980/6, 331.

[35] Parry, TV; Wronski, AS. "Kinking and compressive failure in uniaxially aligned carbon fibre composite tested under superposed hydrostatic pressure" *J. Mat. Sci.* **17** (1982) 893-900.

[36] Hawthorne, HM; Teghtsoonian, E. "Axial compression fracture in carbon fibers" *J. Mat. Sci.*, **10** (1975) 41.

[37] Prandy, JM; Hahn, HT. "Compressive strength of carbon fibers" *35th International SAMPE Symp.*, April 1990, 1657.

[38] Sinclair, D. "A Bending Method for Measurement of the Tensile Strength and Young's Modulus of Glass Fibers" *J. Appl. Phys.* **21** (1950) 380-86.

[39] Bazhenov, SL; Kozey, VV. "Compression fracture of unidirectional carbon fibre-reinforced plastics" *J. Mat. Sci.* **26** (1991) 6764-76.

[40] Vlattis, C. and Galiotis, C. "Monitoring the behavior of polymer fibers under axial compression" *Polymer* **32** (1991) 1788-93.

[41] DeTeresa, SJ. "Piezoresistivity and failure of carbon filaments in axial compression" *Carbon* **29** (1991) 397-409.

[42] Miwa, M; Tsushima, E; Takayasu, J. "Axial Compressive Strength of Carbon Fiber with Tensile Strength Distribution" *J. Appl. Polym. Sci.* **43** (1991) 1467-74.

[43] Allen, SR. "Tensile recoil measurement of compressive strength for polymeric high-performance fibers" *J. Mat. Sci.* **22** (1987) 853.

[44] Kozey, VV; Berlin, AA. "Characterization of compressive properties of advanced fibers" Paper N22-P, 3rd Japan- USSR Joint Symposium on Advanced Composite Materials, Oct. 1991.

[45] Crasto, AS; Kumar, S. "Recoil compression testing of advanced carbon fibers" *35th International SAMPE Symp.*, April 1990, 318.

[47] Arridge, RGC; Folkes, MJ. "Effect of sample geometry on the measurement of mechanical properties of anisotropic materials" *Polym.* **17** (1976) 495-500.

[48] Freeston, WD, Jr; Schoppee, MM. "A Note on Filament Compressive Modulus" *Text. Res. J.* **42** (1972) 314-17.

[49] Dmitruk, LN; Gureeva, NN; Shelyubskii, VI. "Measuring the Bending Strength of Sapphire Fibers" tr. from *Zavodskaya Laboratoriya* **44** (1978) 1284-85.

[50] Moalli, JE; McGarry, FJ. "New Single Fiber Test Methods" *45th Annual Conf. Comp. Inst.*, SPI (1991).

[51] Allen, SR; Farris, RJ. "Mechanical behavior of rigid rod polymeric fibers" in The Materials Science and Engineering of Rigid-Rod Polymers. WW Adams, RK Eby and DE McLemore eds. *Mat. Res. Soc. Symp. Proc.* **134** (1989) 297-307.

[52] Moalli, JE; McGarry, FJ. "New Single Fiber Test Methods" 45th Annual Conf. Comp. Inst., SPI (1991)

[53] SR Allen, personal communication.

[54] duPont product information: Kevlar Aramid Fiber Technical Guide., 12/ 92.

[55] Hercules product data sheet

[56] Amoco Thornel product sheets

[57] Knox, CE. "Fiberglass Reinforcement" in Handbook of Composites, G. Lubin, ed. Van Nostrand Reinhold, New York, 1982, p136-159.

[58] Barford, NC. Experimental Measurements: Precision, Error and Truth, 2nd Ed. John Wiley and Sons, Chichester, UK. 1985.

Biographical Note

Maureen Fahey received all of her university education at the Massachusetts Institute of Technology between September 1986 and September 1993. She earned the Bachelor of Science degree in Materials Science and Engineering in June 1990 and the Doctor of Science through the Program in Polymer Science and Technology in September 1993. Both the bachelor's thesis, "Mechanical Property Characterization and Enhancement of Rigid Rod Polymer Fibers," and the doctoral thesis, "Nonlinear and Anisotropic Behavior of High Performance Fibers," were supervised by Professor Frederick J. McGarry. Industrial experience before graduate studies included a summer co-op at the Allied- Signal Engineered Materials Research Center in Des Plaines, IL, and a summer fellowship with Imperial Chemical Industries at Wilton Centre, England. Dr. Fahey will join the 3M Company in Austin, Texas in October 1993.

Maureen is a member of Tau Beta Pi and Sigma Xi. She received the John Wulff Award for Excellence in Graduate Teaching for her two semesters as a teaching assistant in the upper-level materials science laboratory investigating the structure-processing-properties relationships in magnetic and piezoelectric materials. In addition, Maureen received many awards for her accomplishments on the basketball court, including the Malcolm G. Kispert award for top graduating female student- athlete and an NCAA Postgraduate Scholarship. She was the assistant coach of the women's basketball team from 1990-1992.